POLITECNICO DI MILANO

SCHOOL OF ENGINEERING

MASTER OF SCIENCE IN CIVIL ENGINEERING FOR RISK MITIGATION

M.Sc. THESIS

BEHAVIOR OF HIGH PERFORMANCE FIBER REINFORCED CONCRETE BEAM EXPOSED TO FIRE

Supervisor :

Prof. Matteo COLOMBO

Authors

Fatemeh POURSAFFARI (814216)

APRIL 2016

Acknowledgements

I would like to express my gratitude to my supervisor, Professor Matteo Colombo for his useful comments, remarks and engagement through the learning process of this mater thesis.

I would like to thank my parents, for their support and encourage. I could not have completed this thesis without them.

I would like to gift this thesis to those who are seeking knowledge in this field.

Abstract

The topic of structural damage caused by fire has been discussed extensively by many researchers for over a decade. High performance concrete (HPC) can't resist under fire exposure and the problem of spalling was seen in experimental tests. Using steel fibers in concrete not only develops concrete performance against fire and reduces spalling, but also increases structural resistance like resisting bending moment by taking into account tensile behavior of fibers. This study focuses on fire behavior of high performance fiber reinforced concrete (HPFRC) and presents the bending moment capacity of HPFRC beam exposed to fire using plane section approach (2D) and finite element method (3D). The time-temperature curve used in the thesis is based on standard fire named ISO834. The variation in material properties, caused by elevated temperature, has been studied, including strength and stiffness degradation. Compressive and tension constitutive laws change as temperature of the material increases according to EC3 Part 1.2. The behavior of the HPFRC beam when subjected to thermal loading followed by fire is presented and shows that there is degradation in bending moment capacity. Moreover, this degradation also has been studied under situation when there is cooling phases. Time of collapse in both approaches; 2D and 3D modeling are presented and compared with each other. The results from this study shows that the 3D model predicted a greater time to resist against fire while in 2D model the beam will fail sooner. We demonstrate neither models were able to simulate the spalling effect clearly in the experimental tests. At the end we suggest an effective way to solve this problem by adding polypropylene fibers which should get the concrete to resist better against spalling.

Astratto

Il tema dei danni strutturali causati dal fuoco è stato discusso in modo estensivo da molti ricercatori da oltre un decennio. Il calcestruzzo ad alte prestazioni (HPC) non può resistere ad alte temperature per via del problema di "spalling" riscontratosi nei test. L'utilizzo di fibre di acciaio all'interno del calcestruzzo, non solo riduce l'effetto di "spalling" ma ne aumenta anche la resistenza strutturale come per il momento flettente, tenuto in considerazione il comportamento a trazione delle fibre in acciaio. Questo studio si concentra sul comportamento della fibra nel cemento armato (HPFRC) e sull'analisi del momento flettente HPFRC durante l'esposizione alle alte temperature, utilizzando l'approccio "sezione piano" (2D) e il metodo degli elementi finiti (3D). La curva tempo-temperatura utilizzata nella tesi è stata ripresa da quella di "fuoco standard" ISO 834. Sono state studiate le variazioni delle proprietà del materiale sotto l'effetto delle elevate temperature, comprendendo anche la forza e il degrado di rigidezza. Le leggi costitutive di compressione e tensione cambiano in funzione della temperatura del materiale e si modificano in base alla EC3 parte 1.2. Si dimostrerà che esiste una degradazione nei parametri resistivi a momento flettente nelle travi UHPFRC sottoposte a carico termico a seguito di un incendio. Abbiamo voluto estendere l'analisi sul degrado del materiale anche nella fase di raffreddamento così da avere un'analisi più completa. I risultati di questo studio mostrano che il modello 3D ha predetto un tempo di resistenza al fuoco superiore rispetto a quello dell'analisi 2D. Dimostreremo che nessun modello è stato in grado di simulare l'effetto di "spalling" in modo chiaro. Alla fine suggeriremo che l'uso di fibre di polipropilene dovrebbe risultare un efficace metodo per ridurre il problema di spalling alle alte temperature.

Contents

Notation

l/d	Fibers Aspect ratio
℃	Degree of Celsius
E_d	Design effect of actions in normal temperature design
Q	Heat flow
λ	Thermal conductivity
α_c	Heat transfer coefficient or thermal convection coefficient
P	Emissive power
σ	Stefan-Boltzmann constant.
q	Global thermal flux of the black body towards vacuum
ε_{res}	Resultant emissivity
ϕ	Configuration factor
∇T	Temperature gradient
α	Thermal diffusivity
T	Temperature
T	Time
ρ	Density
c	Specific heat
α_{ci}	Coefficient of convective heat transfer
ϵ	Surface emissivity
$\dot{q}_b''$	Heat flow at the boundary
T_g	Gas temperature
T_b	Boundary temperature
α_c	Convection heat transfer coefficient
ϵ_{res}	Resulting emissivity
θ	Concrete temperature
$C_{c,peak}$	Specific heat at the peak
ΔT	Temperature interval
$f_{c,\theta}$	Characteristic value of the compressive strength of concrete at elevated temperature
$\varepsilon_{c1,\theta}$	Strain corresponding to $f_{c,\theta}$
$\varepsilon_{cu1,\theta}$	Ultimate strain
f_{R1k}	Serviceability characteristic flexural residual strength
f_{R3k}	Ultimate characteristic flexural residual strength
l	Length at 20℃
Δl	Temperature induced elongation
θ_a	Steel temperature
Q_{1k}	Live load
G_{1k}	Permanent load

G_{2k}	Imposed load
M_{Ed}	Acting moment
V_{Ed}	Acting shear
S_{rm}	Mean distance between cracks
l_{cs}	Characteristic length
Y	Distance between the neutral axis and the tensile side of the cross-section
c	Concrete cover
τ_{bm}	Mean bond strength between steel and concrete
f_{ctm}	Mean concrete tensile strength
k	Parameter to take into account the influence of concrete cover
$\emptyset_s$	Rebar diameter
$\rho_{s,ef}$	Effective reinforcement ratio
$A_{c,ef}$	Effective area of concrete in tension
R_{ck}	Cubic compression resistance
ε_{c1}	Deformation at pick
ε_{cu}	Ultimate deformation
γ_{c2}	Material coefficient
E_{c1}	Second module of elastic
E_{c0}	Tangent module of elastic

Table of Figures :

Tables:

1 : Introduction

Normal concrete is typically resistant against fire and elevated temperatures, but the HPC may result in failure. The high packing density of HPC results in low permeability and superior durability over normal concretes. The failure that typically occurs for HPC is explosive spalling at high temperatures. Thermal spalling is mainly due to combination of two phenomena;

1- Increasing of vapor pressure caused by the evaporation of free and bound water trapped in the cementitious matrix.

2- Unequal thermal expansion between the concrete core and surface

Spalling is more crucial for steel reinforced concrete, because by reducing the cross section the convention steel reinforcement may expose to high temperatures. The use of steel and polypropylene or steel fibers has shown to mitigate the problem of spalling at high temperatures. By adding these fibers to HPC mix the resistance of matrix to elevated temperature increases. Also, the addition of fibers allows for higher ductility and energy dissipation capacity. Moreover, it allows to optimize the elements sections, while reducing the total masses and the execution costs. Addition of fibers increase the tensile strength of concrete and constitutive law can be also established for tensile zone.

The focus of this research is to investigate the residual mechanical properties of high performance fiber reinforced concretes at elevated temperatures. Heating of the beam is studied in two different heating regimes, with cooling phase and without cooling phase. The body of thesis consists of seven chapters as follows;

Chapter 1 represents an overview to the thesis

Chapter 2 represents an introduction to HPFRC both in ambient temperature and in elevated temperature according to articles and experimental works already done by researchers.

Chapter 3 is mainly about the heat transfer and an introduction of engineering problem regarding thermal transmission trough the matters.

Chapter 4 presents engineering problem of this work including geometry of the problem, material properties, fire exposure, acting loads and any other parameters required to model the problem numerically.

In Chapter 5 the plane section approach used for finding the bending moment capacity. Applying this approach, the problem was modeled in two dimension and the plane section approached has been introduced and discussed.

Chapter 6 works with 3D model of the whole problem using software of Abaqus CAE (FEM) and its aim is to find the overall behavior of the HPFRC beam exposed to fire in 3D.

Chapter 7 is going further by considering the beam with its slab and finding the results in both 2D and 3D approaches to understand the contribution of slab in bearing capacity of the problem.

Chapter 8 is conclusion on the results of the last three chapters and gives more perspective for future studies.

2 : Literature Review

In the last two decades, concrete technology has enabled the manufacturing of concrete that has a uniaxial compression strength of about (or more than) 100 MPa, implementing conventional mixing technologies. This concrete has been commonly referred to as high strength concrete (HSC). Subsequently, study of the structural behavior of HSC has increased during this period together with the research and development on the material properties. Research on HSC material properties has shown that, besides its increased strength, HSC is also characterized by relatively increased brittleness. Adding steel fibers is one way of enhancing the structural performance of HSC through an increase in the concrete toughness, yielding high performance concrete (HPC). The use of steel fibers has been developed in recent years (Dancygier & Savir, 2006).

Therefore, in order to have a better understanding about High performance fiber reinforced concrete (HPFRC) the behavior of HPC and FRC according to different articles and reports have been discussed separately. After that, the behavior of HPFRC was presented according to articles and studies that were performed on HPFRC directly and the result of tests and studies will be presented. After that the performance of HPFRC when exposed to fire in different researches presented.

2.1 Literature review (Concrete in Ambient Temperature)

2.1.1 HPC

Based on the compressive strength; concrete is normally classified as normal strength concrete, high strength concrete and ultra-strength concrete. To achieve high strength, it is necessary to use high cement content with the lowest possible w/c ratio which invariable affect the workability of the matrix (Krstulovic, Haghayeghi, & Uang, 1995). Therefore, the main difference between conventional concrete and High-Performance Concrete is essentially the use of chemical and mineral admixtures (Kanmalai, Partheeban, & Felix, 2008). The admixtures can be added to cement concrete as a partial replacement of cement along with superplasticiser as a water reducer to get the high performance. Generally speaking, the definition 'high performance' is meant to distinguish structural materials from the conventional ones, as well as to optimize a combination of properties in terms of final applications related to the civil engineering. The most interesting properties are, for example, strength, ductility, toughness, durability, stiffness, thermal resistance, even though it is necessary to take into account the final cost of the material and, above all, of the produced structural members (GUERRINI, 2000).

2.1.1.1 Mixture of HPC

Mineral and chemical admixtures play an important role in the production of High Performance Concrete. Mineral Admixtures form an essential part of the High Performance Concrete mix. They are used for various purposes depending upon their properties. Table 2-1 shows different types of mineral admixtures with their particle characteristics. Different Chemical admixtures (Super plasticizers) are extensively used in development of High Performance Concrete with very low water cement ratio are represented in Table 2-2 with their functions (Vatsal & Niraj, 2013).

Mineral Admixtures	Classification	Particle characteristics
Ground granulated blast furnace slag	Cementitious and pozzolanic	Unprocessed material are grain like sand, ground to size< 45 μm particles and have atough texture
Fly ash	Cementitious and pozzolanic	Powder consists of particles size 45 μm, 10% to 15% are more than 45 μm, solid spheres and general smooth
Silica fume	Highly active pozzolanic	Fine powder consisting of solid spheres of 0.1 μm average diameter
Rice husk ash	Highly active pozzolanic	Particles are <45 μm in size and have cellular and porous structure

Table 2-1: Different mineral admixtures used in HPC

Chemical Admixtures	Function
Superplasticizer	To reduce the water requirement by 15 % to 20% without affecting the workability leading to a high strength and dense concrete
Accelerator	To reduce the setting time of concrete thus helping early removal of forms and therefore used in cold weather concreting
Retarder	To increase the setting time by slowing down the hydration of cement and therefore are preferred in places of high temperature concerting
Water reducing admixture	To achieve certain workability (slump)at low water cement ratio for a specified strength thus saving on the cement
Air entraining admixture	To entrain small air bubbles in concrete which act as rollers thus improving the workability and therefore very effective in freeze-thaw cycles as they provide a cushioning effect on the expanding water in the concreting in cold climate

Table 2-2: Different chemical admixtures used in HPC

The composition of HPC usually consists of cement, water, fine sand, superplasticizer, fly ash and silica fume. Sometimes, quartz flour and fiber are the components as well. The key elements of high performance concrete can be summarized as follows:

- Low water-to-cement ratio,

- Large quantity of silica fume (and/or other fine mineral powders),
- Small aggregates and fine sand,
- High dosage of superplasticizers,
- Heat treatment and application of pressure which are necessary for ultra high strength concrete after mixing (at curing stage).

The microstructure of concrete can be described in three aspects, namely composition of hydrated cement paste, pore structure and interfacial transition zone. The hydrated cement paste is in fact the hydration products when cement is reacted with water. The pore structure refers to the gel pores, capillary pores and voids, as well as their connections within the hardened concrete. The interfacial transition zone refers to the boundaries between the cement paste, and aggregates or particles of admixtures. The composition of NSC is relatively simple, which consists of cement, aggregate and water. Figure 2-1 shows the microstructure of NSC.

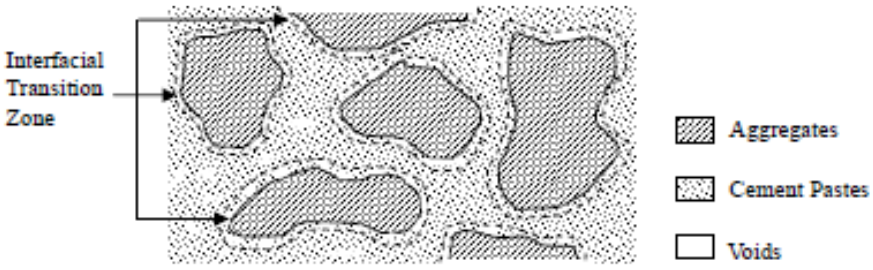

Figure 2-1 Microstructure of NSC

In HPC, very fine admixture, such as silica fume or fly ash, is added into the design mix so that the empty space inside concrete can be reduced significantly. Meanwhile, the pore connectivity is lowered because the very fine particles effectively block the capillary network. Thirdly, the interfacial transition zone can be toughened by lowering the locally high water-to-cement ratio and by improving the particle packing in this zone. Superplasticizer is added into the concrete mix so that a very low water-to-cement ratio (less than 0.2) become feasible to be adopted. Fine admixtures, like silica fume or fly ash, is added as well to improve the particle packing in the interfacial transition zone. It is noticed that in order to improve the concrete performance, admixture is a necessary

component which must be added into the design mix in order to generate HPC. Hence, its microstructure is quite different from that of NSC. Figure 2-2 (Oral & Denvid).

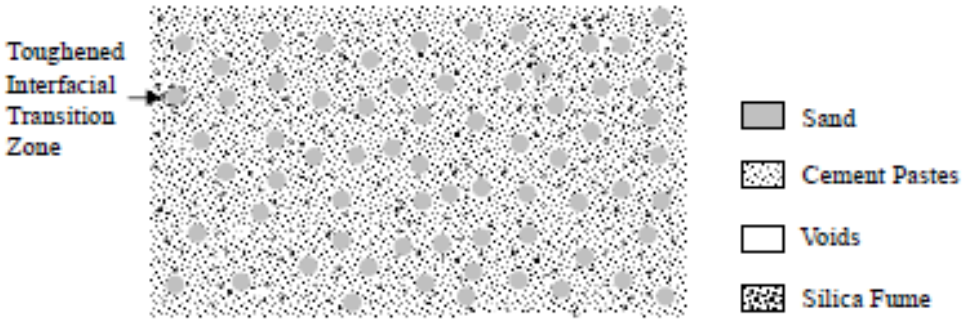

Figure 2-2Microstructure of HPC

2.1.1.2 Strength of HPC

In practice, concrete with a compressive strength less than 50MPa is regarded as NSC, while high strength concrete (HSC) may be defined as that having a compressive strength of about 50MPa. Recently, concrete with the compressive strength of more than 200MPa has been achieved. Table 2-3 shows the characteristics of different type of HSC with various compositions (Oral & Denvid).

It is also studied by Kanmalali and he stated that it is recognized that the use of silica fume as a partial replacement for cement provides a significant increase in strength of concrete (Kanmalai, Partheeban, & Felix, 2008).

	Regular	High strength	Very high strength
Compressive strength (MPa)	<50	50-100	100-150
Water-to-cement ratio	>0.45	0.45-0.30	0.30-0.25
Chemical admixtures	Not required	Water-reducing admixture or superplasiticizer	Superplasticizer
Mineral admixtures	Not required	Fly ash	Silica fume
Permeability (m/s)	$>10^{-12}$	10^{-13}	$<10^{-14}$

Table 2-3: Characteristics of High Strength Concretes

2.1.1.3 Ductility of HPC

Research on HPC material properties has shown that, besides its increased strength, HPC is also characterized by relatively increased brittleness (Dancygier & Savir, 2006). Meanwhile, HPC has a larger Young's modulus than NSC and the post-peak softening branch is steeper. HPC behaves linearly up to a stress level which is about 90% of the peak stress, whereas lower strength concrete shows nearly no linear part at all. When the peak stress has been reached, the stress decays rapidly in high strength concrete. A qualitative comparison of uniaxial compressive stress-strain curve of HSC with that of NSC is given in Figure 2-3.

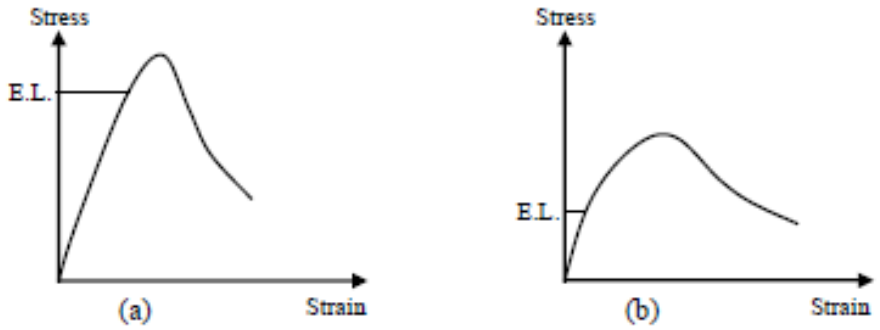

Figure 2-3 Schematic of Stress-Strain curve in (a) HPC and (b) NSC under Uniaxial Compression

2.1.2 FRC

Fibers have been used to reinforce brittle materials since ancient times. The use of straw in sun baked clay bricks; mixing of horse hair in plasters were widespread in early civilizations. Apart from the role of fibers is essentially to arrest any advancing cracks by applying pinching forces at the cracks tips, thus delaying their propagation across the matrix and both these methods provide tensile strength to the concrete members, and they however do not increase the inherent tensile strength of concrete itself creating a distinct slow crack propagation stage (Meikandaan, Arunkumar, & PonPaul, Dec 2012).

Fiber reinforced concrete (FRC) may be defined as a composite materials made with Portland cement, aggregate, and incorporating discrete discontinuous fibers (Chanh).

Fibers are produced from different materials in various shapes and sizes. Typical fiber materials are;

- Steel Fibers: Straight, crimped, twisted, hooked, ringed, and paddled ends. Diameter range from 0.25 to 0.76mm.

- Glass Fibers: Straight. Diameter ranges from 0.005 to 0.015mm (may be bonded together to form elements with diameters of 0.13 to 1.3mm).

- Natural Organic and Mineral Fibers Wood, asbestos, cotton, bamboo, and rock-wood. They come in wide range of sizes.

- Polypropylene Fibers: Plain, twisted, fibrillated, and with buttoned ends.

- Other Synthetic Fibers Kevlar, nylon, and polyester. Diameter ranges from 0.02 to 0.38mm.

A convenient parameter describing a fiber is its aspect ratio (LID), defined as the fiber length divided by an equivalent fiber diameter. Typical aspect ratio ranges from about 30 to 150 for length of 6 to 75mm (WAFA, 1990).

Addition of fibers to concrete influences its mechanical properties which significantly depend on the type and percentage of fiber. Fibers with end anchorage and high aspect ratio were found to have improved effectiveness. It was shown that for the same length and diameter, crimped-end fibers can achieve the same properties as straight fibers using 40 percent less fibers. In determining the mechanical properties of FRC, the same equipment and procedure as used for conventional concrete can also be used.

2.1.2.1 Mixture of FRC

As with any other type of concrete, the mix proportions for SFRC depend upon the requirements for a particular job, in terms of strength, workability, and so on. Several procedures for proportioning SFRC mixes are available, which emphasize the workability of the resulting mix. However, there are some considerations that are particular to SFRC.

In general, SFRC mixes contain higher cement contents and higher ratios of fine to coarse aggregate than do ordinary concretes, and so the mix design procedures the apply to conventional concrete may not be entirely applicable to SFRC. Commonly, to reduce the quantity of cement, up to 35% of the cement may be replaced with fly ash. In addition, to improve the workability of higher fibre volume mixes, water reducing admixtures and, in particular, superlasticizers are often used, in conjunction with air entrainment.

The second factor which has a major effect on workability is the aspect ratio (l/d) of the fibres. The workability decreases with increasing aspect ratio, in practice it is very difficult to achieve a uniform mix if the aspect ratio is greater than about 100 (Chanh).

2.1.2.2 Compressive and tensile strength of FRC

The presence of fibers may alter the failure mode of cylinders, but the fiber effect will be minor on the improvement of compressive strength values (0 to 15 percent). Many experimental researches have been written in order to describe the effect of fibers on Compressive and tensile strength of concrete. For example Meikndaan performed number of tests on a FRC beam and the results indicated that there is 13.29% increase in compressive strength as compared with normal plain concrete (without fibers). Meanwhile adding fibers increases 11.96% of splitting tensile strength as compared with normal plain concrete. Moreover, there is 26.56% increase in Modulus of elasticity as compared with normal plain concrete (Meikandaan, Arunkumar, & PonPaul, Dec 2012).

According to Johnston, (Figure 2-4) fibres do little to enhance the static compressive strength of concrete, with increases in strength ranging from essentially nil to perhaps 25%. Even in members which contain conventional reinforcement in addition

to the steel fibres, the fibres have little effect on compressive strength. However, the fibres do substantially increase the post-cracking ductility, or energy absorption of the material (Johnston, 1974).

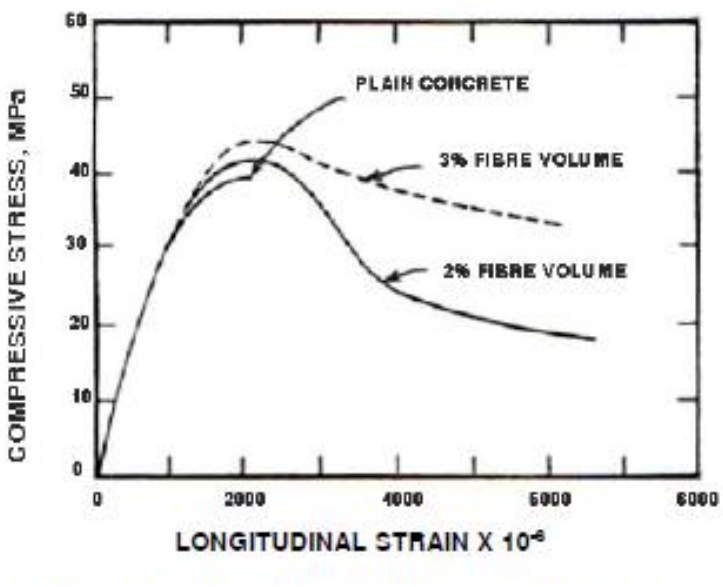

Figure 2-4: Stress-strain curves in compression for SFRC

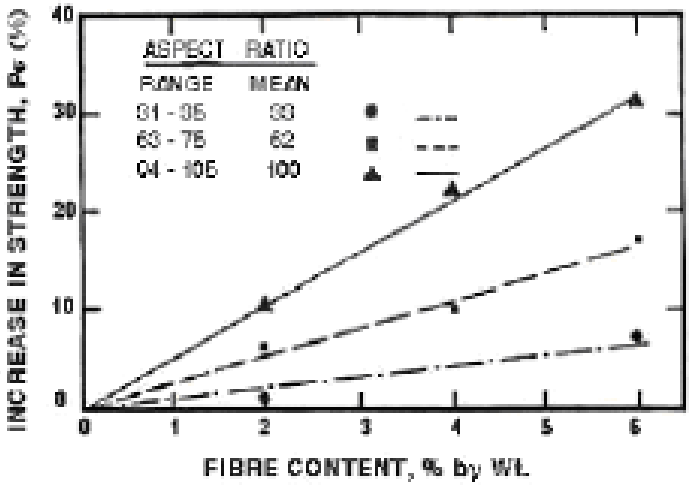

Figure 2-5: influence of fiber content on tensile strength

According to Johnston, for more or less randomly distributed fibers, the increase in tensile strength is much smaller, ranging from as little as no increase in some instances to perhaps 60%, with many investigations indicating intermediate values, as shown in

Figure 2-5. Splitting-tension test of SFRC show similar result. Thus, adding fibers merely to increase the direct tensile strength. However, as in compression, steel fibers do lead to major increases in the post-cracking behavior or toughness of the composites (Chanh; Johnston, 1974).

The addition of steel fibers to a reinforced concrete beam is known to increase its shear strength and if sufficient fibers are added, a brittle shear failure can be suppressed in favor of more ductile behavior (Adebar, Mindess, Pierre, & Olund, 1997).

According to Kwak et al , the fibers appeared to be effective in delaying the formation of cracks, or at least in arresting their initial growth. As the steel fiber volume increase the failure mode changed to a combination of shear and flexure. The experimental results form 12 fiber-reinforced concrete beams demonstrate the steel fiber volume fraction, a/d (shear span-depth ratio), and concrete compressive strength on the onset of shear cracking, shear strength, ultimate deflection and failure mode. The increase in strength was particularly large (69 to 80%) for beams with the smallest a/d (Kwak, Eberhard, Kim, & Kim, 2002).

The presence of 3 percent fiber by volume was reported to increase the splitting tensile strength of mortar about 2.5 times that of the unreinforced one.

2.1.2.3 Ductility of FRC

Concrete is a brittle material, and usage of steel fibers considerably increases its toughness, the energy absorption capacity, among other contributions, like more ductile behavior prior to the ultimate failure, reduced cracking, and improved durability (Fatih , Tefaruk, & Kamura, 2007).

In a research study, the effect of SFs on cracks in RC beams was investigated, and it was concluded that a SF dosage of 30–40 kg/m_3 was appropriate to have an appreciable improvement on cracks (Dupont and Vandewalle).

2.1.2.4 Durability of steel fibers

A ten-year exposure of steel fibrous mortar to outdoor weathering in an industrial atmosphere showed no adverse effect on the strength properties. Corrosion was found to be confined only to fibers actually exposed on the surface. Steel fibrous mortar continuously immerse in seawater for 10 years exhibited a 15 percent loss compared to 40 percent strength decrease of plain mortar.

2.1.2.5 Modulus of elasticity of FRC

Modulus of elasticity of FRC increases slightly with an increase in the fibers content. It was found that for each 1 percent increase in fiber content by volume there is an increase of 3 percent in the modulus of elasticity.

2.1.2.6 Shear capacity of FRC

Addition of fibers increases shear capacity of reinforced concrete beams up to 100 percent. Addition of randomly distributed fibers increases shear-friction strength, the first crack strength, and ultimate strength.

High Strength Concrete Fibers increases the ductility of high strength concrete. The use of high strength concrete and steel produces slender members. Fiber addition will help in controlling cracks and deflections.

2.1.2.7 Cracking and Deflection

Tests have shown that fiber reinforcement effectively controls cracking and deflection, in addition to strength improvement. In conventionally reinforced concrete beams, fiber addition increases stiffness, and reduces deflection

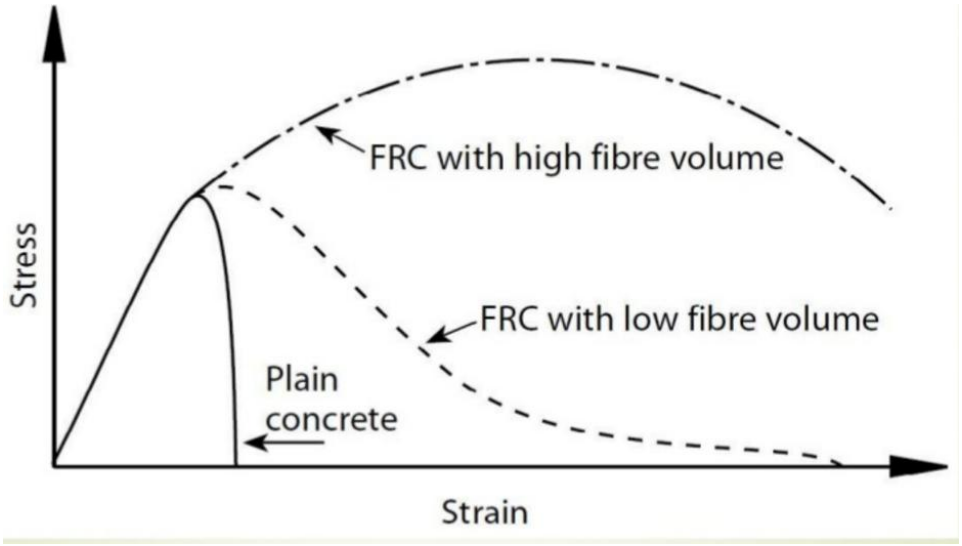

Figure 2-6:overall behavior of NC, FRC with loa and high fiber volume

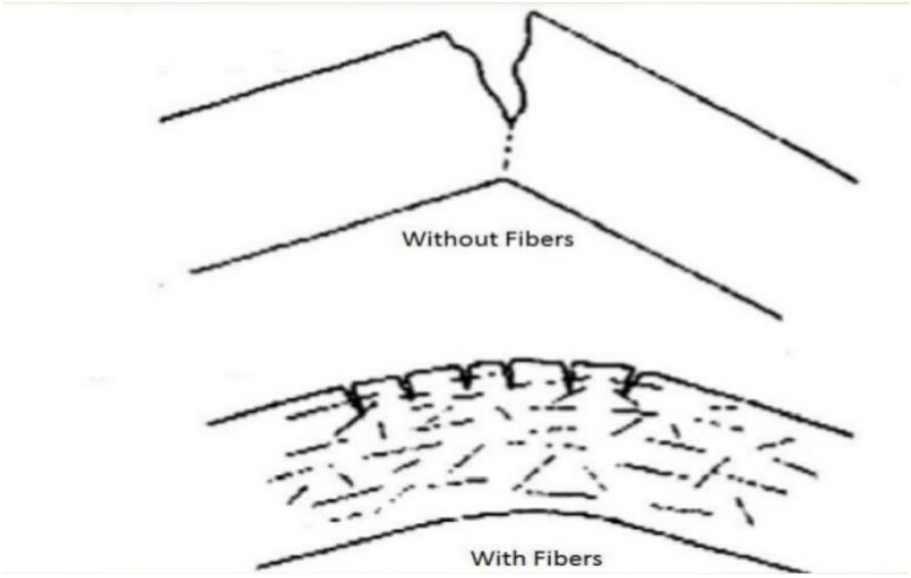

Figure 2-7: Type of cracks occur in concrete with fibers and without fibers

2.1.3 HPFRC

The development from normal strength (plain) concrete to high strength (plain) concrete with a cylinder strength of about 100 N/mm$_2$ took approximately a decade. A concrete compressive strength of 100–110 N/mm$_2$ was regarded to be a practical

maximum, since the strength of the aggregate particles does not allow a further increase of the bearing capacity of the concrete.

Fiber reinforced concrete is as well a material which has encountered limits in its development due to reasons related to its composition. In this case it was the reduced workability of concretes with increasing volumes of fibers which impeded the step to becoming a real high performance material. As a reaction on this limitation due to workability, interesting concepts were developed to increase the maximum volume of fibers and their efficiency (Joost, 2009) .

2.1.3.1 Examples of HPFRC

High-performance fiber-reinforced cement-based composites were derived starting from high-performance materials currently defined using acronyms such as:

- SIFCON (Slurry Infiltrated Fiber Concrete)
- SIMCON
- DSP (Densified with Small Particle systems)
- RPC (Reactive Powder Concrete) or BPR (Bétons de Poudres Réactives)
- BSI (Béton Spécial Industriel – Special Industrial Concrete)
- MDF (Macro-Defect-Free) cements

The main result obtained from the development of these materials is the optimum combination of strength and ductility/toughness, approaching the structural properties of steel and other common building materials (plastics, composites) Figure 2-8 (Shah, 1995).

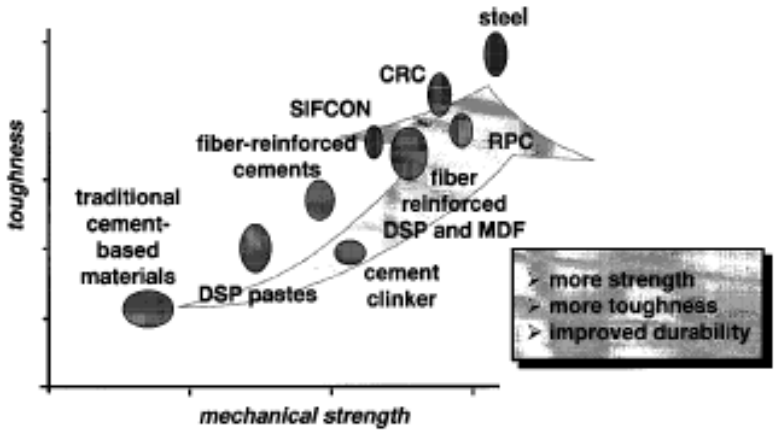

Figure 2-8 Trends of Cement-based materials

SIFCON and SIMCON are the most popular type of HPFRC, therefore it is better to have a brief introduction on them.

In the nineties the material SIFCON (Slurry Infiltrated Fibre CONcrete) was developed, the fibers of which are placed and compacted first, after which the space between them was filled with a cement-based slurry. On the other words, SIFCON is a type of fibre reinforced concrete but it is produced using a method very different from that for ordinary fibre concrete. Fibre concrete is usually produced by adding fibres into fresh concrete. All components are then mixed together and cast into a mould (Svermova & Bartos, 2002). In this way a fiber content of 12–13% volume can be reached, which is about 10 times the maximum volume obtained in conventional fiber concrete. Very large strain capacities (10–15%) and high strengths (120–140 MPa) can be achieved in this way (Naaman A. , 23 Jun 1991) (Joost, 2009) .

Another concept was SIMCON (Slurry Infiltrated Mat Concrete). To produce this concrete, a manufactured continuous mat of interlocking discontinuous steel fibers is placed in a form, subsequently infiltrated with a flowable cement-based slurry (Kristulovic, Dogan, Uang, & Haghayeghi, 1997). However, on the basis of advanced ideas with regard to the composition of fiber reinforced concrete mixtures, new types of fiber reinforced concretes with compressive strengths up to 200 N/mm^2 and fiber contents up to 2.5 vol.%(175 kg/m^3) became available (Joost, 2009).

SIFCON and SIMCON are made by pre-placing short, discontinuous steel fibers or continuous stainless steel fiber-mats (from 5 to 20% by volume), respectively, followed

by infiltrating the fibers with a cement-based slurry. SIMCON can successfully interact with existing structural elements, substantially increasing load capacity, compressive and flexural strength, energy-absorption capacity, ductility and toughness. However, to achieve the maximum benefit of SIMCON retrofit it is important to prevent delamination of the SIMCON layer. Based on the observed cracking mechanism, it can also be anticipated that the use of SIMCON would markedly improve durability of retrofitted elements (Krstulovic, Haghayeghi, & Uang, 1995).

Fiber contents in HPFRC plays significant role but it doesn't mean that by increasing to a high value, the strength improved with the same order. On the other hand, extremely high fiber contents do not increase the compressive strength by as much as might be expected. For instance, San et al (Sun, Pan, Yan, Qi, & Chen, 1999) found that SIFCON with fiber contents of up to 10% by volume had compressive strengths only in the range of about 25–50% higher than the plain concrete matrix; different fiber geometries led to quite different increases in strength. Similarly, using SIMCON, Krstulovic (Krstulovic, Haghayeghi, & Uang, 1995) found an increase of about 30% in going from a fiber volume of 2.16% to 5.39%. It may be that for these very high fiber volume materials, difficulties in achieving full compaction may lead to increased matrix porosities (Bentur & Mindess, 1990).

However, Very high fiber volumes, appear to be more effective in tension than in compression. (Krstulovic, Haghayeghi, & Uang, 1995) found about a 150% increase in the tensile strength of SIMCON on increasing the steel fiber content from 2.16% to 5.25% (Naaman & Reinhardt, 2006).

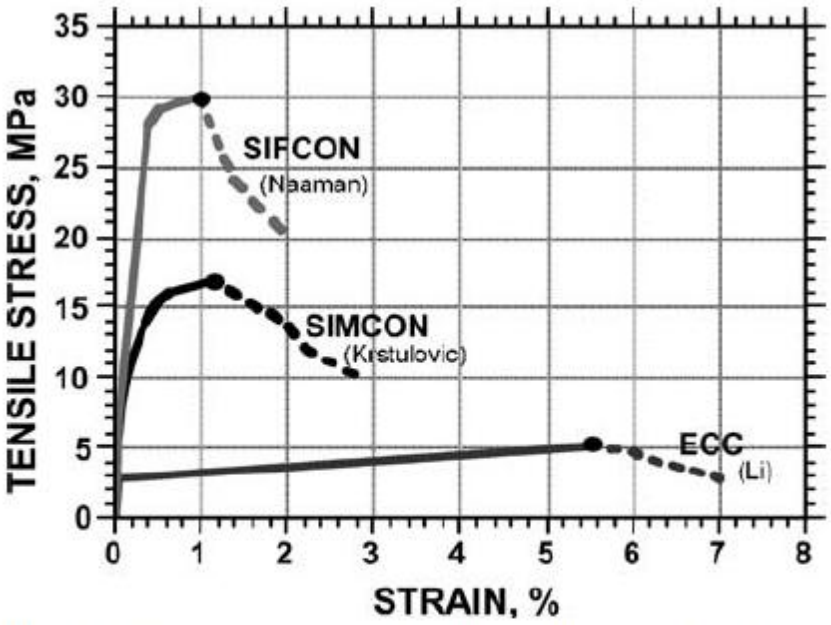

Figure 2-9 Schematic comparison of the tensile response of three different strain-hardening FRC composites illustrating the tradeoff between strength and ductility (strain is to peak point only).

Moreover, it is worth noticing that, in conventional reinforced fiber concrete the fibers are relatively large in comparison with the aggregate particles. The fibers are activated as soon as a major crack in the concrete occurs: In HPFRC the fibers are much finer: they are already activated when micro-cracks occur in the concrete (Markovic, 2006) (Joost, 2009). There are considerable differences between concretes with only one type of fiber and concretes with combinations of fibers. Figure 2-10 shows for instance that a mixture with 2 vol.% of fibers (155 kg/m$_3$) with l = 13 mm reached a flexural tensile strength of 25 N/mm$_2$ whereas a mixture with 1 vol.% short fibers (13 mm) plus 1 vol.% long fibers (40 mm) reaches a flexural tensile strength of 40 N/mm$_2$. t can as well be seen in the diagram that 1 vol.% of short fibers combined with 0.5 vol.% of long fibers (40 mm) offers the same flexural tensile strength as 2 vol.% of short fibers. This shows that by combining different types of fibers optimization of mechanical properties can be achieved (Joost, 2009). As the fiber content increased, both the maximum applied load and ultimate deflection increased also (Kwak, Elberhard, Kim, & Kim, August 2002).

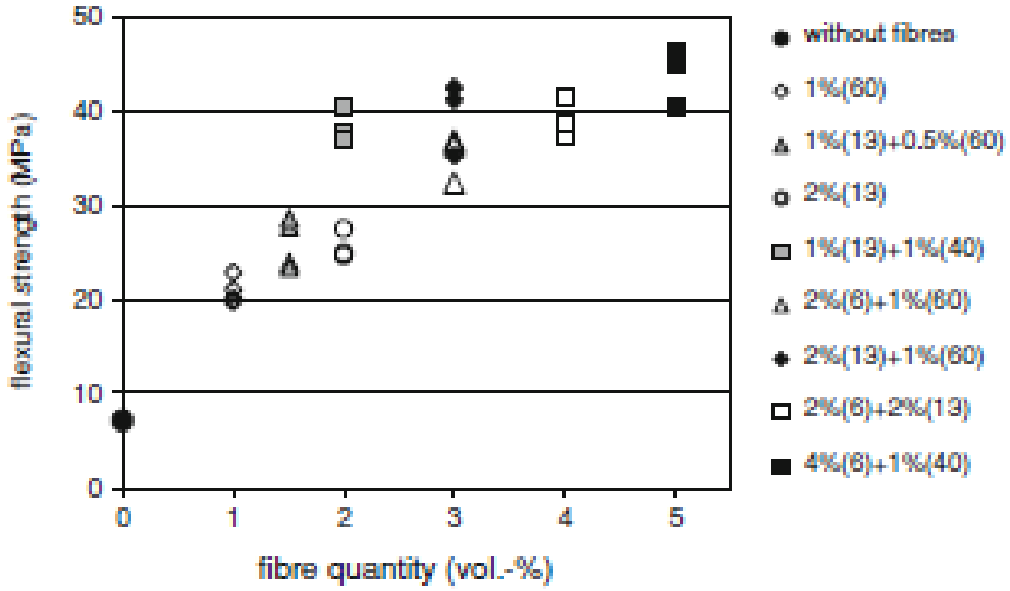

Figure 2-10: Fiber Quantity (vol,-%)

2.1.3.2 Strength of HPFRC

The addition of fibers to NSC and HPC columns increases the maximum strength. The percentage increase in peak strength at constant steel fiber volume fraction is slightly decreased with the increase in fiber aspect ratio. The percentage increase for HPC columns containing 0.75% steel fibers is about 42% and 21% for specimens with short fibers (aspect ratio 60)and long fibers(aspect ratio 100), respectively (Wasan, Ikbal, & Zeinab, 2012). It was observed that the same percentage of fibers had different effects on the behavior of NC and HPC concrete mixes.

The maximum strength capacity results for normal strength and HPC columns with and without steel fibers reinforced with different longitudinal reinforcement ratio are indicated in Table-4. It can be concluded that the peak strength of concrete columns significantly increases as the compressive strength of concrete increases. For non-fibrous HPC columns (column No. 3), the percentage increase is about 98% relative to non-fibrous NSC columns (column No.1). The percentage increase in peak stress of fiber reinforced columns over non fibrous concrete in the case of HPC is comparatively less marked compared to the NSC columns with the same fiber content and aspect ratio. The addition of 0.5% steel fibers with aspect ratio 100 to NSC (column No. 2) causes an increase in column peak strength of about 54% relative to non-fibrous NSC columns

(column No.1), while the percentage increases for HPC columns containing 0.5% steel fibers (column No.6) is about 23% in comparison with non-fibrous HPC columns (column No.3). This suggests that HPC requires more fibers to acquire the same percentage increase in strength and ductility as that provided by normal strength fibrous concrete. Thus, the same percentage of fibers had different effects on the behavior of two concrete mixes with different concrete strengths (Wasan, Ikbal, & Zeinab, 2012). It can be seen that the inclusion of steel fibers in reinforced normal strength and HPC columns increases the deformability of the specimens. It can also be observed that at the same applied stress, non-fibrous and fibrous HPC columns have lower deformability relative to non-fibrous and fibrous NSC columns (Wasan, Ikbal, & Zeinab, 2012).

The addition of fibers to HPC columns increases the maximum strength with respect to non-fibrous HPC columns specimens. The increase of steel fiber volume fraction from 0.5% to 0.75% with aspect ratio 100 causes a slight decrease in maximum strength of HPC columns. This may be due to the fact that the increase in volume fraction of fibers leads to a reduction in the compatibility of the mix, thus increasing the entrapped air, and this is followed by a decrease in strength and density (Tamim, Faisal, & Talal, 1999).

The results also demonstrate that at a constant steel fiber volume fraction, the percentage increase in peak strength decreases with the increase in the aspect ratio from 60 to 100. The percentage increase in peak strength for HPC columns containing 0.75% steel fibers is about 42% and 21% for specimens with short fibers (aspect ratio 60) and long fibers (aspect ratio 100), respectively. This is probably due to the fact that short fibers become active earlier than longer fibers to control the initiation and propagation of initial micro-cracks, as well as under the increasing loads, once the cracks become quite wide in this stage, the short fibers begin to pullout of the matrix, and their crack bridging capability is relatively diminished as compared to longer fibers. For a given volume fraction of fibers added to the matrix, the short fibers are greater in number and, therefore, much closer together. Thus, short fibers influence to a greater degree the early part of matrix cracking, thereby enhancing the strength of the composite as compared to longer fibers (Bhargava, Sharama, & Kaushik, 2006).

The addition of fibers to NSC and HPC columns increases the maximum strength. The percentage increase in peak strength at constant steel fiber volume fraction is slightly decreased with the increase in fiber aspect ratio. The percentage increase for HPC columns containing 0.75% steel fibers is about 42% and 21% for specimens with short fibers (aspect ratio 60)and long fibers(aspect ratio 100), respectively (Wasan, Ikbal, & Zeinab, 2012) At the same applied load, non-fibrous and fibrous HPC columns have lower deformability relative to non-fibrous and fibrous NSC columns; The deformability of steel fiber high performance concrete columns after concrete cracking increases as the fibers aspect ratio is increased (Wasan, Ikbal, & Zeinab, 2012).

The results of maximum cylindrical compressive strength show that in each series, slight increase in the compressive strength was observed up to 2% fiber volume; however at 3% fiber volume, compressive strength observed to be decreased from 2.37% to 15.1% (Ayub, Shafiq, & Nuruddin, 2013).

2.1.3.3 Shear effect

The addition of steel fibers to a reinforced concrete beam is known to increase its shear strength and, if sufficient fibers are added, a brittle shear failure can be suppressed in favor of more ductile behavior (Kwak, Elberhard, Kim, & Kim, August 2002) (ACI c. , 1997).

Soltanzadeh carried an experimental study on replacement of stirrups with fibers and he found that "discrete steel fibers is an interesting reinforcement, mainly for high strength concrete, since they can totally replace steel stirrups without occurring shear failure" (Soltanzadeh, Mazaheripour, Barros, & Sena, 2013).

According to Hung, one of the beneficial effects of HPFRC is that the system had 30% reduction in the shear reinforcement of the coupling beams (Hung & Tawil, December 2011). Also he stated that the 20% reduction in the flexural reinforcement in the flange and boundary zone of the wall piers, and 50% reduction in confinement reinforcement in the boundary zone is another beneficial effects of HPFRC.

As well as it is stated that “the use of steel fibers is particularly attractive for high-strength concrete, which can be relatively brittle without fibers, or if conventional stirrups can be eliminated, which reduces reinforcement congestion” (Kwak, Elberhard, Kim, & Kim, August 2002).

2.1.3.4 Failure mode

High performance fiber cementations composites are characterized by high toughness and a hardening behavior in bending. Fibers enhance the ductility of brittle materials like concrete, and this improvement is strictly related to the process by which load is transferred from the matrix to the fibers and the bridging effect of fibers across the cracks. Hence fiber pull-out is the principal mechanism contributing to the high toughness of the material and it is the preferable failure mode rather than fracture failure mechanism (Caverzan, Cadoni, & di Prisco, Dynamic tensile behaviour of high performance fibre reinforced cementitious composites after high temperature exposure, 2013) . Also the shape of fibers effect on the result of failure mechanism since the HPFRCC specimen with twisted fibers are generally sensitive to strain rate, whereas their counterparts with hooked fibers are generally not (Kim, El-Tawil, & Naaman, 2009).

An experimental study done by Ayub et al (2013) on HPFRC shows that strains corresponding to the maximum compressive strength as well as splitting tensile strengths increase with the increasing of fiber volume and this increment was significantly higher than samples without fiber, and it shows the ductile behavior of the concretes with the use of Basalt fibers (Ayub, Shafiq, & Nuruddin, 2013).

Other investigation revealed that, as the steel fiber volume increase the failure mode changed to a combination of shear and flexure. In such failures, significant diagonal shear cracks and vertical flexural cracks both formed and may have interacted to produce the failure (Kwak, Elberhard, Kim, & Kim, August 2002).

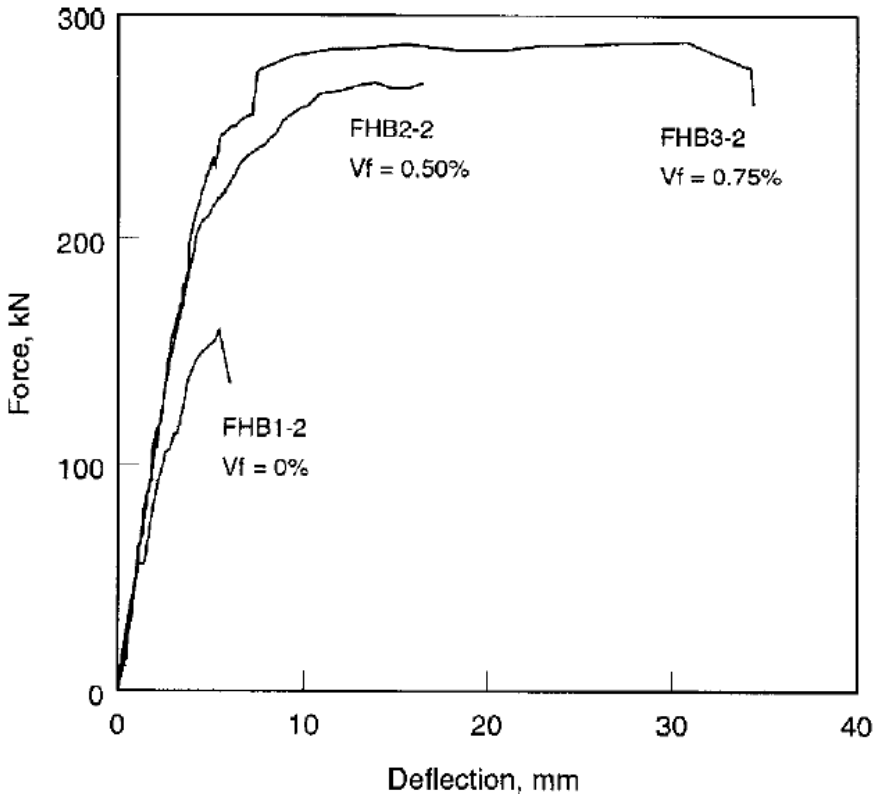

Figure 2-11: Typical force-deflection histories (Yoon,Marc,Woo 2002)

The addition of steel fibers consistently increase the strength, decreased crack spacing and sizes, increased deformation capacity and changed a brittle mode to a ductile one (Kwak, Elberhard, Kim, & Kim, August 2002).

2.2 Literature review (Concrete at elevated temperature)

Fire represents one of the most severe risks to buildings and structures. While normal concrete is typically considered to be resistant against fire and high temperatures, the low permeability of high performance fiber reinforced concrete (HPFRC) may result in failure by explosive spalling at high temperatures. Explosive spalling is the process of concrete explosively breaking away as a result of elevated temperatures. Spalling reduces the cross section area of critical sections and may expose conventional steel reinforcement to high temperatures. The use of steel and polypropylene fibers has shown to mitigate the problem of spalling at high temperatures. As Mitsuo and Hiroaki presented in their article on 2014 (Mitsuo & Hiroaki , 2014), concrete exposed to fire spalls owing to two phenomena: (1) the restrained thermal dilation of the water inside the concrete pores, which generates biaxial compressive stress parallel to the heated surface,

subsequently leading to tensile stress developing in the direction perpendicular to the heated surface Figure 2-12; and (2) the build-up of pressure in the concrete pores as a consequence of the physically/chemically bound water in the cement vaporizing, thereby loading tensile stress in the heated concrete microstructure Figure 2-13. Several studies have examined and found that some combinations of fibres increased the fire-resistance of the HPC. Adding synthetic fibres, especially polypropylene (PP) fibres, to HPC is a widely used and effective method of preventing explosive spalling. Figure 2-14 shows how spalling is reduced when PP fibres are mixed into concrete. Under normal conditions, the PP fibres mixed into concrete exist in a dispersed condition in the concrete. If the concrete surface gets heated during a fire, surface cracking occurs first. Then, as the fire continues to burn, and the temperature of the concrete rises, the free water existing within the concrete turns into vapor, forming vapor bubbles. It is thought that, in the absence of the PP fibres, the vapor pressure within these vapor bubbles results in tensile stress. If the tensile stress exceeds the tensile strength of the concrete, spalling results. However, when the PP fibres are present, they melt at 165–170 _C and form a vapor pressure dissipation network, which effectively dissipates the vapors within the concrete and prevents spalling. (Mitsuo & Hiroaki , 2014)

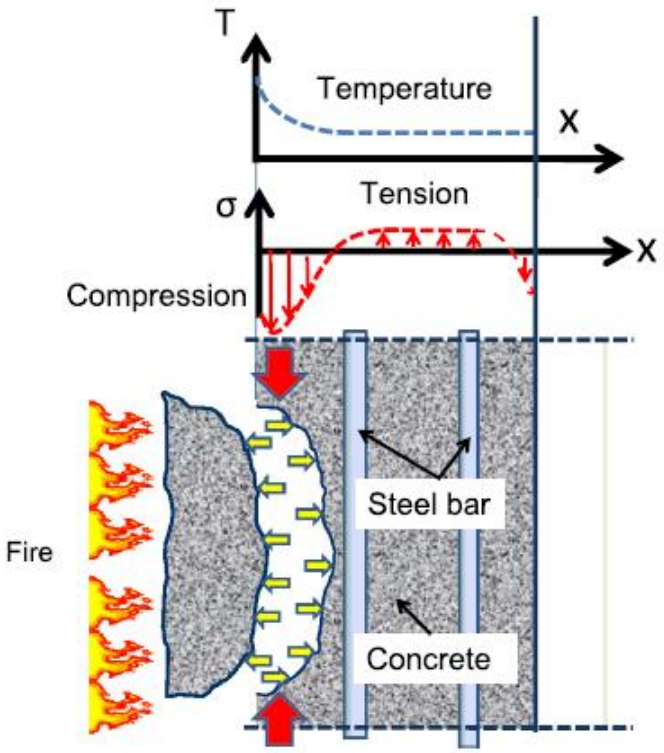

Figure 2-12:Thermal dilation, (Mitsuo and Hiroaki 2014)

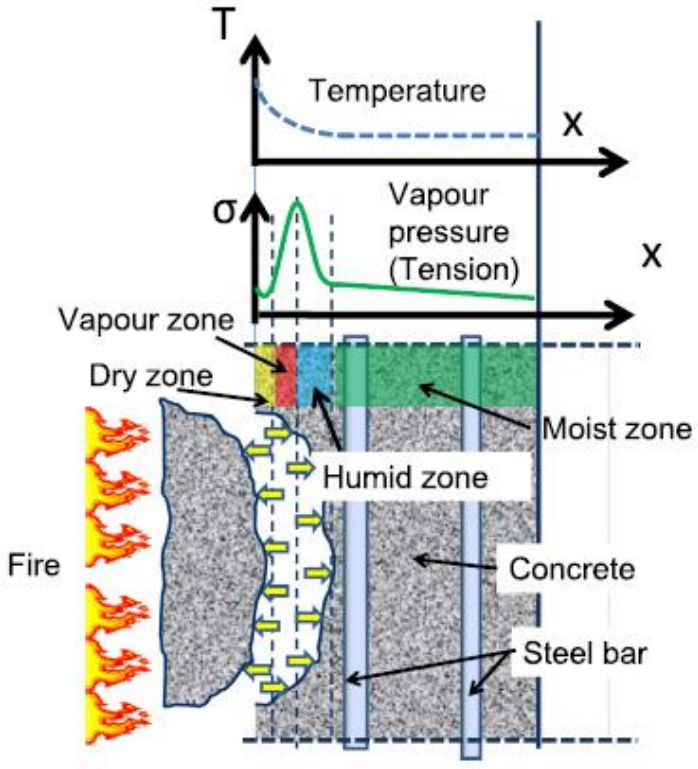

Figure 2-13: Vapor pressure (Mitsuo and Hiroaki 2014)

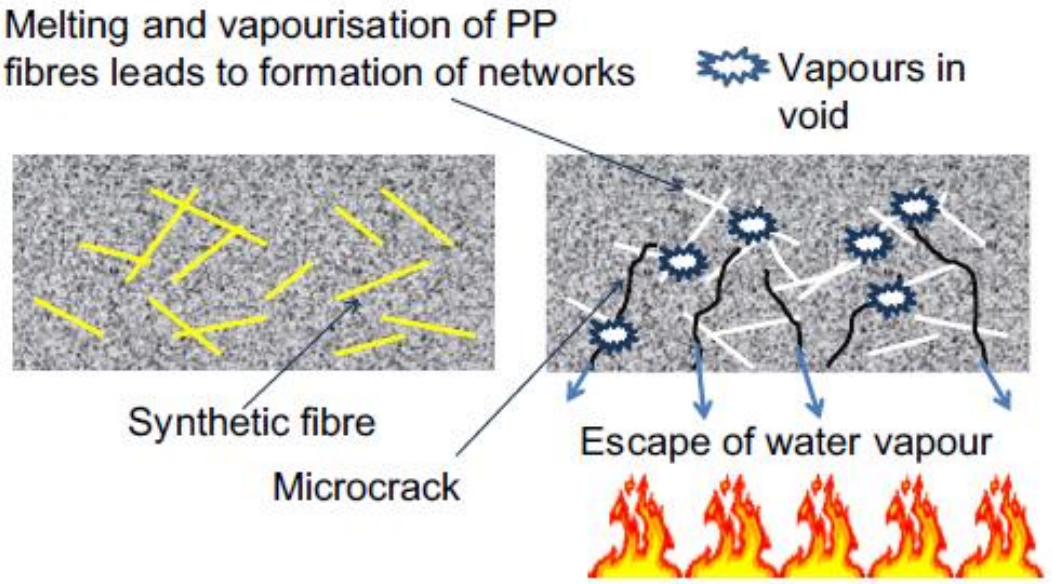

Figure 2-14: Effect of PP fibres (Mitsuo and Hiroaki 2014)

2.2.1 FRC degradation in elevated temperature

Mechanical properties of steel fibers will decrease by increasing the temperature. An experimental study has been done by Caverzan et all (2015) to investigate the mechanical degradation of fibers when exposed to high behavior of high performance cementitious composite reinforced by microfibers, when exposed to high temperatures. In order to investigate mechanical properties of the fiber at room condition and their decay after a thermal treatment, several steel wires were tested in uniaxial tension. A mix design HPFRCC was used, the mix design is specified in Table 2-4.

Constituent	Dosage (kg/m3)
Cement type I 52.5	600
Slag	500
Water	200
Super plasticizer	33 l/m3
Sand 0-2 mm	983
Fibers (lf=13mm, df=0.16mm)	100

Table 2-4: Mix design (Caverzan et all 2015)

The high fiber content and the favorable orientation imposed by the casting flow control allowed to guarantee a small dispersion of the response before and after single-crack localization and a hardening behavior in uniaxial tension . (Figure 2-15)

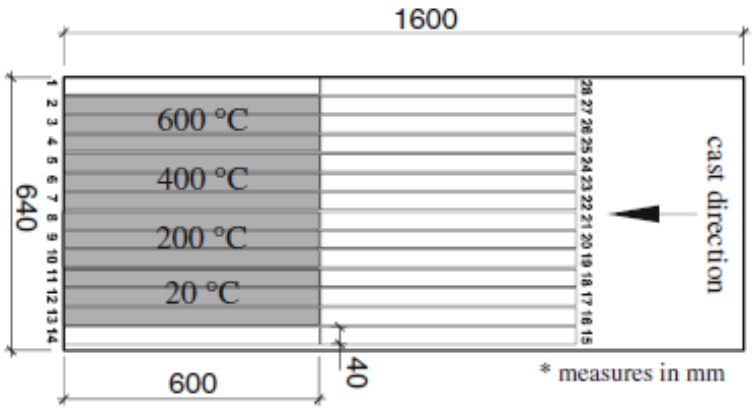

Figure 2-15: Slab cast applying a unidirectional flow (Carvezan et all 2015)

In order to investigate mechanical properties of the fibre at room condition and their decay after a thermal treatment, several steel wires were tested in uniaxial tension. Two meter long steel wire samples were cut from a skein (Figure 2-16) used to produce the fibres Uniaxial tension tests.

Figure 2-16:Skein used to produce the fibers (a) (Carvezan et all 2015)

The mechanical strength of the tested specimens are shown in Figure 2-17and Figure 2-18 for temperatures 20, 200, 400 and 600 _C, respectively; The meaning of each parameter is explained as follows:

f_{If} : First cracking strength, representing the matrix flexural tensile strength, is the maximum strength in the COD range 0–0.1 mm. Due to the hardening behavior in bending

after first cracking, the maximum value, in the investigated range, is always considered, and it is referred to as w_1;

w_1 : Conventional COD when the first crack is assumed to propagate;

f_{eq1}: Average nominal strength in COD range between $3w_l$ and $5w_l$ (0.3–0.5 mm) that is considered as a reference for Serviceability Limit State (SLS) residual strength;

f_{eq2}: Average nominal strength in COD range between $0{:}8w_u$ and $1{:}2w_u$, which is regarded as ultimate limit state (ULS), when material behavior is governed only by pull-out mechanism.

w_u: is the ultimate COD. Minimum crack opening between 0.02 lcs and 3mm.

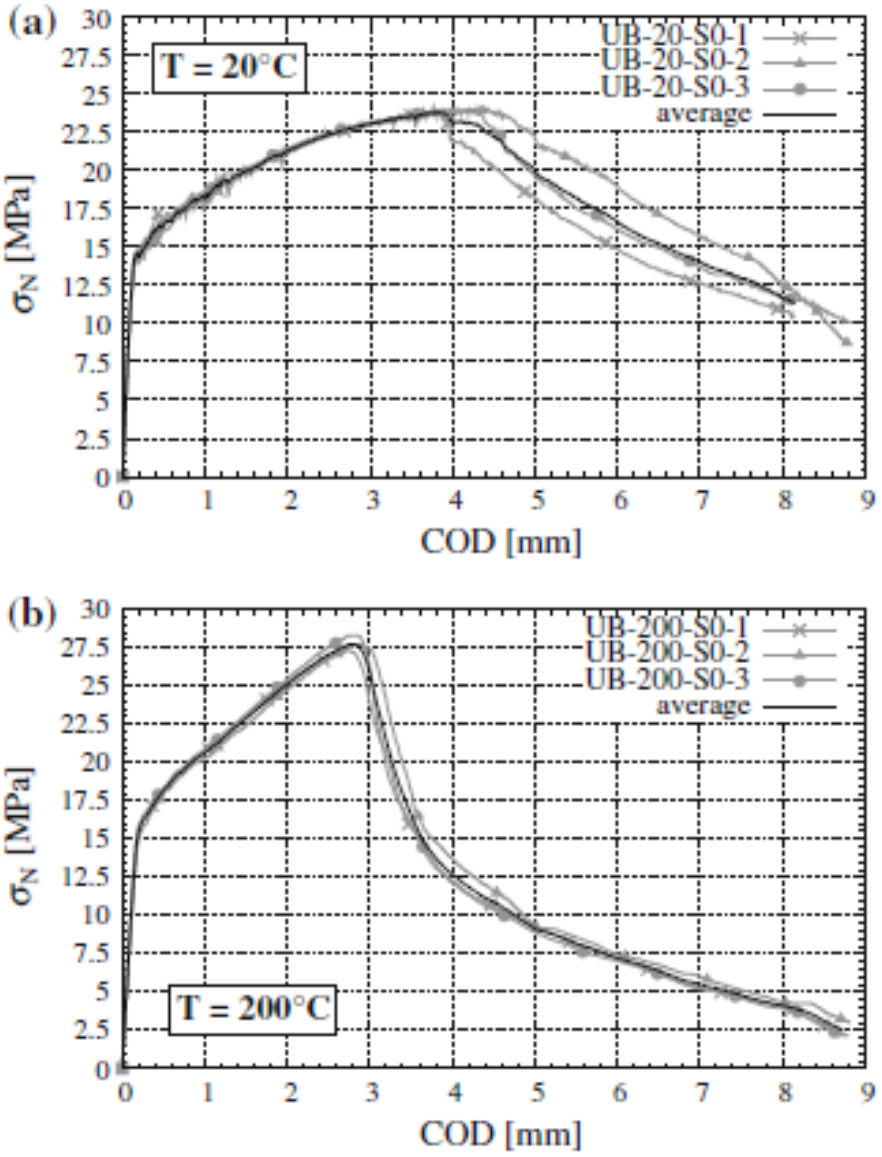

Figure 2-17: Stress versus COD curves. Tests carried out on an undamaged specimens 20C; b specimens exposed up to 200 C

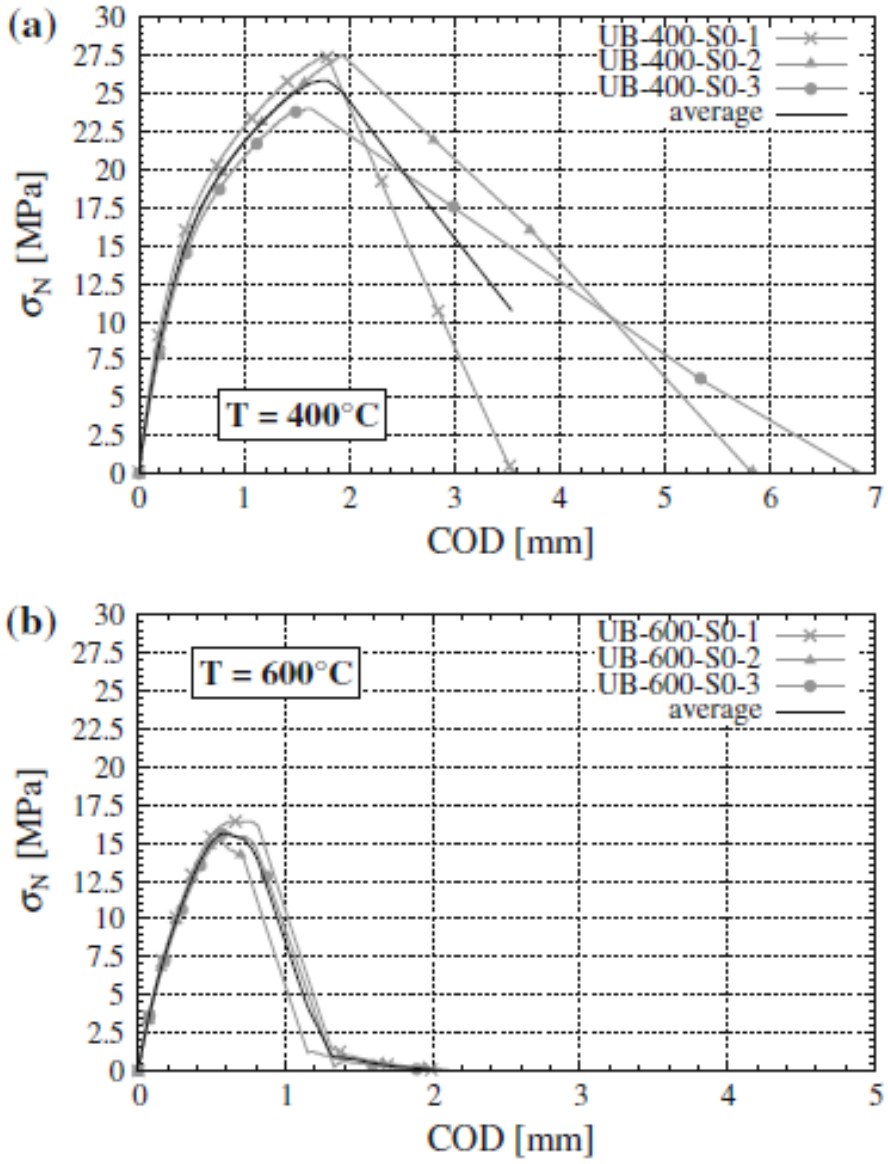

Figure 2-18: Stress versus COD curves. Tests carried out on: a specimens exposed up to 400 C; b specimens exposed up to 600 C (Carvezan et all 2015)

Finally, on the basis of the equivalent strengths, defined by taking into account the pre-peak ductility, it is possible to show that the residual equivalent strengths change with the increase in temperature (Figure 2-19) differently from steel fiber reinforced concrete characterized by a low content of fibers (0.7 %). The comparison clearly highlights the surprising performances of such materials in terms of its fire resistance behavior.

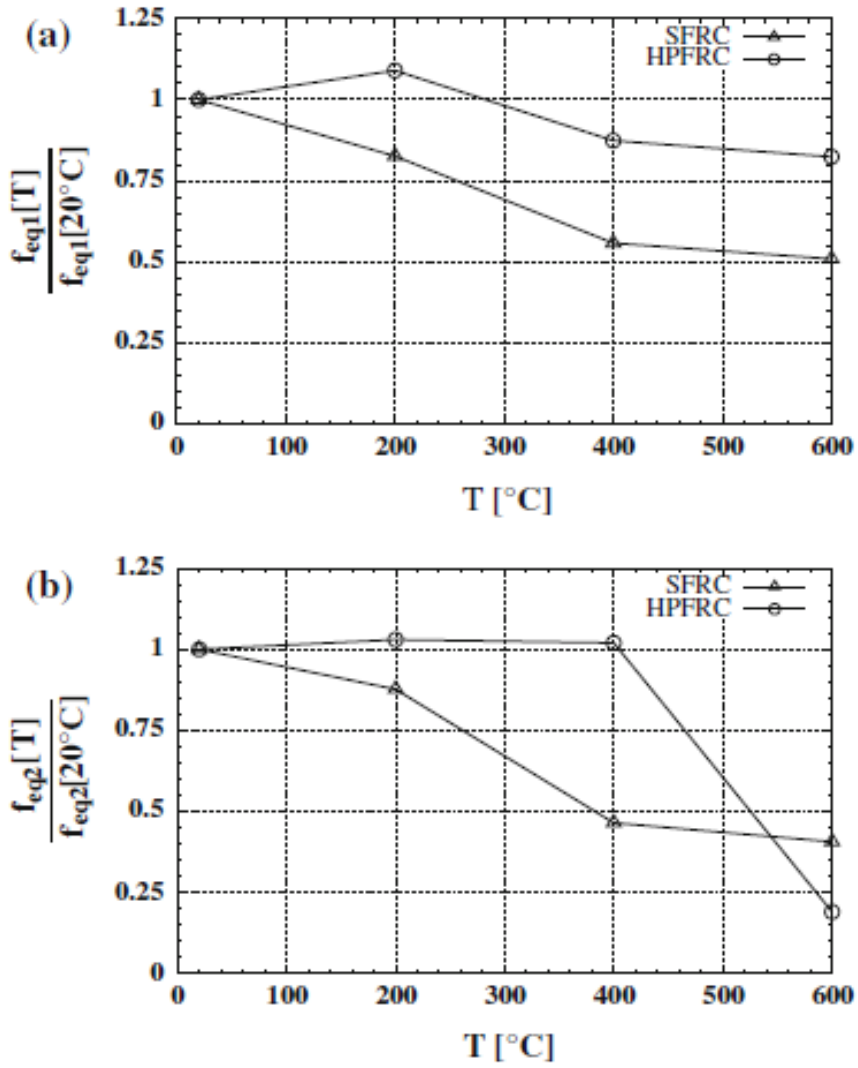

Figure 2-19: Residual strengths versus temperature for SFRC and HPFRC feq1(T)/feq1(20) versus temperature (a); feq2(T)/feq2(20) versus temperature (b)

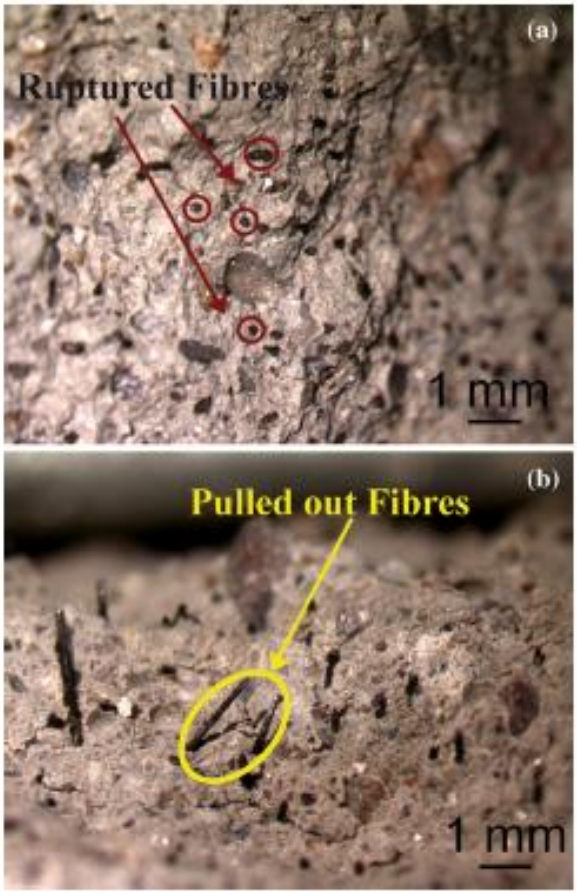

Figure 2-20: Fracture surfaces on specimen exposed to a thermal cycle up to 600 C;

fibers failed (a), Pulled out (b)

The type of fiber failure shows a significant ductility up to 400 _C and the ratio between f_{eq2} and f_{eq1} confirms the hardening in bending definition ($f_{eq2}/f_{eq1} = 1.66$). The material exposed to 600 C fails due to steel fiber rupture, this behavior being prevailingly due to the damage caused to the fibers by the high temperature. Thermal treatment up to 600 C was shown in Figure 2-20. The significant decay of the fibers mechanical properties can be ascribed to the change in the fiber microstructure and an evident reduction of the cross section. Moreover, fibers exposed to 600 C appear covered by an oxide film, which could affect the bond between the fibers and the matrix. (Caverzan, Colombo, Di Prisco, & Rivolta, 2015)

2.2.2 HPFRC degradation in elevated temperature

HPC has advantages but suffers from weakness of higher brittleness. When exposed to high temperature HPC exhibits more serious degradation that normal concretes do, such as spalling and cracking. Fibers have been used to improve the ductility of concrete. It has been found that a number of fibers can also improve the residual properties of concrete after exposure to elevated temperatures. (Poon, Shui, & Lam, Compressive behavior of fiber reinforced high performance concrete subjected to elevated temperatures, 2004)

The presence of steel fibers increases the tensile strength of concrete, at high temperatures, and thus reduces spalling and enhances fire resistance. Also, the increased deformation capacity from the addition of steel fibers contributes to minimizing spalling. The type of load and its intensity have significant influence on spalling and the resulting fire resistance. The fire intensity, fire size and heat output, and rate of heating influence the degree of spalling and fire endurance duration. The main parameters that influence fire performance of high performance concrete are: concrete strength, silica fume, concrete moisture content, concrete density, fiber reinforcement, and type of aggregate. (Kodur & Phan, 2007)

An experimental investigation was conducted on behavior of high performance steel-fiber concrete subjected to high temperature, in terms of explosive spalling and permeability. A series of concretes incorporated steel fiber at various dosages were prepared. Explosive spalling tests were conducted on control plain concrete and steel fiber concrete. The results prove that steel fibers efficient to avoid spalling concrete under high temperature. The permeability increases significantly after thermal exposure. Therefore it is concluded that steel fiber can play a positive effect on explosive spalling of high performance concrete under high temperature, as well as on permeability after thermal exposure. (Peng, Duan, Yang, & Hao, 2014)

2.2.2.1 Compressive and flexural strength

The compressive strength results of a series of experimental tests performed by (Lau & Anson, Effect of high temperatures on high performance steel fibre reinforced concrete, 2006)for heated specimens are shown in Figure 2-21 It can be observed that the reduction in strength is noticeable, but not disastrous, if concrete is not heated above 400 °C. However, the reduction in strength is considerable between 400 and 800 °C but even then remains useful at around the 30 MPa mark for HPC. At 1000 °C maximum temperature all mixes have negligible strengths of between 4 MPa and 12 MPa, and at 1200 °C, between 6 MPa and 19 MPa. For all three mixes, the addition of fibres gives small increases of about 5% to 15% regardless of mix and regardless of maximum temperature of heating. Thus, the addition of fibres to concrete is of some compressive strength benefit. Increased saturation percentage decreases strength for all mixes and this remains the case regardless of the maximum temperature of heating. Fully saturated concretes are 5 to 12 MPa weaker than concrete 20% saturated.

Figure 2-22 shows that for all values of maximum temperature, steel fibre reinforced concretes have better flexural strength than concretes without steel fibres, although there is no significant difference in flexural strength between SFRC and the non-fibre mixes after exposure to a temperature of 1000 °C. The reduction in flexural strength occurs progressively from 105 °C up to about 1000 or 1100 °C. For concrete exposed to a maximum heating temperature of 1100 °C, it is observed that in some cases, the residual flexural strength is a little greater than that for concrete exposed to 1000 °C.

Concrete mixes	Initial saturation levels (%)	Maximum heating temperatures (°C)									
		25	105	200	300	400	600	800	1000	1100	1200
M-1	20	–	40	38	36	32	24	14	6	5	11
	60	–	37	35	34	30	21	12	6	5	10
	100	39	35	32	30	28	18	10	4	4	6
M-2	20	–	50	46	39	36	34	17	8	8	15
	60	–	47	39	38	33	29	16	8	7	15
	100	53	45	36	34	32	22	13	6	6	10
M-3	20	–	101	99	96	94	56	33	12	11	19
	60	–	98	97	93	87	56	30	12	11	18
	100	99	96	95	90	85	50	26	8	19	15
M-1F	20	–	46	42	38	35	32	16	8	7	14
	60	–	42	38	36	32	24	14	7	6	13
	100	45	41	34	32	30	20	12	5	5	8
M-2F	20	–	60	58	54	50	37	19	8	9	18
	60	–	53	50	47	44	36	18	8	8	17
	100	60	50	48	45	40	33	17	6	8	14
M-3F	20	–	112	106	102	100	69	37	14	12	19
	60	–	107	104	96	94	69	33	14	11	19
	100	110	100	97	94	90	65	28	12	10	17

Figure 2-21: Compressive strength after heating (Mpa) (Lau, 2004)

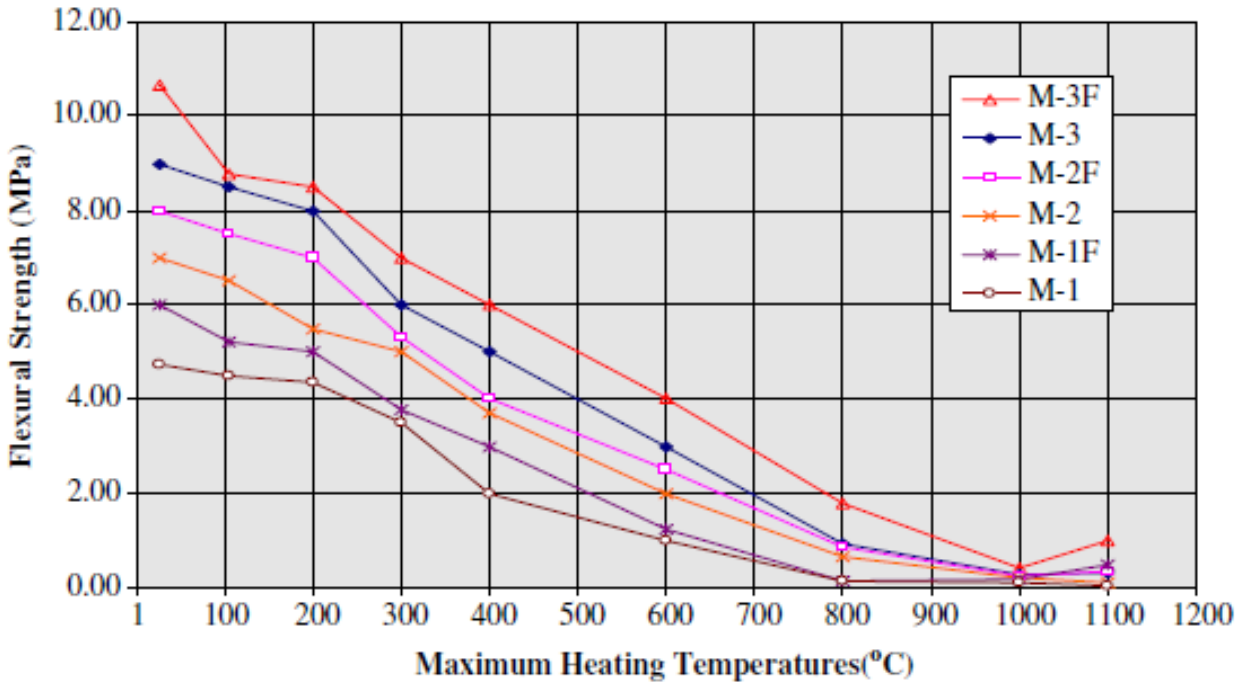

Figure 2-22: Flexural strength VS maximum heating temperature (Lau, 2004)

Another experimental tests was performed by Poon et al(2004) on HPFRC and the results shows in Figure 2-23 that the compressive strength obtained from the cylinder tests is, on average, 0.83 times of that obtained from the cube tests. Replacement of cement by MK resulted in an increase of 20% to 25% in the compressive strength, while a 10% replacement of cement by steel fibers increased the strength by 15 to 20%. Comparing with the use of steel fibers at the level of 1%, which resulted in a small increase in the compressive strength, the use of 0.11% or 0.22% PP fibers had negative effects on the compressive strength. Similar results had been reported by other researchers such as (Qian & Stroeven, 2000).

Mix	Addition of fibers	Cube tests		Cylinder tests			
		Apparent density (kg/m^3)	Compressive strength (MPa)	Compressive strength (MPa)	Strain at cylinder peak stress (%)	Area under stress–strain curve (MPa × 10^{-2})	Specific toughness (%)
PC-0	No	2409	84.3	69.1	0.374	34.20	0.495
PC-1	1% steel	2442	86.6	71.4	0.410	66.41	0.930
PC-2	0.22% PP	2384	83.4	68.5	0.360	36.8	0.537
PC-3	1% steel + 0.22% PP	2411	83.9	69.6	0.433	62.43	0.897
MK-0	No	2382	105.1	86.1	0.397	35.97	0.418
MK-1	1% steel	2426	109.5	87.5	0.420	75.49	0.863
MK-2	0.11% PP	2370	105.4	86.1	0.397	37.64	0.437
MK-3	0.22% PP	2365	98.4	84.6	0.391	39.76	0.470
MK-4	1% steel + 0.22% PP	2409	100.3	86.0	0.402	73.35	0.853
SF-0	No	2395	97.3	82.8	0.388	35.83	0.433
SF-1	1% steel	2433	99.9	83.7	0.390	64.53	0.771
SF-2	0.11% PP	2384	96.7	81.8	0.371	39.46	0.482
SF-3	0.22% PP	2374	95.8	81.2	0.368	42.28	0.521
SF-4	1% steel + 0.22% PP	2415	97.6	82.9	0.391	71.19	0.859

Figure 2-23: Compressive strength (poon et al 2004)

Figure 2-24 shows the effect of temperature on the residual compressive strength of the HPCs, where the compressive strengths were given as relative values, with reference to the compressive strength of the unheated concrete mixes. Figure 2-24a shows that for the PC concrete prepared without any fibers, the relationship between the residual compressive strength and exposure temperature can be approximated by the dash line, assuming that the compressive strength maintains constant up to 200 jC and then drops linearly with increasing temperatures. This dash line is also shown in Figure 2-24b and c as a reference to compare the performance of the MK and SF series mixes. Clearly, the use of MK and SF resulted in a quicker loss of compressive strength, although they increased the compressive strength of the unheated concrete. The use of steel fibers slightly reduced the rate of degradation of compressive strength. (Poon, Shui,

& Lam, Compressive behavior of fiber reinforced high-performance concrete subjected to elevated temperature, 2004)

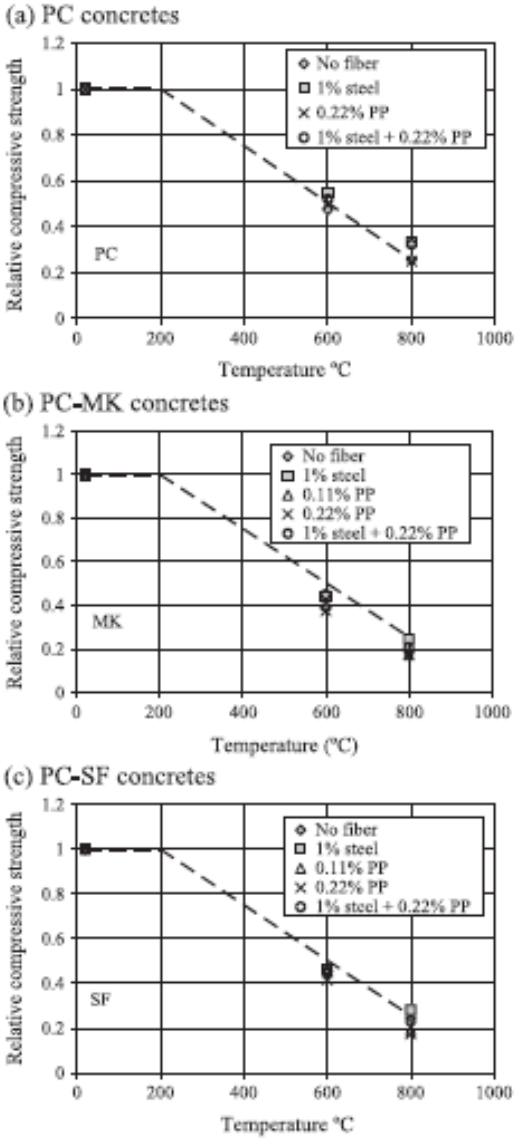

Figure 2-24: effect of temp. on compressive strength (Poon 2004)

2.2.2.2 Modulus of elasticity and Poisson's ratio

According to Lau(2006), Figure 2-25 illustrates the effects of different heating temperatures on the modulus of elasticity. It can be seen from the results that the loss in modulus of elasticity, for concrete mixes increased significantly. Concrete mixes reinforced with steel fibres consistently show higher values of modulus of elasticity than non-fibre mixes. It can be seen from the results that the loss in modulus of elasticity,

Concrete mixes reinforced with steel fibres consistently show higher values of modulus of elasticity than non-fibre mixes.

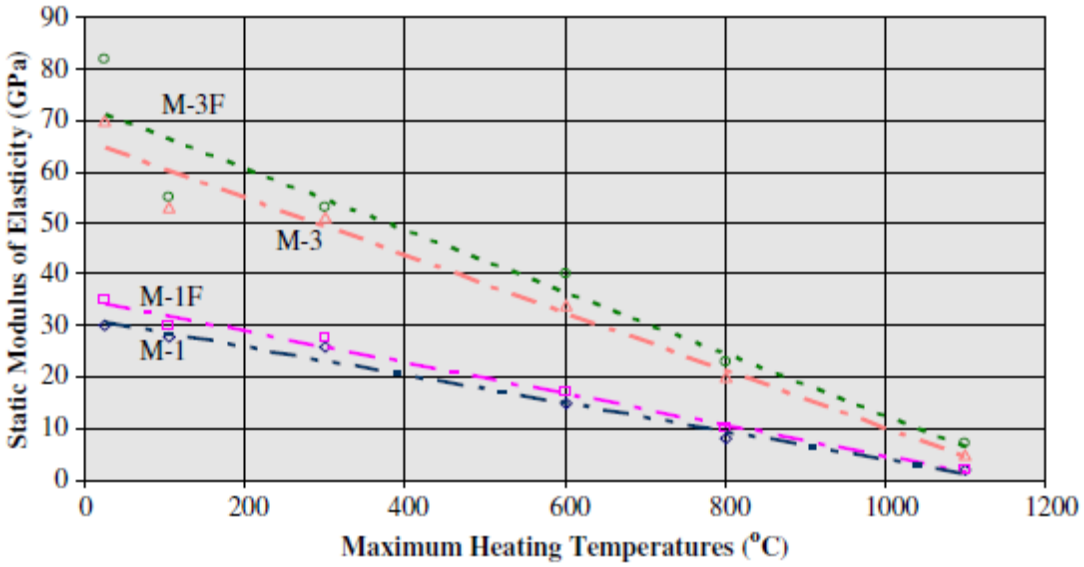

Figure 2-25:Elastic modulus VS. temperatures (Lau, 2006)

According to other tests, it was observed that the use of steel fibers slightly reduced the rate of degradation of compressive strength. The decrease in elastic modulus with increasing temperature. The results show that the degradation of elastic modulus is much quicker than that of compressive strength. Only 18% of the elastic modulus original sample was retained, on average, after the concretes were exposed to 600 jC. This was further decreased to 11% after exposure to 800 jC.

Wu et al. observed that for high-strength concrete prepared without any fibers, the elastic modulus dropped quickly from 200 to 600 jC, but the decrease was more gradual from 100 to 200 jC and from 600 to 900 jC. The slower drop of elastic modulus after heating to 600 jC was also observed in this study for both the concretes prepared with and without the use of fibers the mixes with 1% steel fibers seemed to preserve the elastic modulus to a higher percentage than those concretes prepared with the PP fibers or a combination of the PP and steel fibers.

Since Poisson's ratio is related to modulus of elasticity, the Poisson's ratio for concrete cylinders heated at different temperatures up to 1100 °C is also determined. It indicates that Poisson's ratio reduces after high temperature exposure Figure 2-26. (Lau & Anson, Effect of high temperatures on high performance steel fibre reinforced concrete, 2006)

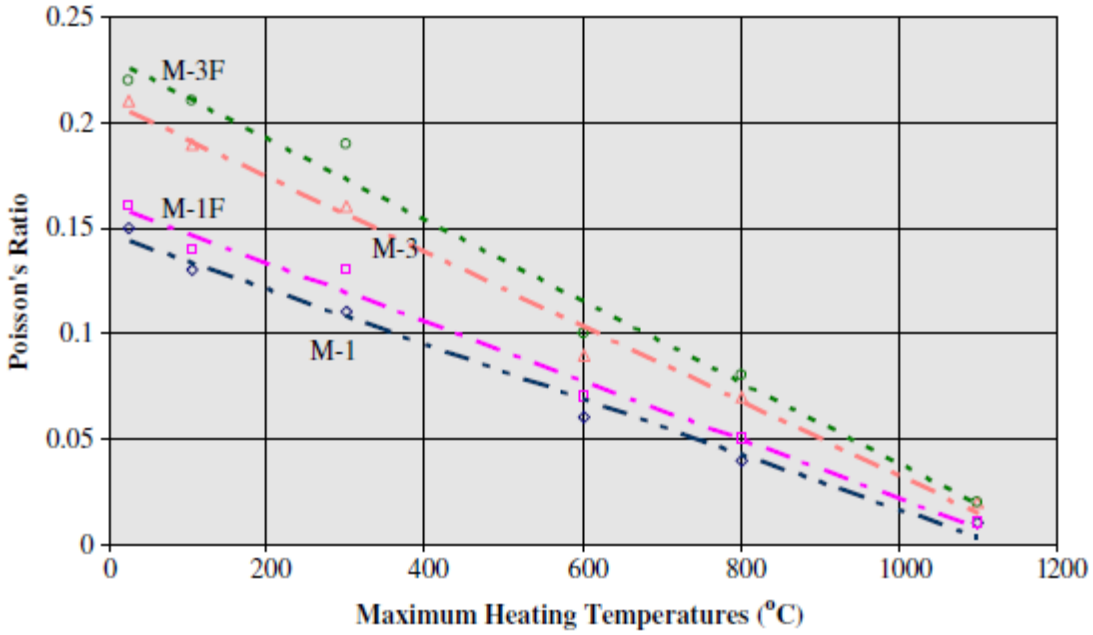

Figure 2-26: Poisson's ratio vs temperature (Lau, 2006)

2.2.2.3 Fracture Energy

According to an experimental test performed by Felicetti et al, The fracture energy (which was measured only in the residual tests), CRC exhibits a strong increase up to 250–300 °C, followed by a steep decrease. In contrast, the lower fracture energy of RPC is hardly affected by the temperature and the extremely reduced fracture energy of HSC (one order of magnitude) is scantly affected by the temperature. (Felicetti, Gambarova, Natali Sora, & Khoury, 2000) These different fracture energy trends point out the role played by steel fibres and suggest a change in the mechanical properties of the fibres and/or the matrix surrounding them with temperature growth as observed by Biolzi et al. (2004) In particular, the steel microfibers became weak and brittle and specimens showed a response not influenced by fibers. No fiber pullout was detected in the specimens treated at highest temperature. When the maximum temperature reached was

equal to 750°C, a fiber partial melting occurred and the internal core of fibers was clearly different from the external portion in terms of both morphology and composition. The steel fibers partially melted tended to fill the cracks formed in the concrete.

By increasing the maximum temperature exposure, pull-out energy decreases while the energy associated to the failure of fibres increases, this being justified by the change in the ratio of G pull out/G failure. We can say at last the specimens exposed up to 600 _C have a brittle behavior associated with fibre failure.

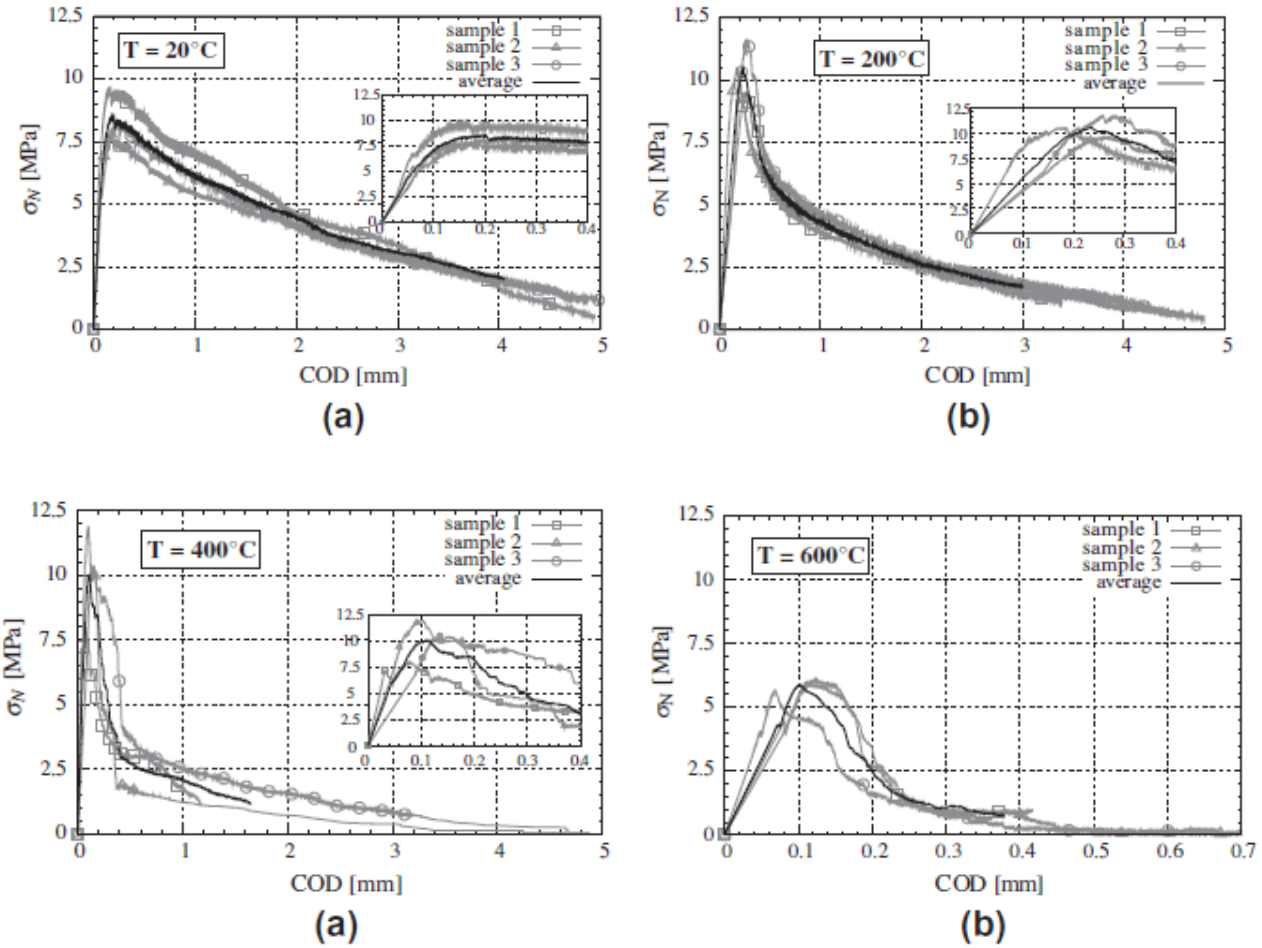

Figure 2-27: COD vs Stress in T=20, 200, 400 and 600 C (Felliceti et al 2000)

The total energy Gf shows a significant decay starting from 200 _C as exhibited it can be observed that the fracture energies computed from the average curves up to 0.1 mm and at the peak strength are less affected by the thermal damage with respect to the total one as reported for the tests at medium strain rate.

3 Heat Transfer

3.1 What is Heat and Temperature?

All matter is made up of molecules and atoms which are always in different types of motion. The motion can be translating, rotating or vibrating which creates thermal energy. Therefore all matters have thermal energy and the level of motion defines heat of a matter. The more motion the atoms or molecules have the more heat they will have.

All movement of atoms and molecules are not similar to each other, some move faster than others. Temperature is a definition to cope with this variety and unified it in theory. Temperature is an average value of energy for all the atoms and molecules in a given system and it is independent of how much matter there is in the system. It is simply an average of the energy in the system.

3.2 How is heat transferred?

If there is a temperature difference between two systems, heat will always find a way to transfer from the higher to lower system in order to fulfill balance between two systems.

Heat transfer takes place in three ways. Conduction, Convection and Radiation. Both conduction and convection require matter to transfer heat.

3.2.1 CONDUCTION

Conduction takes place in matter. Conduction is one way to transfer heat between substances that are in direct contact with each other. It is transmission of kinetic energy among the molecules without matter transport. It is possible to classify matters according to the rate of heat transfer by conduction and define matters to be a good conductor or

less conductor. The better the conductor, the faster heat will be transferred. For example metal is defined as a good conductor because heat transfer faster.

Conduction occurs when a substance is heated, particles will gain more energy, and vibrate more. These molecules then bump into nearby particles and transfer some of their energy to them. This then continues and passes the energy from the hot end (more energetic particles) down to the colder end (less energetic particles) of the substance due to energy gradient. Conduction takes place in solids, liquids and gases. Fourier found an empirical relation for this type of heat transmission.

Fourier's law is a law based on observation. It states that the rate of heat flow $\frac{dQ}{dt}$, through a homogeneous solid is directly proportional to the area, A, of the section at right angles to the direction of heat flow, and to the temperature difference along the path of heat flow, $\frac{dT}{dx}$.

$$\frac{dQ}{dt} = -\lambda A \frac{dT}{dx}$$

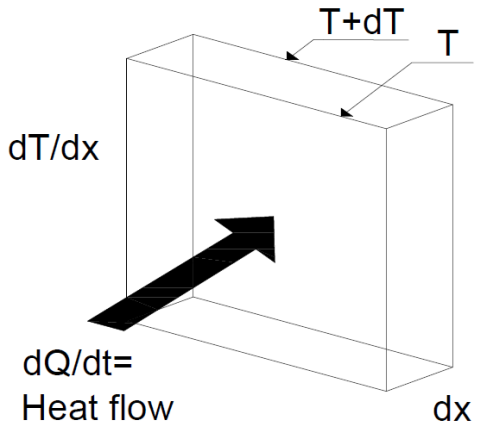

Figure 3-1 Conduction

Heat flow in a unit of time over length of L is therefore:

$$Q = \lambda A(T_1 - T_2)/L$$

$Q = Heat\ Flow\ (W)$

$\lambda = Theram\ Conductiviy\ (\frac{W}{mc})$

Thermal conductivity of a substance is defined as the heat flow per unit area per unit time when the temperature decreases by one degree in unit distances. The SI unit of thermal conductivity is $\frac{W}{mC}$.

3.2.2 CONVECTION

One other way for heat transmission is Convection. Thermal energy can be transferred from hot places to cold places in fluids or gases due to bulk or macroscopic motion. Convection occurs when warmer areas of a liquid or gas rise to cooler areas in the liquid or gas. Cooler liquid or gas then takes the place of the warmer areas which have risen higher. This results in a continuous circulation pattern. Water boiling in a pan is a good example of these convection currents. Another good example of convection is in the atmosphere. The earth's surface is warmed by the sun, the warm air rises and cool air moves in.

The heat transfer from the solid surface to the fluid can be described by Newton's law of cooling[1]. This empirical law states that the heat transfer ($\frac{dQ}{dt}$) from a solid surface of area A, at a temperature$t_{surface}$, to a fluid of temperaturet_{Fluid}, is:

$$\frac{dQ}{dt} = \alpha_c A\left(t_{surface} - t_{Fluid}\right)$$

$$considering\ a\ unit\ time; \quad Q = \alpha_c A(t_{surface} - t_{Fluid})$$

[1] At contact surfaces between a fluid and a solid wall, there is always a thin layer of fluid through which the heat is transferred by conduction. Whenever there is an appreciable movement of the fluid, conduction heat transfer in fluid may be neglected compared with convection heat transfer.

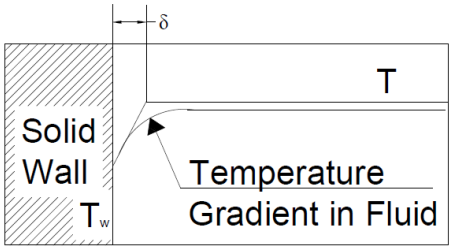

Figure 3-2: Convection

Where

$Q = heat\ flow\ (W)$

α_c is the heat transfer coefficient or thermal convection coefficient. $\left(\frac{W}{m^2 C}\right)$

Matter	α_c $\frac{W}{m^2 C}$
Air – natural convection	1-20
Water- natural convection	250-750
Still air (sides not exposed to fire)	4
Still air (sides not exposed to fire) Including radiation in linearized form	9
Air in turbulent regime (sides exposed to fire) ISO 834 and external nominal fires	25
Air in turbulent regime (sides exposed to fire) hydrocarbon nominal fire	50
Air in turbulent regime (sides exposed to fire) parametric fire and zone models	35

Table 3-1: Typical values of α_c

3.2.3 RADIATION

Radiation is a method of heat transfer that does not rely upon any contact between the heat source and the heated object as is the case with conduction and convection. Heat can be transmitted through empty space by thermal radiation often called infrared radiation. Energy emitted by matter due to changes in electron configuration that results in changes in energy via electromagnetic waves or photons. No mass is exchanged and no medium is required for its propagation. Radiation is propagation of electro-magnetic waves in vacuum or in transparent matters. Examples of radiation is the heat from the sun, or heat released from the filament of a light bul.

Heat transfer by radiation occur between solid surfaces, although radiation from gases is also possible. Solids radiate over a wide range of wavelengths, while some gases emit and absorb radiation on certain wavelengths only.

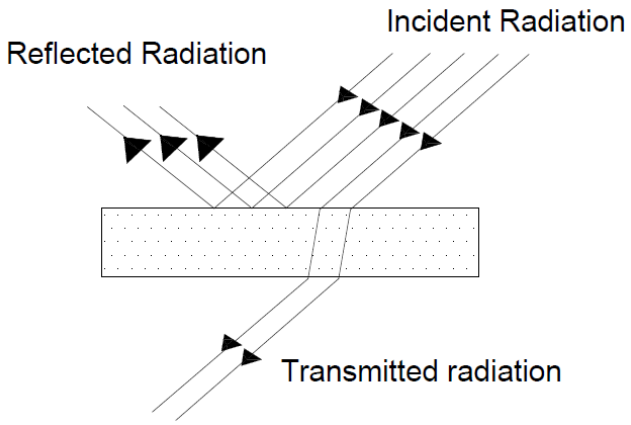

Figure 3-3: Radiation

When thermal radiation strikes a body, it can be absorbed by the body, reflected from the body, or transmitted through the body (Figure 3-3). The fraction of the incident radiation which is absorbed by the body is called absorptivity (α). Other fractions of incident radiation which are reflected and transmitted are called reflectivity (ρ), and transmissivity (τ). The sum of these fractions should be unity.

$$\alpha + \rho + \tau = 1$$

Therefore there is no reflection from a black body[2]. Applying the Kirchoff's law[3] to a black body results in that it should have an emissivity of unity. $\varepsilon = 1$

Emissivity (ε) is a property of the body surface and is dependent on the temperature of the body and the wavelength of the emitted radiation. It is dimensionless value.

[2] Black body by definition is an object that absorbs all radiation falling on it or in other words it has an absorptivity equal to unity (α=1) .

[3] Kirchoff's law states that the absorptivity and emissivity of a grey body are equal at any given temperature.

This means that a good absorber of radiation is also a good emitter of radiation. There are no totally black bodies in practice, but many surfaces approximate to the definition[4].

Empirical relation for radiation is Stefan-Boltzmann law. The Stefan-Boltzmann law states that the emissive power, P, from a black body is directly proportional to the forth power of its absolute temperature.

$$P = \sigma T^4$$

Where

$P=$ Emissive power is defined as the energy radiated from a body per unit area per unit time. [5]

σ is the Stefan-Boltzmann constant. $(\sigma = 5.67E-08\ \frac{W}{m^2c^4})$

$$q = \mathrm{PA} = \sigma T^4 A$$

$q = global\ thermal\ flux\ of\ the\ black\ body\ towards\ vacuum\ (W)\ in\ area\ A$

$$q = \sigma_n A(T_1^4 - T_2^4)/(\frac{1}{\varepsilon_1} + \frac{1}{\varepsilon_2} - 1)$$

Under the assumption of unit view factor $(\phi = 1)$

Where

ε_i is the surface emissivity.

T_{i} is the surface temperature

On the other hand;

[4] Grey body is defined as a body with constant emissivity over all wavelengths and temperatures. Such an ideal body does not exist in practice but the assumption is good approximation for many objects used in engineering.

[5] The emitted power, P, for a non-black body depends also on its emissivity ε (P= $\varepsilon\sigma T^4$).

$$q = \sigma_n A(T_1^4 - T_2^4)\varepsilon_{res}$$

$$\varepsilon_{res} = resultant\ emissivity\ (0.56\ in\ the\ italian\ code\ INI9502)$$

$$\varepsilon_{res} = \phi.\varepsilon_{member}.\varepsilon_{fire} = 1.0\ .\ 0.8\ .\ 1.0\ \ (EN\ 1991-1-2)$$

According to Eurocode1991-1-2; In general $\varepsilon_{fire} = 1$ is assumed, which makes the rigorous formula for the resultant emissivity much simpler.

$$q = \sigma_n A(T_1^4 - T_2^4)/(\frac{1}{\varepsilon_{res}} + \frac{1}{\varepsilon_{fire}} - 1) = \sigma_n A(T_1^4 - T_2^4)/(\frac{1}{\varepsilon_{res}} + 0) = \varepsilon_{res}\sigma_n A(T_1^4 - T_2^4)$$

Where

ϕ is the configuration factor, accounting for the visibility of the flames.

ε_{member} For some material is given in Table 3-2.

Member	ε_{member}
Generic	0.8
Concrete	0.7
Carbon steel	0.7
Stainless steel	0.4

Table 3-2: Typical values for ε_{member}

3.3 FOURIER EQUATION

Fourier's law defines heat conduction in continuous medium as follows;

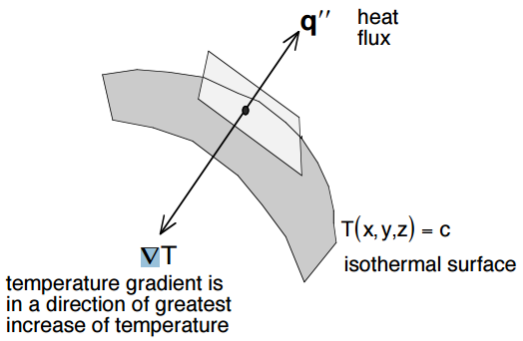

Figure 3-4 Fourier equation for heat flux

$$q'' \cong -\lambda \nabla \mathrm{T}$$

Where

q'' is heat flux

λ is coefficient of thermal conductivity

∇T is temperature gradient

Heat Equation

$$\rho c \frac{\partial T}{\partial t} = \nabla . (\lambda \nabla T) + q$$

To simplify the equation two hypotheses are presented;

Hyp. 1: constant conductivity

$$\rho c \frac{\partial T}{\partial t} = \lambda \nabla (\nabla T) + q$$

Therefore;

$$\frac{\partial T}{\partial t} \cong \frac{\lambda}{\rho c} (\nabla^2 T) + \frac{q}{\rho c}$$

In equation above, term of $\frac{\lambda}{\rho c}$ is called thermal diffusivity (m^2 /s)

Hyp. 2: No internal sources

$$\frac{\partial T}{\partial t} \cong \frac{\lambda}{\rho c} (\nabla^2 T)$$

(Equation 1)

$\frac{\lambda}{\rho c}$ is called diffusivity and in order to know the rate of heat flow in a substance it is necessary to know the conductivity, specific heat and density of the substance. These parameters are called thermal properties of materials.

The temperature field in a construction is controlled by Fourier's differential equation for heat balance as follows:

3.3.1 Coordinate system

The various distances and angles involved when describing the location of a point in different coordinate systems (Figure 3-5). Since in this study, rectangular coordinates has been chosen, only the final Fourier equation for rectangular coordinates will be discussed.

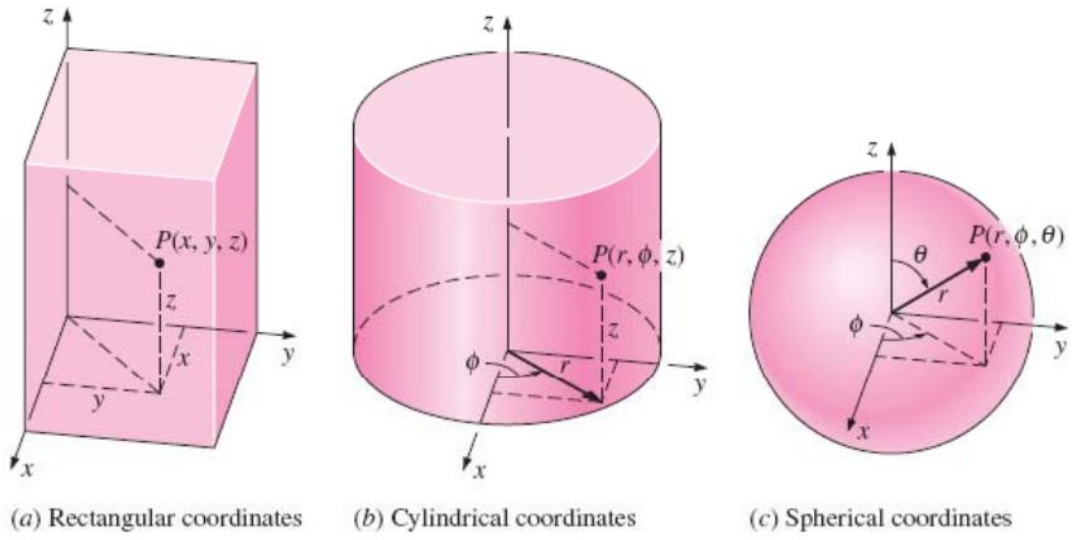

Figure 3-5: coordinates systems

By considering case "a" in Figure 3-5 ;

$$\nabla^2 T = \frac{\partial^2 \mathrm{T}}{\partial x^2} + \frac{\partial^2 \mathrm{T}}{\partial y^2} + \frac{\partial^2 \mathrm{T}}{\partial z^2}$$

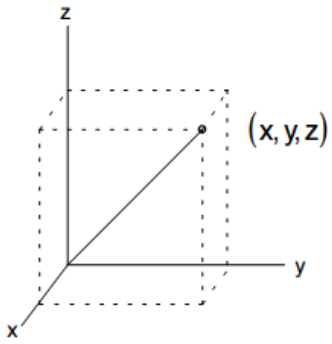

Figure 3-6: Rectangular coordinate

Substituting in Equation 1;

$$\frac{\partial^2 T}{\partial x^2} + \frac{\partial^2 T}{\partial y^2} + \frac{\partial^2 T}{\partial z^2} = \frac{1}{\alpha}\frac{\partial T}{\partial t}$$

(Equation 2)

Where

α is thermal diffusivity [λ / ρc]

T is temperature (°C)

t is time (s)

ρ is density (kg/m3)

c is specific heat

Equation 2, gives an approximation for the temperature distribution since it doesn't consider moisture and vapor movements. These factors are considered by varying the thermal factors like thermal capacity according to experiments and laboratory tests.

Knowing that $\frac{\partial T}{\partial t}$ is the rate of heat transfer that can be found through conduction, convection or radiation empirical formulas.

3.4 Steady versus transient heat transfer

In reality heat flux may change or remain constant with time at any point within the medium. In order to simplify the calculation an assumption have been considered that called steady state which implies no change with time at any point within the medium and in the contrast the transient state has been defined that implies variation with time or time dependence (Figure 3-7). Therefore, the temperature or heat flux remains unchanged with time during steady heat transfer through a medium at any location, although both quantities may vary from one location to another.

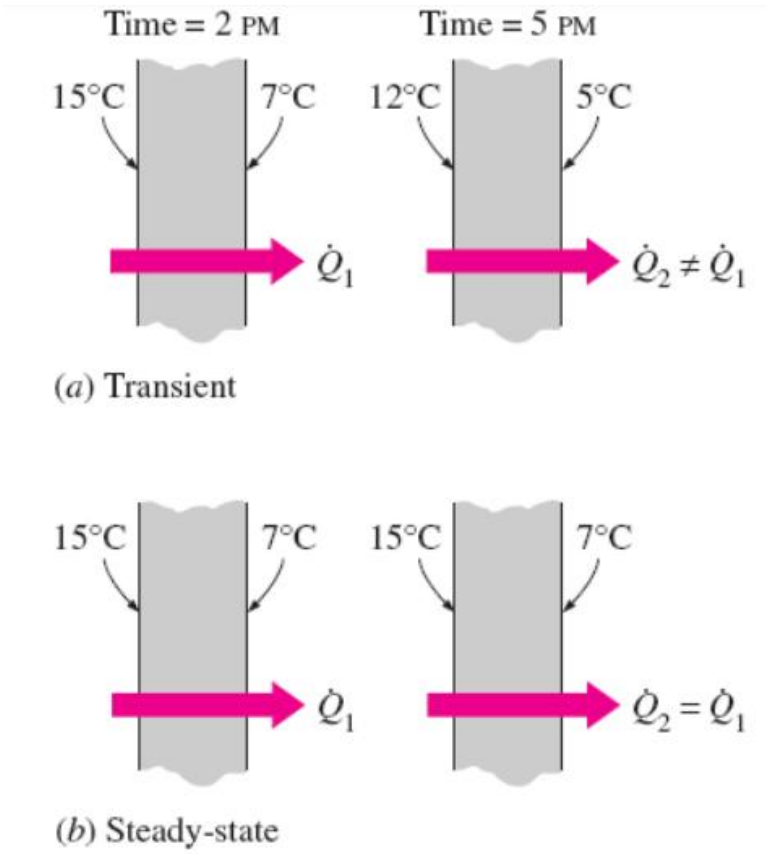

Figure 3-7: Steady Vs. Transient state

3.5 Boundary and Initial conditions

The temperature distribution in a medium depends on the conditions at the boundaries of the medium as well as the heat transfer mechanism inside the medium. To describe a heat transfer problem completely, two boundary conditions must be given for

each direction of the coordinate system along which given for each direction of the coordinate system along which heat transfer is significant.

1. Initial condition

A condition, which is specified at time t=0 is called the initial condition. T(x,y,z,0)=f(x,y,z)

Note that under steady conditions, the heat conduction equation does not involve any time derivatives, and thus we do not need to specify an initial condition.

The heat conduction equation is first order in time, and thus the initial condition cannot involve any derivatives (it is limited to a specified temperature). However, the heat conduction equation is second order in space coordinates, and thus a boundary condition may involve first derivatives at the boundaries as well as specified values of temperature.

2. Temperature boundary condition

The temperature of an exposed surface can usually be measured directly and easily. Therefore, one of the easiest ways to specify the thermal conditions on a surface is to specify the temperature. For one dimensional heat transfer through a plane wall of thickness L, for example, the specified temperature boundary conditions can be expressed as

$$T(0,t) = T_1$$

$$T(L,t) = T_2$$

3. Heat flux boundary condition

The sign of the specified heat flux is determined by inspection: positive if the heat flux is in the positive direction of the coordinate axis and negative if it is in the opposite direction. Note that it is extremely important to have the correct sign for the specified heat flux.

Another classification of boundary conditions is to define prescribed boundary conditions or prescribed boundary heat flux.

A. Prescribed boundary conditions

- A-1: Non-linear boundary conditions:

At x=0 $-\lambda\frac{\partial T}{\partial x} \cong \alpha_{c1}[T_1 - T_0] + \epsilon_1\sigma_n\left[T_{1,sur}^4 - T_0^4\right]$

At x=L $-\lambda\frac{\partial T}{\partial x} \cong \alpha_{c2}[T_2 - T_L] + \epsilon_2\sigma_n\left[T_{2,sur}^4 - T_L^4\right]$

Where

σ_n 5.67e-08 stefan-bolzmann constant [W/m2K4]

α_{ci} Coefficient of convective heat transfer [W/m2.K]

ϵ Surface emissivity

- A-2: Classification of linearized boundary conditions:

1- Dirichlet (Specify temperature)

$T_{x=0} = T_1$ Constant surface temperature $T_{x=L} = T_2$

2- Neumann

$\left(-\lambda\frac{\partial T}{\partial x}\right)_{x=0} = q''_{s,1}$ Constant heat flux at the wall $\left(-\lambda\frac{\partial T}{\partial x}\right)_{x=L} = q''_{s,2}$

3- Robin

$\left(-\lambda\frac{\partial T}{\partial x} + \mathrm{h_1T}\right)_{\mathrm{x=0}} = \mathrm{f_1}$

Convective boundary condition $\left(-\lambda\frac{\partial T}{\partial x} + \mathrm{h_2T}\right)_{\mathrm{x=L}} = \mathrm{f_2}$

B. Prescribed boundary heat flux

- The heat flow at the boundary is based on convection and radiation and so;

$$-\dot{q}_b'' \cong \alpha_c\left[T_g - T_b\right] + \epsilon_{res}\sigma_n\left[T_g^4 - T_b^4\right]$$

Where

$\dot{q}_b''$ is heat flow at the boundary [W/m2]

T_g is gas temperature [C]

T_b is boundary temperature [C]

α_c is convection heat transfer coefficient [W/m2C]

ϵ_{res} is resulting emissivity

σ_n is Stefan-Bolzman constant [W/m2K4]

Heat transfer coefficients at boundaries:

In order to find the heat exchange at the boundaries of the fire exposed member the heat transfer coefficients of both emissivity and convection are required. Eurocode (ENV 1992-2-2, 1994) provide[6] the value for emissivity and convection factors as follows;

Emissivity/convection	ϵ_r	α_c
Unexposed surface	0.8 (landersson, 1974)	9
Exposed surface	0.56	25

Table 3-3: Emissivity/Convection values for Un/Exposed surfaces

[6] The heat transfer at the structure surfaces is dependent on factors such as distance from burning objects and gases to the actual surface, properties and direction of the actual surface and surrounding gas turbulence.

4 : Engineering Problem

The main object of this study is to evaluate bearing capacity of the structural elements in exceptional conditions such as those exposed to fire. The geometry of slab and beam under study has been shown in Figure 4-1 and Figure 4-2. It is assumed that the beam is simple supported beam and each beam carries load of slab with one-meter length. Material used for slab is normal fiber reinforced concrete (NFRC) and for beam is high performance fiber reinforced concrete (HPFRC). The load acting on the system is considered as live load, permanent load and weight of elements (slab and beam). Behavior of the beam and its bearing capacity under different scenarios of fire time-temperature curves has been studied. It is worth noticing that for high performance concrete which is used for the beam material, the mechanical performance at elevated temperatures are higher than those of an ordinary concrete, but its thermal conductivity is similar, and this implies that the steel reinforcement present in the elements can still reach very high temperatures and therefore be ineffective in purposes of structural strength. In order to have an effective contribution of steel bars after fire exposure, it is required to consider a larger value for concrete cover. It is designed to use bars with diameter of 10 mm to obtain a cover net of 40 mm. In order to still ensure the bearing capacity also the ultimate limit states have been provided for two additional longitudinal reinforcement bars with diameter of 12 mm placed underneath the previous with concrete cover equal to 16 mm as shown in Figure 4-3.

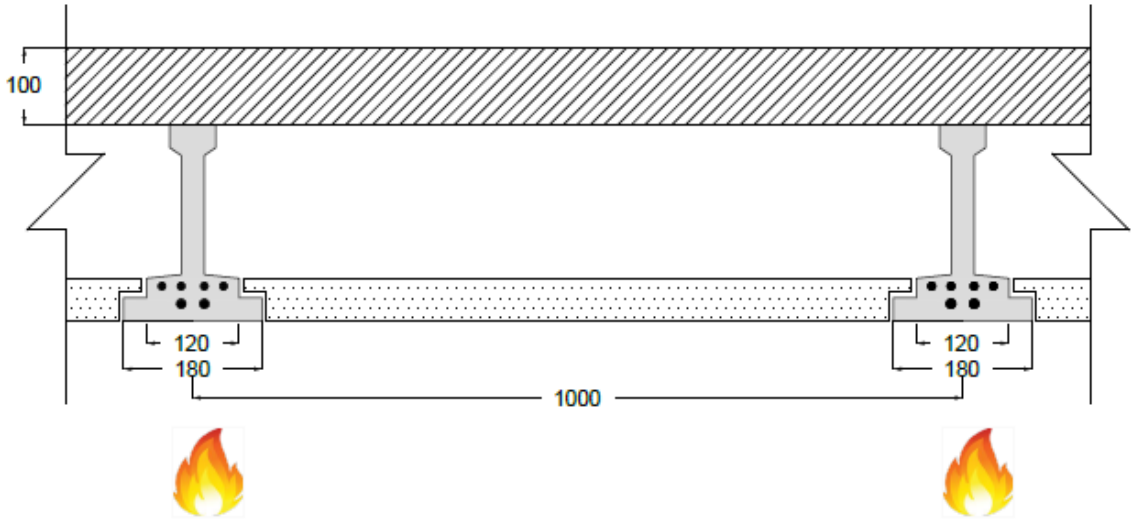

Figure 4-1: Geometry of beam and slab (values in mm)

4.1 Geometry of the problem

Geometry of the beam considering the whole section and the section with hole is presented in Figure 4-2. The beam is reinforced by longitudinal steel bars located at bottom as it is shown in Figure 4-3.

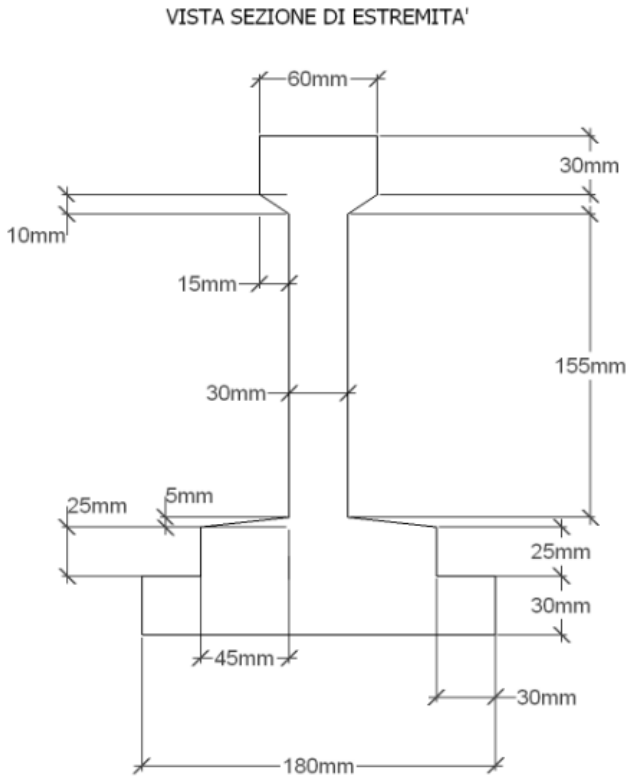

Figure 4-2: Geometry of beam section in detail

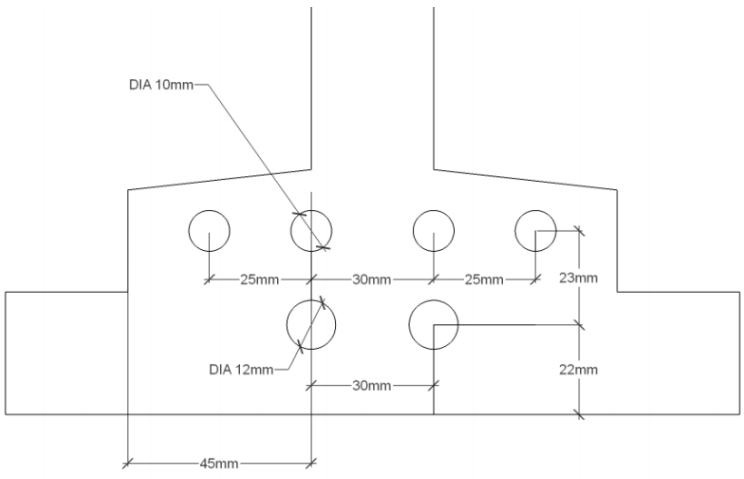

Figure 4-3: Section Details of reinforcement bars

Geometry Specifications:	Values (mm)
Length of the beam	6 m
Width of the beam	180 mm
Distance between beams	1000 mm
Slab height	100 mm
Bars diameter	10mm and 12 mm
Hole diameter	100 mm

Table 4-1:Geometry specifications

4.2 Admixture of the beam

The mix design of the HPFRC beam was iteratively optimized so as to obtain a self compacting material. An amount of 1.2% by volume of straight high-carbon steel microfibers (length 13 mm, diameter 0.16 mm, aspect ratio of about 80) was added to the mix, as shown in Table 4-2: HPFRCC- mix compositionTable 4-2.

Component	Content
Cement I 52.5	600 kg/m^3
Sand 0-2 mm	977 kg/m^3
Water	200 l/m^3
Superplasticizer	33 kg/m^3
Slag	500 kg/m^3
Steel fibers	100 kg/m^3

Table 4-2: HPFRCC- mix composition

4.3 Exposing Fire

Fire exposing on a system can be considered in the model by using a relation of temperate variation over time. The most used time- temperature relation for designing structures under fire is standard fire ISO 834 that has been presented in standard national codes. This temperature-time relation on the boundary of the member is defined in Equation 3 and in Figure 4-4:

$$T_b = 345 * \log_{10}(8t + 1) + T_0 \qquad t > 0$$

(Equation 3)

Where

T_b is boundary temperature [C]

T_0 is ambient temperature [C] (assumed 20 C)

T is time [min]

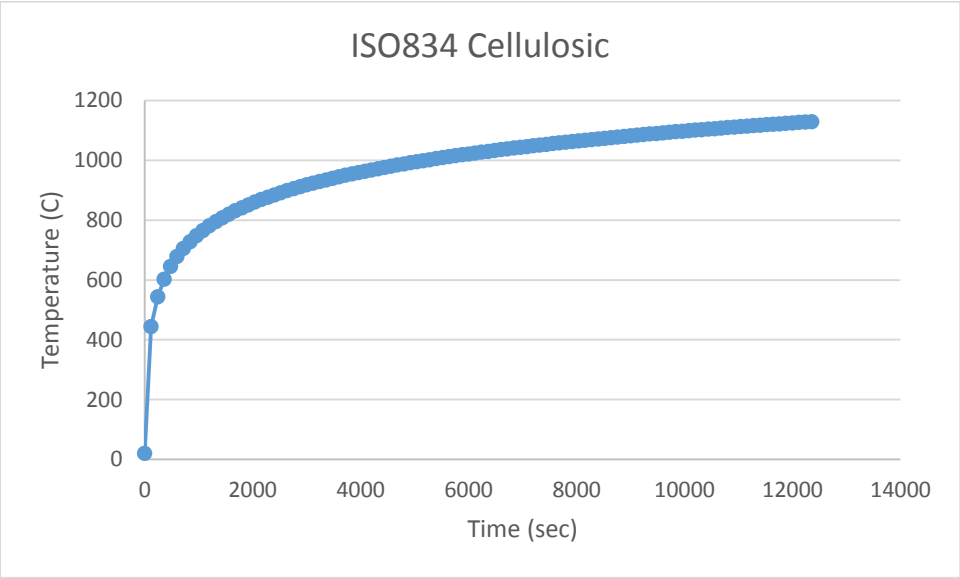

Figure 4-4: Standard fire IS0834 curve (Time-Tempreature)

4.4 Material properties

4.4.1 Introduction

Fire behavior of concrete structure is related to the mechanical, thermal and deformation properties of concrete. Results obtained from fire tests show that these properties are varied with respect to temperature and also they depend on the composition and characteristics of concrete mix. Thermal properties of materials defines rate of heat flux and thermal diffusion in cross section while mechanical properties of material are needed to determine the extent of strength loss and stiffness deterioration of the member. The material properties degradation are given by Eurocode (EN1992-1-2-2004) and in this study the decreasing of strength and modulus of elasticity were defined according to Eurocode. It is worth noticing that the mechanisms behind the

behavior of the material or underlying physical and chemical phenomena are not addressed in the Eurocode.

4.4.2 Thermal Properties of Materials

Thermal properties of materials are those affect the temperature distribution or define the rate of heat transfer. Specific heat, Conductivity and density are the parameters required to determine diffusivity. These parameters also vary with temperature and for both materials, steel and HPFRC these parameters and its variation with respect to temperature are presented.

4.4.2.1 Thermal Properties of Concrete

4.4.2.1.1 Specific heat

Specific heat, denoted as C_p or C, is the heat required to raise the temperature of a unit mass of material by one degree. The common units for specific heat are kcal/kg-ºC and kJ/kg-ºC. The specific heat of concrete at room temperature varies in the range of 0.84 KJ/kg·C and 1.800 KJ/kg·C for different aggregate types. The specific heat property is sensitive to various physical and chemical transformations that take place in concrete at elevated temperatures. This includes the vaporization of free water at about 100°C, the dissociation of $Ca(OH)_2$ into CaO and H_2O between 400–500°C, and the quartz transformation of some aggregates above 600°C. Specific heat is therefore highly dependent on moisture content and considerably increases with higher water to cement ratio. In this study, normal concrete has been used for slab and high performance concrete has been applied for construction of the beam, therefore the values of specific heat for both material NC and HPC will be discussed.

4.4.2.1.1.1 Specific heat of Normal Strength concrete (used for slab)

The specific heat $c_p(\theta)[kJ/kg°C]$ of siliceous and calcareous concrete, as a function of concrete temperature, is given according to EN2-part 1-2. As it is shown in Figure 4-5 the specific heat depends on moisture content. There is a peak between 100

°C and 200 °C due to the heat needed to evaporate the water inside the concrete. Jansson[7] states that this peak has a certain width due to a variable boiling point for the water as a result of pore size and pore pressure.

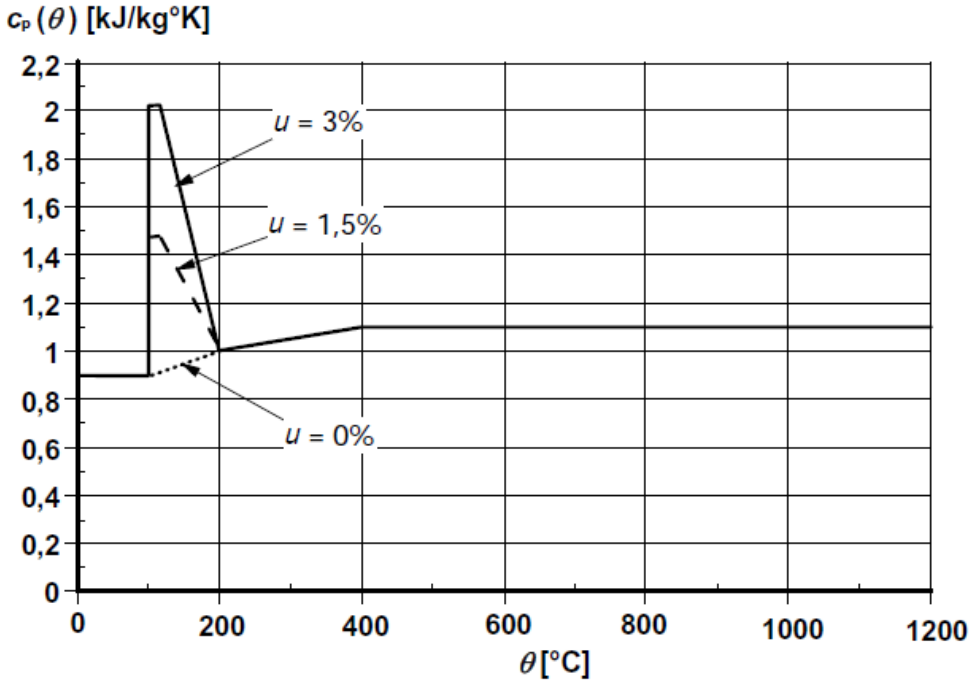

Figure 4-5: specific heat, as function of temperature at 3 different moisture (u=0, 1.5 and 3%) EN2-1-2

The mathematical expression for dry concrete (u=0%) is:

Siliceous and calcareous aggregates:

$$C_P(\theta) = 900\ (J/kg°C) \qquad 20°C \leq \theta \leq 100°C$$

$$C_P(\theta) = 900 + (\theta - 100)(J/kg°C) \qquad 100°C \leq \theta \leq 200°C$$

$$C_P(\theta) = 1000 + \frac{\theta - 200}{2}\ (J/kg°C) \qquad 200°C \leq \theta \leq 400°C$$

$$C_P(\theta) = 1100\ (J/kg°C) \qquad 400°C \leq \theta \leq 1200°C$$

Where

[7] (Jansson, 2008)

θ is the concrete temperature (°C)

Where the moisture content is not considered explicitly in the calculation method, the function given for the specific heat of concrete with siliceous or calcareous aggregates may be modelled by a constant value, $C_{P,peak}$, situated between 100 °C and 115 °C with linear decrease between 115 °C and 200 °C.

$$C_{P,peak} = 900\ (J/kg°C) \quad for\ moisture\ content\ of\ 0\%\ of\ concrete\ weight$$

$$C_{P,peak} = 1470\ (J/kg°C) \quad for\ moisture\ content\ of\ 1.5\%\ of\ concrete\ weight$$

$$C_{P,peak} = 2020\ (J/kg°C) \quad for\ moisture\ content\ of\ 3\%\ of\ concrete\ weight$$

And linear relationship between (115°C, $C_{P,peak}$) and (200°C,1000 J/kg°C). For moisture contents a linear interpolation is acceptable. The peaks of specific heat are illustrated in Figure 4-5.

4.4.2.1.1.2 Specific Heat of High Strength Concrete:

For high strength concrete an equation is given by ENV 1992-1-2, for determination of the specific heat as function of temperature for both siliceous and calcareous concrete:

$$C_c = 900 + \frac{80T}{120} - 4\left(\frac{T}{120}\right)^2$$

Where

C_c is specific heat (J/kg K)

T is temperature where the peak is situate (ºC)

Due to steam generation the curve describing the specific heat will have to be modified. As the thermal properties of water are known and the amount of water needed to account for the moisture in the concrete is known, the area under the c_c curve can be

calculated. The value of the specific heat peak in EN 1992-1-2, /1995/ is declared for the water content 2 and 4 % by weight as 1875 and 2750 J/Kg K respectively.

The following equation, is adopted to determine the peak of the specific heat curve for an arbitrary water content in HPC;

$$C_{c,peak} = 2\frac{2500.10^3(1-0.001\theta)\delta}{\Delta T} + C_{c,p}$$

$C_{c,peak}$ is value of specific heat at the peak [J/kg K]

θ is temperature where the peak is situated [ºC]

δ is water content by weight [-]

ΔT is temperature interval where the steam is generated [k]

$C_{c,p}$ is specific heat already determined at the temperate T [J/kg K]

Similarly to NC, the specific heat for HPC depends on moisture content, therefore the above equation was modified and different curves can be determined for different amount of water content in concrete.

The specific heat at elevated temperatures for high strength concrete has been determined for concrete characterized by a water cement ratio of 0.3, a cement weight of 465 kg/m3, 10 % silicafume of cement, concrete density of 2450 kg/m3 and the relative humidity of 40 and 60 %. The specific heat curves are illustrated in Figure 4-6. In this figure also the value of specific heat of dry HPC and NC (according to EN1992-1-2) are presented.

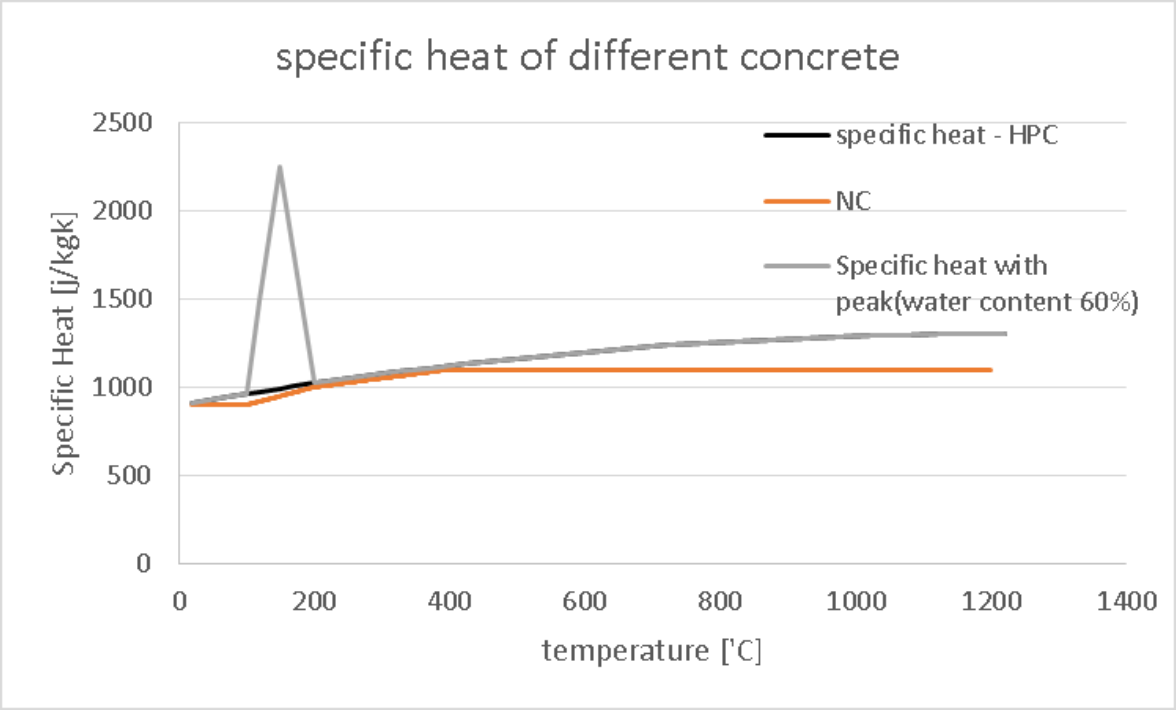

Figure 4-6: Specific heat for normal concrete NC, dry HPC and HPC with 60% humidity

4.4.2.1.2 Thermal conductivity

The thermal conductivity of concrete is the rate of heat transferred through a unit thickness of the material per unit temperature difference, with common units $w/m\ K$ and kcal/m-h-ºC. It is dependent upon the type of aggregate, porosity of the concrete, and the moisture content. Also, thermal conductivity values for concrete elements are dependent on the temperature of the concrete.

4.4.2.1.2.1 Thermal conductivity of NC

The Eurocode determines only a lower and an upper limit for the thermal conductivity λc [W/m°C] of concrete. Additional rules may be given in the National Annex of the Member State. For example, in Sweden, the lower limit most be applied. In Belgium, the lower limit is used for calcareous concrete and the average of the two limits for siliceous concrete (Wit, 2011). It can be read in the Eurocode (EN 1992-1-2, 2004) that the lower limit of thermal conductivity was obtained through the comparison of temperatures measured in fire tests performed on different types of concrete. This limit

gives more realistic temperatures than the upper limit, which was obtained from tests on composite steel/concrete structures.

According to Eurocode 1992-1-2, the thermal conductivity λ_c of concrete may be determined between lower and upper limit of values as;

The upper limit:

$$\lambda_c = 2 - 0.2451\left(\frac{\theta}{100}\right) + 0.0107\left(\frac{\theta}{100}\right)^2 \quad w/m\,K$$

The lower limit :

$$\lambda_c = 1.36 - 0.136\left(\frac{\theta}{100}\right) + 0.0057\left(\frac{\theta}{100}\right)^2 \quad w/m\,K$$

θ is the concrete temperature

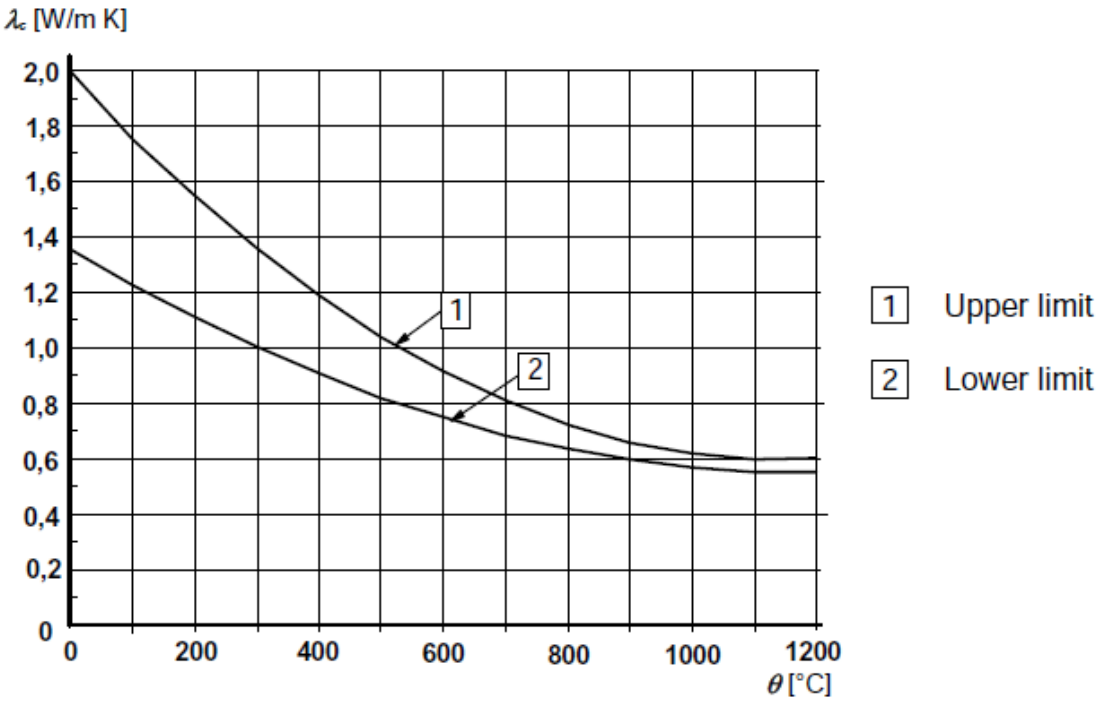

Figure 4-7: Upper and lower limit of the thermal conductivity of concrete as a function of the concrete temperature. EN 1992-1-2

4.4.2.1.2.2 Thermal conductivity of HPC:

According to Eurocode 1992-1-2, the value of thermal conductivity for high strength concrete for use in a Country may be given in its National Annex within the range defined by lower and upper limit.

In this report the values for the thermal conductivity of HPC according to Holst (1994), have shown an acceptable agreement with values for normal concrete given by the EN, where a 2nd degree polynomial has be adapted. The equation below only considers temperature as a variable, although λ_c is known to vary with moisture content as well. This is assumed to be of sufficient accuracy but gives a somewhat high temperature.

$$\lambda_c = 2 - \frac{0.24\theta}{120} + 0.012\left(\frac{\theta}{120}\right)^2$$

λ_c is thermal conductivity [W/mk]

θ is temperature [ºC]

Thermal conductivity as a function of temperature is shown in Figure 4-8 for comparison the thermal conductivity for normal concrete is plotted in the same graph.

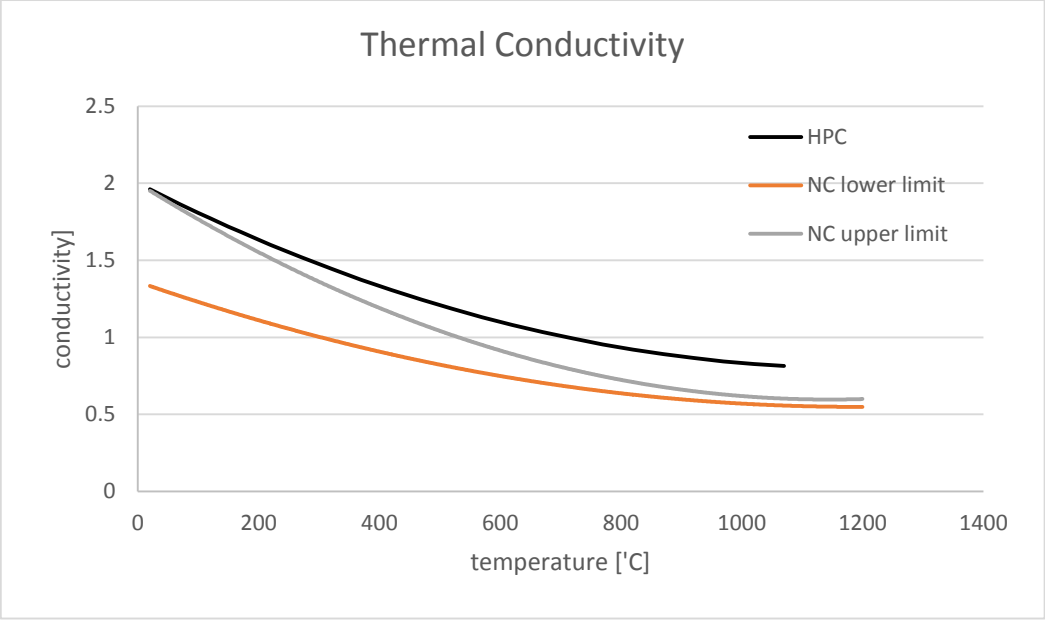

Figure 4-8: Thermal conductivity of HPC and comparison with NC

The two previously given thermal properties summarized: for an increase in temperature, the thermal conductivity will decrease and the specific heat will increase. As a result, the thermal diffusivity decreases with increasing temperature.

4.4.2.1.3 Density

Type of aggregate in concrete primarily defines the density of concrete. Concretes made of dense aggregates have densities ranging from 2000 kg/m3 to 2400 kg/m3. Lightweight aggregate concretes have densities ranging from 1000kg/m3 to 1500kg/m3.

When concrete is heated free moisture is driven away once the temperature in the section exceeds 100ºC. Vapor migrates through the capillaries and forces the moisture to the outer surfaces of the concrete element. On an exposed side of an element it will turn into steam but an unexposed side it will condense. Losses in moisture reduce the density of concrete by a small amount but for practical purposes it is commonly neglected (Levesque, 2006).

4.4.2.1.3.1 Density of NC

According to EN 1992-1-2:2004, the variation of density for NC with temperature is influenced by water loss and is defined as follows:

$$\rho(\theta) = \rho(20℃) \qquad \text{for } 20℃ \leq \theta \leq 115℃$$

$$\rho(\theta) = \rho(20℃).(1 - 0.02(\theta - 115)/85) \qquad \text{for } 115℃ \leq \theta \leq 200℃$$

$$\rho(\theta) = \rho(20℃).(0.98 - 0.03(\theta - 200)/200) \qquad \text{for } 200℃ \leq \theta \leq 400℃$$

$$\rho(\theta) = \rho(20℃).(0.95 - 0.07(\theta - 400)/800) \qquad \text{for } 400℃ \leq \theta \leq 1200℃$$

4.4.2.1.3.2 Density of HPC

For high performance concrete the density has been chose according to UNI 9502-2001 for calcareous concrete with 2% of moisture.

$$\rho(\theta) = 2300 \quad \text{for } \theta \leq 100°C$$

$$\rho(\theta) = 2250 \quad \text{for } \theta \geq 100°C$$

The variation of density for NC and HPC for concrete with a density of 2300kg/m3 is illustrated in Figure 4-9.

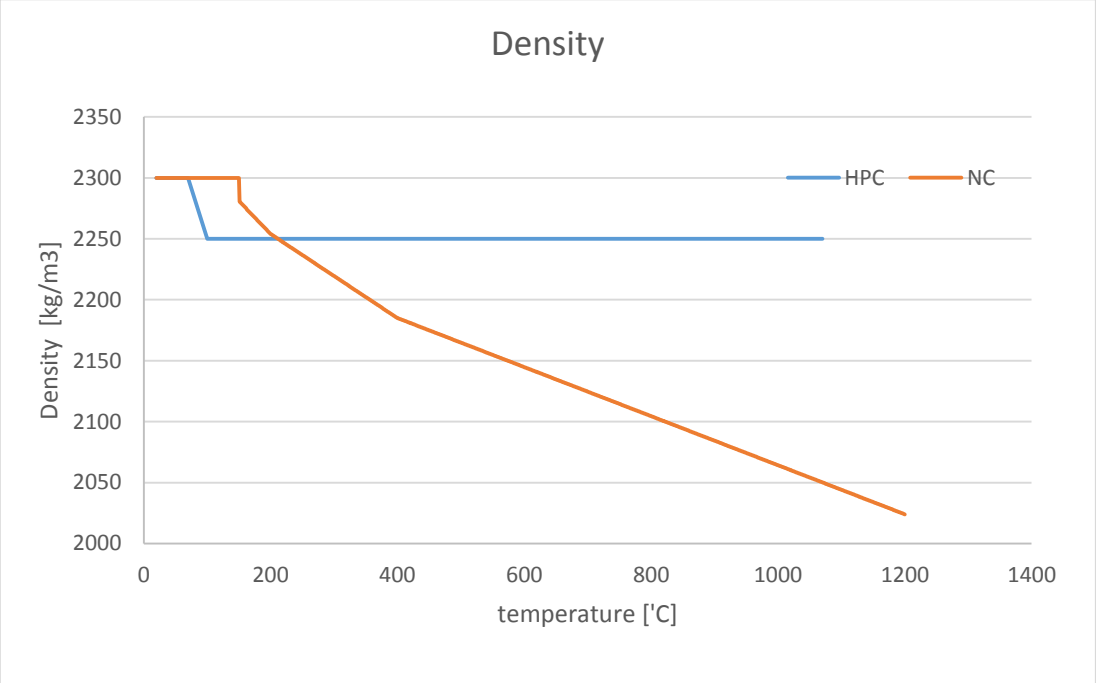

Figure 4-9: Density of concrete as a function of temperature

4.4.2.1.4 Overview on Normal strength concrete and high strength concrete

High performance concrete has less porous than normal strength concrete. Thermal conductivity and specific heat is higher for denser materials. Higher conductivity means that the heat transfers faster in the concrete. Whereas higher value of specific heat means that the heat transfer slower because it provides an enhanced heat storage potential. The product of density and specific heat is called volumetric specific heat (in EN 1992-1-2) or capacitivity and is often used to indicate the potential for transfer heat. Moreover, Anderberg and Pettersson(1992) presented properties for normal strength concrete. The higher value of conductivity can be cancelled by higher value of specific

heat in HPC but it is still difficult to judge about the behavior of HSC and make a comparison with NSC.

Although in this study the thermal properties of HPC has been applied for the beam, according to Eurocode, values given for normal strength concrete may be applied also for high strength concrete.

In this study the specific heat has been considered without peak (dry u=0) and the results are in the conservative side. The higher value of specific heat works in favor of the section thermal diffusion while the smaller value of specific heat indicates that the material can't store thermal energy and the temperature of section increases more.

4.4.2.2 Thermal Properties of steel

The amount of steel is in most concrete structures so low that it hardly influences the total temperature distribution (Donoel, 2007). When nevertheless needed, the other properties can be found in Eurocode 3 (EN 1993-1-2, 2005). In the next chapters, the beam has been modelled in 2D and 3D. In plane section approach (2D), the cross section has been modelled without the steel bars since their existence does not affect the overall temperature distribution, while in FEM beam model (3D) the steel bars have been drawn in the model, therefore it is needed to present the thermal properties of steel.

4.4.2.2.1 Specific Heat

According to EN 1993 1-2, Specific heat of steel can be calculated as;

$C_a = 425 + 0.773\theta - 1.69E-03\theta^2 + 2.22eE-06\theta^3$ [J/kgK] for $20℃ \leq \theta \leq 600℃$

$C_a = 666 + \frac{13002}{738-\theta}$ [J/kgK] for $600℃ \leq \theta \leq 735℃$

$C_a = 545 + \frac{17820}{\theta-731}$ [J/kgK] for $735℃ \leq \theta \leq 900℃$

$C_a = 650$ [J/kgK] for $900℃ \leq \theta \leq 1200℃$

θ is the steel temperature [C]

The variation of the specific heat with temperature is illustrated in Figure 4-10.

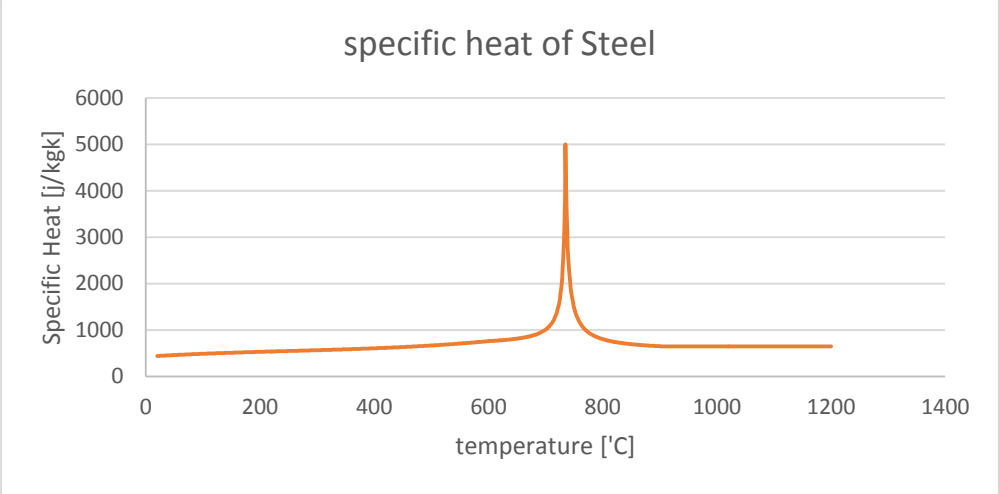

Figure 4-10: Specific heat of steel as a function of temperature

4.4.2.2.2 Thermal conductivity

Thermal conductivity of steel is presented in EN 1993. 1-2 (2005) as follow;

$\lambda_a(t) = 54 - 0.0333\theta \quad W/m℃$ for $20℃ \leq \theta \leq 800℃$

$\lambda_a(t) = 27.3 \quad W/m℃$ for $800℃ \leq \theta \leq 1200℃$

Where

θ is the steel temperature [C]

The variation of the thermal conductivity with temperature is illustrated in Figure 4-11.

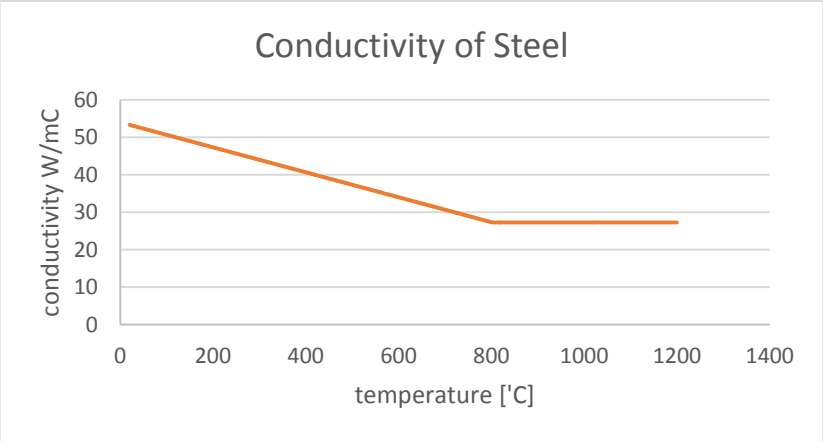

Figure 4-11: Thermal Conductivity of carbon steel as a function of the temperature

4.4.2.2.3 Density

According to En 1993-1-2, the unit mass of steel or density may be considered to be independent of the steel temperature and it is proposed a constant value of 7850 Kg/m3 for steel.

4.4.3 Mechanical Properties of Materials

General

Fire behavior of concrete members are also related to their mechanical properties such as compressive and tensile strength, young modulus of materials, and finally constitutive laws for stress-strain response at elevated temperatures.

Compressive strength of concrete at elevated temperature depends on water/cement ratio, aggregate interface transition zone, curing condition, aggregated type and size admixture types and type of stress.

The tensile strength of concrete is much lower than compressive strength, due to this cracks can propagate under tensile loads. Concrete is weak in tension, and for NSC, tensile strength is only 10% of its compressive strength and for HSC tensile strength ratio is further reduced. Thus, tensile strength of concrete is often neglected in strength calculations at room and elevated temperatures. However, it is an important property, because cracking in concrete is generally due to tensile stresses and the structural damage of the member in tension is often generated by progression in micro-cracking. Under fire conditions tensile strength of concrete can be even more crucial in cases where fire induced spalling occurs in a concrete structural member. In fiber reinforced concrete by use of fibers the tensile strength of concreted increases. Also in this case the tensile strength varied with temperature.

Another property that influences fire resistance is the modulus of elasticity of concrete which decreases with temperature. At high temperature, disintegration of hydrated cement products and breakage of bonds in the microstructure of cement paste

reduce elastic modulus and the extent of reduction depends on moisture loss, high temperature creep, and type of aggregate.

4.4.3.1 Mechanical Properties of Concrete

In fib model code, mechanical properties of concrete are given by a reduction factor that represents the decrease of the property for an increase of the material temperature (Table 4-3).

Concrete	Siliceous aggregates			Calcareous aggregates		
temp. θ	$f_{c,\theta}/f_{ck}$	$\varepsilon_{c1,\theta}$	$\varepsilon_{cu1,\theta}$	$f_{c,\theta}/f_{ck}$	$\varepsilon_{c1,\theta}$	$\varepsilon_{cu1,\theta}$
[°C]	[-]	[-]	[-]	[-]	[-]	[-]
1	2	3	4	5	6	7
20	1,00	0,0025	0,0200	1,00	0,0025	0,0200
100	1,00	0,0040	0,0225	1,00	0,0040	0,0225
200	0,95	0,0055	0,0250	0,97	0,0055	0,0250
300	0,85	0,0070	0,0275	0,91	0,0070	0,0275
400	0,75	0,0100	0,0300	0,85	0,0100	0,0300
500	0,60	0,0150	0,0325	0,74	0,0150	0,0325
600	0,45	0,0250	0,0350	0,60	0,0250	0,0350
700	0,30	0,0250	0,0375	0,43	0,0250	0,0375
800	0,15	0,0250	0,0400	0,27	0,0250	0,0400
900	0,08	0,0250	0,0425	0,15	0,0250	0,0425
1000	0,04	0,0250	0,0450	0,06	0,0250	0,0450
1100	0,01	0,0250	0,0475	0,02	0,0250	0,0475
1200	0,00	-	-	0,00	-	-

Table 4-3: values of the main parameters of the stress-strain relationships of normal weight concrete with siliceous or calcareous aggregates concrete at elevated temperatures. Linear interpolation may be used. Copied from EN 1992-1-2 (2004).

The corresponding mechanical property at normal temperature (20°C) can be found in EN 1992-1-1 and it is represented in Table 4-4. Since creep effects are not explicitly considered, the given material models are only applicable for heating rates

between 2 and 50°C per minute. If the heating rate deviates from this range, the reliability of the strength and deformation properties must be demonstrated explicitly.

Concrete properties			
Slab		**Beam**	
fc	45 Mpa	fc	110 Mpa
ε_{c1}	0.0024	ε_{c1}	0.0025
ε_{cu}	0.02	ε_{cu}	0.02
Ec0	28050 Mpa	Ec0	65824 Mpa

Table 4-4:Mechanical properties of Concrete for Slab and Beam

4.4.3.1.1 Constitutive law for concrete in Compression

Both the compressive strength and the stiffness of uniaxial stressed concrete are reduced when the temperature rises. The reduction of the modulus of elasticity is even bigger since the peak stress strain increases with temperature. This is all reflected by Figure 4-13 where different stress-strain diagrams are plotted for different temperatures and for a certain type of concrete. Note, that the Eurocode makes a difference between siliceous aggregate concrete and calcareous aggregate concrete. The latter is defined as a concrete containing calcareous aggregates. The stress-strain relationship is characterized by the following three variables, which are also illustrated in Figure 4-12:

$f_{c,\theta}$ is the characteristic value of the compressive strength of concrete at elevated temperature

$\varepsilon_{c1,\theta}$ is the strain corresponding to $f_{c,\theta}$

$\varepsilon_{cu1,\theta}$ is the strain that defines the end of the descending branch

The mathematical expression of the ascending branch is:

$$\sigma = \frac{3\varepsilon f_{c,\theta}}{\varepsilon_{c1,\theta}\left[2+\left(\frac{\varepsilon}{\varepsilon_{c1,\theta}}\right)^3\right]} \quad for\ \varepsilon \le \varepsilon_{c1,\theta} \qquad \text{Eq. 1}$$

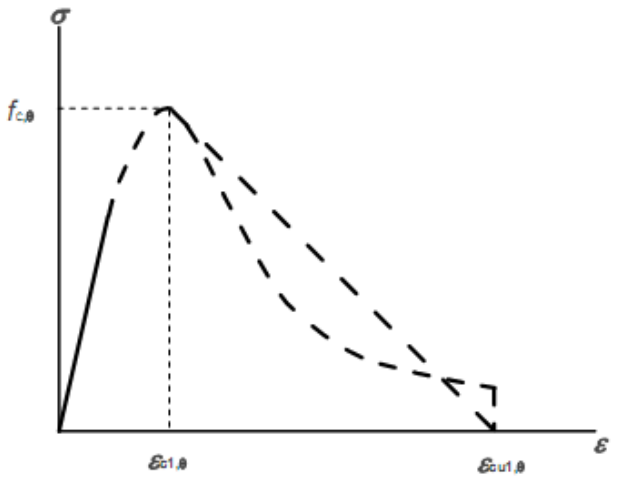

Range	Stress $\sigma(\theta)$
$\varepsilon \leq \varepsilon_{c1,\theta}$	$\frac{3\varepsilon f_{c,\theta}}{\varepsilon_{c1,\theta}\left(2+\left(\frac{\varepsilon}{\varepsilon_{c1,\theta}}\right)^3\right)}$
$\varepsilon_{c1(\theta)} < \varepsilon \leq \varepsilon_{cu1,\theta}$	For numerical purposes a descending branch should be adopted. Linear or non-linear models are permitted.

Figure 4-12: Mathematical model for stress-strain relationships of concrete under compression at elevated temperatures. From EN 1992-1-2(2004)

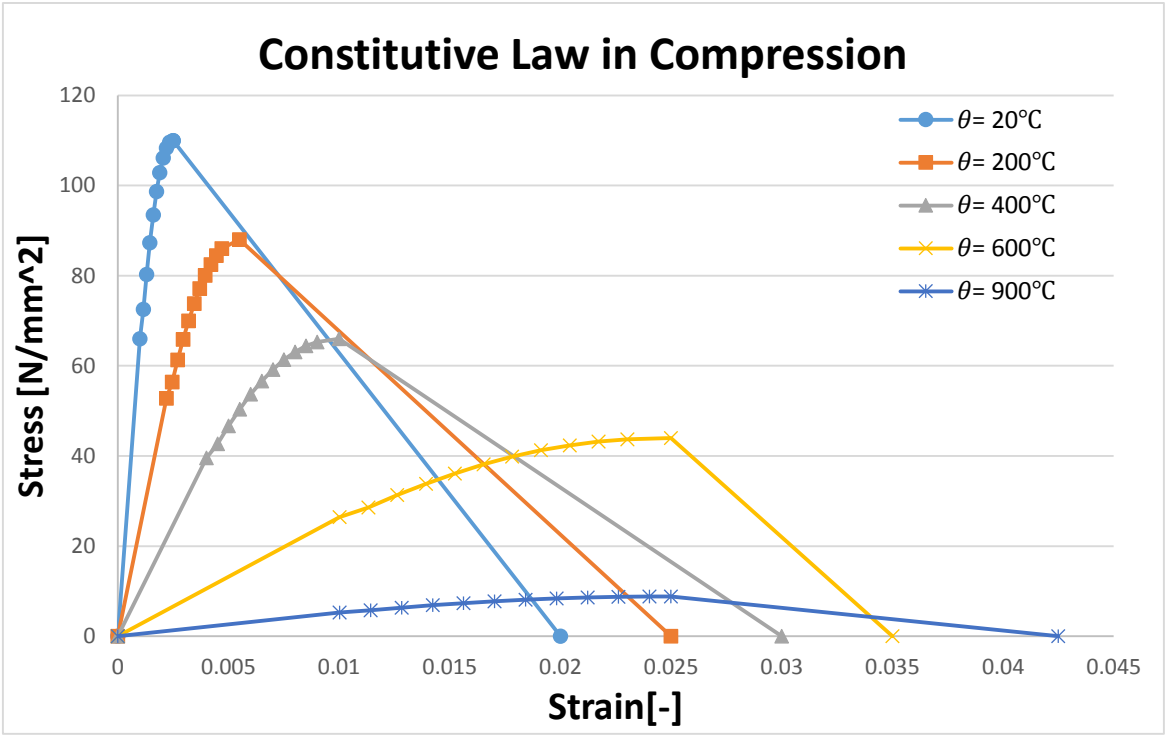

Figure 4-13: compressive stress- strain relationship of concrete c110 for different values of the concrete temperature. The descending branch is chosen to be linear. Based on a figure from the fib Bulletin 46 (2008)

The descending branch must be adopted to avoid numerical instability during modelling. The shape may be chosen linear or nonlinear (see also Figure 4-12). The main parameters of the stress-strain curve are dependent on temperature and their value, intended for normal weight concrete, is found in Table 4-3 . Linear interpolation may be used.

4.4.3.1.2 Constitutive law for Concrete in Tension

In general, the tensile strength of concrete should be ignored. By adding steel fibers into the matrix the tensile strength of the concrete mix increases considerably and the model presented in fib MC can be used. The procedure to find the tensile behavior of FRC is illustrated in four steps:

1- Classification of Fibers

According to fib model code, to classify the post-cracking strength of FRC a linear elastic behavior can be assumed, by considering the characteristic flexural residual strength values that are significant for serviceability (f_{R1k}) and ultimate (f_{R3k}) conditions. In particular two parameters, namely f_{R1k} (representing the strength interval) and a letter a, b, c, d or e (representing thef_{R3k}/f_{R1k}ratio). The strength interval is defined by two subsequent numbers in the series: 1.0, 1.5, 2.0, 2.5, 3.0, 4.0, 5.0, 6.0, 7.0, 8.0 … [MPa] while the letters a, b, c, d, e correspond to the residual strength ratios:

- a if $0.5 \leq f_{R3k}/f_{R1k} < 0.7$
- b if $0.7 \leq f_{R3k}/f_{R1k} < 0.9$
- c if $0.9 \leq f_{R3k}/f_{R1k} < 1.1$
- d if $1.1 \leq f_{R3k}/f_{R1k} < 1.3$
- e if $1.3 \leq f_{R3k}/f_{R1k}$

The designer has to specify the residual strength class and the f_{R3k}/f_{R1k} ratio as well as the material of the fiber.

Properties of fibers used in slab:

$f_{R1k} = 4$ Mpa, $f_{R3k} = 3.6$ Mpa

$f_{R3k}/f_{R1k} = 0.9 \rightarrow$ c Fiber class: 4C

Properties of fibers used in beam:

$f_{R1k} = 15$ Mpa, $f_{R3k} = 16.5$ Mpa

$f_{R3k}/f_{R1k} = 0.9 \rightarrow$ c Fiber class: 16.5d

2- Define tension behavior of fibers

A stress-crack opening law in uniaxial tension is defined for the post-cracking behavior of FRC. Two simplified stress-crack opening constitutive laws may be deduced from the bending test results: a plastic rigid behavior, or a linear post- cracking behavior (hardening or softening) as schematically shown in Figure 4-14, where f_{Fts}represents the serviceability residual strength, defined as the post-cracking strength for serviceability crack openings, and f_{Ftu} represents the ultimate residual strength. In this study a linear post-cracking behavior (softening) is considered for calculations.

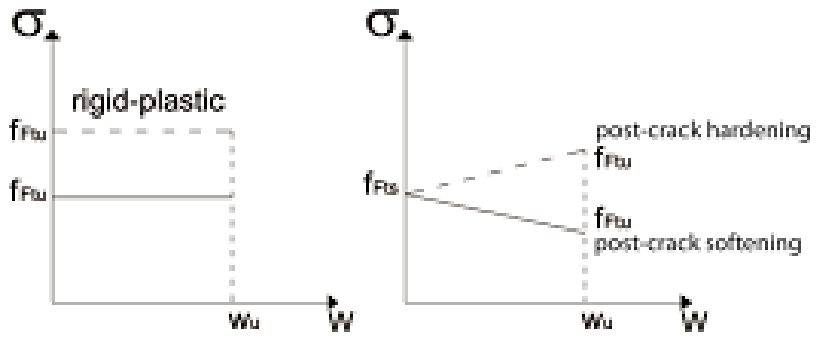

Figure 4-14: Simplified post-cracking constitutive laws: stress-crack Opening (continuous and dashed lines refer to softening and hardening post-cracking behavior, respectively)

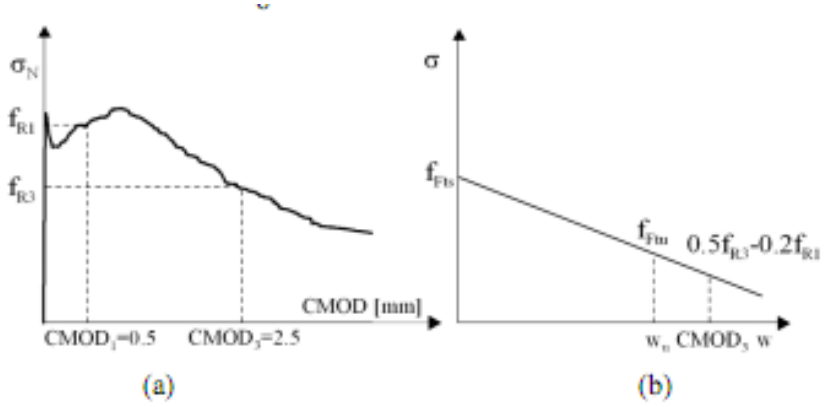

Figure 4-15: Typical results from a bending test on a softening material (a); linear post-cracking constitutive law (b) For numerical analyses, more advanced constitutive laws are recommended, including first crack tensile strength.

When considering softening materials, the definition of the stress-strain law is based on the identification of the crack width and on the corresponding structural characteristic length (lcs) of the structural element. Thus, the strain can be assumed equal to: $\varepsilon = \frac{w}{l_{cs}}$

3- Define characteristic length

Characteristic length is a value needed for converting displacement to strain. It can be computed as the minimum value between the mean distance between cracks S_{rm} and the distance y between the neutral axis and the tensile side of the cross-section.

$l_{cs} = \min(s_{rm}, y)$

$S_{rm} = 1.5 l_{s,max}$

$$l_{s,max} = kc + \frac{1}{4}\frac{(f_{ctm} - f_{Ftsm})}{\tau_{bms}}\frac{\emptyset_s}{\rho_{s,ef}}$$

Where

$k = 1.0$ Empirical parameter to take into account the influence of concrete cover

$c = 22$ mm concrete cover

$\tau_{bm} = 1.8 f_{ctm} = 10.08\ Mpa$ is the mean bond strength between steel and concrete

$f_{ctm} = 5.6\ Mpa$ Mean concrete tensile strength

$f_{Ftsm} = 5.067\ Mpa$

$\emptyset_s = 10\ mm$ Rebar diameter

$\rho_{s,ef} = \frac{A_s}{A_{c,ef}} = 0.058$ Effective reinforcement ratio

$A_{c,ef}$ Effective area of concrete in tension

$l_{s,max} = 24.27\ mm$

$l_{cs} = \min(1.5 \times l_{s,max}, 180) = 36.40\ mm$

	Crack formation stage	Stabilized cracking stage
Short term, instantaneous loading	$\tau_{bms} = 1.8 \cdot f_{ctm}(t)$ $\beta = 0.6$ $\eta_r = 0$	$\tau_{bms} = 1.8 \cdot f_{ctm}(t)$ $\beta = 0.6$ $\eta_r = 0$
Long term, repeated loading	$\tau_{bms} = 1.35 \cdot f_{ctm}(t)$ $\beta = 0.6$ $\eta_r = 0$	$\tau_{bms} = 1.8 \cdot f_{ctm}(t)$ $\beta = 0.4$ $\eta_r = 1$

Table 4-5:Values for τ_bm for deformed reinforcing bars (fib MC2010, Table 7.6-2)

4- Find stress-strain relationship

Fib MC 2012 presented two models to define the stresses of fibres.

A) Rigid-plastic model

B) linear model

Rigid plastic model identifies an unique reference value, f_{Ftu}, based on the ultimate behavior. This value is determined as :

$$f_{Ftu} = \frac{f_{R3}}{3}$$

Linier model identifies two reference values, namely f_{Ftu} and f_{Fts}. They have to be defined through residual values of flexural strength using the following equations:

$$f_{Fts} = 0.45 f_{R1}$$

$$f_{Ftu} = f_{Fts} - \frac{w_u}{CMOD_3}(f_{Fts} - 0.5 f_{R3} + 0.2 f_{R1}) > 0$$

Where

w_u is the maximum crack opening accepted in structural design; its value depends on the ductility required.

The equation for f_{Ftu} when $w_u = CMOD_3$ is obtained from the rotational equilibrium at ULS, when a stress block in tension along the section is taken into account, Figure 4-16

Figure 4-16: Stress diagrams for determination of the residual tensile strength f_Fts)b) and f_Ftu(C) for the linear model respectively

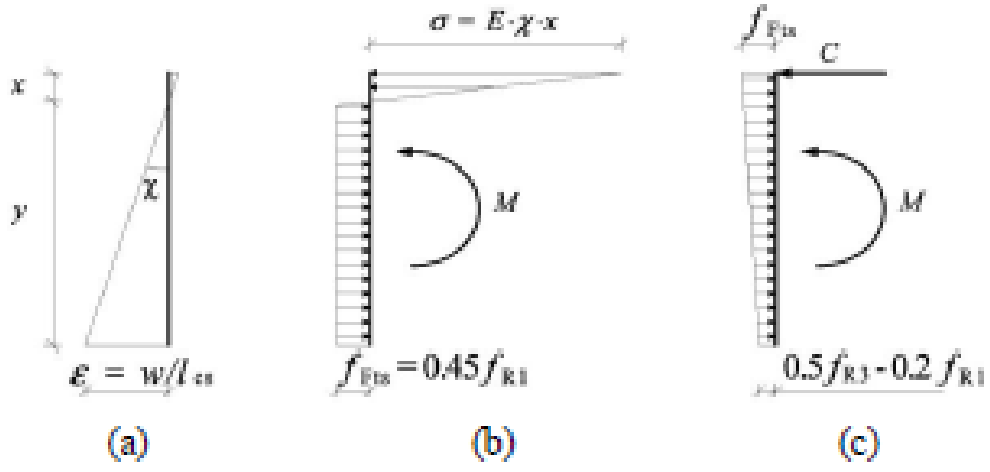

In this study a linear model is assumed and for the beam the corresponding values are:

$$f_{Fts} = 0.45 f_{R1} = 6.75\ MPA$$

$$f_{Ftu} = f_{Fts} - \frac{CMOD_3}{CMOD_3}(f_{Fts} - 0.5 f_{R3} + 0.2 f_{R1}) = 0.5 f_{R3} - 0.2 f_{R1} = 5.2\ MPA$$

For Slab:

$$f_{Fts} = 0.45 f_{R1} = 1.8\ MPA$$

$$f_{Ftu} = f_{Fts} - \frac{CMOD_3}{CMOD_3}(f_{Fts} - 0.5 f_{R3} + 0.2 f_{R1}) = 0.5 f_{R3} - 0.2 f_{R1} = 1 MPA$$

It is assumed that the elasticity modulus in tension and compression are equal. Therefore it is possible to calculate correspond strain of f_{Fts}&f_{Ftu};

Beam: $E_c = 65824\ MPa, \varepsilon_1 = f_{Fts}/E_c = 0.0001, \quad \varepsilon_u = \frac{w_b}{l_{cs}} = 0.06867$

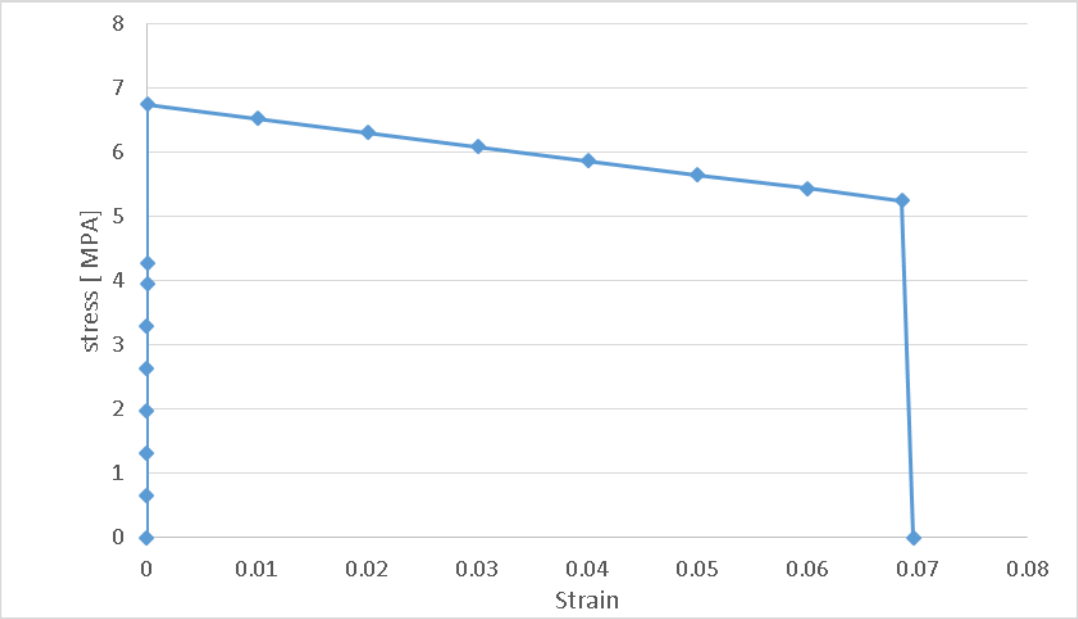

Figure 4-17: Constitutive law for HPFRC beam in tension

Slab: $E_c = 65824\ MPa, \quad \varepsilon_1 = f_{Fts}/E_c = 0.0001, \quad \varepsilon_u = \frac{w_b}{l_{cs}} = 0.06867$

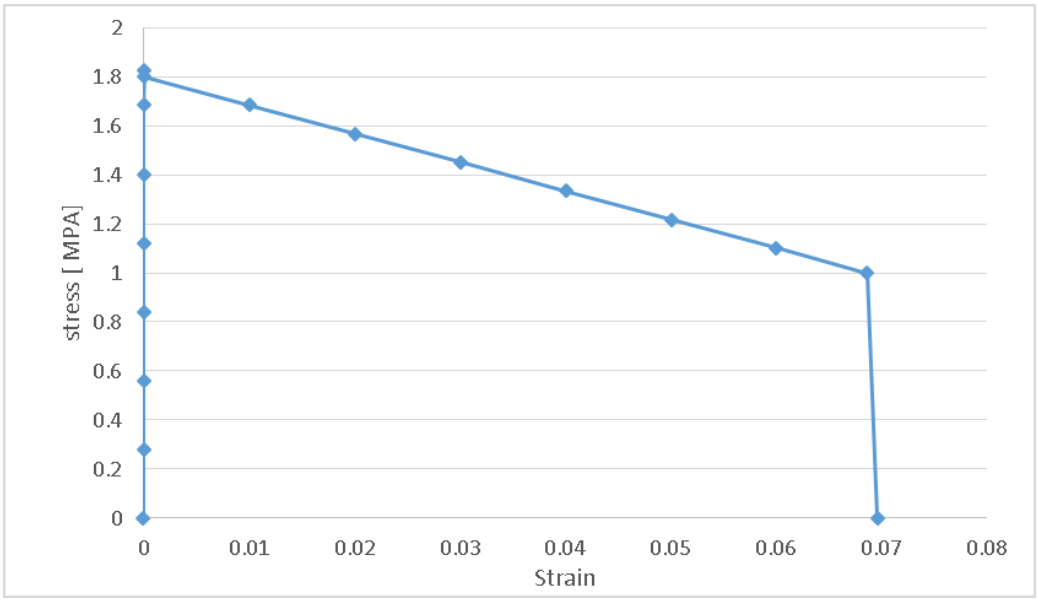

Figure 4-18: Constitutive law for FRC Slab in tension

5- Define degradation of FRC strength in elevated temperature

In elevated temperature the fibers strength decreases and this degradation is according to experimental tests presented in chapter 2 by Carvazan et all (2013).

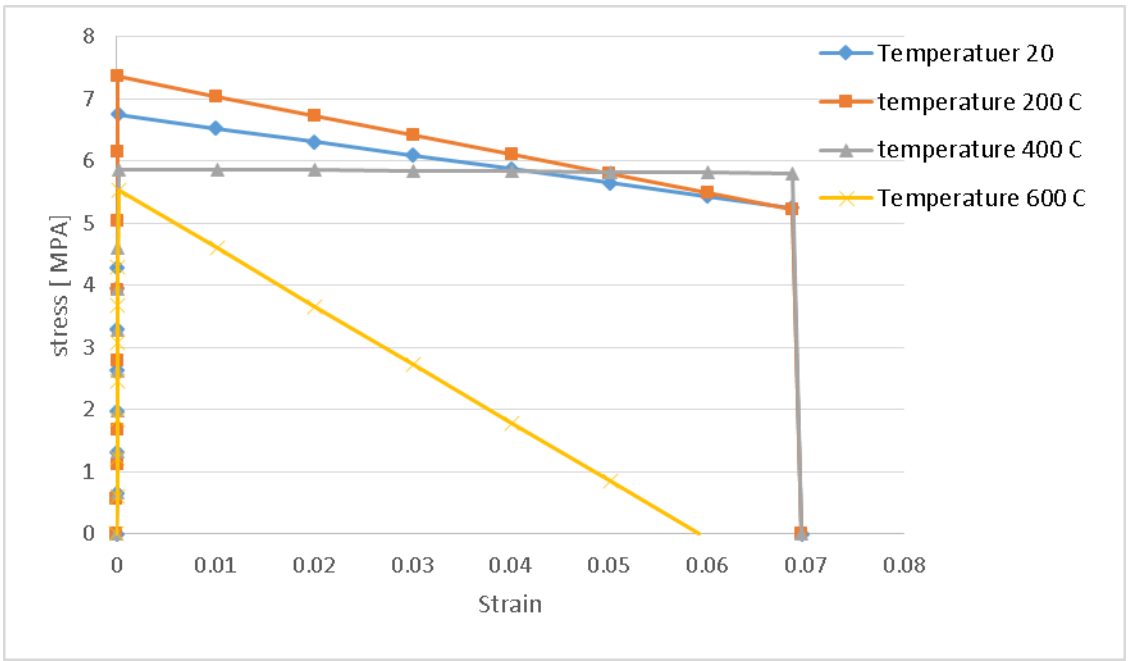

Figure 4-19: Constitutive law for HPFR in tension for different temperatures

4.4.3.2 Mechanical Properties of steel

In reinforced concrete structures reinforced steel bars play significant role when structural elements are exposed to fire. It becomes more significant when the steel bars have a primary load bearing capacity like in the case of slabs or beams. These elements are more vulnerable in case of increase of temperature due to fire, because position of steel bars in slabs or beams are near the surface, to gain a maximum moment capacity at ordinary temperature. Therefore, in case of fire the steel bars temperature rises and the time to reach to maximum temperature depends on concrete cover and thermal properties of concrete. In continue, when temperature increases in the steel, the strength reduces and this reduction is proportion to the residual strain considered. The effect of temperature in steel bars in high performance concrete is more critical than ordinary strength concrete due to existence of more amount of reinforcement.

According to EN1993, part 1-2, the strength and deformation properties of reinforcing steel at elevated temperatures shall be obtained from the stress-strain relationships specified in Figure 4-20. The relationship given in Figure 4-20 should be used to determine the resistances to tension compression moment or shear.

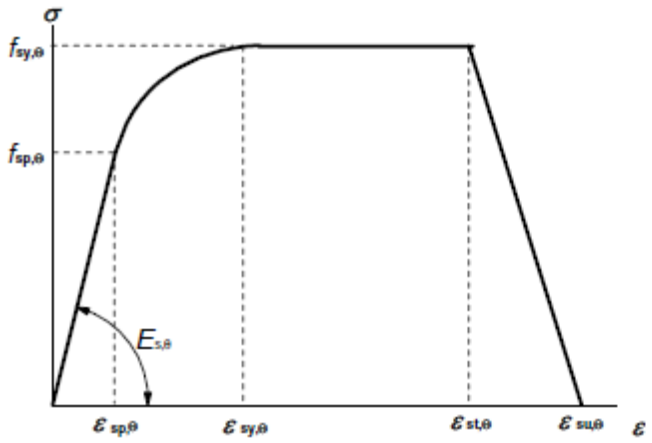

Range	Stress $\sigma(\theta)$	Tangent modulus
$\varepsilon_{sp,\theta}$	$\varepsilon E_{s,\theta}$	$E_{s,\theta}$
$\varepsilon_{sp,\theta} \le \varepsilon \le \varepsilon_{sy,\theta}$	$f_{sp,\theta} - c + (b/a)[a^2 - (\varepsilon_{sy,\theta} - \varepsilon)^2]^{0,5}$	$\frac{b(\varepsilon_{sy,\theta} - \varepsilon)}{a\left[a^2 - \left(\varepsilon - \varepsilon_{sy,\theta}\right)^2\right]^{0,5}}$
$\varepsilon_{sy,\theta} \le \varepsilon \le \varepsilon_{st,\theta}$	$f_{sy,\theta}$	0
$\varepsilon_{st,\theta} \le \varepsilon \le \varepsilon_{su,\theta}$	$f_{sy,\theta}[1-(\varepsilon - \varepsilon_{st,\theta})/(\varepsilon_{su,\theta} - \varepsilon_{st,\theta})]$	-
$\varepsilon = \varepsilon_{su,\theta}$	0,00	-
Parameter *)	$\varepsilon_{sp,\theta} = f_{sp,\theta} / E_{s,\theta}$ $\varepsilon_{sy,\theta} = 0,02$ $\varepsilon_{st,\theta} = 0,15$ $\varepsilon_{su,\theta} = 0,20$ Class A reinforcement: $\varepsilon_{st,\theta} = 0,05$ $\varepsilon_{su,\theta} = 0,10$	
Functions	$a^2 = (\varepsilon_{sy,\theta} - \varepsilon_{sp,\theta})(\varepsilon_{sy,\theta} - \varepsilon_{sp,\theta} + c/E_{s,\theta})$ $b^2 = c\,(\varepsilon_{sy,\theta} - \varepsilon_{sp,\theta})\,E_{s,\theta} + c^2$ $c = \frac{(f_{sy,\theta} - f_{sp,\theta})^2}{(\varepsilon_{sy,\theta} - \varepsilon_{sp,\theta})E_{s,\theta} - 2(f_{sy,\theta} - f_{sp,\theta})}$	

Figure 4-20: Stress-strain relationship for carbon steel at elevated temperatures. EN1993.1.2

$f_{y,\theta} = 430\ Mpa$ Effective yield strength

$f_{p,\theta} = 300\ Mpa$ Proportional limit

$E_{a,\theta} = 205000\ Mpa$ Slope of the linear elastic range

$\varepsilon_{p,\theta} = 0.0015$ Strain at the proportional limit

$\varepsilon_{y,\theta} = 0.02$ Yield strain

$\varepsilon_{s,\theta} = 0.15$ Limiting strain for yield strength

$\varepsilon_{u,\theta}$=0.2 Ultimate strain

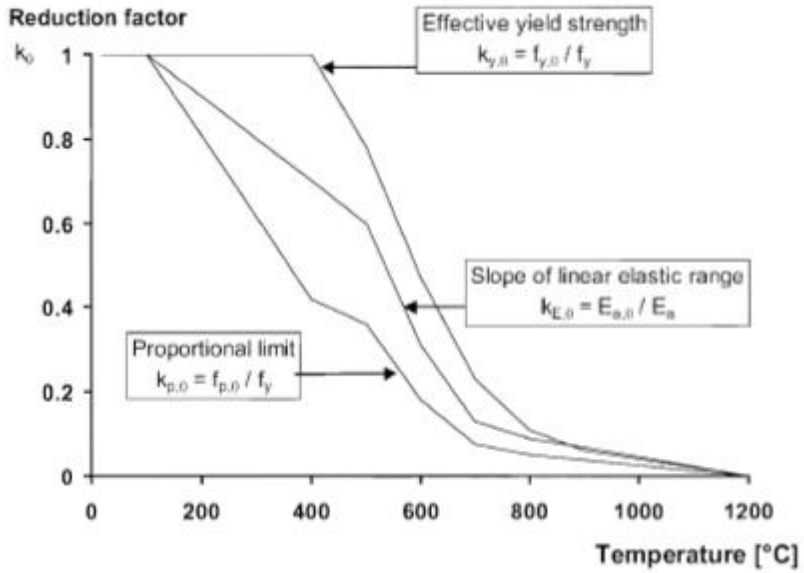

Figure 4-21: Reduction factors for the stress-strain relationship of steel at elevated temperatures (EN1993.1.2)

Steel Temperature θ_a	Reduction factors at temperature θ_a relative to the value of f_y or E_a at 20°C		
	Reduction factor (relative to f_y) for effective yield strength $k_{y,\theta} = f_{y,\theta}/f_y$	Reduction factor (relative to f_y) for proportional limit $k_{p,\theta} = f_{p,\theta}/f_y$	Reduction factor (relative to E_a) for the slope of the linear elastic range $k_{E,\theta} = E_{a,\theta}/E_a$
20°C	1,000	1,000	1,000
100°C	1,000	1,000	1,000
200°C	1,000	0,807	0,900
300°C	1,000	0,613	0,800
400°C	1,000	0,420	0,700
500°C	0,780	0,360	0,600
600°C	0,470	0,180	0,310
700°C	0,230	0,075	0,130
800°C	0,110	0,050	0,090
900°C	0,060	0,0375	0,0675
1000°C	0,040	0,0250	0,0450
1100°C	0,020	0,0125	0,0225
1200°C	0,000	0,0000	0,0000

Figure 4-22: Reduction factors for stress-strain relationship of carbon steel at elevated temperatures (EN1993.1.2)

After finding the stress-Strain relationship for ambient temperature, it is possible to use the degradation coefficient suggested by Eurocode to find the stress-strain relationship at elevated temperature. The results are shown in Figure 4-23 and Table 4-6.

Parameters	Temperature (℃)							
	20	**400**	**500**	**600**	**700**	**800**	**900**	**1000**
Fsy (Mpa)	430	430	335.4	202.1	98.9	47.3	25.8	17.2
fsp(Mpa)	300	126	108	54	21	15	12	6
Es(Mpa)	205000	143500	123000	63550	26650	18450	14350	8200
ε_{sp}	0.001463	0.000878	0.000878	0.00085	0.000788	0.000813	0.000836	0.000732

Table 4-6: strength of steel bars at elevated temperature

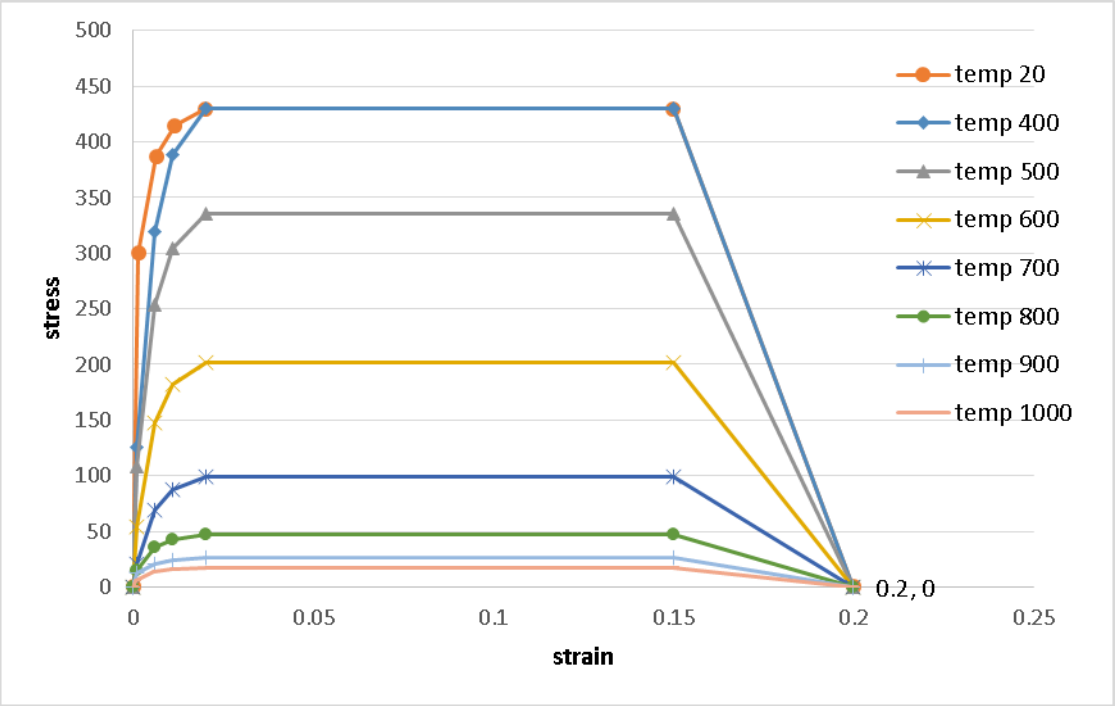

Figure 4-23: Constitutive law for steel bars at elevated temperature, Compression and tension

4.4.4 Deformation properties of materials:

Thermal expansion, creep strain are deformation properties of materials are dependent on the chemical composition, aggregate type, and chemical reactions during heating in the concrete and for steel the thermal expansion depends on the molecule composition of the steel bars.

4.4.4.1 Thermal expansion of concrete

When concreted exposed to fire it goes under expansion. The thermal expansion varies with temperature. The thermal expansion of concrete increases from zero at room temperature to about 1.3% at 700°C and then generally remains constant through 1000°C. This increase is substantial in the 20–700°C temperature range and is mainly due to high thermal expansion resulting from constituent aggregates and cement paste in concrete. Thermal expansion of concrete is complicated by other contributing factors such as additional volume changes caused by variation in moisture content, by chemical reactions (dehydration, change of composition), and by creep and micro-cracking resulting from non-uniform thermal stresses. In some cases, thermal shrinkage can also result from loss of water due to heating, along with thermal expansion, and this might lead to the overall volume change to be negative, that is, shrinkage rather than expansion.

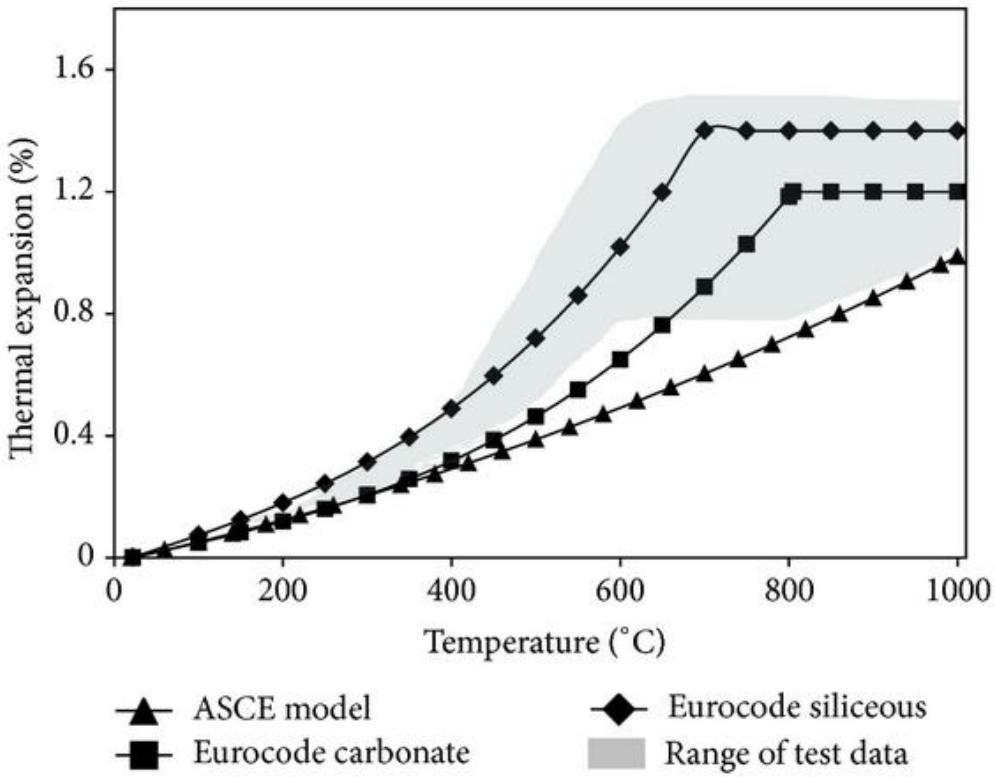

Figure 4-24: Thermal expansion of Concrete(Kodur 2014)

Eurocodes accounts for the effect of type of aggregate on variation of thermal expansion than of concrete with temperature. Concrete made with siliceous aggregate has a higher thermal expansion than that of carbonate aggregate concrete. However, ASCE provisions provide only one variation for both siliceous and carbonate aggregate concrete.

The strength of concrete and presence of fiber have moderate influence on thermal expansion. The rate of expansion for HSC and fiber-reinforced concrete slows down between 600–800°C; however the rate of thermal expansion increases again above 800°C. The slowdown in thermal expansion in the 600–800°C range is attributed to the loss of chemically bound water in hydrates, and the increase in expansion above 800°C is attributed to a softening of concrete and excessive micro- and macrocrack development. (Kodur V. , 2014)

4.4.4.2 Thermal expansion of steel

Steel rebar show elongation behavior under elevated temperatures. If the grades of rebar was higher it shows less elongation and it depends on ductile behavior of the steel. At high temperatures the steel reinforcement show ductile behavior and it causes increase in deflection of the structural members. The elongation ratio were increased up to 300°C, while the material becomes brittle with decrease of the elongation values.

The elongation ratios were slightly increased up to 300°C, however, above this temperature material becomes brittle with decrease of the elongation values. According to EN 1993.1.2 the relative thermal elongation of steel $\Delta l/l$ should be determined from the following:

For $20℃ \leq \theta_a < 750℃$

$$\frac{\Delta l}{l} = 1.2 \times 10^{-5}\theta_a + 0.4 \times 10^{-8}\theta_a^2 - 2.416 \times 10^{-4}$$

For $750℃ \leq \theta_a < 860℃$

$$\frac{\Delta l}{l} = 1.1 \times 10^{-2}$$

For 860℃ $\leq \theta_a <$ 1200℃

$$\frac{\Delta l}{l} = 2 \times 10^{-5}\theta_a - 6.2 \times 10^{-3}$$

Where

l is the length at 20℃

Δl is the temperature induced elongation

θ_a is the steel temperature (℃)

The variation of the relative thermal elongation with temperature is illustrated in Figure 4-25.

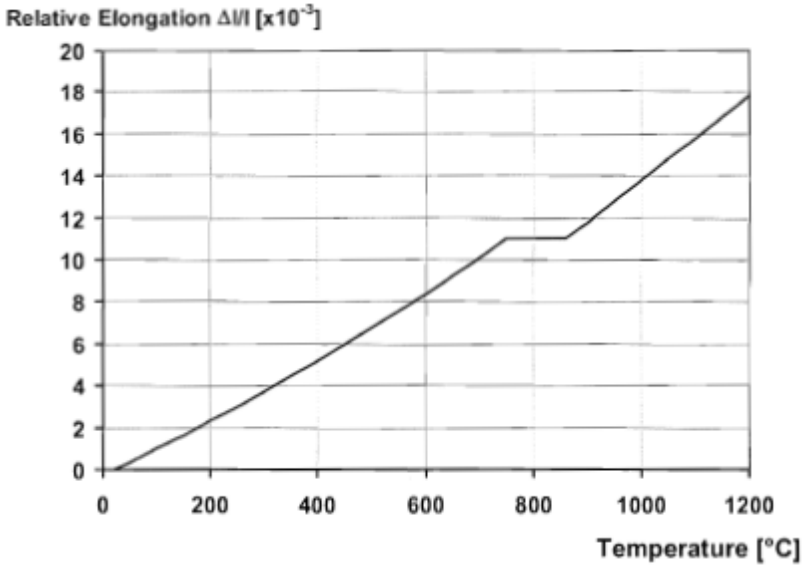

Figure 4-25: Relative thermal elongation of carbon steel as a function of the temperature

This behavior is not sufficient for rebar steel in reinforced concrete structures. In this study the steel bars are considered to have a fixed expansion of1.1×10^{-2}.

4.4.5 Spalling properties

There are large number of factors that are interdependence and makes prediction of spalling quite complex. A review of the literatures presents that major causes for fire induced spalling in concrete are low permeability of concrete and moisture migration in concrete at elevated temperatures. In many laboratory tests explosive spalling has been observed which refers to a sudden and violent braking away of a surface layer concrete. (Diederichs, Jumppanen, & Schneider, 1995) (Castillo, C. , Durrani, A.J., Jan-Feb 1990) (Phan L. , 2005) (Phan, L.T., Carion, N.J., 2003) (Kodur V. , 2003) (Kalifa, P., Menneteau, D., Quendard, D., 2000).

Two theories has been presented for explaining of this phenomenon.

1- Pressure Build-Up

According to this theory, spalling is caused by the increasing of pore pressure during heating. Free water residing in the concrete pores and chemically-bound water in the concrete matrix undergo transformation from liquid to a gaseous phase. The extremely high water vapor pressure, generated during exposure to fire, cannot escape due to the high compactness and low permeability of higher strength concrete. So concrete especially HPC has inability to successfully mitigate the buildup of internal pressure as, expand in volume, and transport through the concrete with increasing concrete temperature. (Phan l. , 2007) When the effective pore pressure (porosity times pore pressure) exceeds the tensile strength of concrete, chunks of concrete fall off from the structural member. This pore pressure is considered to drive progressive failure; that is, the lower the permeability of concrete, the greater the fire induced spalling. This falling-off of concrete chunks can often be explosive depending on fire and concrete characteristics.

2- Restrained thermal dilation. (Kodur V. K., May 2000) .

This hypothesis considers that spalling results from restrained thermal dilatation close to the heated surface, which leads to the development of compressive stresses parallel to the heated surface. These compressive stresses are released by brittle fracture

of concrete (spalling). The pore pressure can play a significant role on the onset of instability in the form of explosive thermal spalling (Bažant, 1997)

Although spalling might occur in all concretes, high-strength concrete is believed to be more susceptible to spalling than normal-strength concrete because of its low permeability and low water-cement ratio. Another factors such as strength, aggregate type, relative humidity, amount of silica fume, and other admixtures are interdependent and influence on spalling. But the most significant factor is the variation of porosity with temperature which is higher in HSC than NSC. (Dwaikat, M.B., Kodur, V.K.R., 2009)

The additions of PP fibers cause a significant reduction in maximum pore pressure and prevent explosive spalling. The polypropylene fibers melt when temperatures in concrete reach about 160–170°C and this creates pores in concrete that are sufficient for relieving vapor pressure developed in the concrete.

4.5 Acting Loads

Let us now calculate the acting forces on the slab and beam. It is assumed that the most appropriate static scheme which has the maximum positive moment is a simply supported beam. Regarding load combinations, one load combination as suggested by EUR codes has been considered. This load has been used for design of the beam in ambient temperature. The loads acting on beam are: permanent loads, imposed loads and live loads.

4.5.1 Permanent loads (G_{1k})

Permanent load is a constant load over time in a structure (slab, beam, or …) that is due to the weight of the members itself. Permanent loads are also known as dead loads or static loads. Weight of a member may be usually determined as a product of the volume and the density.

The determination of the characteristic values of self-weight, and of the densities shall be in accordance with EN 1990, given in Table 4-7.

Materials	Density γ [kN/m^3]
concrete (see EN 206)	
lightweight	
density class LC 1,0	9,0 to 10,0 [1)2)]
density class LC 1,2	10,0 to 12,0 [1)2)]
density class LC 1,4	12,0 to 14,0 [1)2)]
density class LC 1,6	14,0 to 16,0 [1)2)]
density class LC 1,8	16,0 to 18,0 [1)2)]
density class LC 2,0	18,0 to 20,0 [1)2)]
normal weight	24,0 [1)2)]
heavy weight	> [1)2)]
mortar	
cement mortar	19,0 to 23,0
gypsum mortar	12,0 to 18,0
lime-cement mortar	18,0 to 20,0
lime mortar	12,0 to 18,0
[1)] Increase by 1kN/m^3 for normal percentage of reinforcing and pre-stressing steel [2)] Increase by 1kN/m^3 for unhardened concrete	
NOTE See Section 4	

Table 4-7: nominal density of construction materials

In this study the permanent load on the beam is the summation of self-weight of the slab and self-weight of the beam itself which is equal to $G_{1k} = 2.395\ KN/m$.

4.5.2 Imposed loads (G_{2k})

Imposed loads on buildings are those arising from occupancy and the values given include:

- Normal use by persons;

- Furniture and moveable objects;

- Vehicles;

- Rare events such as concentrations of people and furniture, or the moving or stacking of objects during times of reorganization and refurbishment.

The imposed loads specified in this part are modelled by uniformly distributed loads. For the determination of the imposed loads, floor and roof areas in buildings should be sub-divided into categories according to their use.

Category	Specific Use	Example
A	Areas for domestic and residential activities	Rooms in residential buildings and houses; bedrooms and wards in hospitals; bedrooms in hotels and hostels kitchens and toilets.
B	Office areas	
C	Areas where people may congregate (with the exception of areas defined under category A, B, and D[1)])	**C1**: Areas with tables, etc. e.g. areas in schools, cafés, restaurants, dining halls, reading rooms, receptions. **C2**: Areas with fixed seats, e.g. areas in churches, theatres or cinemas, conference rooms, lecture halls, assembly halls, waiting rooms, railway waiting rooms. **C3:** Areas without obstacles for moving people, e.g. areas in museums, exhibition rooms, etc. and access areas in public and administration buildings, hotels, hospitals, railway station forecourts. **C4**: Areas with possible physical activities, e.g. dance halls, gymnastic rooms, stages. **C5**: Areas susceptible to large crowds, e.g. in buildings for public events like concert halls, sports halls including stands, terraces and access areas and railway platforms.
D	Shopping areas	**D1:** Areas in general retail shops **D2**: Areas in department stores

[1)] Attention is drawn to 6.3.1.1(2), in particular for C4 and C5. See EN 1990 when dynamic effects need to be considered. For Category E, see Table 6.3

NOTE 1 Depending on their anticipated uses, areas likely to be categorised as C2, C3, C4 may be categorised as C5 by decision of the client and/or National annex.

NOTE 2 The National annex may provide sub categories to A, B, C1 to C5, D1 and D2

NOTE 3 See 6.3.2 for storage or industrial activity

Figure 4-26; Category of imposed loads

Table 6.2 - Imposed loads on floors, balconies and stairs in buildings

Categories of loaded areas	q_k [kN/m^2]	Q_k [kN]
Category A		
- Floors	1,5 to2,0	2,0 to 3,0
- Stairs	2,0 to4,0	2,0 to 4,0
- Balconies	2,5 to 4,0	2,0 to 3,0
Category B	2,0 to 3,0	1,5 to 4,5
Category C		
- C1	2,0 to 3,0	3,0 to 4,0
- C2	3,0 to 4,0	2,5 to 7,0 (4,0)
- C3	3,0 to 5,0	4,0 to 7,0
- C4	4,5 to 5,0	3,5 to 7,0
- C5	5,0 to 7,5	3,5 to 4,5
category D		
- D1	4,0 to 5,0	3,5 to 7,0 (4,0)
- D2	4,0 to 5,0	3,5 to 7,0

Table 4-8: Imposed loads on floors, balconies and stairs in buildings according to Eurocode

NOTE Values for qk and Qk are given in Table 4-8. In this study the slab is considered in category A so $G_{2k} = 2\ KN/m$ (considering one meter length of slab).

4.5.3 Variable loads (Q_{1k})

A moving, variable weight added to the dead load or intrinsic weight of a structure.
$Q_{1k} = 2\ KN/m$

4.5.4 Load combination

Load combination suggested by Eurocode is :

$$G_{1k} + G_{2k} + Q_{1k} \qquad \text{Eq. (1)}$$

$$= 2.395 + 2 + 2 = 6.395\ KN/m$$

4.5.5 Acting Bending moment and shear force

On the basis of these considerations it is possible to calculate the acting bending moment and shear force for the beam with span of 6 meters.

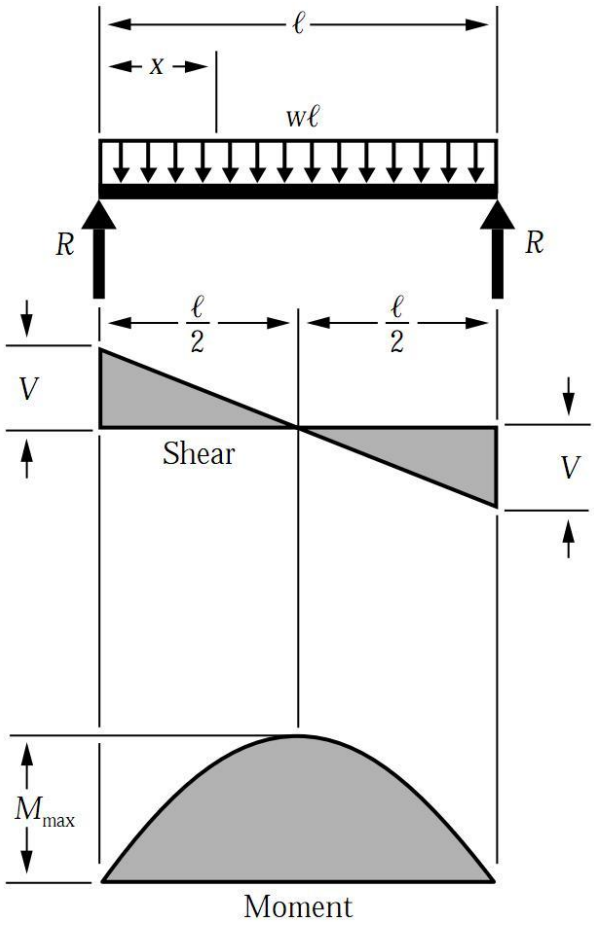

Acting moment (M_{Ed}) and shear (V_{Ed}) for a simple supported beam in the center is:

$$M_{Ed} = \frac{wl^2}{8} = \frac{6.39(6)^2}{8} = 28.75\ KN.m$$

5 : 2D model

5.1 Introduction

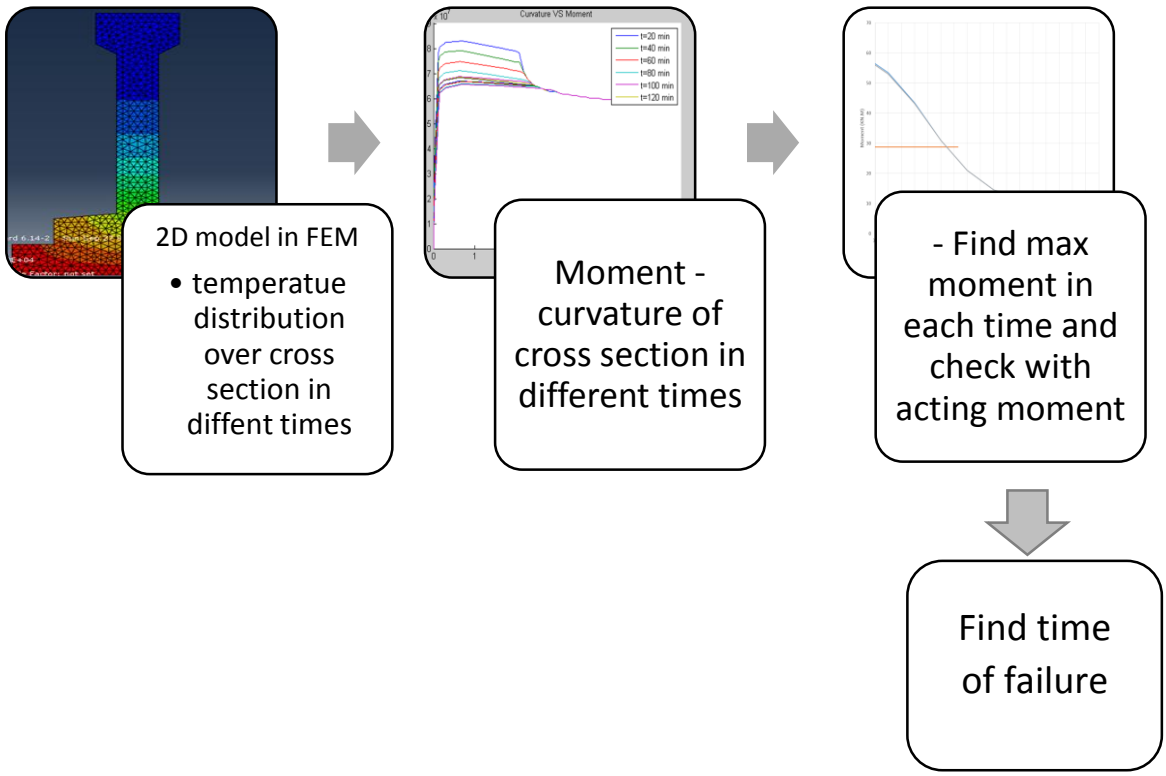

Figure 5-1: main procedure of the plane section approach

The aim of this chapter is to find the time of failure when beam is exposed to fire. To reach this aim, it is necessary to follow the plane section approach to find the bearing capacity of the beam section in the middle of the span and compare it with maximum acting moment.

5.2 Creating numerical model

The section was modelled in Abaqus CEA software in order to find the temperature distribution over the cross section in different times of exposure. The software program requires number of parameters and characteristics' inputs to analyze the problem. The following steps have been used to produce the model and read the results.

5.2.1 Part

In Abaqus there is a section which called "Part". In this section model can be drawn by knowing the geometry of the beam. The coordinates of the points were determined in meter unit, therefore in all other sections, if it is referred to length, the unit is considered to be in meter.

Part attributes:

Part: "HPC", Modeling space: 2D Planar, Type: Deformable

It is a shell part (1 shell face, 17 edges and 17 vertices)

Coordinates of the points:

Points	Coordinates (x, y, z)	points	coordinates(x, y, z)
1	0., 0. , 0.	10	-30.E-03,255.E-03,0.
2	90.E-03,0.,0.	11	-30.E-03,225.E-03,0.
3	90.E-03,30.E-03,0.	12	-15.E-03,215.E-03,0.
4	60.E-03,30.E-03,0.	13	-15.E-03,60.E-03,0.
5	60.E-03,55.E-03,0.	14	-60.E-03,55.E-03,0.
6	15.E-03,60.E-03,0.	15	-60.E-03,30.E-03,0.
7	15.E-03,215.E-03,0.	16	-90.E-03,30.E-03,0.
8	30.E-03,225.E-03,0.	17	-90.E-03,0.,0.
9	30.E-03,255.E-03,0.		
Number of geometries: 17 & Number of constraints: 21			

Table 5-1: Coordinates of he point in 2D model

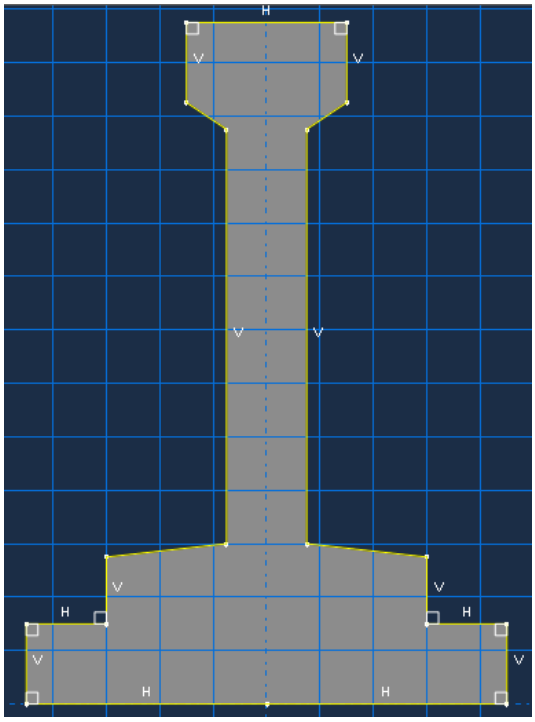

Figure 5-2: create part (Geometry of the beam)

5.2.2 Property

In this part the property of the material used for beam is defined. The material used for beam is high performance fiber reinforced concrete (HPFRC), therefore the required fields were filled with the data of HPFRC given in chapter 2. It is summarized in continue;

1- Density (General properties)

Used as uniform distribution and temperature dependent data

Density (kg/m3)	2300	2300	2250	2250
Temperature (C)	20	70	120	1220

Table 5-2: Density over temp input of numerical model

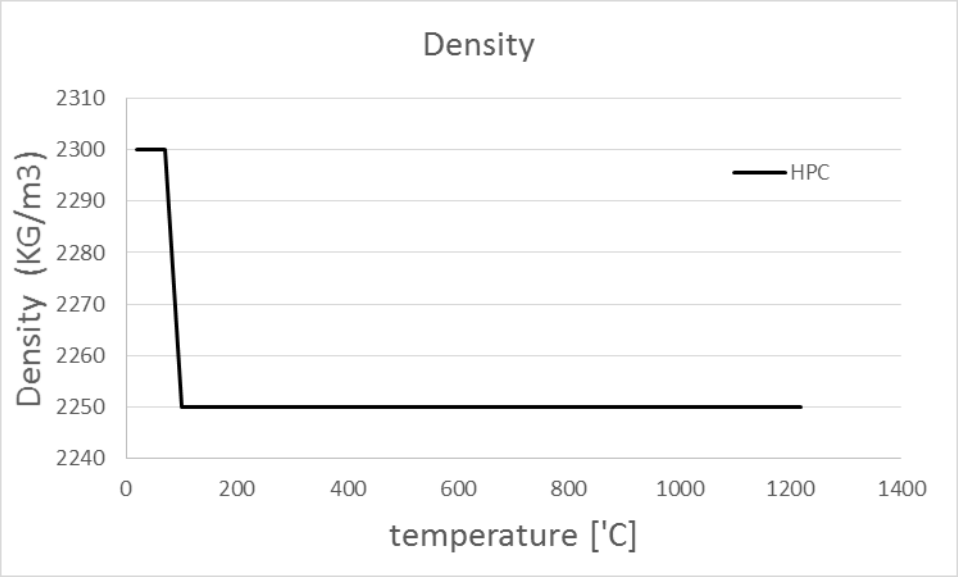

Figure 5-3: Density over temperature of HPC

2- Conductivity (Thermal properties)

Used type as isotropic and temperature dependent data

Temperature (°C)	Conductivity (W/MK)	Temperature (°C)	Conductivity (W/MK)
20	1.960333	570	1.13075
70	1.864083	620	1.080333
100	1.808333	670	1.034083
120	1.772	720	0.992
150	1.71875	770	0.954083
170	1.684083	820	0.920333
200	1.633333	870	0.89075
220	1.600333	920	0.865333
270	1.52075	970	0.844083
320	1.445333	1020	0.827
370	1.374083	1070	0.814083
420	1.307	1120	0.805333
470	1.244083	1170	0.80075
520	1.185333	1220	0.800333

Table 5-3: Conductivity over temperature input of numerical model

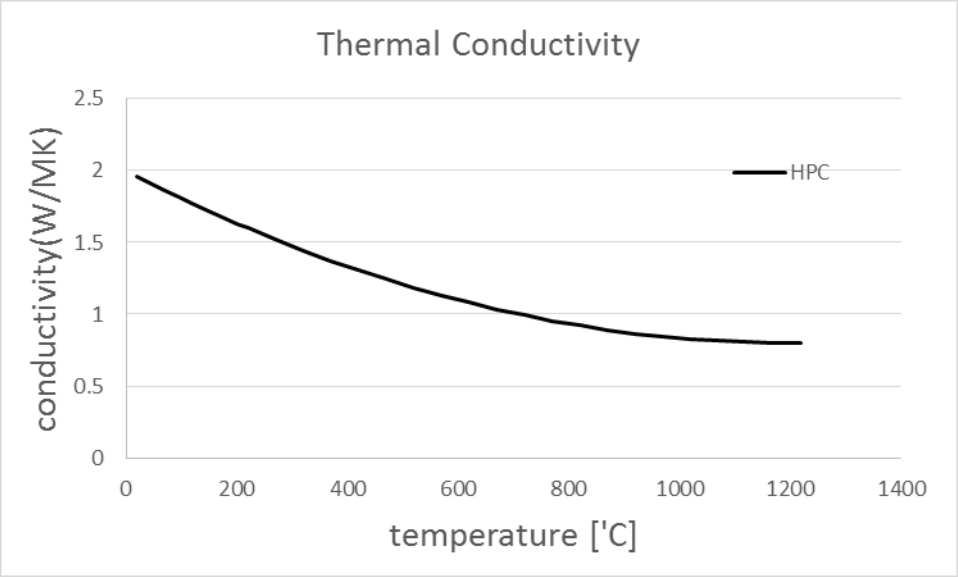

Figure 5-4: Thermal conductivity of HPC

3- Specific Heat (Thermal properties)

Used constant volume and temperature dependent data.

Temperature (C)	Specific Heat(J/kgK)	Temperature (C)	Specific Heat(J/kgK)
20	913.2222	570	1189.75
70	945.3056	620	1206.556
100	963.8889	670	1221.972
120	976	720	1236
150	993.75	770	1248.639
170	1005.306	820	1259.889
200	1022.222	870	1269.75
220	1033.222	920	1278.222
270	1059.75	970	1285.306
320	1084.889	1020	1291
370	1108.639	1070	1295.306
420	1131	1120	1298.222
470	1151.972	1170	1299.75
520	1171.556	1220	1299.889

Table 5-4: temperature-specific heat value for concrete input of Abaqus

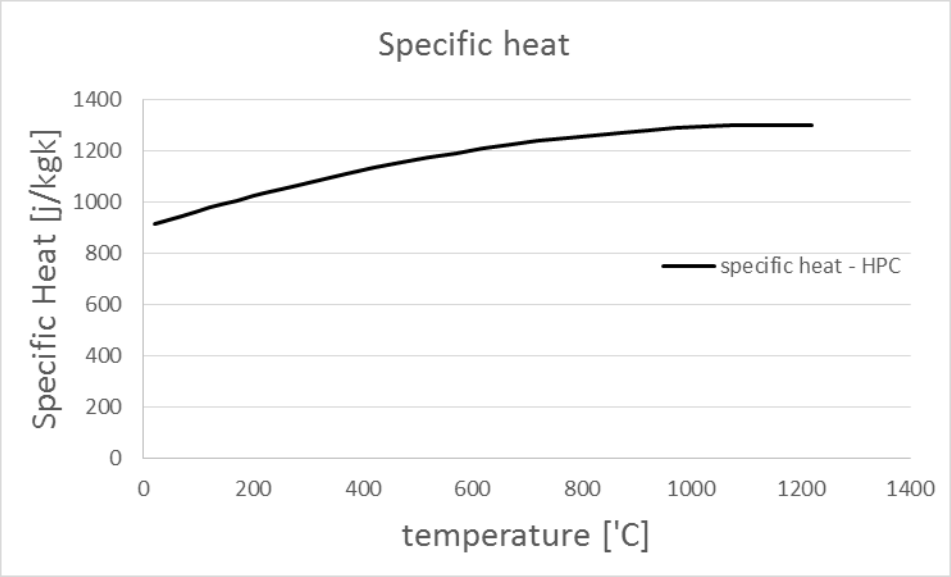

Figure 5-5: Specific heat over temperature

Note: the results using specific heat with peak is more and less similar to final results of using specific heat without peak. Therefore in order to be also in conservative side it is assumed that there is no peak in the trend.

After defining the material it is possible to assign the material to the beam section drawn in previous part.

5.2.3 Assembly

In this part the model can be assembled if there are more than one parts in different stances and postures. Since here the geometry of beam consists only one part, it is simply assembled as it is.

5.2.4 Step

Defining the procedure or method to analyze the problem has been considered in step. Since the problem refers to beam exposed to fire and we want to know the temperature distribution the procedure type is chosen as “General Heat transfer”. The basic inputs are time period which is equal to time of fire exposure 12000 seconds (Time period of ISO834 is 200 minutes). The response is consider as transient which is closer

to what happens in reality rather than steady-state (Explained in chapter2). The results will be found in specific times according to incrementation. Maximum number of increments is 10000. Increment sizes are: Initial=30, minimum=5 and maximum=60 seconds. Maximum allowable temperature change per increment is 20 and maximum allowable emissivity change per increment is 0.1. The equation solver method is direct and matrix storage is solver default. Solution techniques is full newton and default load variation with time is instantaneous. Extrapolation of previous state at start of each increment is considered linear.

The output is assumed to be found as thermal results which is nodal temperature and heat flux vector at each increment for the whole model.

5.2.5 Interaction

The interaction is the part where the fire will be defined by introducing two parameters. First, surface film condition (Embedded coefficient) which is defined for heat transfer step and has been assigned to the bottom side of the beam where fire has effect. Film coefficient is 15 and is instantaneous, sink definition is uniform with temperature of 1. Table of time-temperature ISO834 is used for sink amplitude. Second parameter is surface radiation which is also defined in heat transfer step. Radiation type is to ambient and it has been assigned to the bottom side of the beam. Emissivity distribution is uniform for simplicity. Emissivity is 0.5, ambient temperature is 1 and amplitude by table of time-temperature of ISO834. Second parameter illustrates radiation while the first one means both convection and conduction.

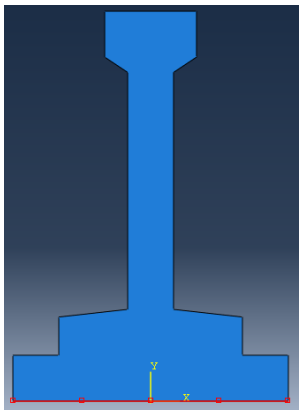

Figure 5-6: interaction assigned to the bottom side of the beam

5.2.6 Load

In this part loads, boundary conditions and predefined fields can be defined into the model. Since this numerical model is aimed to render the thermal results there is no need to input loads or constrains to the model and only by selecting predefined temperature field in initial step, the temperature of 20 can be assigned to the whole model.

5.2.7 Mesh

Meshing is very important in numerical analyses because type and number of meshes can affect the results. Triangle was used as element shape of mesh which gives better results rather than rectangular. Element type was selected as standard library, linear geometric order and heat transfer family. Meshing was done in part object with sizes approximately equal to 0.005 (m). Total number of nodes are 771 and total number of elements are 1358.

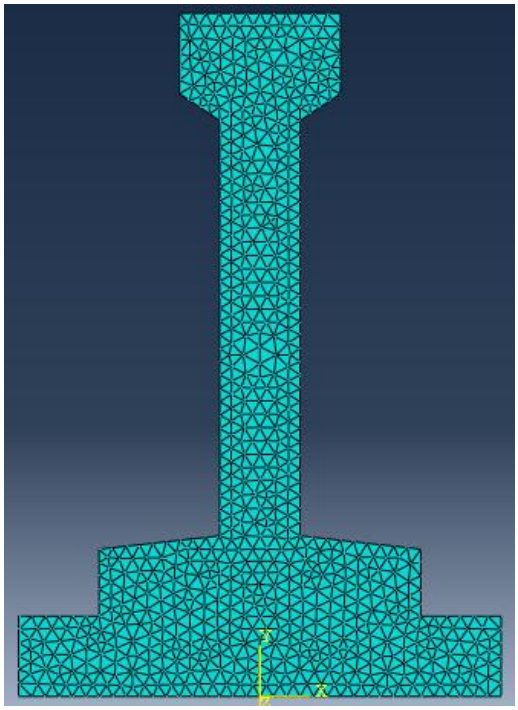

Figure 5-7: Mesh elements of the beam section

5.2.8 Job and visualization

By creating a job, it is possible to run the model. The results will be presented in visualization part. In this part the results can be presented over depth of the section (field output) and/or over time of exposure (history output). Figure 5-8/4-7 shows nodal temperature and heat flux at the end of exposure period. This results can also be extracted for other times.

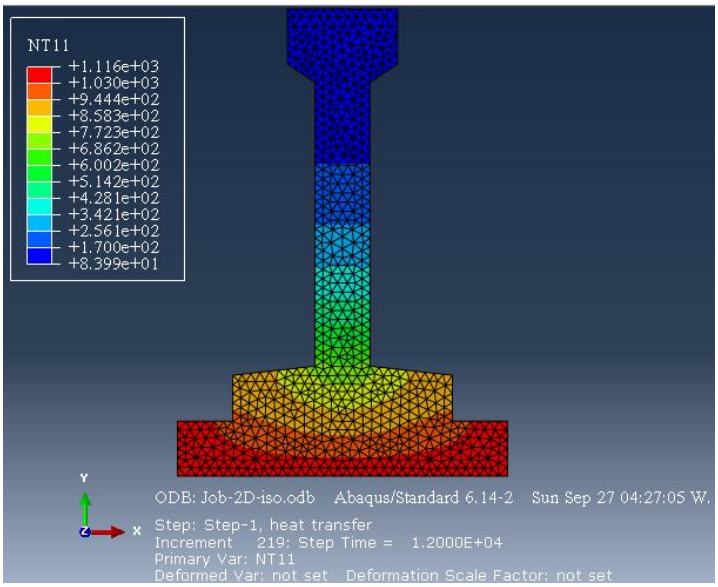

Figure 5-8: Nodal temperature after 200 min

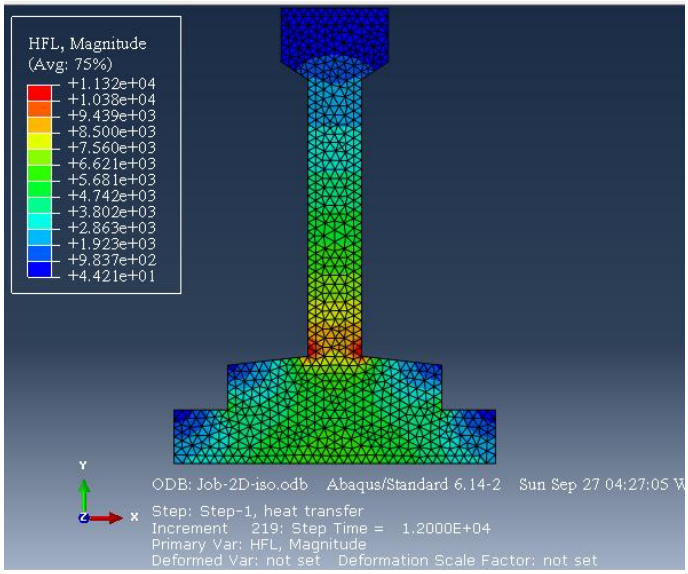

Figure 5-9: Heat Flux after 200 min

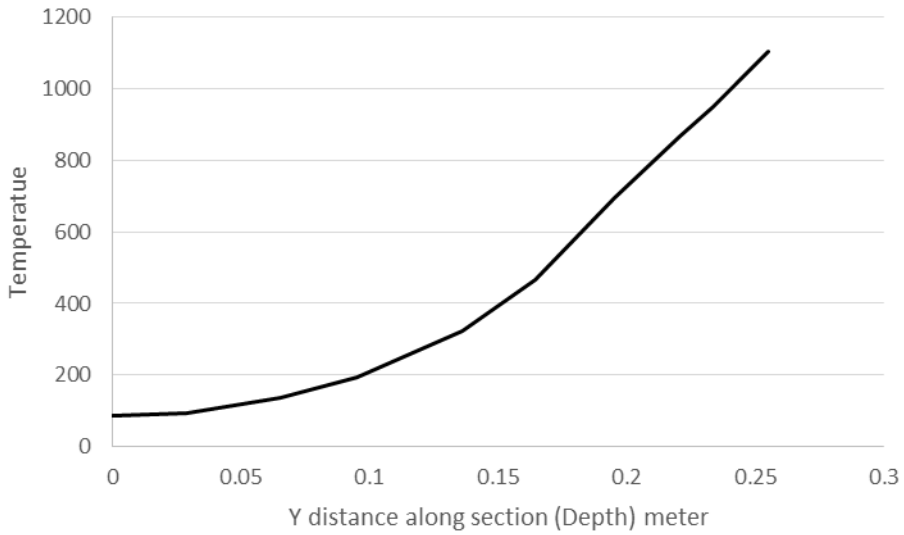

Figure 5-10: Field output (temperature over depth of cross section after 200 min)

Figure 5-10 shows the result of nodal temperature at the end of the period over the center line of cross section (zero is top of the beam and 0.25 m is located at bottom of the beam). In case of need for other times it is possible to render the results for those times by simply change the time step.

5.3 Fire analysis

The steps for producing model and find the results were explained above. In the following, the required results and the way to apply them for plane section analysis will be described in details.

5.3.1 Find temperature distribution

The first goal of this chapter is to reach the temperature distribution over the cross section. By knowing the temperature distribution, it is possible to find the strength and modulus elasticity degradation for steel and concrete in different layer of the section. These parameters are required to calculate bending moment capacity. To achieve this aim number of points in different layers of section were chosen in order to find their temperature over time. These points are shown in Figure 5-11.

.

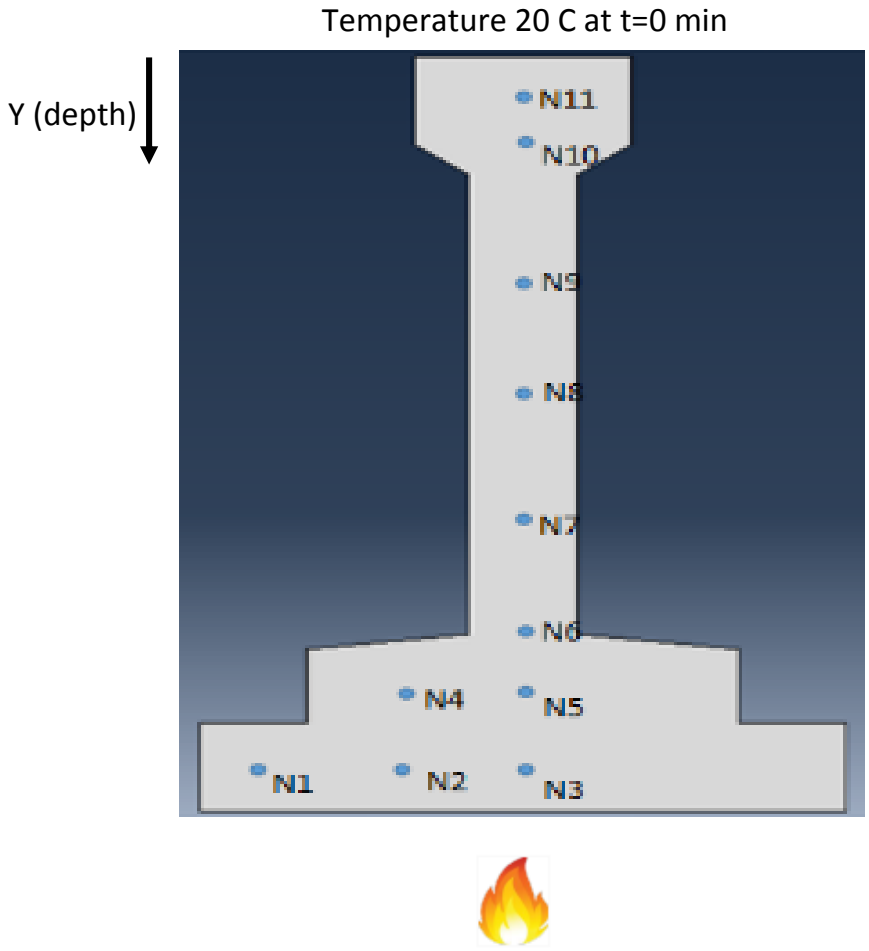

Figure 5-11: Defining points over cross section

The results obtained from model were extracted on these 11 nodes (8 layers). For the first two layers an average value of temperature in corresponding nodes has been considered ($T_{layer1} = \frac{(T_{N1}+T_{N2}+T_{N3})}{3}$ and $T_{layer2} = \frac{(T_{N4}+T_{N5})}{2}$) while for the other layers its assumed that the temperature is equal to the temperature of corresponding node($T_{layeri} = T_{Ni}$).

Temperature distribution varies over depth as well as over time. Therefore for each node it is needed to find the temperature in different times. Figure 5-12 shows temperature variation over time in each 11 nodes. As well as, it is possible to find temperature over section in different time steps which will be used later in plane section approach (Figure 5-13).

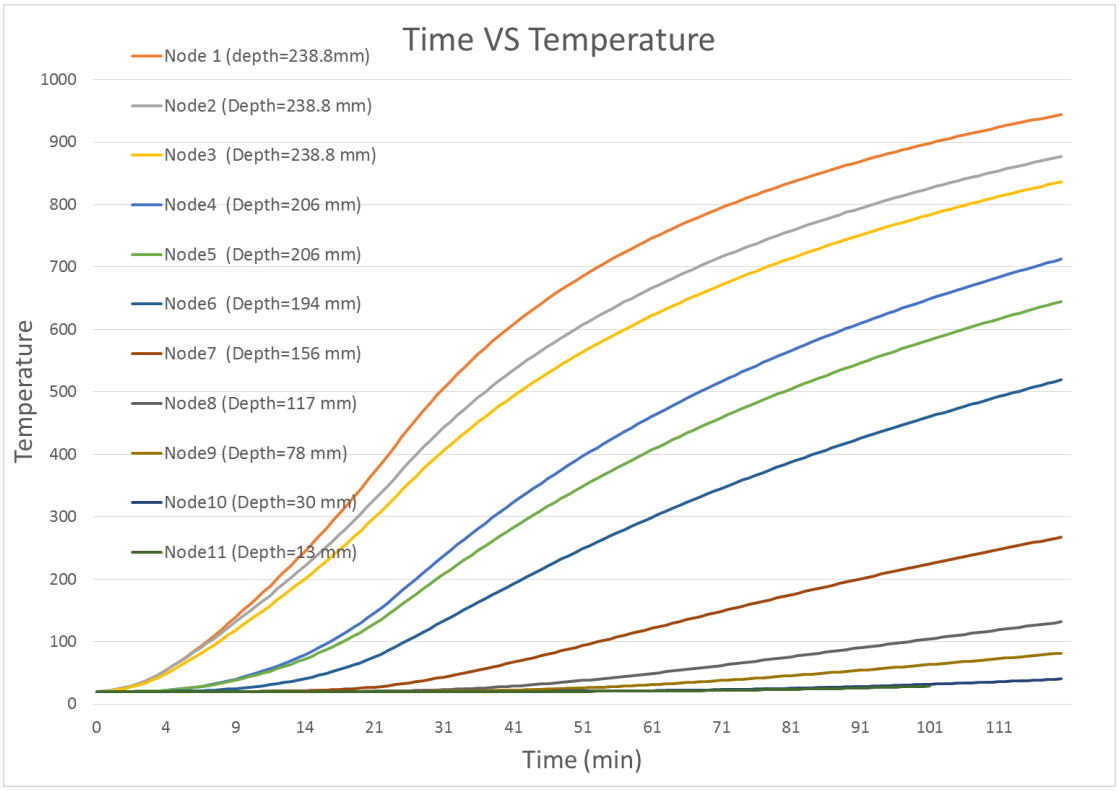

Figure 5-12: Temperature over time in different nodes

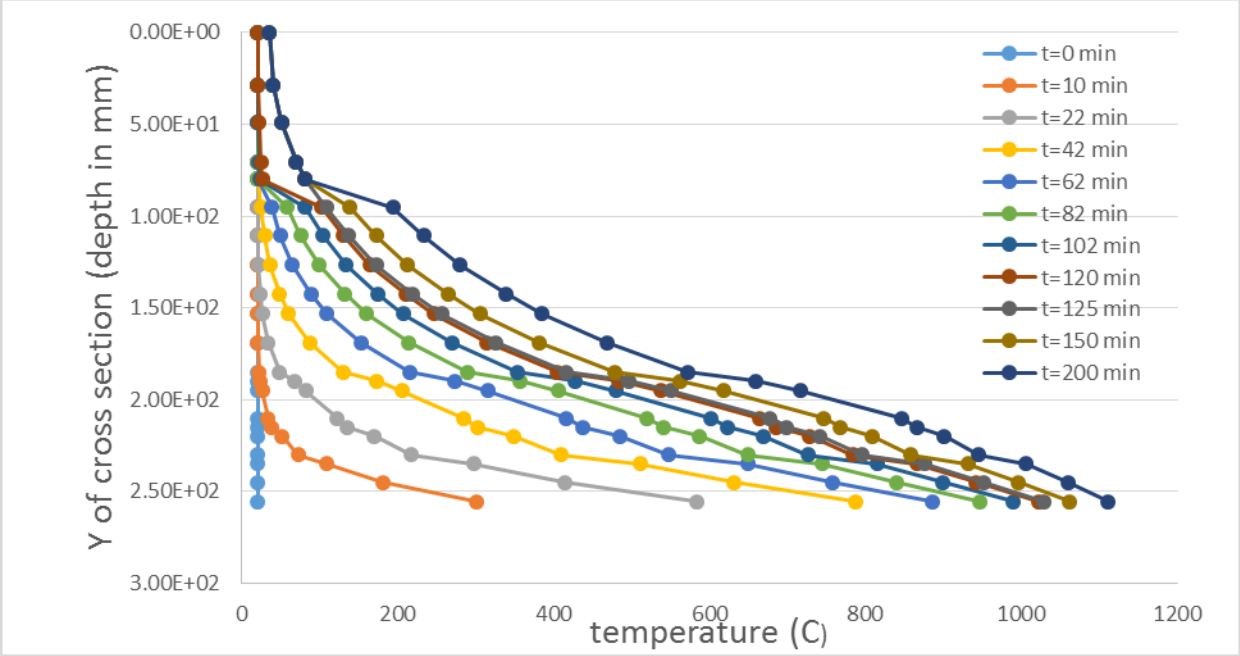

Figure 5-13: Temperature distribution of section in different times

5.4 Plane section approach

The bending moment vs. curvature diagrams are obtained following a plane section approach and the provisions provided by the Fib Model Code 2010.

In case of fire exposure the material suffers degradation. Since the temperature varies over time this degradation also differs over time. By fixing time, it is possible to find degradation of material which gives us constitutive laws and finally the bearing capacity of the section.

The process of finding bending moment capacity of the beam section has been done by Matlab code using finite element method. This code requires temperature distribution over the cross section (which has already obtained in previous part), then it automatically considered its corresponding degradation in different layers of the beam according to coefficients given by Eurocode. By fixing a specific curvature the Matlab code look for a neutral axis imposing translational equilibrium. After finding neutral axis, strains in tension and compression zones are known and it is possible to find the stress in each layer according to constitutive laws already defined. Finally, bending moment of the section can be calculated by integrating the stresses over cross section multiplying by its distance. The failure mode were estimated on the basis of the simplified piecewise-linear constitutive laws were derived for both the fiber-reinforced matrix and the reinforcing bars. It is worth noticing that the acceptable failing in HPFRC beams are those with flexural failure and not brittle. This procedure should be repeat for the next curvature until the whole diagram of moment-curvature is achieved and also should be done for the next time of exposure. The whole process has been shown in an algorithm in the following page.

Geometry of the section, Characteristic length

Temperature distribution over section in a fixed time

Bars, Fibers and Concrete Properties in T=20C

Constitutive laws in Tension and Compression

Discretize the section

Discretize the curvature axis

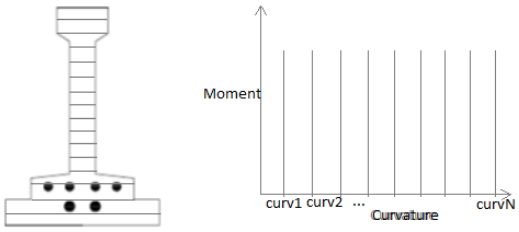

Calculate degradation of material Properties

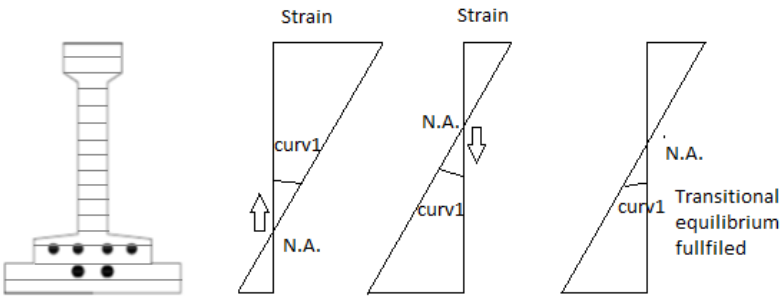

Constitutive laws for damaged materials in tens. and Comp.

i=1

$\vartheta = \vartheta_i$

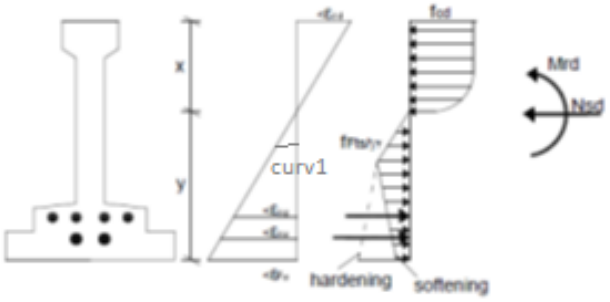

Translational Equilibrium and find Neutral Axis (NA)

Bending moment capacity

i=i+1

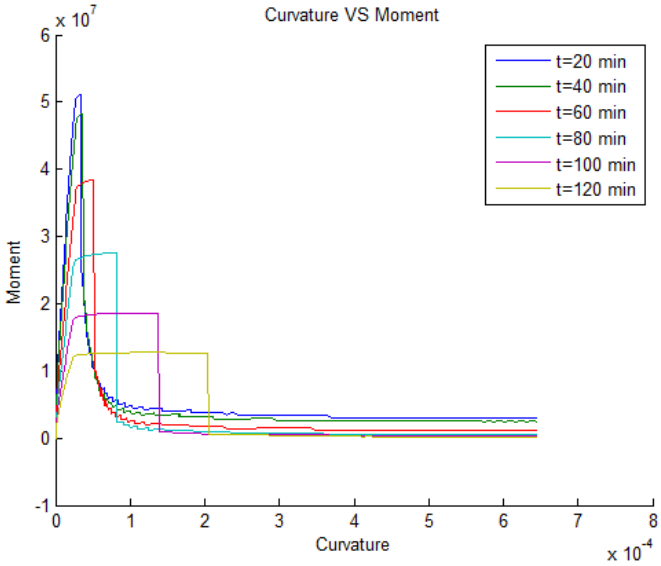

Moment curvature curves

5.4.1 Section Geometry and Discretization

The primary step of performing plane section analysis is defining geometry and then discretizing the cross section. The Geometry in Matlab code is defined by rectangular giving the depth and width. So the inputs are:

Depth (mm)	Width (mm)
0	60
30	60
40	30
195	30
200	120
225	120
225.00001	180
255	180

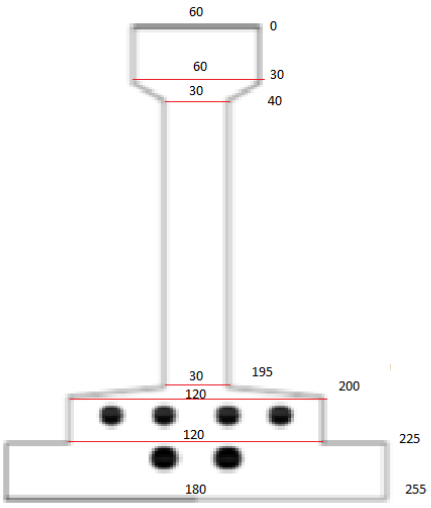

Figure 5-14: Defining geometry in Matlab code

Discretizing of section performed horizontally dividing into 30 parts. In Matlab code, the input is "n_sez=30" in PS_SFRC_tegolo2.m script.

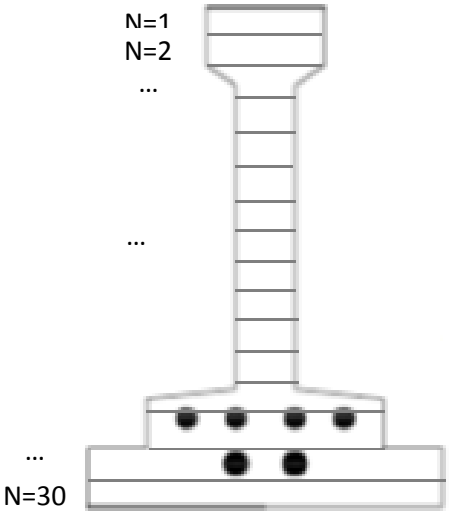

Figure 5-15: Discretization of cross section

Define characteristic length

Characteristic length has been calculated in chapter 3. This value is needed for converting displacement to strain. The summarized result of characteristic length is as follows:

$l_{cs} = \min(s_{rm} = 1.5 l_{s,max}, y)$

$$l_{s,max} = kc + \frac{1}{4}\frac{(f_{ctm} - f_{Ftsm})}{\tau_{bms}}\frac{\emptyset_s}{\rho_{s,ef}}$$

Where

$k = 1.0$ Empirical parameter (effect of concrete cover)

$c = 22$ mm concrete cover

$\tau_{bm} = 1.8 f_{ctm} = 10.08\ Mpa$ is the mean bond strength between steel and concrete

$f_{ctm} = 5.6\ Mpa$ Mean concrete tensile strength

$f_{Ftsm} = 5.067\ Mpa$

$\emptyset_s = 10\ mm$ Rebar diameter

$\rho_{s,ef} = \frac{A_s}{A_{c,ef}} = 0.058$ Effective reinforcement ratio

$A_{c,ef}$ Effective area of concrete in tension

$l_{s,max} = 24.27\ mm \longrightarrow l_{cs} = \min(1.5 \times l_{s,max}, 180) = 36.40\ mm$

In Matlab code this value is located in PS_SFRC_tegolo2.m script as `lcar=24.27*1.5 and lcar_leg=lcar.`

5.4.2 Temperature distribution over section in a fixed time

The output of numerical modelling (Abaqus) is needed in this part because in continue the temperature of each layer is needed. This input for Matlab is a text file using results of part 4.3.1 . First row is time in minutes, first column is depth of cross section and the values inside are the temperatures at the corresponding time and depth. (These values are the same as Figure 5-13)

0	0	9.35	21.96666667	41.65	61.65	81.65	101.65	120	124.65	150.65	200
0.00E+00	20	20	20	20	20.0001	20.0053	20.0542	20.2522	35.3878	35.3878	35.3878
2.90E+01	20	20	20	20	20.0009	20.0227	20.1602	20.5846	39.7535	39.7535	39.7535
4.89E+01	20	20	20	20.0001	20.0054	20.0942	20.5225	21.5984	50.5062	50.5062	50.5062
7.06E+01	20	20	20	20.0011	20.0297	20.3563	21.567	24.1044	69.8024	69.8024	69.8024
8.01E+01	20	20	20	20.0026	20.06	20.6091	22.423	25.9418	80.6489	80.6489	80.6489
9.51E+01	2.00E+01	2.00E+01	2.02E+01	2.47E+01	3.82E+01	5.80E+01	8.07E+01				
1.11E+02	2.00E+01	2.00E+01	2.05E+01	2.88E+01	4.90E+01	7.55E+01	1.04E+02				
1.27E+02	2.00E+01	2.00E+01	2.13E+01	3.58E+01	6.46E+01	9.88E+01	1.34E+02				
1.42E+02	2.00E+01	2.00E+01	2.32E+01	4.79E+01	8.82E+01	1.32E+02	1.74E+02				
1.53E+02	2.00E+01	2.01E+01	2.57E+01	5.99E+01	1.09E+02	1.60E+02	2.07E+02				
1.69E+02	2.00E+01	2.04E+01	3.31E+01	8.69E+01	1.53E+02	2.14E+02	2.69E+02				
1.85E+02	2.00E+01	2.16E+01	4.83E+01	1.30E+02	2.15E+02	2.89E+02	3.53E+02				
1.90E+02	2.00E+01	2.39E+01	6.70E+01	1.73E+02	2.73E+02	3.57E+02	4.28E+02				
1.95E+02	2.00E+01	2.63E+01	8.22E+01	2.05E+02	3.15E+02	4.05E+02	4.80E+02				
2.10E+02	2.00E+01	3.35E+01	1.22E+02	2.84E+02	4.16E+02	5.19E+02	6.01E+02				
2.15E+02	2.00E+01	3.78E+01	1.35E+02	3.02E+02	4.37E+02	5.41E+02	6.23E+02				
2.20E+02	2.00E+01	5.15E+01	1.70E+02	3.48E+02	4.85E+02	5.88E+02	6.68E+02				
2.30E+02	2.00E+01	7.21E+01	2.17E+02	4.10E+02	5.48E+02	6.49E+02	7.26E+02				
2.35E+02	2.00E+01	1.09E+02	2.98E+02	5.11E+02	6.48E+02	7.44E+02	8.15E+02				
2.45E+02	2.00E+01	1.81E+02	4.13E+02	6.32E+02	7.57E+02	8.40E+02	8.99E+02				
2.55E+02	2.00E+01	3.01E+02	5.83E+02	7.87E+02	8.85E+02	9.47E+02	9.90E+02				

5.4.3 Material Properties and their constitutive laws in ambient and degradation in high temperature

By knowing temperature distribution over the cross section, it is possible to apply the coefficient given by Eurocode for reducing young modulus, compression strength and tensile resistance of materials.

A) Bars properties and constitutive laws

Bars were not defined in the geometry of cross section in previous step. Therefore they are needed to define numerically in the code script. The area and location of bars were putted in main script (PS_SFRC_tegolo2.m) in the name of "barre" as follows;

```
barre=[210., 314.15;   [Area of the bars in 1st layer, its location (y)]
       233., 226.188]; [Area of the bars in 2nd layer, its location (y)]
```

Then for material properties of bars the inputs will be written in sforzzo_barre.m script. The values are the ones illustrated in chapter 3 part 3.52 and 3.5.3. As a summary the inputs of this part are ;

```
fsy_20=430.; fsp_20=300.; Es_20=205000.;
```

andamento_fsy=[20.,1.; 400., 1.; 500., 0.78; 600., 0.47; 700., 0.23; 800., 0.11; 900., 0.06; 1000., 0.04; 1100., 0.02; 1200., 0.];	andamento_fsp=[20.,1.; 100., 1.; 200., 0.81; 300., 0.61; 400., 0.42; 500., 0.36; 600., 0.18; 700., 0.07; 800., 0.05; 900., 0.04; 1000., 0.02; 1100., 0.01; 1200., 0.];	andamento_Es=[20.,1.; 100., 1.; 200., 0.9; 300., 0.8; 400., 0.7; 500., 0.6; 600., 0.31; 700., 0.13; 800., 0.09; 900., 0.07; 1000., 0.04; 1100., 0.02; 1200., 0.];

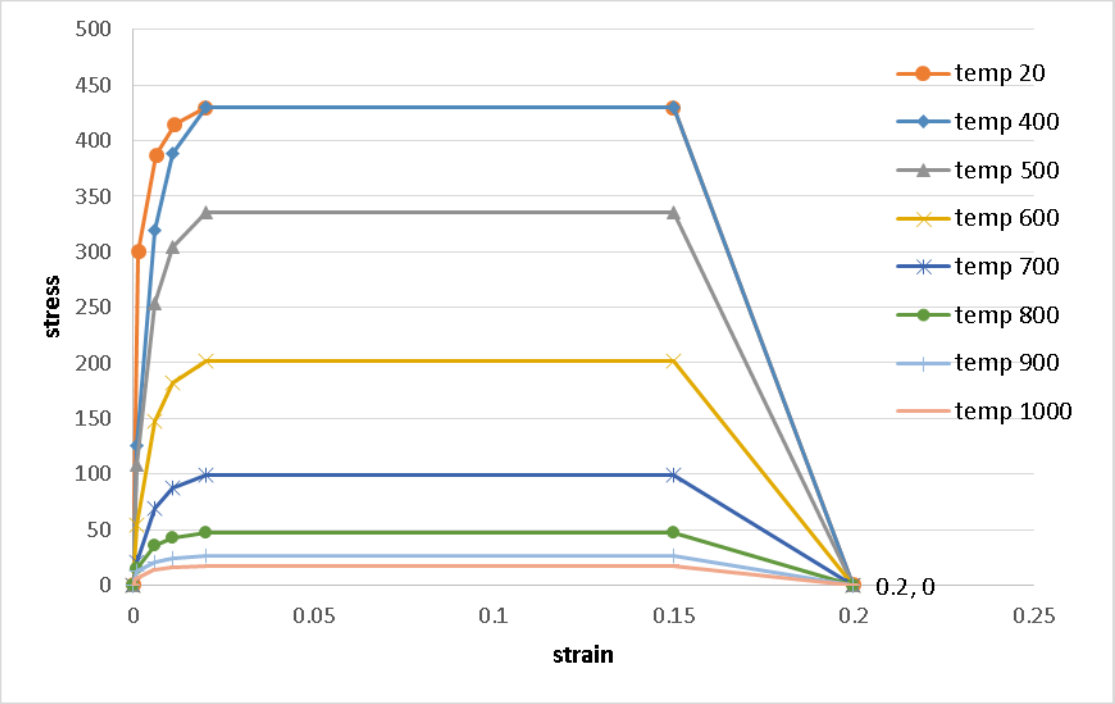

Figure 5-16: Constitutive law for steel bars at elevated temperature, Compression and tension

B) Concrete properties and constitute laws

It is assumed that concrete only work in compression zone and fibers are the only material that stands against tensile forces. Therefore, in Comprssione.m script the inputs are concrete properties which has been illustrated in chapter 3 part 3.5.3.1.1. As short the constitutive law is also presented in Figure 5-23

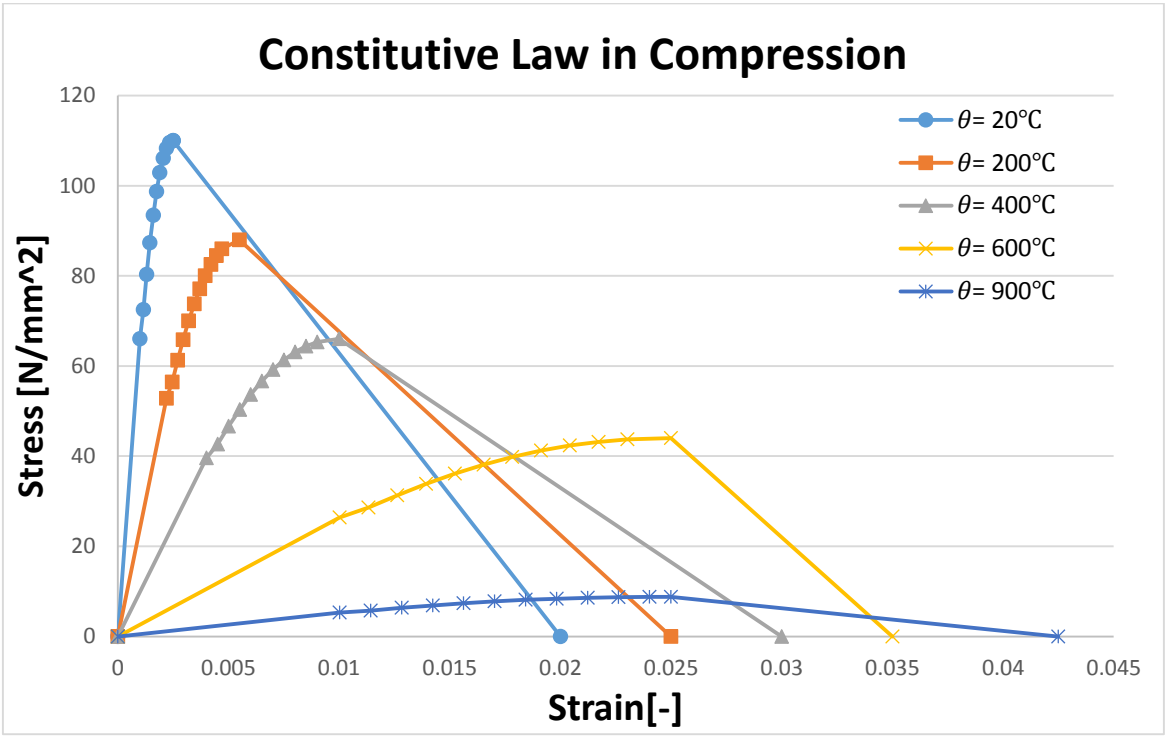

Figure 5-17: compressive stress- strain relationship of concrete c110 for different values of the concrete temperature. The descending branch is chosen to be linear. Based on a figure from the fib Bulletin 46 (2008)

```
fc_20=110.;
```

andamento_fc=[20, 1.; 200, 0.8; 400, 0.6; 600, 0.4; 900, 0.08; 1200, 0.];	andamento_ec1=[20., 0.0025; 100., 0.0040; 200., 0.0055; 300., 0.0070; 400., 0.01; 500., 0.015; 600., 0.025; 1100., 0.025];	andamento_ecu=[20., 0.02; 100., 0.0225; 200., 0.025; 300., 0.0275; 400., 0.03; 500., 0.0325; 600., 0.0350; 700., 0.0375; 800., 0.04; 900., 0.0425; 1000., 0.0450; 1100., 0.0475];

C) Fibers properties and constitutive laws

Fibers are the material that stands against tensile forces arising on cross section. The fiber properties has been already introduced in chapter 3 part 3.5.3.1.2 which should be input of Matlab script named "trazione.m'. To summarize they are;

Properties of fibers used in slab:

$f_{R1k} = 4$ Mpa, $f_{R3k} = 3.6$ Mpa

$f_{R3k}/f_{R1k} = 0.9 \rightarrow$ c Fiber class: 4C

```
feq006_20=4;%Mpa
feq063_20=3.6;%Mpa
fIf_20=5.78;%Mpa
Ec_20=65824.; %Mpa
wb=2.5;    %mm
```

Properties of fibers used in beam:

$f_{R1k} = 15$ Mpa, $f_{R3k} = 16.5$ Mpa

$f_{R3k}/f_{R1k} = 0.9 \rightarrow$ c Fiber class: 16.5d

```
feq006_20=15;%Mpa
feq063_20=16.5;%Mpa
fIf_20=5.78;%Mpa
Ec_20=65824.; %Mpa
wb=2.5;    %mm
crack opening
```

andamento_f006=[20., 1.; 200., 1.09; 400., 0.87; 600., 0.82];	andamento_f063=[20., 1.; 200., 1.03; 400., 1.02; 600., 0.19];	andamento_fIf=[20., 1.; 200., 0.97; 400., 0.46; 600., 0.49];	andamento_Ec=[20., 1.; 200., 0.850343225; 400., 0.500442835; 600., 0.466763092];

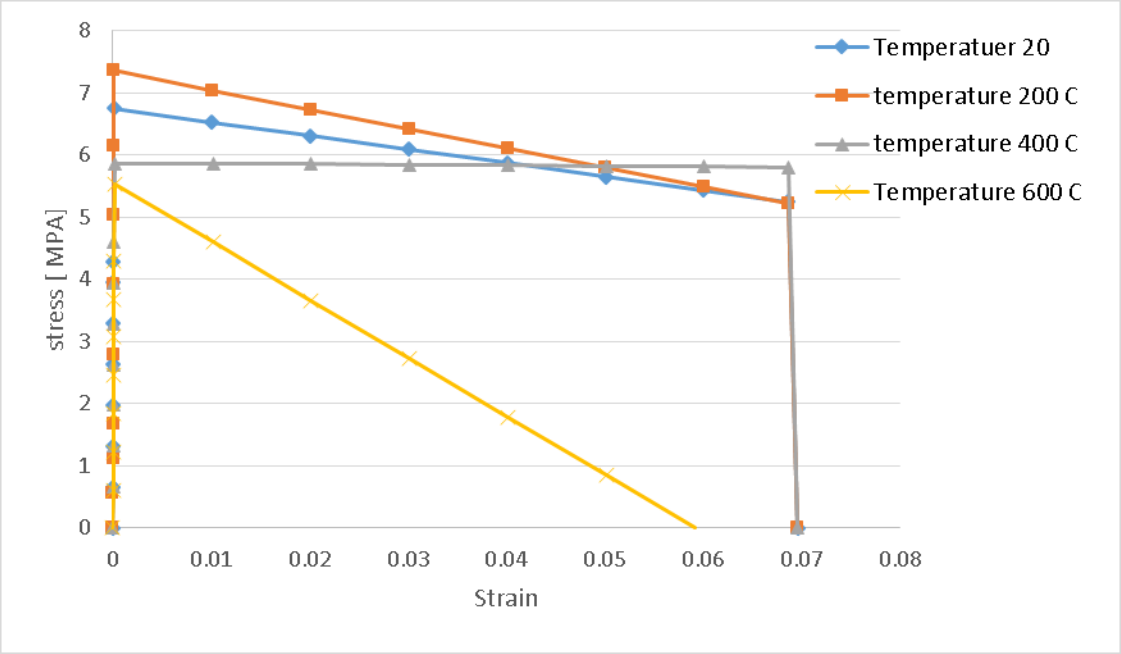

Figure 5-18: Constitutive law for HPFR in tension for different temperatures

5.4.4 Discretize the curvature axis

The procedure for finding moment-curvature diagram is based on discretization of curvature axis and finding for each curvature its corresponded bending moment. In this study the curvature of the first part of the diagram was discretize into number of 200 curvatures and for the rest part of the diagram the axis of curvature was discretize into 30 parts. So totally the bending moment will be calculated in 230 points.

```
%Numero di punti del diagramma momento-curvatura prima parte

np1=200;

%Numero di punti del diagramma momento-curvatura seconda parte
np2=30;
```

5.4.5 Translational Equilibrium and find Neutral Axis (NA)

In this part for each curvature the neutral axis will be calculated using translational equilibrium. In order to reach the equilibrium, tensile and compressive

forces should be equal to each other. It is illustrated in Figure 5-19 and in script equilibrioflex.m. (The constitutive law for each temperature and layer can be calculated by applying the results of pervious steps.)

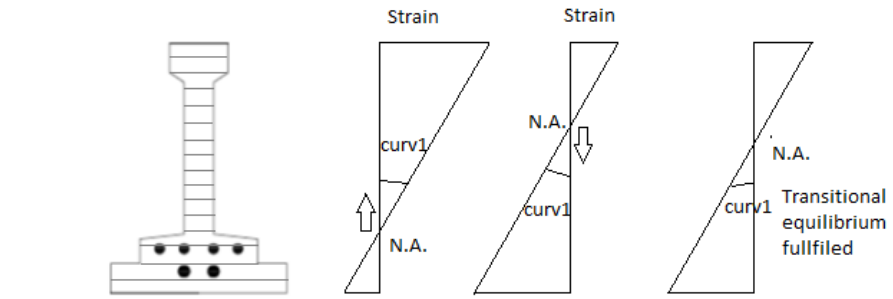

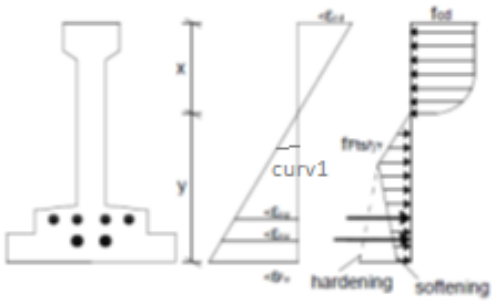

Figure 5-19: Establish translational equilibrium to find N.A

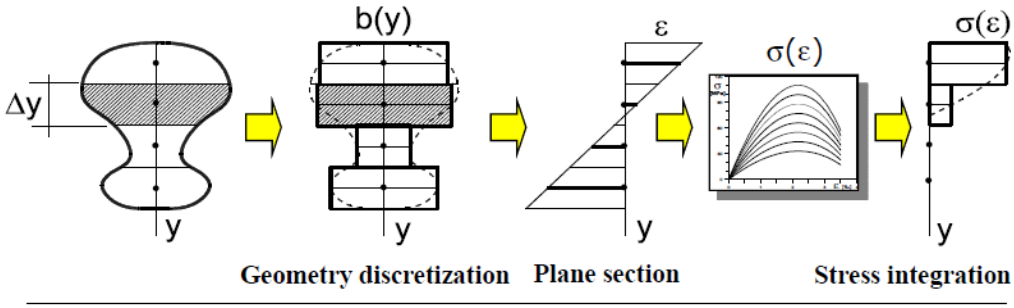

$$N(\varepsilon_{sup}, \vartheta) = \int_0^h \sigma_c[\varepsilon_c(y)]b(y)dy + \sum \sigma_s[\varepsilon_s(y)]A_s + \sum \sigma_p[\varepsilon_p(y) + \varepsilon_{p\infty}]A_p$$

Figure 5-20: General equation for translational forces acting on the section

The matlab code use a trial value for N.A and solve the equation. If the equilibrium does not full filled then it change the position of N.A and resolve the equation until the equilibrium full filled. In this time the value of N.A will be stored to calculate bending moment capacity in the next steps.

5.4.6 Bending moment capacity

After finding the position of neutral axis it is possible to find the bending moment capacity of the cross section by integrating the tensile and compressive stresses in each layer.

$$M(\varepsilon_{sup},\vartheta)=\int_0^h \sigma_c[\varepsilon_c(y)]b(y)(y-y_{GC})dy+\sum\sigma_s[\varepsilon_s(y)]A_s(y-y_{GC})+\sum\sigma_p[\varepsilon_p(y)+\varepsilon_{p\infty}]A_p(y-y_{GC})$$

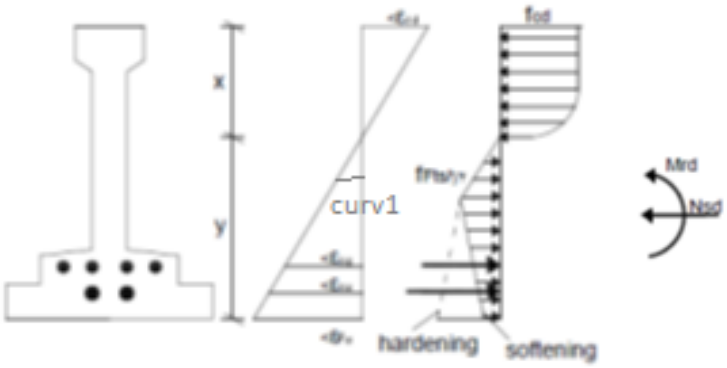

Figure 5-21: Calculating bending moment capacity of the beam by knowing strains and its corresponding stresses over cross section.

5.4.7 Moment-curvature curves

By choosing new curvature and performing all steps mentioned above, it is possible to find the bending moment for each curvature and draw the final and complete diagram of moment-curvature for a fixed time of fire exposure. Then, by changing the time of exposure in the inputs of Matlab code the new moment-curvature will be obtained for new time. At the end, it is possible to draw out all the moment-curvature diagrams for different times of exposure in one plot to simply compare them with each other. Final result are presented in Figure 5-22 for beam section exposed to ISO834.

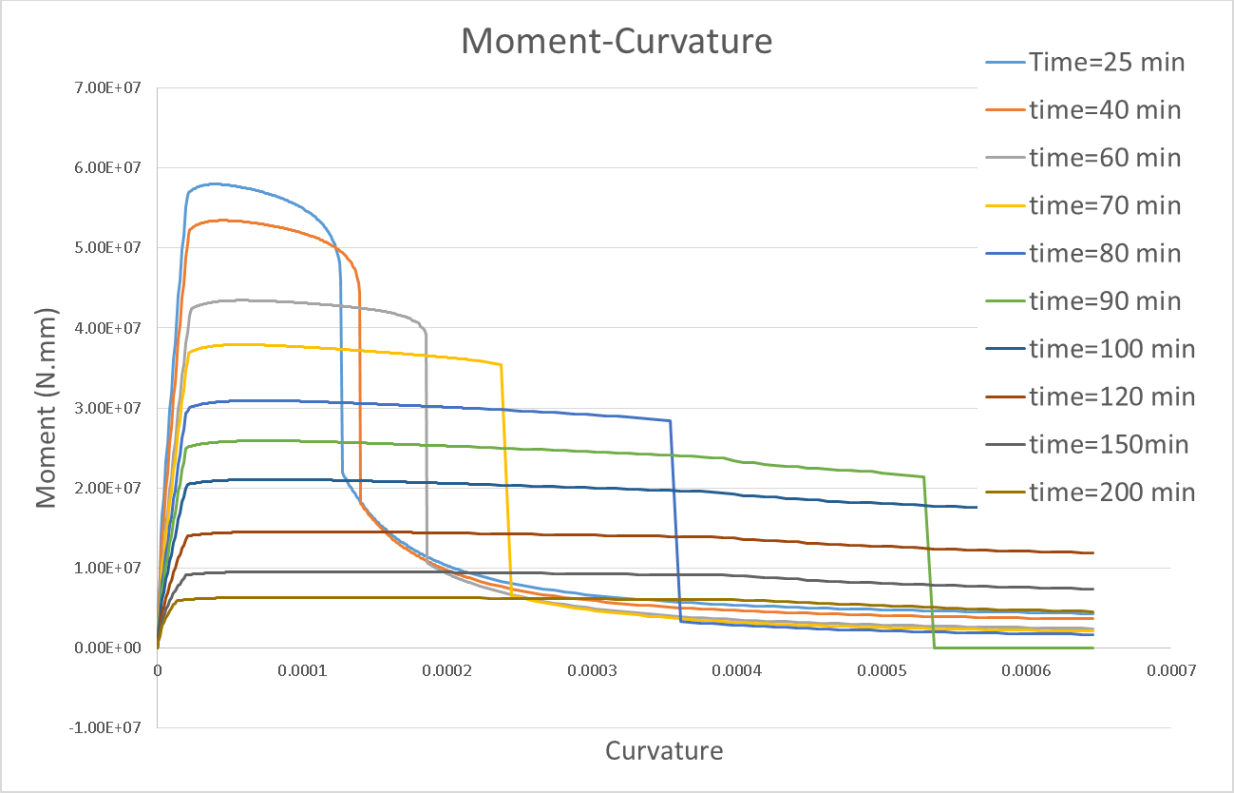

Figure 5-22: Moment curvature at different times

By comparing the results it is obvious that the maximum bending moment decreases as the time increases because of the degradation of material strength in high temperature. One another result obtained by comparing the diagrams is that the ductility increases as time evolves. Also, the results indicate that the initial slope of the curves decreases, as we know this slope in Moment-curvature diagram is the bending stiffness (EJ) and it reduces by increasing time and it is due to the degradation of material stiffness in high temperature.

5.5 Results

5.5.1 Time of failure

After comparing the results, it is possible to draw the bending capacity of the section over time by considering the maximum moment capacity for each time and collect these maximum moments and their corresponding time in a table to draw the diagram.

This diagram has been shown in Figure 5-23. Then, it is assumed that the acting bending moment calculated in previous chapter (caused by live load, dead load and permanent load) does not change over time. The intersection of constant acting bending moment and capacity bending moment curve gives us the time of failure. Therefore, In this case, failure will occur after 85 minutes of fire exposure as it can be observed in Figure 5-23. Acting bending moment already calculated and the value is Med=27.8 KN.M.

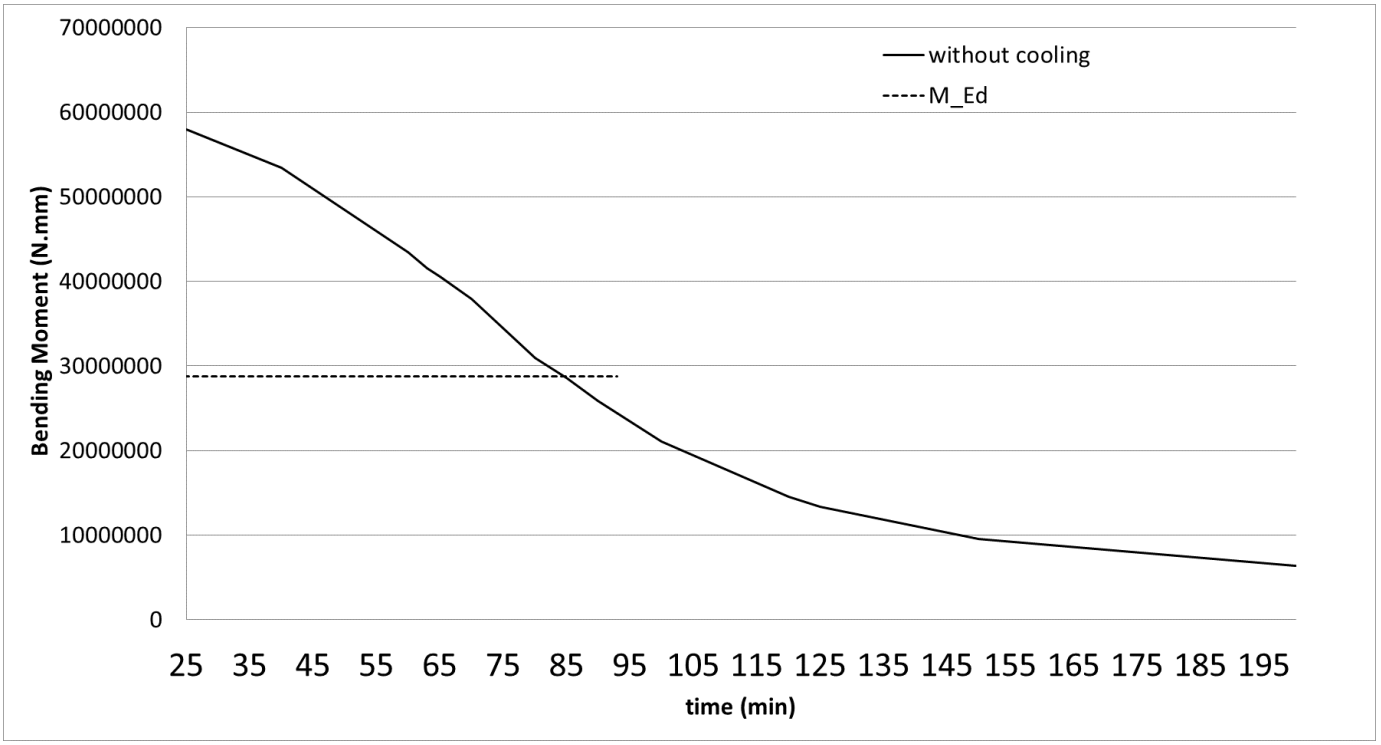

Figure 5-23: Bending moment capacity over time

5.6 : 500 C isotherm method

Number of different methods has been introduced by Eurocode 2 part 1-2 for finding capacity of structures exposed to fire. One of simplified calculation method is 500°C isotherm method which has been introduced in Annex B of EN 2. This method is applicable to a standard fire exposure. This method simplified calculation by comprising a general reduction of the cross section size with respect to a heat damaged zone at the concrete surfaces. It is assumed that concrete with temperature over 500 °C is damaged and have no strength. Moreover, it is assumed that the damaged concrete do not contribute to the load bearing capacity of the member, while the residual concrete cross section retains its initial values of strength and modulus of elasticity (Figure 5-24). The thickness of the damaged concrete, is made equal to the average depth of the 500 isotherm in the compression zone of the cross section. On the basis of these assumptions the procedure for calculating the resistance of a reinforced concrete beam in the fire situation may be carried out as follows:

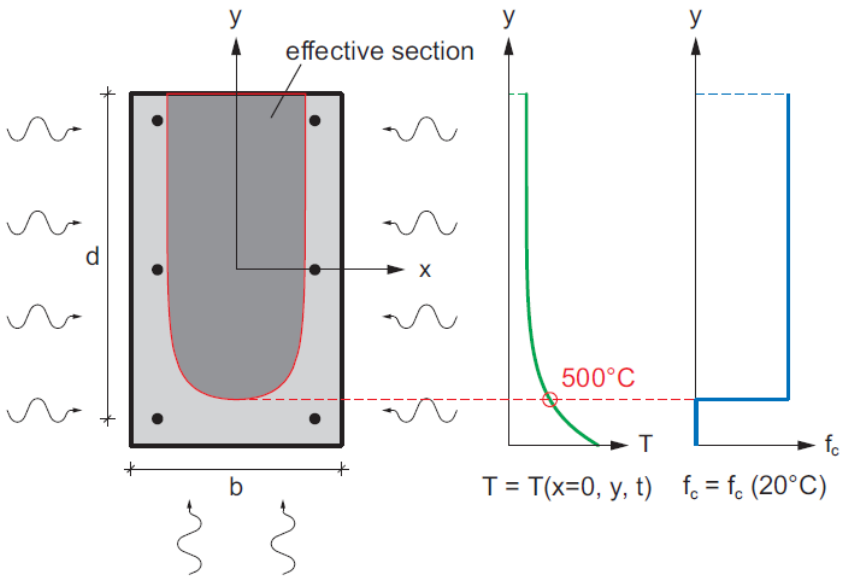

Figure 5-24: 500 Degree isotherm and simplified assumptions for concrete strength

1. Determine the position of isotherm 500 °C

Thermal distribution over time has been calculated in previous part. Therefore it is possible to find the penetration of 500 C isotherm over time in the cross section of the

beam. The results has been presented in Table 5-5 and graphically shown in Figure 5-25 in eight steps.

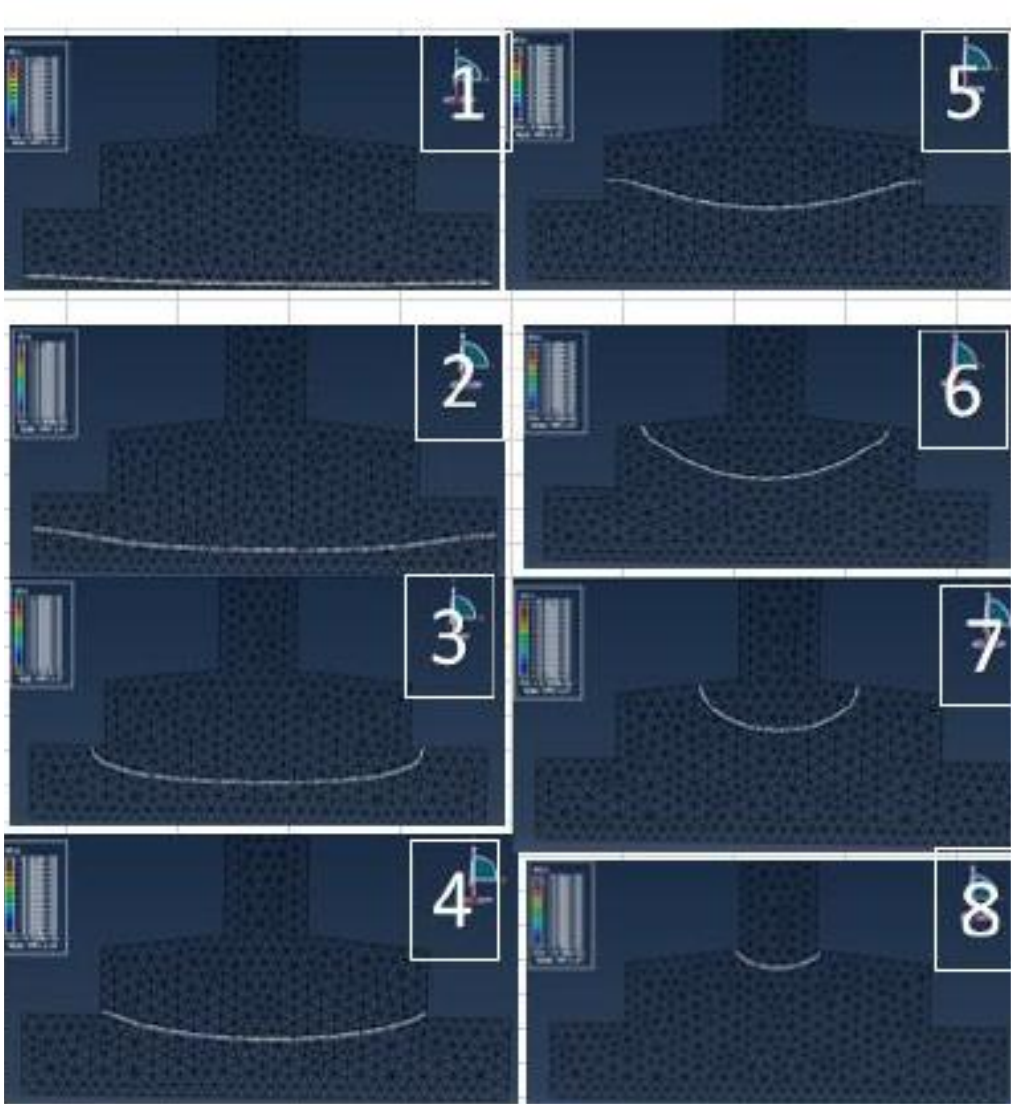

Figure 5-25: Position of 500 C isothrem in different steps

Number	Time (min)	Approximate depth of 500 ℃ (mm)
1	19.6	1
2	30.016667	15
3	40.016667	25
4	50.016667	27
5	60.016667	31
6	70.016667	42
7	80.016667	49
8	100.01667	53

Table 5-5Penetration of 500 degree isotherm

2. Determine a new width and height

By excluding the concrete outside the 500 °C isotherm the new width and effective height of undamaged concrete can be calculated. The rounded corners of isotherms can be regarded by approximating the real form of the isotherm to a rectangle or a square.

Number	Time (min)	Approximate depth of 500 °C (mm)	New width (mm)	New height (mm)
1	20	1	180	254
2	30	15	180	239
3	40	25	140	226
4	50	27	120	223
5	60	31	120	219
6	70	42	70	213
7	80	49	45	206
8	100	53	30	202

Table 5-6: New width and height after penetration of 500 C isotherm

3. Determine the temperature of reinforcing bars in the tension and compression zones.

The temperature of the individual reinforcing bar can be evaluated from the temperature profiles results of FEM (Abaqus) and is taken as the temperature in the center of the bar. The values of temperature in each step is given in Table 5-7. Some of the reinforcing bars may fall outside the reduced cross-section, they may be included in the calculation of the ultimate loadbearing capacity of the fire exposed cross-section;

Number	Time (min)	Temperature at the center of Bar 1	Temperature at the center of Bar 2	Temperature at the center of Bar 3
1	20	243.949	129.469	104.707
2	30	359.739	228.427	188.23
3	40	448.889	314.484	263.62
4	50	521.823	389.475	330.997
5	60	582.729	454.525	390.576
6	70	634.535	511.267	443.357
7	80	679.275	561.161	490.382
8	100	752.969	644.893	570.606

Table 5-7: Temperature of bars over time of exposure

4. Determine the reduced strength of the reinforcement due to the temperature

After knowing the temperature of each bar it is possible to apply the table suggested by Eurocode to find level of degradation in strength and elastic modulus of steel bars. The values of strength and stiffness for different steps has been presented in Table 5-8.

Time (min)	Bar1		Bar2		Bar3		Bar1		Bar2		Bar3	
	$\frac{f_{sy,t}}{f_y}$	$\frac{E_{s,t}}{E_s}$	$\frac{f_{sy,t}}{f_y}$	$\frac{E_{s,t}}{E_s}$	$\frac{f_{sy,t}}{f_y}$	$\frac{E_{s,t}}{E_s}$	$f_{sy,t}$	$E_{s,t}$	$f_{sy,t}$	$E_{s,t}$	$f_{sy,t}$	$E_{s,t}$
20	1.00	0.86	1.00	0.97	1.00	1.00	430	175685	430	199055	430	204180
30	1.00	0.74	1.00	0.87	1.00	0.91	430	151905	430	178760	430	186960
40	0.97	0.65	1.00	0.79	1.00	0.84	415	133660	430	161130	430	171585
50	0.79	0.54	1.00	0.71	1.00	0.77	340	110516	430	145755	430	157850
60	0.68	0.36	0.95	0.65	1.00	0.71	293	74251	409	132430	430	145550
70	0.61	0.25	0.81	0.57	0.98	0.66	264	51004	350	116461	422	134685
80	0.57	0.17	0.72	0.42	0.86	0.61	247	34399	308	86736	370	125050
100	0.54	0.11	0.60	0.23	0.70	0.40	233	22386	260	47314	302	81385

Table 5-8: Results of degradation of steel bars due to increasing of temperature

5. Use conventional methods to calculate bending moment capacity

Bending moment capacity of the reduced cross-section can be determined by finding the position of neutral axis and integrating the stresses over the cross section. Since the cross section is not a simple rectangular, one can apply "Response2000" or "VcaSlu" program to find the moment capacity of the complicated sections. Here, Matlab program was used to integrate the forces and find the bending capacity of the section. The procedure however is shown in Figure 5-26.

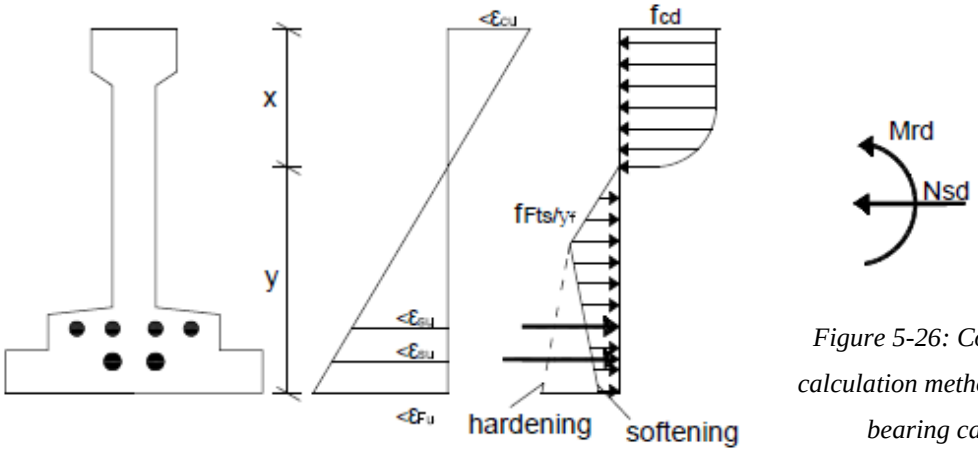

Figure 5-26: Conventional calculation methods: ultimate bearing capacity

The final results of Matlab program has been represented in Table 5-9 and shown graphically in Figure 5-27: Bending Moment Vs Time (500'C method)Figure 5-27.

Number	Time (min)	Resisting Bending moment KN.m
1	20	59
2	30	55
3	40	52
4	50	50
5	60	48
6	70	44
7	80	40
8	100	34

Table 5-9: Results of Bending Moment Capacity (method : 500'C isotherm)

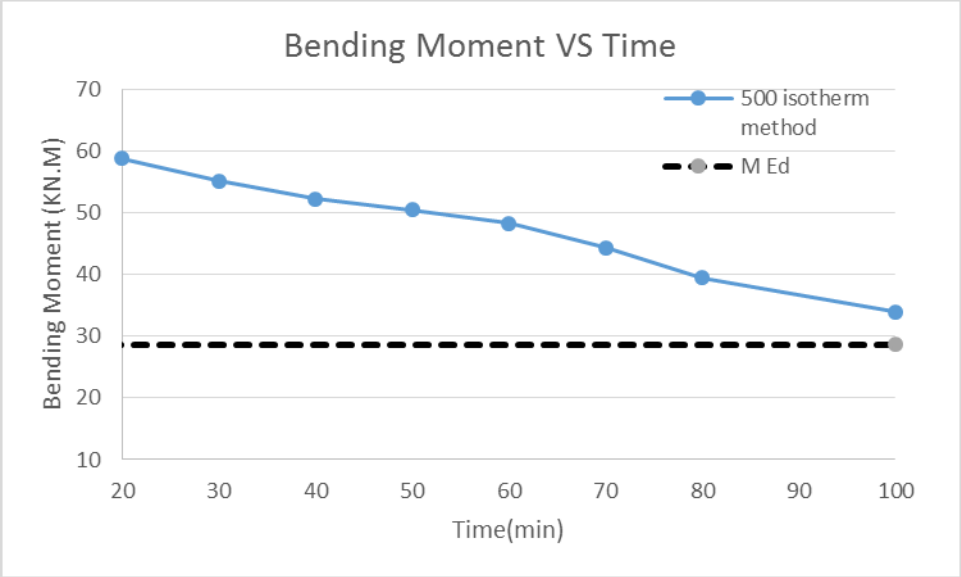

Figure 5-27: Bending Moment Vs Time (500'C method)

6. Compare the ultimate load-bearing capacity with the design load

Acting load is assumed to be constant over time and the value is 28.7 KN.M. Finding the intersection of the acting bending moment and the bending moment capacity curve gives us the time of failure. By extrapolating, time of collapse is approximately equal to 120 minutes as it can be observed in Figure 5-27.

7. Comparing the result of plane section (2D model) and 500 isotherm methods

In order to compare the results, two curves have been drawn in one plot as presented in Figure 5-28. The two method gave similar results until 50 minutes after fire exposed, however after this time the results show some differences with each other and indicates that plane section approach gives lesser value for bending moment capacity and designing according to plane section approach is more on conservative side. As time evolves, this difference becomes more and more, therefore the time of failure will vary significantly from one method to other one.

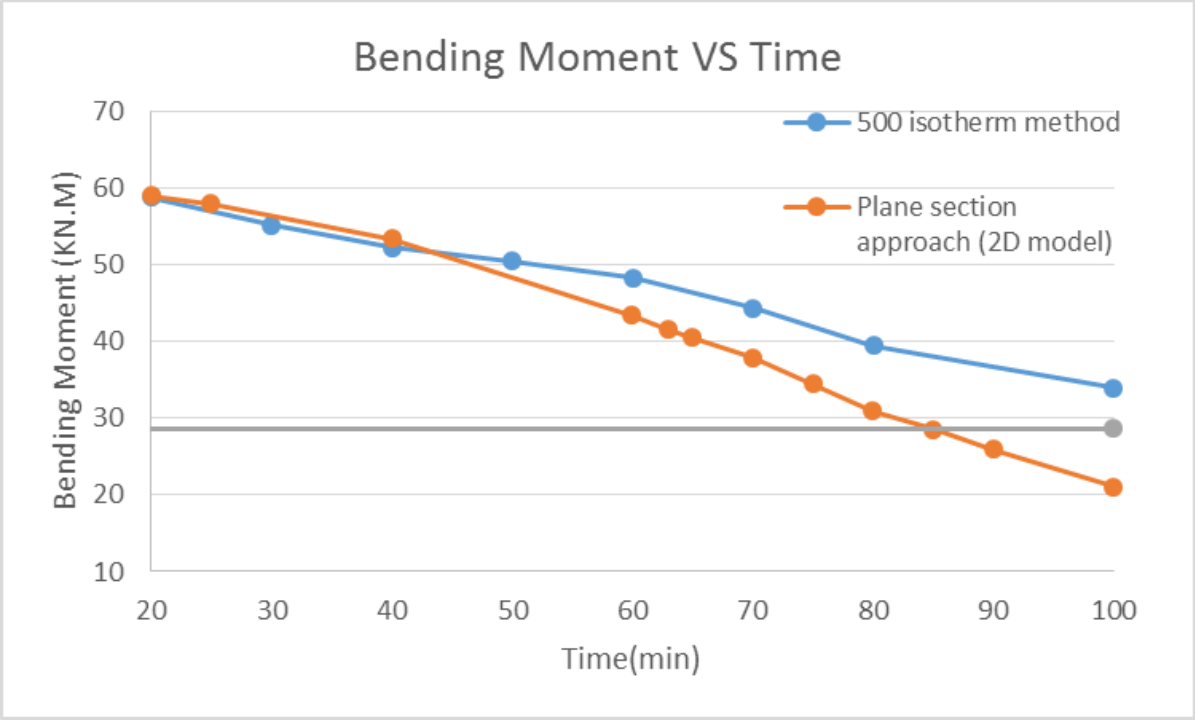

Figure 5-28: Time of failure (acting Bending moment and bending moment capacity of section according to 500'C and FEM)

According to 500 isotherm method, the section will fail after 120 min of fire exposure while the plane section approach calculates time of failure after 85 minutes.

This overestimating of bending moment of the 500-isotherm method can be due to disregarding degradation in concrete with temperature less than 500 °C. While in reality the concrete elasticity and strength reduced at elevated temperatures even if the temperature was lower than 500 degree.

5.6.1 Fire scenarios (Cooling phases)

By considering different cooling phases, it is possible to establish different fire scenarios. In this part, it is assumed that fire ISO834 cooled down linearly after 30, 60, 90 and 120 minutes of exposure. The graph of time-temperature for different cooling phases is presented in Figure 5-29.

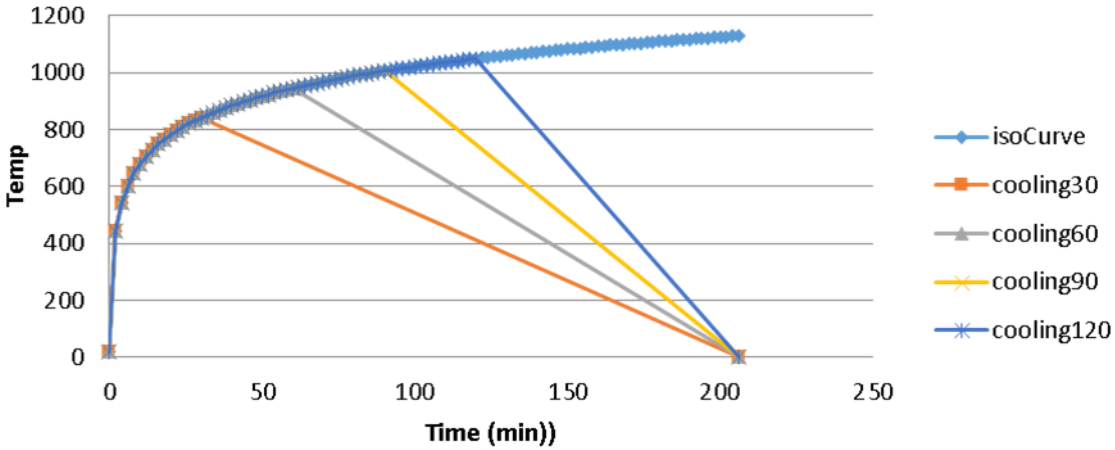

Figure 5-29: Different fire scenarios and cooling phases

The beam model already was defined in Abaqus and only by changing the input of fire temperature-time table it is possible to study other scenarios. Finally, thermal distribution over section in different time of fire exposure can be achieved for each scenarios. The graphs presented in Figure 5-31 and Figure 5-32 show temperature distribution at specific times (60, 100, 130 and 150 minutes) for different scenarios. According to the results by increasing the time the differences among the result of different scenarios become greater. As well as, these differences of temperature value over cross section are more obvious and significant in the bottom of section rather than the top. Another comment on the results are on the cooling effect, since it has shown that after cooling starts, there is still evolution of temperature over specific depth near the outside of the cross section and it doesn't decrease suddenly by cooling down the surface.

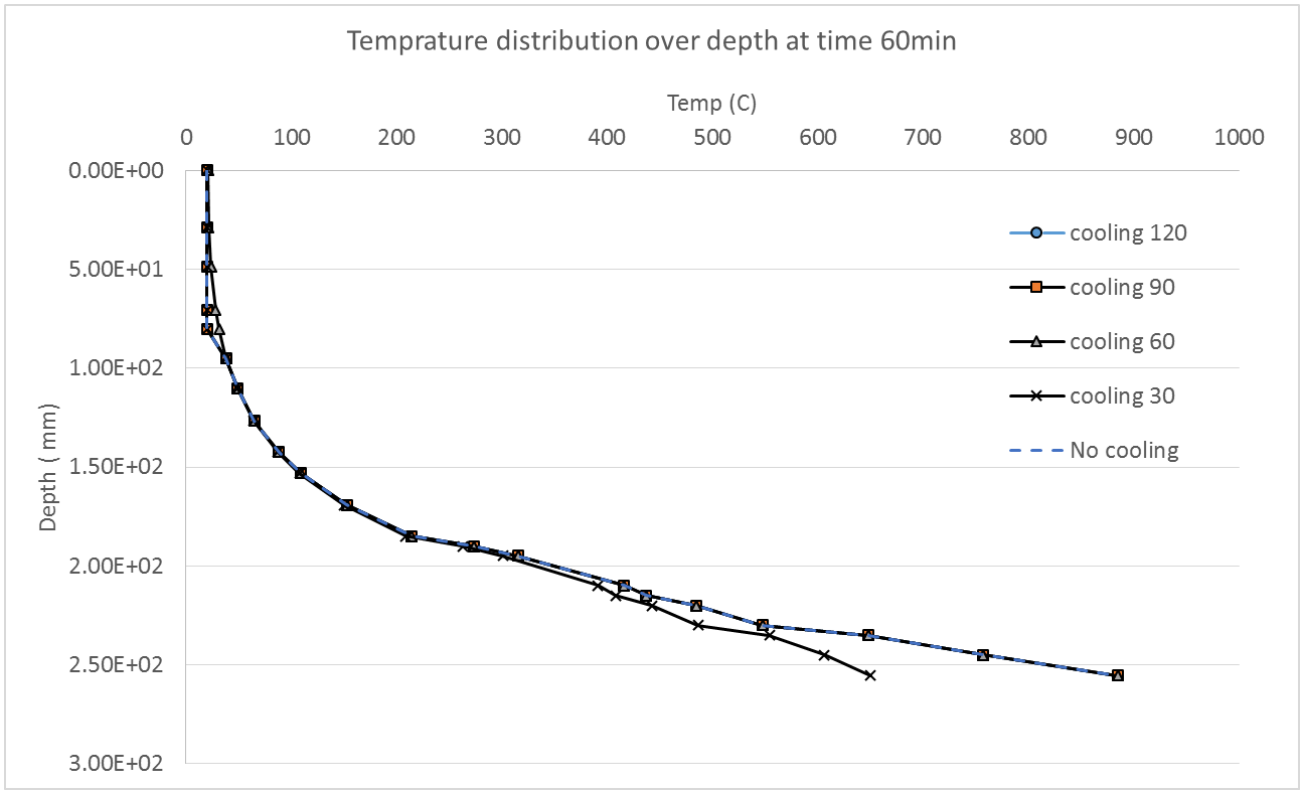

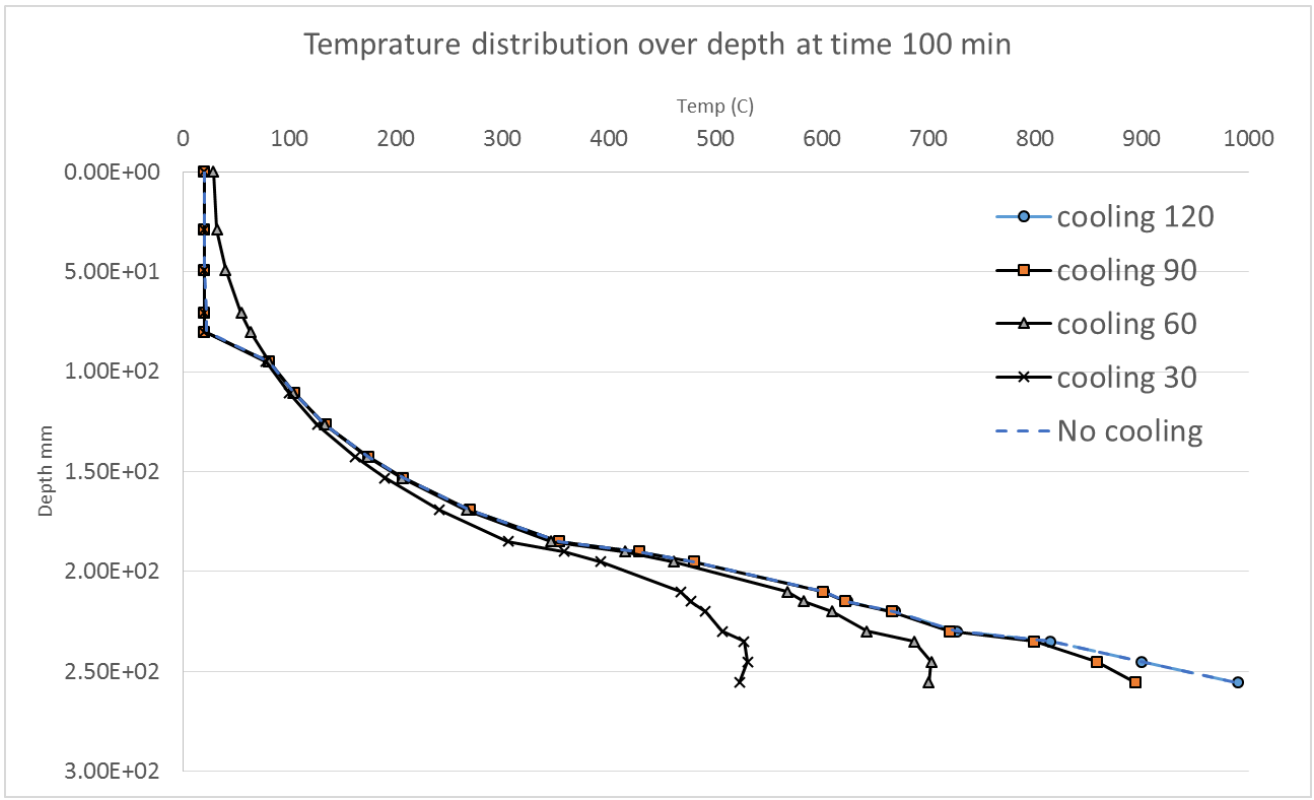

Figure 5-30: Temperature distribution over depth for different fire scenarios at different times

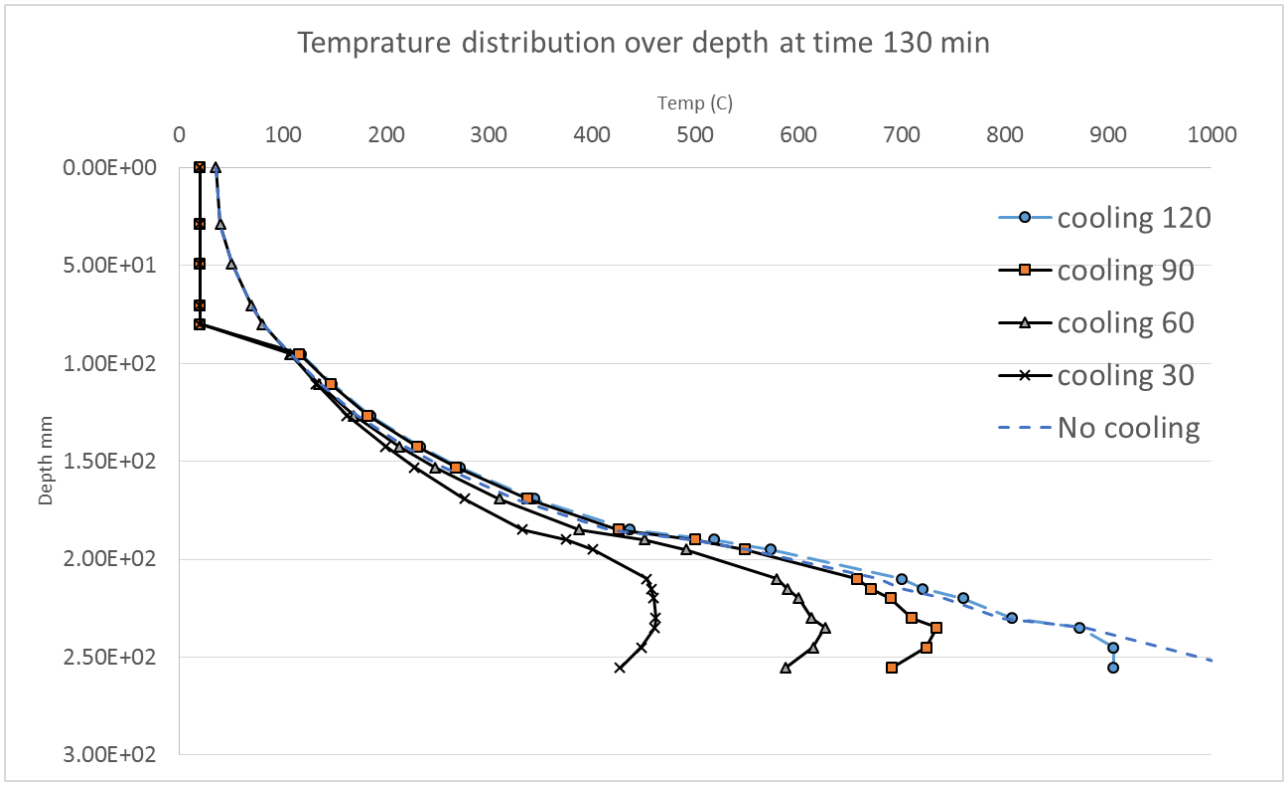

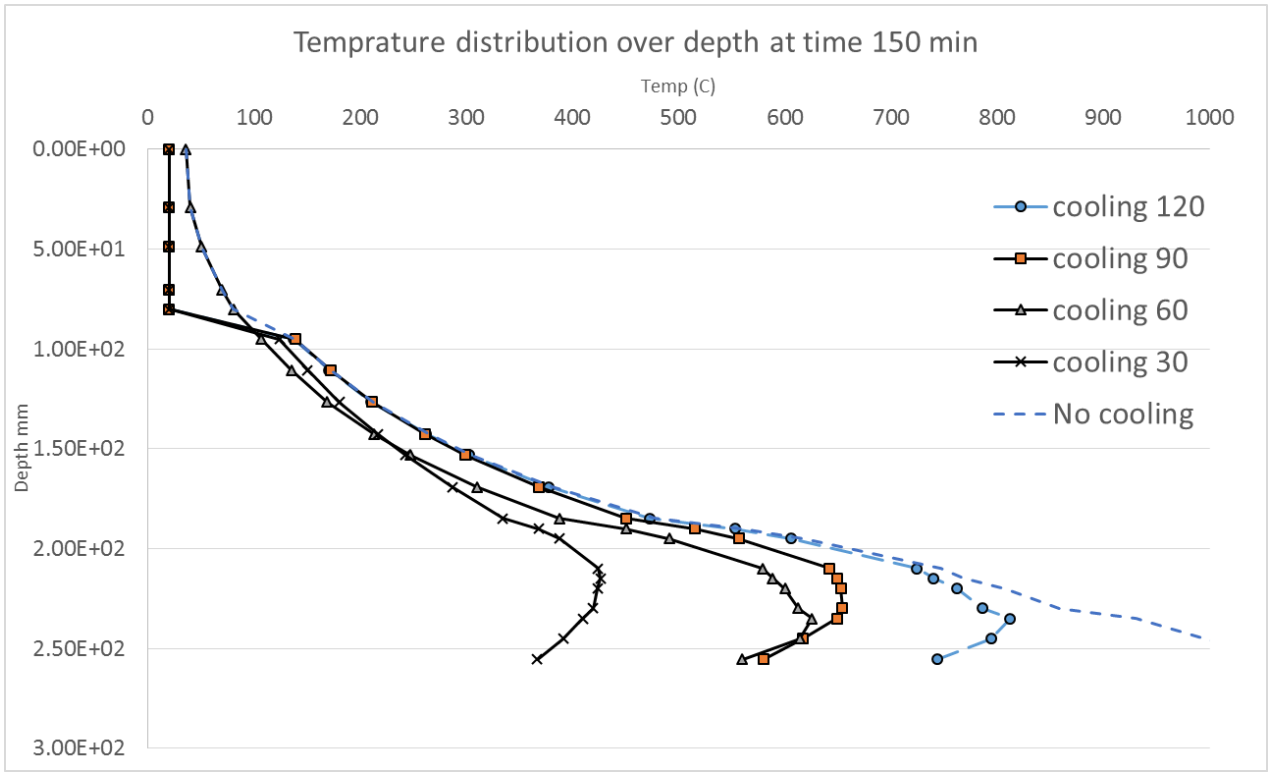

Figure 5-31: Temperature distribution over depth for different fire scenarios at different times

5.6.1.1 Moment-curvature and Moment-time diagrams for each scenarios

The procedure to fine the Moment-curvature diagram is the same as before and only the input of fire (temperature-time) and input of temperature distribution over cross section in different times should be considered as new inputs of the program. Both inputs have been already calculated and presented in previous parts and by substituting them into the model, the final results can be achieved. Moment-curvature diagram of each scenarios and its corresponding moment-time diagram will be presented in this part.

5.6.1.1.1 Scenario 1 (cooling starts after 30 min)

Final results of Moment-curvature diagram are presented in Figure 5-32 .

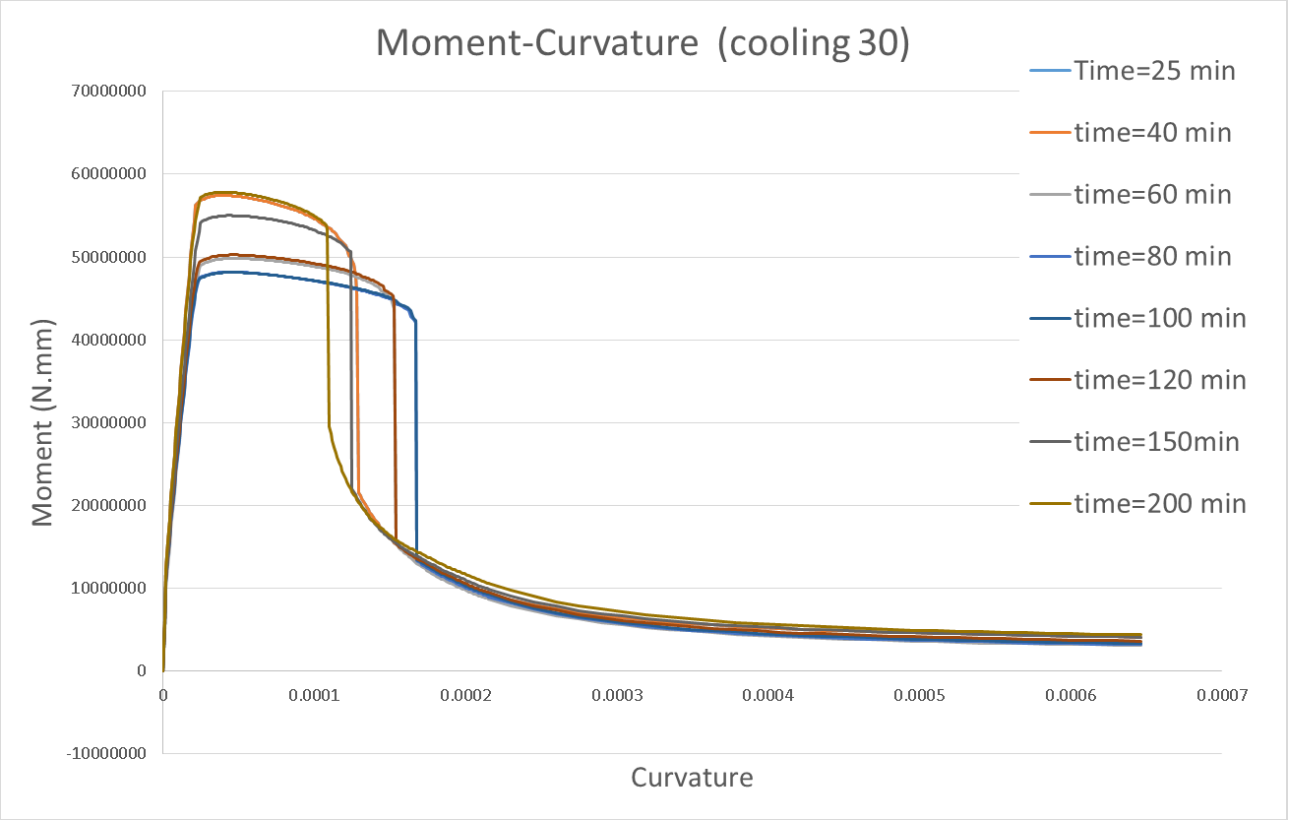

Figure 5-32: Moment-Curvature for fire Scenario 1 at different times

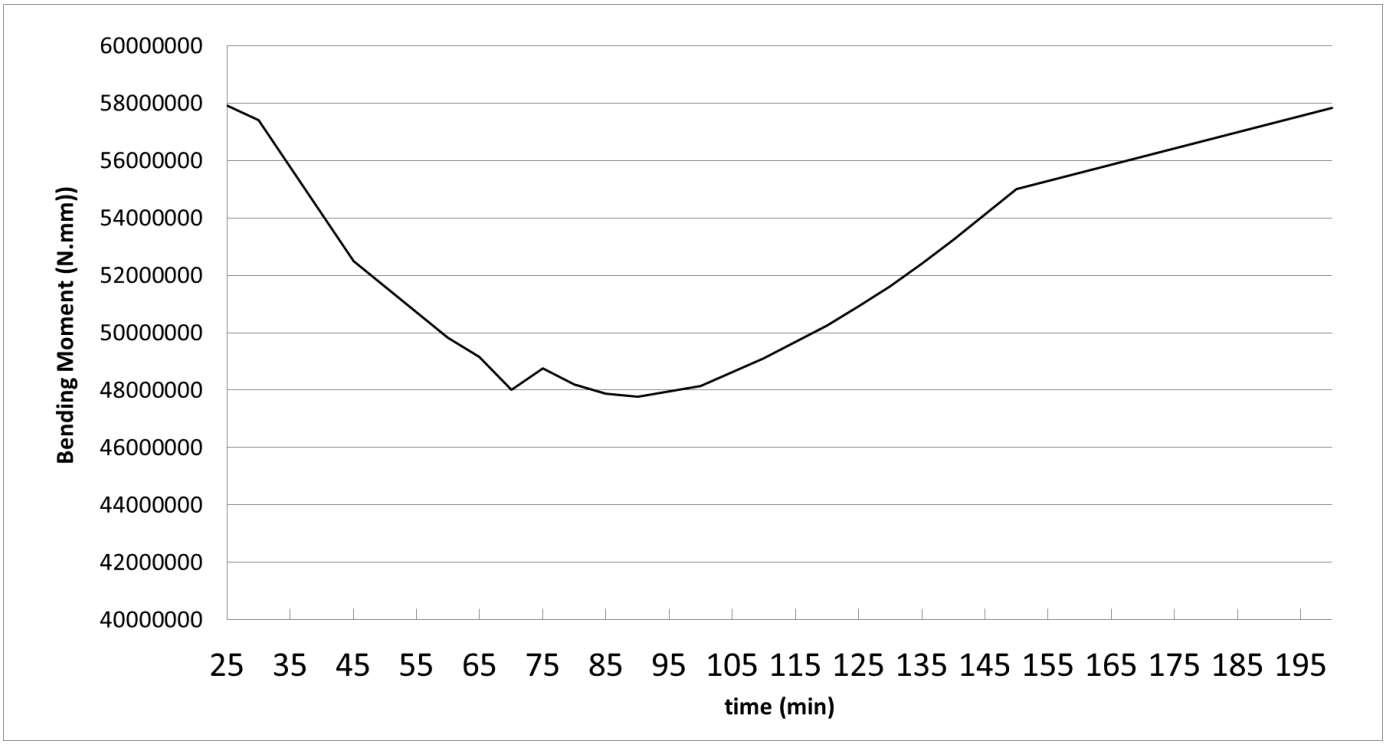

Figure 5-33:Bending moment capacity over time (Cooling 30 min)

As it can be seen in Figure 5-33, the minimum bending moment capacity is around 48 (KN.M) and it happens after 86 minutes.

Cooling started after 30 minutes but the minimum bending moment capacity doesn't occur at that time, while it continuing reducing its capacity till some minutes after 30 min. Finally after 86 minutes it reaches to its minimum bending moment capacity and after that it increases again due to the cooling of the material. It indicates that although cooling started, the temperature still increases inside the cross section and it doesn't reduce suddenly, Therefore the material experiences degradation also for a while after cooling started.

5.6.1.1.2 Scenario 2 (cooling starts after 60 min)

Final results of Moment-curvature diagram are presented in Figure 5-34.

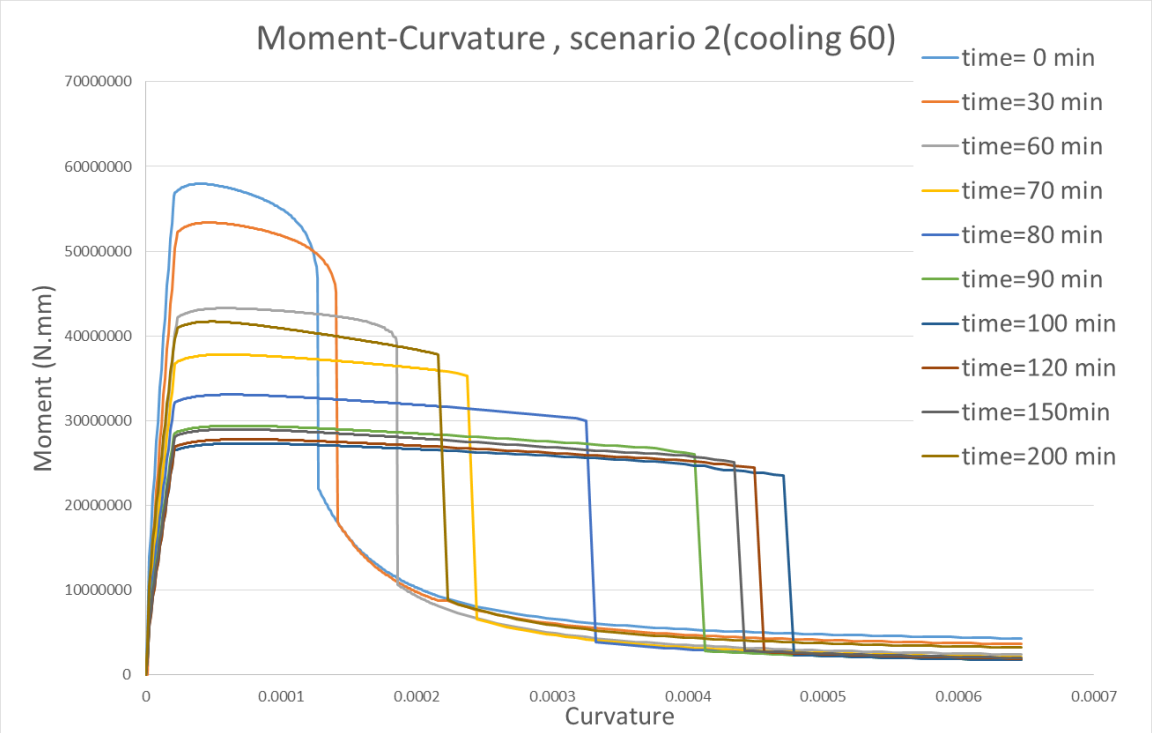

Figure 5-34:Moment-Curvature for fire Scenario 2 at different times

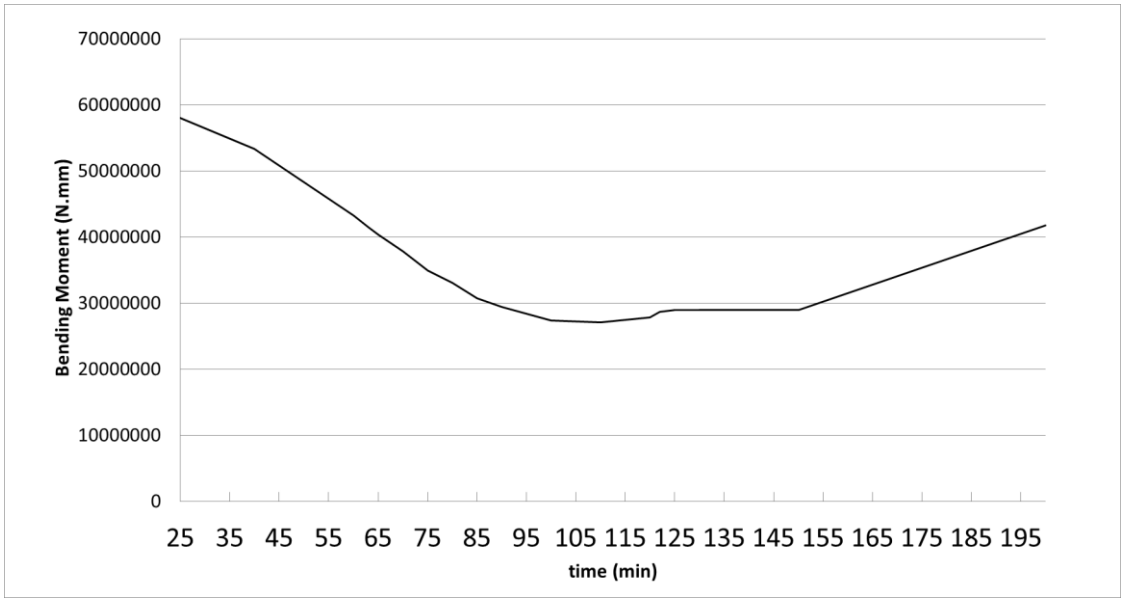

Figure 5-35::Bending moment capacity over time (Cooling 60 min)

As it can be seen in Figure 5-35, the minimum bending moment capacity is around 27 (KN.M) and it happens after 105 minutes.

5.6.1.1.3 Scenario 3 (cooling starts after 90 min)

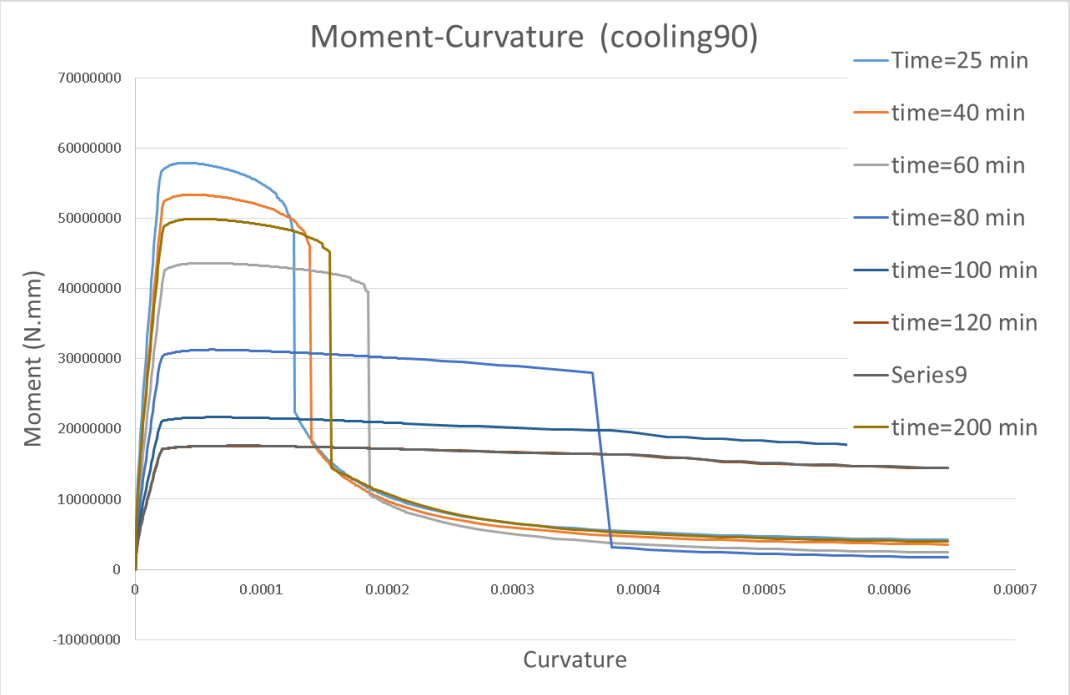

Figure 5-36:Moment-Curvature for fire Scenario 3 at different times

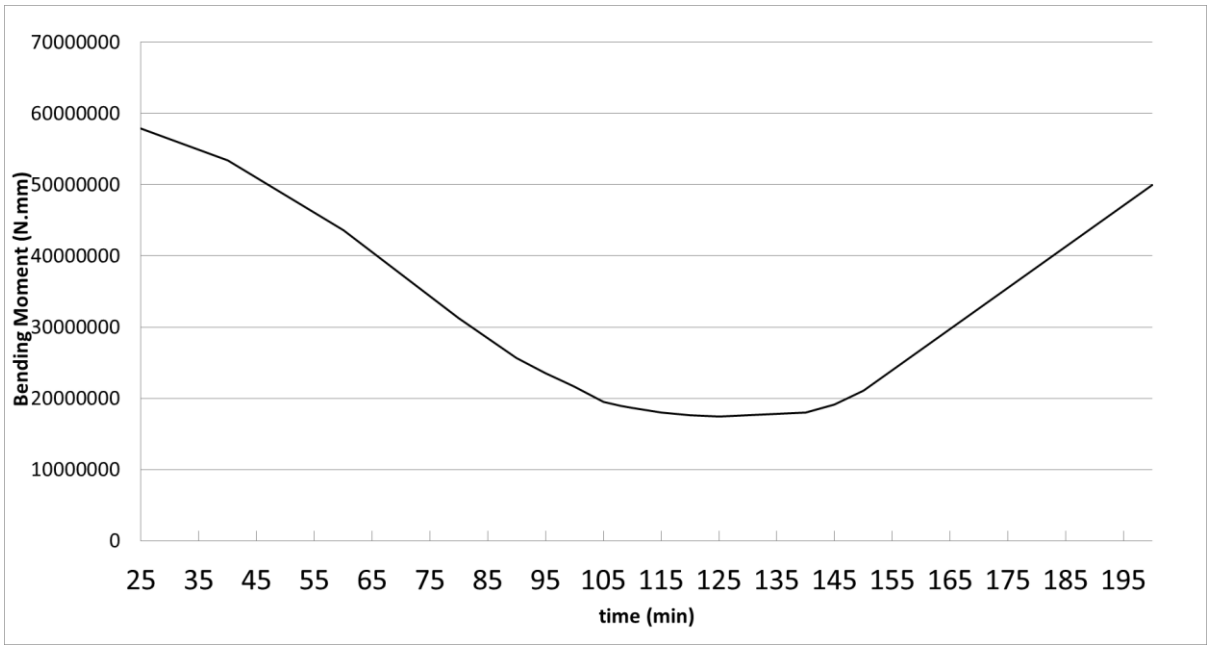

Figure 5-37: Bending moment capacity over time (Cooling 90 min)

As it can be seen in Figure 5-37, the minimum bending moment capacity is around 17 (KN.M) and it happens after 125 minutes.

5.6.1.1.4 Scenario 4 (cooling starts after 120 min)

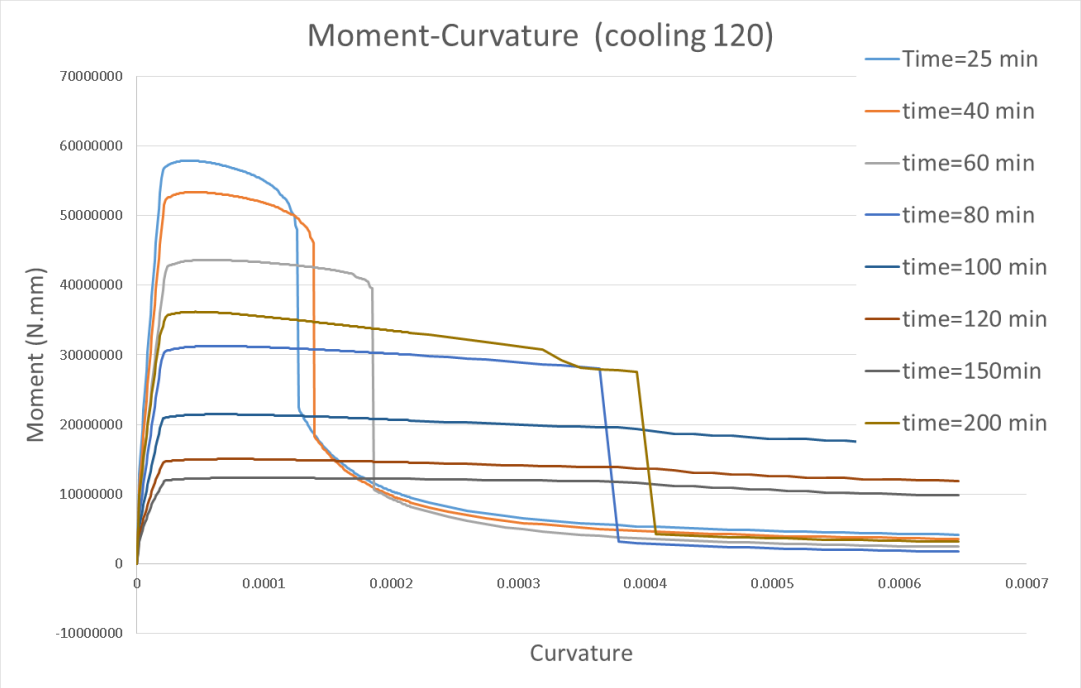

Figure 5-38:Moment-Curvature for fire Scenario 4 at different times

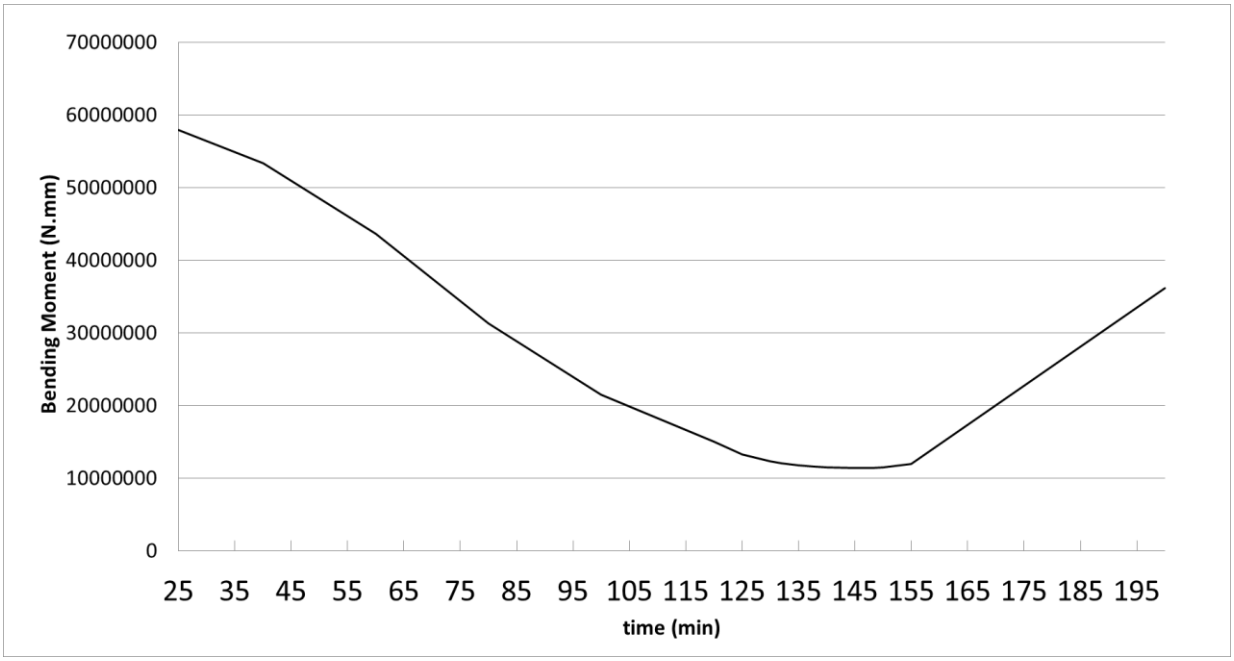

Figure 5-39: Bending moment capacity over time (Cooling 120 min)

As it can be seen in Figure 5-39, the minimum bending moment capacity is around 11 (KN.M) and it happens after 147 minutes.

5.6.1.1.5 Comparing different scenarios

In order to better compare the results all scenarios were shown in one graph (Figure 5-40). As it can be seen, if the cooling phase started sooner, the degradation in the bending moment capacity would be lower. Moreover, the time corresponding to the cooling, is not the time when the section experience its minimum bending moment capacity. The minimum bending moment capacity of the section will occur after a while when cooling started.

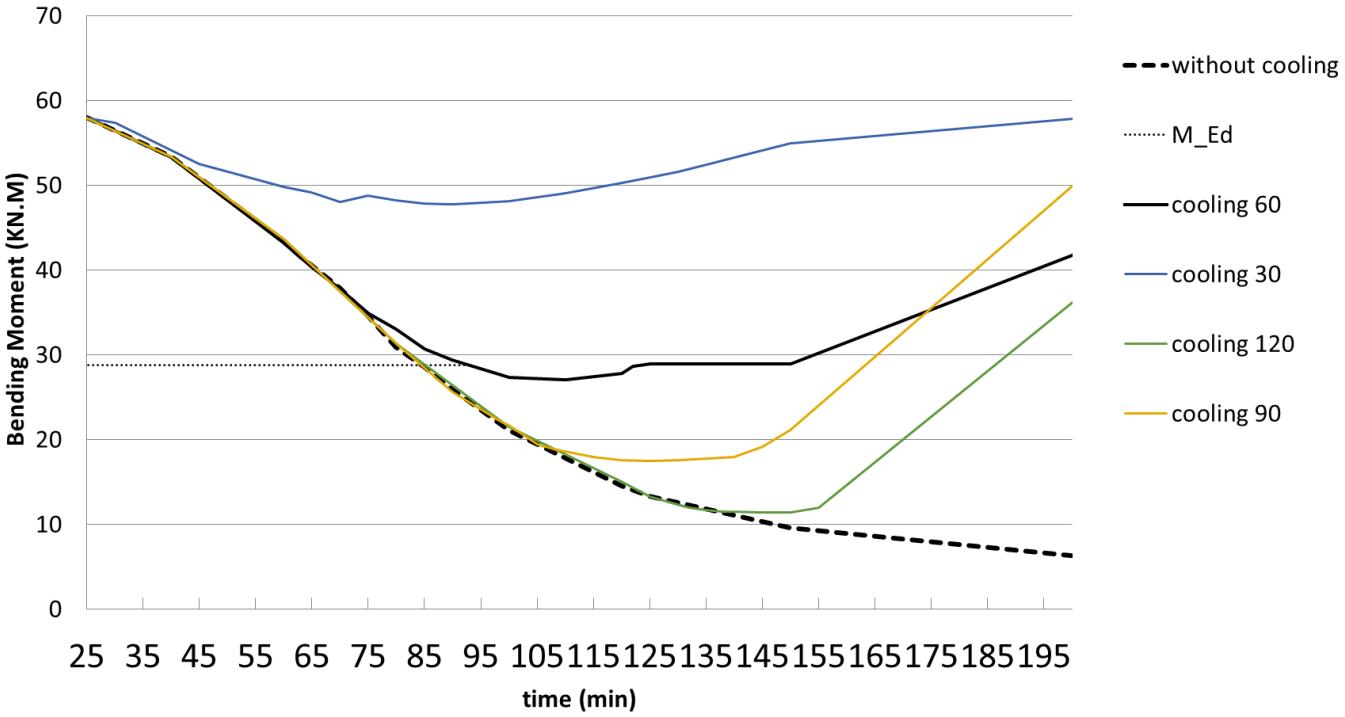

Figure 5-40: Capacity bending moment-time for all scenarios

Summarize the results presented in previous parts:

1st Scenario : Cooling 30→ Mmin=48 (KN.m)

2nd Scenario : Cooling 60→ Mmin=27 (KN.m)

3rd Scenario : Cooling 90→ Mmin=17 (KN.m)

4th Scenario : Cooling 120→ Mmin=11 (KN.m)

The results can be also drawn in a diagram as Figure 5-41. In this diagram it is possible also to compare scenarios results with the result of fire without cooling (ISO834).

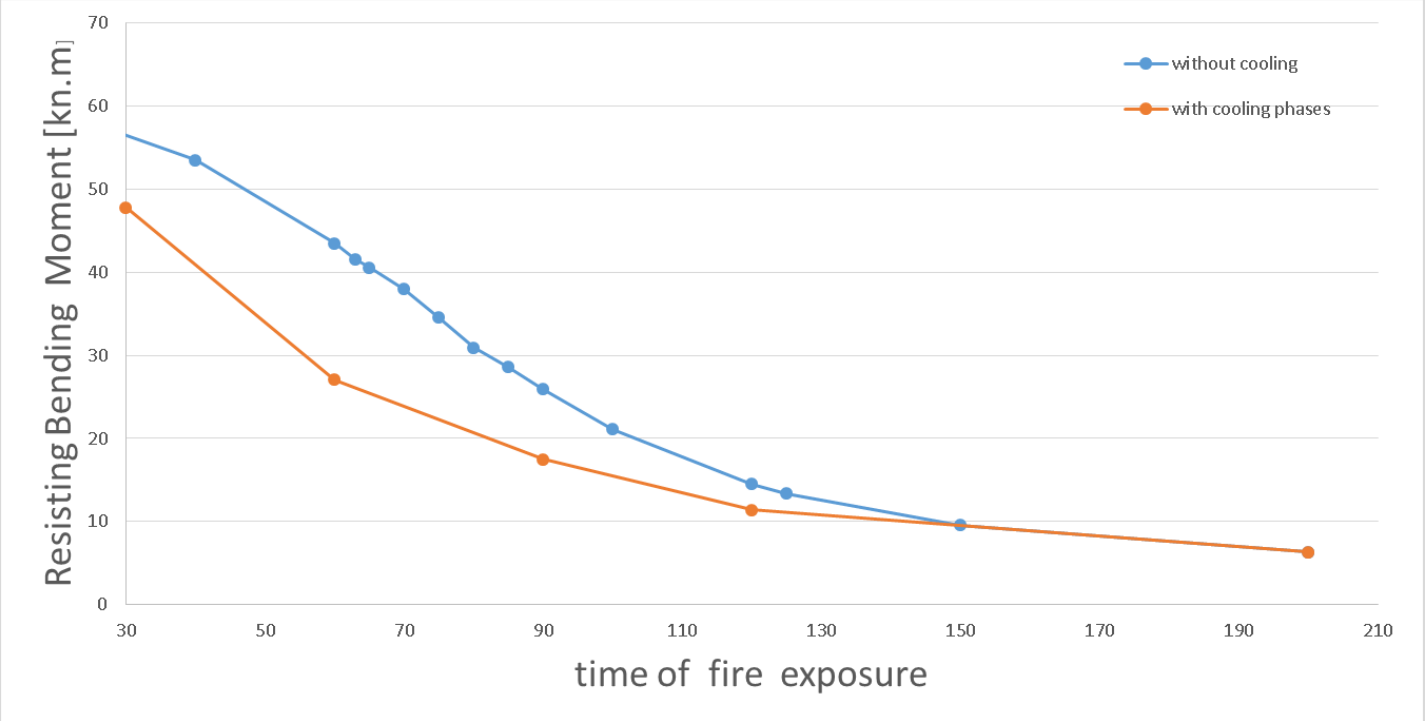

Figure 5-41: Resisting bending moment-time for beam exposed to ISO834 and beam exposed to different cooling phases

The graph indicates that with cooling phases in a specific time, the beam section suffers greater degradation of resisting bending moment and it is more critical. The failure will occur at 58 minutes while in beam exposed to fire ISO834 without cooling the failure occurs after 85 minutes. It shows that temperature penetrates into the certain depth of beam section even for a time after cooling started.

6 : 3D Model

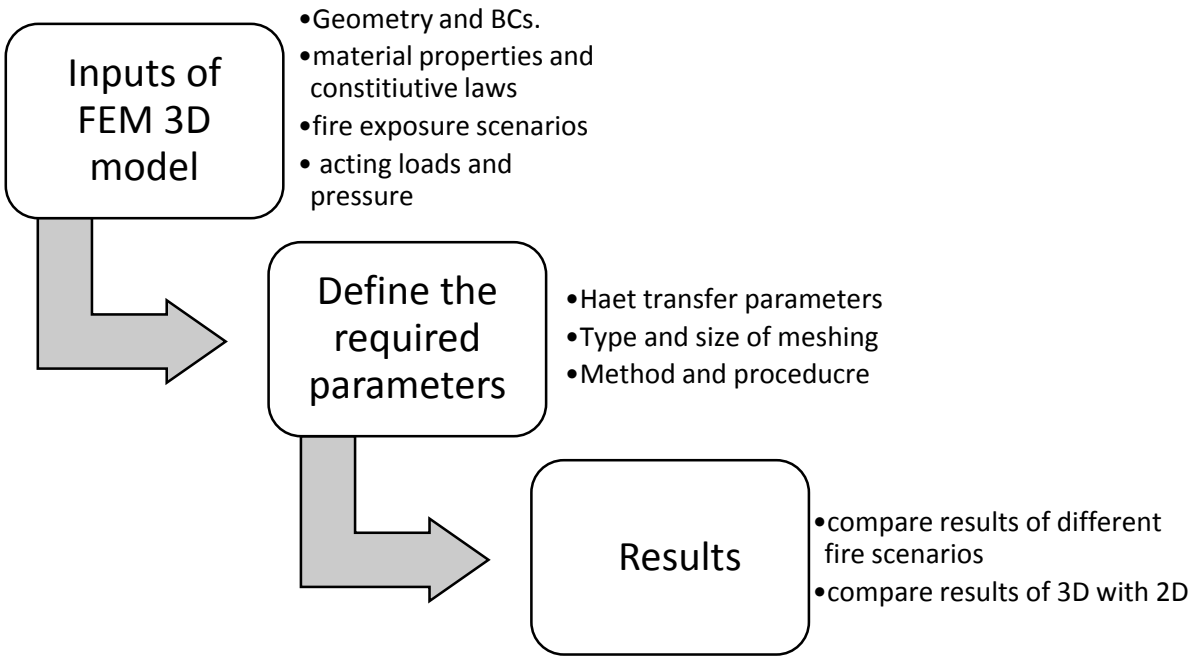

6.1 Numerical Models

The whole beam with and without slab, was modelled in Abaqus. The software is suitable also for 3D modelling and performing numerical analysis (FEM) for engineering purposes. 3D modelling in Abaqus used for analyzing the problem according to given parameters and chosen methods and at the end can visualize the FEM results.

The analysis and the results are highly dependent on the inputs and chosen methods, therefore special care should be given to inputs and other required parameters. One problem here is the way to define a fiber-reinforced concrete because it is not possible to define fibers in the model due to large number of fibers and uncertainly about their orientation and distribution. Therefore, one way to cope this problem is to accept the HPFRC as a homogeneous concrete called “composite” which has compression capacity of high performance concrete and tension capacity of fiber elements. Considering this concept, HPFRC can be modeled by defining its properties into the software.

6.1.1 Geometry

In Abaqus, section “Part”, it is possible to model the beam geometry. In 3D model, steel bars should be defined into the model, because they play role for achieving the bearing capacity of the beam. Therefore, there are 2 separate parts; concrete beam and steel bars. While in 2D model, thermal analysis was done without considering the steel bars, because the temperature at the center of the bars is equal to the temperature of concrete at corresponding point.

Geometry of concrete beam is the same as illustrated in chapter 4 part 4.2.1. The difference is the section was extruded to 3 meters of depth to get the 3D model. Since there is a symmetry in six-meter-length beam, therefore only the half of the beam which is length of 3 meters, was modelled (Figure 6-1).

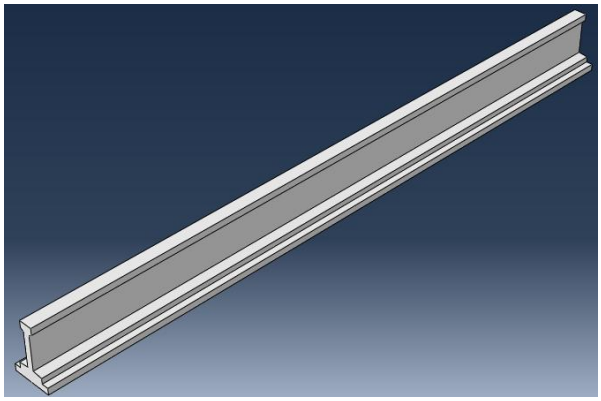

Figure 6-1: Geometry of concrete beam (3D model)

The second part is steel bars. By defining new part in Abaqus the steel bars were drawn in plane and extruded for 3 meters.

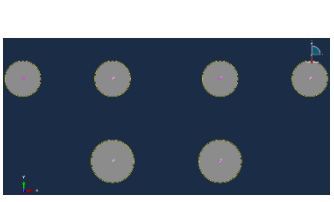

a)

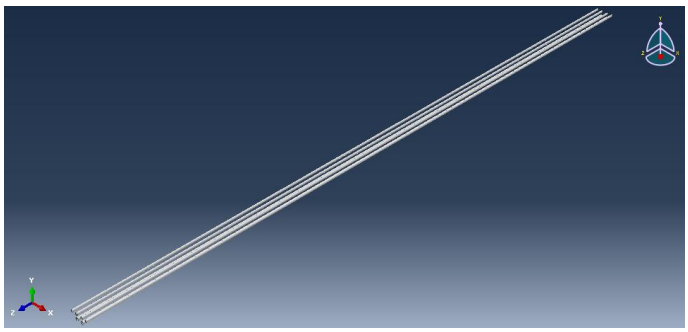

b)

Figure 6-2: Geometry of steel bars ; a)steel bars in plane section b)steel bars after extrusion

The radius of steel bars in the first layer is 6 mm and for the second layer is 5 mm. the coordinates and positions of steel bars are the same as illustrated in chapter 4. Some inputs to draw the steel bars were presented in **Error! Not a valid bookmark self-reference.**.

Center Coordinates of circles with radius of 5 mm (x,y,z)	Center Coordinates of circles with radius of 6 mm (x,y,z)
40.E-03,45.E-03,0.	15.E-03,22.E-03,0.
15.E-03,45.E-03,0.	-15.E-03,22.E-03,0.
-15.E-03,45.E-03,0.	
-40.E-03,45.E-03,0.	

Table 6-1: Coordinates of the steel bars points

6.1.2 Property of the material

In this part the property of the material used in the beam will be defined and assigned to the model. Beam consists of steel and HPFRC material. The mechanical and thermal properties and their degradation in high temperature has been already described in Chapter 3, part 3.5. To have a short view of inputs a summarize description of the material has been presented in the next part. Material properties are mostly temperature dependent while there are also some other properties that presented only in room temperature.

6.1.2.1 HPFRC:

1- Conductivity (inputs varies with temperatures and are the same as 2D model)

2- Density (inputs varies with temperatures and are the same as 2D model)

3- Specific heat (inputs varies with temperatures and are the same as 2D model)

4- Elastic: Young modulus, Poisson's ratio (varies with temperatures)

Young's modulus of the concrete used is $1.49\frac{\varepsilon_{c1}}{f_c}$ and according to the coefficient given in Eurocode 2 part 1-2 (table 3.1), the degradation of compressive strength (f_c) and strain corresponding to f_c (ε_{c1}) and can be calculated for high temperature (as described in 4.4.3.1.1).

Young's Modulus ($\frac{N}{m^2}$)	Poisson's ratio	Temperature (°C)
65824000000	0.2	20
23936000000	0.2	200
9873600000	0.2	400
2632960000	0.2	600
526592000	0.2	900

Table 6-2: Table of Young's Modulus variation by increasing temperature

5- Expansion (Constant and equal to 2E-005)

6- Concrete damaged plasticity:

a) Plasticity (constant),

Plasticity Properties	
Dilation Angle	38
Eccentricity	0.1
f_{b0}/f_{c0}	1/16
K	0.67
Viscosity parameter	0

Table 6-3: plasticity properties of concrete input of 3D model

b) Compressive behavior (varies with temperatures)

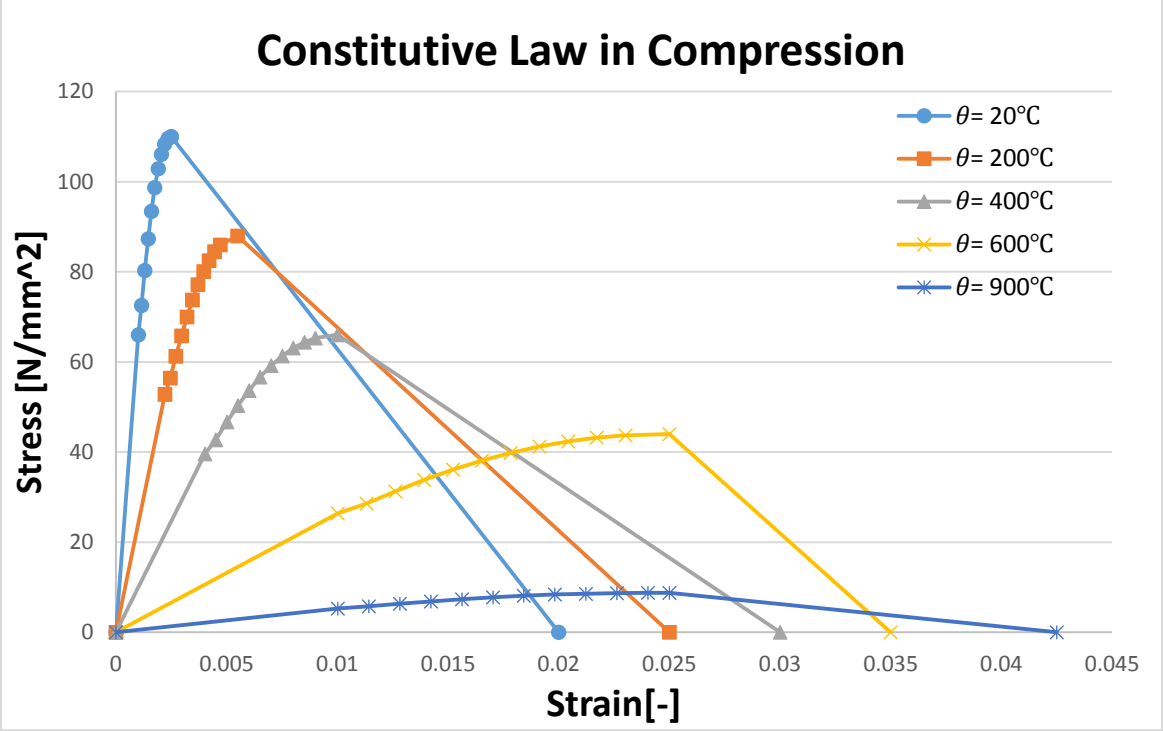

Figure 6-3: compressive stress- strain relationship of concrete c110 for different values of the concrete temperature.(refer to 4.4.3.1.1)

In Abaqus the inputs are inelastic strain and it is assumed that 60% of maximum compressive strength (0.6fc) is the starting point for inelastic strains.

Yield stress (N/ m2)	Inelastic strain	Temperature	Yield stress (N/ m2)	Inelastic strain	Temperature
66000000	0	20	26400000	0	600
72522280	0.00015	20	28573868	0.0013	600
80296408	0.0003	20	31317126	0.0026	600
87311503	0.00045	20	33841445	0.0039	600
93464387	0.0006	20	36118240	0.0052	600
98675871	0.00075	20	38123698	0.0065	600
1.03E+08	0.0009	20	39840111	0.0078	600
1.06E+08	0.00105	20	41256796	0.0091	600
1.08E+08	0.0012	20	42370505	0.0104	600
1.1E+08	0.00135	20	43185328	0.0117	600
1.1E+08	0.0015	20	43712115	0.013	600
1.1E+08	0.001497	20	44000000	0.014973	600
0	0.018997	20	0	0.024973	600
52800000	0	200	5280000	0	900
56429239	0.00025	200	5758390	0.0014	900
61291860	0.0005	200	6344099	0.0028	900
65831678	0.00075	200	6877957	0.0042	900
70008870	0.001	200	7353031	0.0056	900
73788512	0.00125	200	7763762	0.007	900
77142094	0.0015	200	8106316	0.0084	900
80048717	0.00175	200	8378808	0.0098	900
82495883	0.002	200	8581351	0.0112	900
84479817	0.00225	200	8715961	0.0126	900
86005336	0.0025	200	8786324	0.014	900
88000000	0.003294	200	8800000	0.014973	900
0	0.022794	200	0	0.032473	900
39600000	0	400			
42696614	0.0005	400			
46670235	0.001	400			
50343457	0.0015	400			
53677641	0.002	400			
56640042	0.0025	400			
61357778	0.0035	400			
63089983	0.004	400			
64404829	0.0045	400			
65313967	0.005	400			
66000000	0.005989	400			
0	0.025989	400			

Table 6-4: Table of yield stress-Temperature value of concrete input of 3D model

c) Tensile behavior (varies with temperatures)

According to description given in chapter 4 part 4.4.3.1.2, tensile behavior of HPFRC is allocated to steel fibers and it is shown in Figure 6-4.

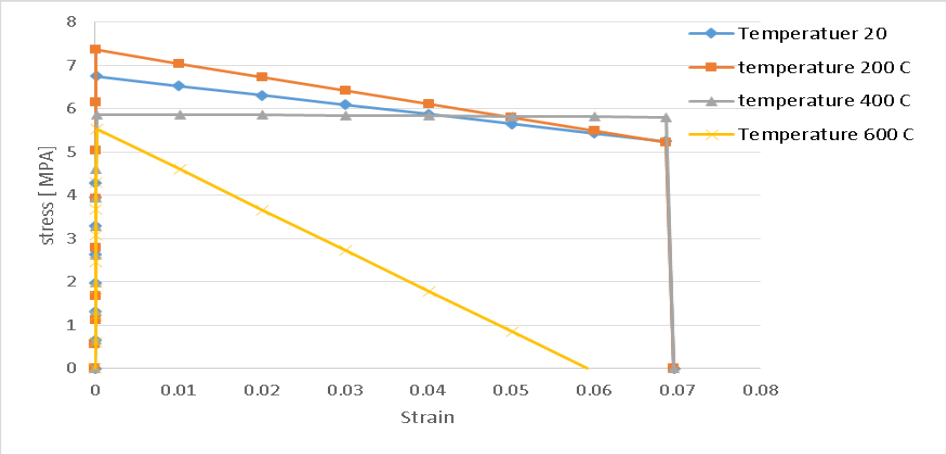

Figure 6-4: Constitutive law for HPFR in tension for different temperatures (refer to 4.4.3.1.2)

The program required displacement instead of strain. In order to convert strain to displacement the characteristic length (4.4.3.1.2) has been used. The inputs of Abaqus are also started from the maximum stress because after that point, cracks propagate.

Yield stress (N/m2)	Displacement (m)	Temperature	Yield stress (N/m2)	Displacement (m)	Temperature
6750000	0	20	0	0.002532	200
6531243	0.000364	20	5872500	0	400
6312487	0.000728	20	5862645	0.000364	400
6093730	0.001092	20	5852790	0.000728	400
5874973	0.001456	20	5842935	0.001092	400
5656217	0.00182	20	5833080	0.001456	400
5437460	0.002184	20	5823225	0.00182	400
5250000	0.002496	20	5813370	0.002184	400
0	0.002533	20	5805000	0.002494	400
7357500	0	200	0	0.00253	400
7046735	0.000364	200	5535000	0	600
6735969	0.000728	200	4596566	0.000364	600
6425204	0.001092	200	3658131	0.000728	600
6114438	0.001456	200	2719697	0.001092	600
5803673	0.00182	200	1781262	0.001456	600
5492907	0.002184	200	842828	0.00182	600
5227500	0.002495	200	0	0.002148	600

6.1.2.2 Steel:

1- Conductivity (constant=46)

2- Density (constant=7750 Kg/m3)

3- Specific heat (constant=490 j/kgC)

4- Elastic: Young modulus, Poisson's ratio

Young's Modulus N/m2	Poisson's ratio	Temperature
2.05E+11	0.3	20
2.05E+11	0.3	100
1.85E+11	0.3	200
1.64E+11	0.3	300
1.44E+11	0.3	400
1.23E+11	0.3	500
6.36E+10	0.3	600
2.67E+10	0.3	700
1.85E+10	0.3	800
1.44E+10	0.3	900

Table 6-5: Young's Modulus over temperature increasing input of steel in 3D model

5- Expansion (constant=1E-020)

6- Plastic

Constitutive law for steel bars has been already presented in 4.4.3.2. Figure 6-5 presents the final results of that part that will be used as input of Abaqus. It is worth noticing that in software the plastic strain is needed, therefore from this graph the corresponding value of plastic strains should be extracted and inserted in the required field. Plastic strain starts when the stress reaches to its maximum value and the results were presented in Table 6-6.

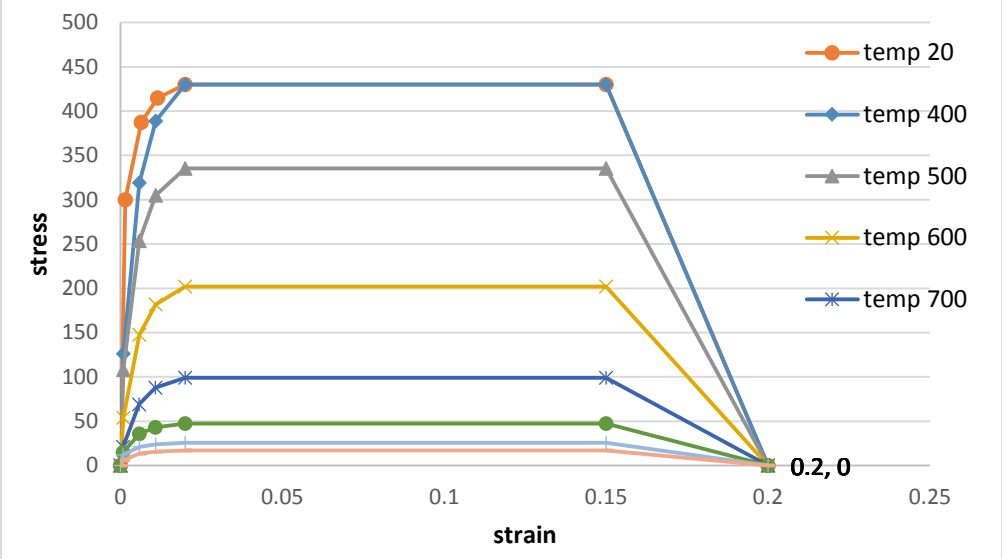

Figure 6-5: constitutive law of steel

Yield Stress (N/m2)	Plastic Strain	Temperature
4.3E+08	0	20
4.3E+08	0.196902	20
4.3E+08	0	400
4.3E+08	0.196003	400
3.35E+08	0	500
3.35E+08	0.196273	500
2.02E+08	0	600
2.02E+08	0.19582	600
98900000	0	700
98900000	0.195289	700
47300000	0	800
47300000	0.196436	800
25800000	0	900
25800000	0.197202	900
17200000	0	1000
17200000	0.196902	1000

Table 6-6: plastic strain of steel bars in different temperature

6.1.3 Assembly

In this section, HPFRC beam (part 1) and Steel bars (part 2) are assembled together. In order to assemble these two parts, firstly it is needed to extract holes corresponding to steel bars from the beam. Then, by adding steel bars to part 1 in the positions of holes the model become complete and new part will be created (Part 3). At the end, it is better to make part 3 dependent in order to have better meshing.

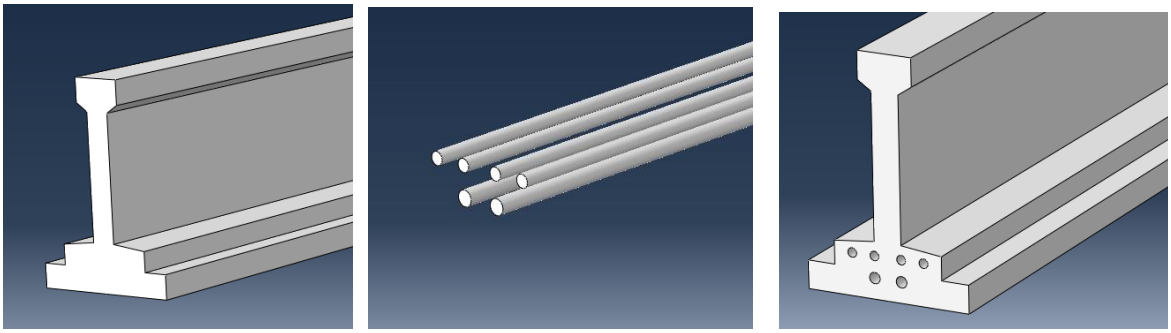

a) Part 1 b) Part2 c) Part 1 with holes

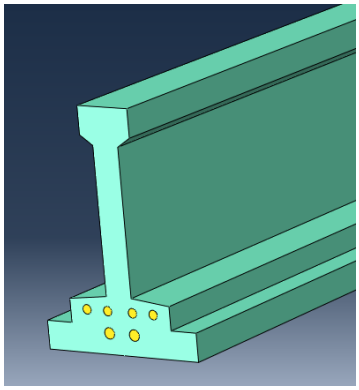

d) Part 3

Figure 6-6: procedure to assemble steel bars and HPFRC beam

6.1.4 Step

In this part, the method of analyzing and its required parameters were defined. Since the model is carrying load and also exposed to fire, the method has been chosen is "coupled temp-displacement". Time period is 12370 seconds and was used transient response. Maximum number of increment is 500000 with initial size of 0.01 and maximum size of 50. Maximum allowable temperature change per increment is 10. Using linear extrapolation between results of two following increments.

The outputs are "stresses", "plastic strains (PE)", "Strains (E)","Nodal temperature (NT)", "Damage" and "displacement (U)" for every increments.

6.1.5 Interaction

Interaction is the part that the property and characteristic of fire will be defined. Surface radiation and surface film condition has been defined same as 2D model and the only difference refers to the surface of exposure which is on the bottom plane of the beam in 3D model.

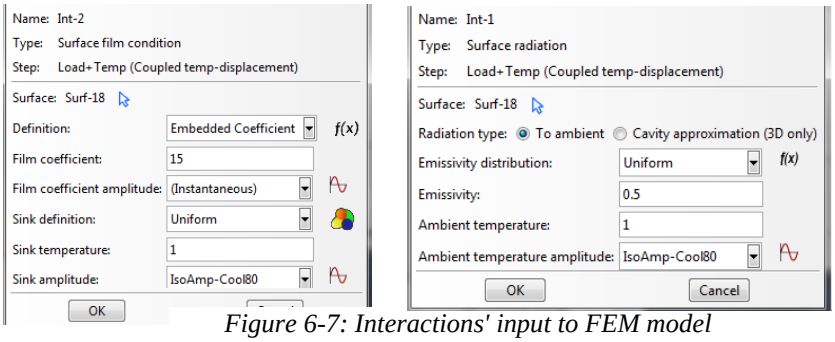

Figure 6-7: Interactions' input to FEM model

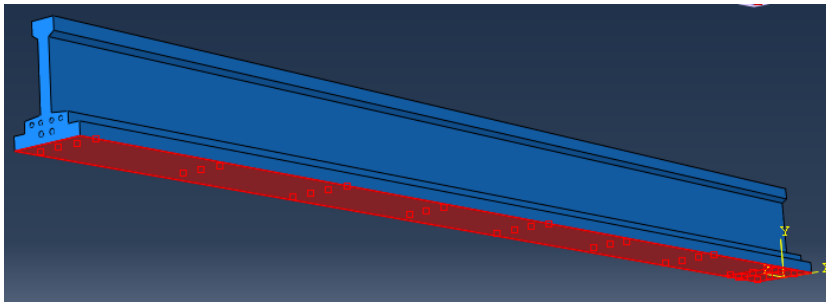

Figure 6-8: Exposed surface

6.1.6 Load , Boundary condition and predefined field

Loads (dead load and live load) are defined as a “Pressure” on the top surface of the beam. The pressure is equal to 106 KN/m2 and is the value of Load divided by the width of the beam at top.

From chapter 3: liniear Load on beam $= 6.395$ KN/m

$$\text{Pressure} = \frac{6395}{0.06} = 106 \frac{\text{KN}}{\text{m}^2}$$

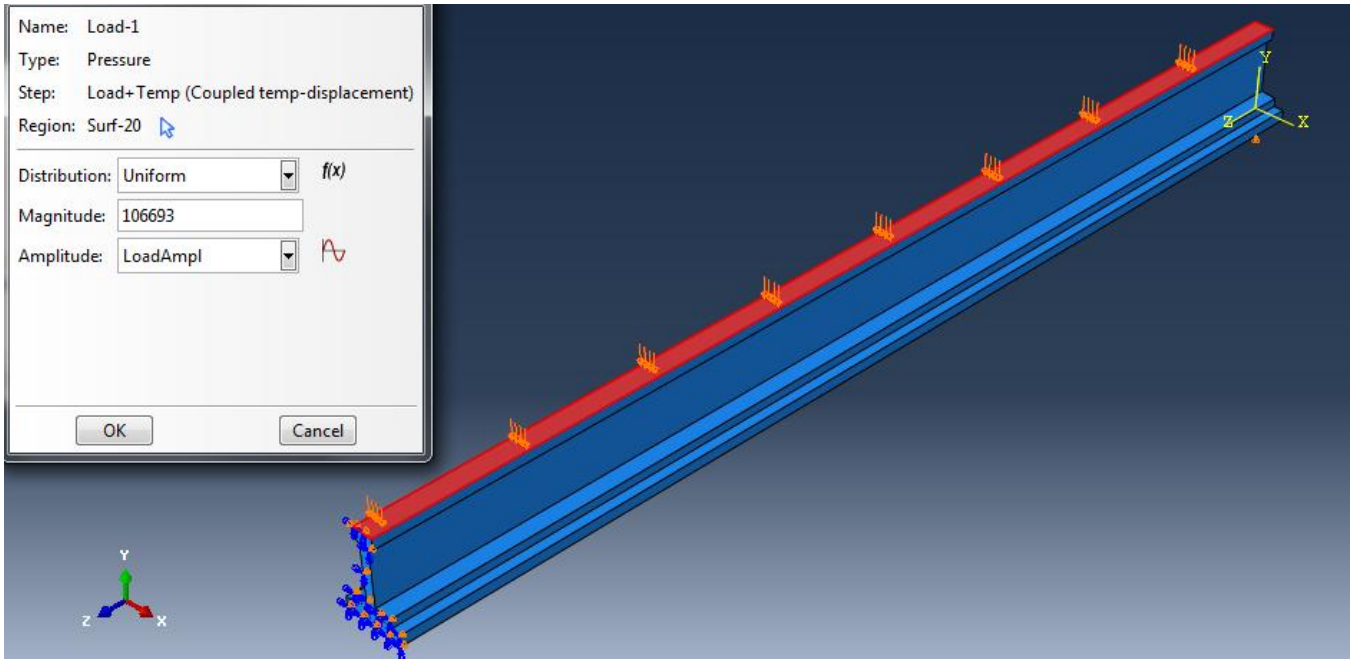

Figure 6-9: Loads in FEM model

Only half of the beam was modelled due to existence of symmetry and therefore a symmetry boundary conditions will be used at the center of the beam. Simple support has been chosen for the beam end by fixing Y and X movements equal to zero. Furthermore,

a constraint is set at the center of the beam for X direction restraining the displacement regarding the rigid body motions.

In predefined field, the whole model has been selected and initial temperature equal to 20 C was assigned.

6.1.7 Mesh

In element types part, “Standard and linier coupled temperature -displacement” is chosen for the analysis. Approximate global size of meshes are 0.02 and using tet mesh.

Total number of nodes: 48176

Total number of elements: 262521

262521 linear tetrahedral elements of type C3D4T

All regions in the assembly that require a mesh are meshed.

6.1.7.1 Meshes and Convergence

Since this model has shown a sensitivity analyzing on meshing, therefore it is important to mesh the model with more care. The results with different meshes reveals that the dependency of response to mesh size and type is high and convergence should be considered. Convergence is a concept in FEM, representing that the smallness of the elements beyond a certain size does not affect its accuracy and final results.

Abaqus is a Finite Element Method and uses numerical techniques to find approximate solution for structural problems. When solving a finite element problem, we have to ensure that the solution we obtained is accurate. One of the approximation in a FEM comes from mesh and discretization of the model. The geometry is discretized into finite number of small elements. Increasing the number of elements in the model will cause the solution to approach the analytical solution. At some point further mesh

refinement yields little or no change in solution, and the mesh is assumed to have converged.

Abaqus offers few convenient ways to evaluate mesh convergence such as Quilt, Discontinuity and SJP (strain jump at nodes). They are effective tools to quickly check mesh convergence and have confidence on the analysis results in the context of the finite element mesh. In this study only the first way has been used. In the visualization module of Abaqus/CAE offers some contour options to check for mesh convergence. One of the contour plot options is Quilt contour. Quilt contour plot is an effective means of displaying results on an element-by-element basis. The values are computed for each element face individually with no averaging across element boundaries. Hence it shows the difference in values across individual elements against neighboring elements thereby giving a reasonable idea about mesh convergence. Quilt plot options are available only for element based outputs. The results are shown in Figure 6-10.

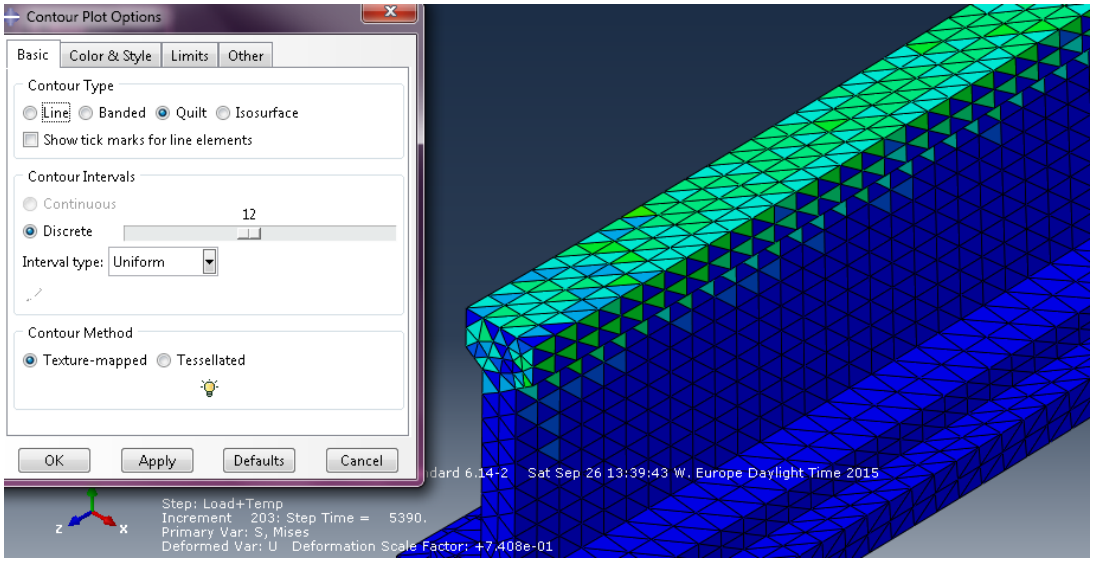

Figure 6-10: Convergence check -Quilt option

Ideally a mesh is fine enough such that for any given node, all the elements attached to it have nearly the same strain. For coarse meshes in areas of rapidly changing strain, adjacent elements sharing one or more of the same nodes may calculate dramatically different strain values. When the adjacent nodes have the same strain values the error is zero and when the nodes have different values the error is positive, naturally the closer the error to zero the higher confidence in results. As the number of elements

increases in the solution, it provides a more accurate representation of the solution field and the discretization error is reduced.

In order to reduce the cost of calculation, it is necessary to avoid very fine meshes. Therefore among three options of mesh type (Hex, Wedge and Tet), Tet has been chosen, because it approaches convergence in meshing with larger size than Hex or wedge.

6.1.8 Job and visualization

By creating a job in the "job" part, the model will be submitted and the results will be stored in visualization part.

6.1.8.1 Results

After submitting the job, an error occurs indicating that "the analyzing has not been completed successfully". This means that the beam will collapse so the analyzing of the problem stops at time of failure. This time is the last step that the results have been calculated. For this model it happens after 5390 seconds, indicating that after about 90 minutes the beam will collapse. Results can be illustrated in different outputs and some of them are presented in this part:

- Nodal temperature

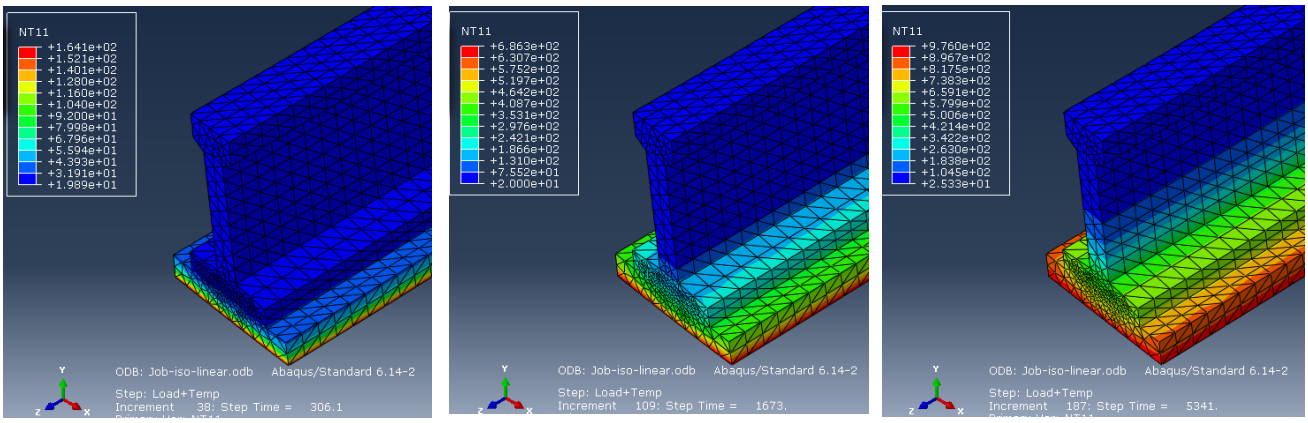

Figure 6-11: evolution of nodal temperature for different steps

As Figure 6-11 shows, temperature increases from the bottom of the beam where there is exposed surface to the top. Degradation of material strength will be more in tensile zone for steel fibers and for steel bars rather than compressive zone or concrete properties of the beam.

- Stresses on the beam:

Stresses on beam evolve by increasing the temperature and when a point reaches to its final strain, the stress become zero. For point B, evolution of stress over time has been plotted in Figure 6-12. There is an initial stress due to initial strain and then there is increasing trend of stress until it experienced its maximum strain and then it reaches to zero means that the point will not any more contribute for the bearing capacity of the beam. Figure 6-13 shows the evolution of stresses over the beam for 3 different steps.

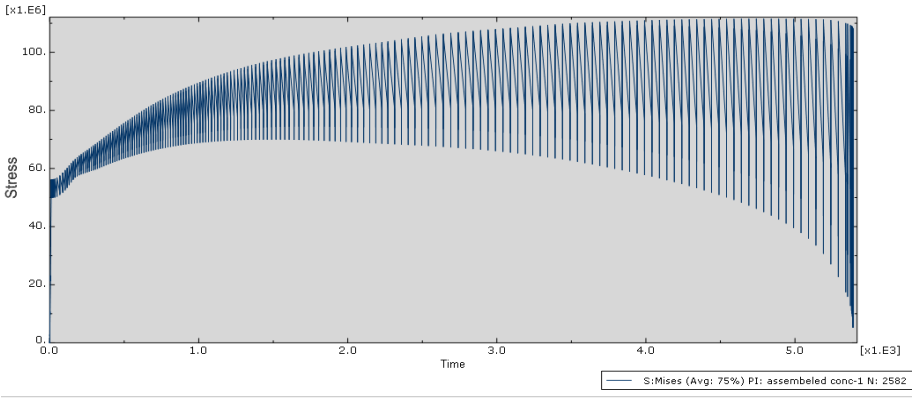

Figure 6-12: Stress over time for point B

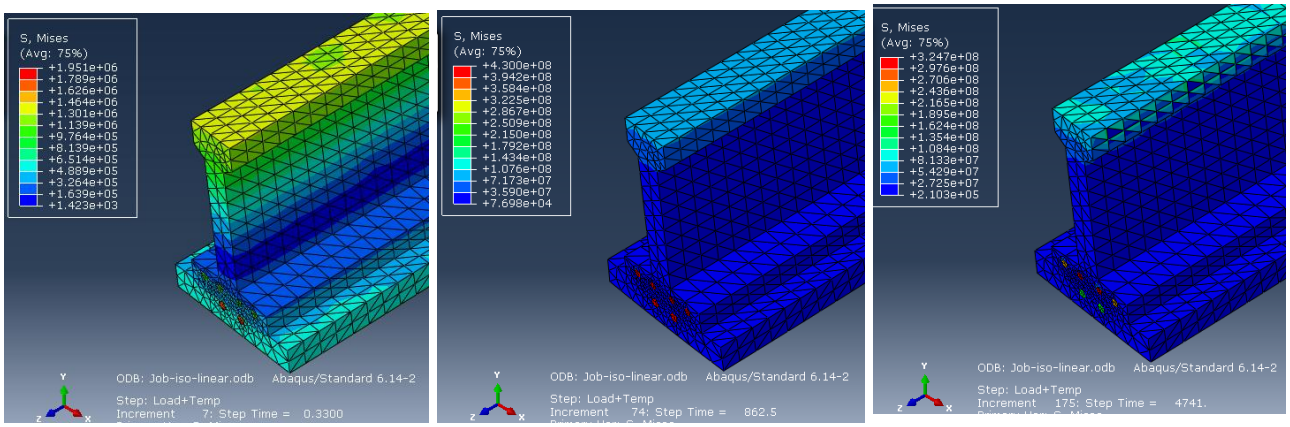

Figure 6-13: Von Mises Stresses evolution for 3 steps

- Plastic strain and total strain

Figure 6-14 shows the plastic strain evolution over the beam. As it can be observed, plastic strain is activated only on small portion of the beam at the last step. As it is shown in figure, other parts (dark blue) have zero plastic strains. For these parts the elastic strain existed and it has been shown in Figure 6-15.

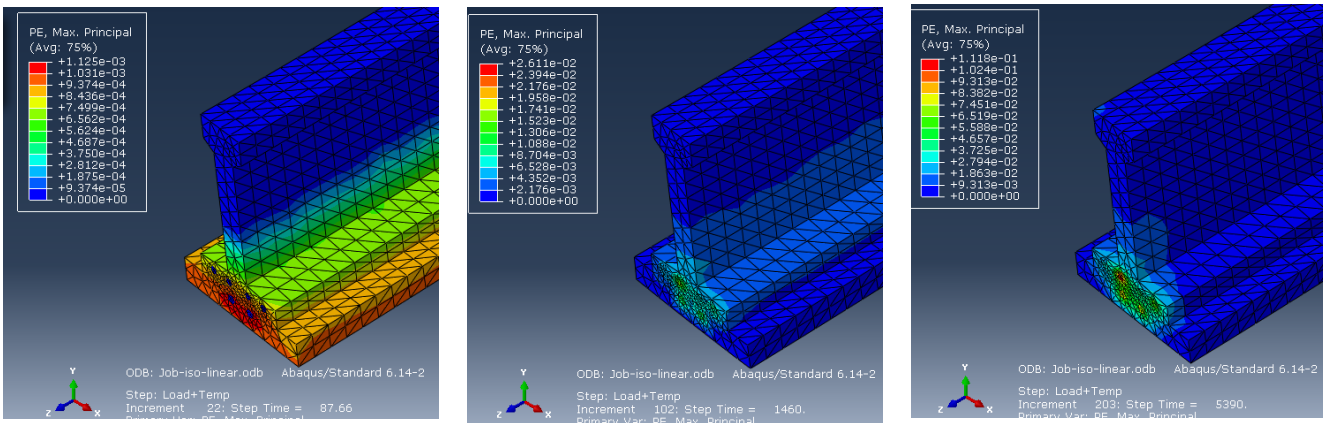

Figure 6-14: Plastic strain evolution over time (for three different steps)

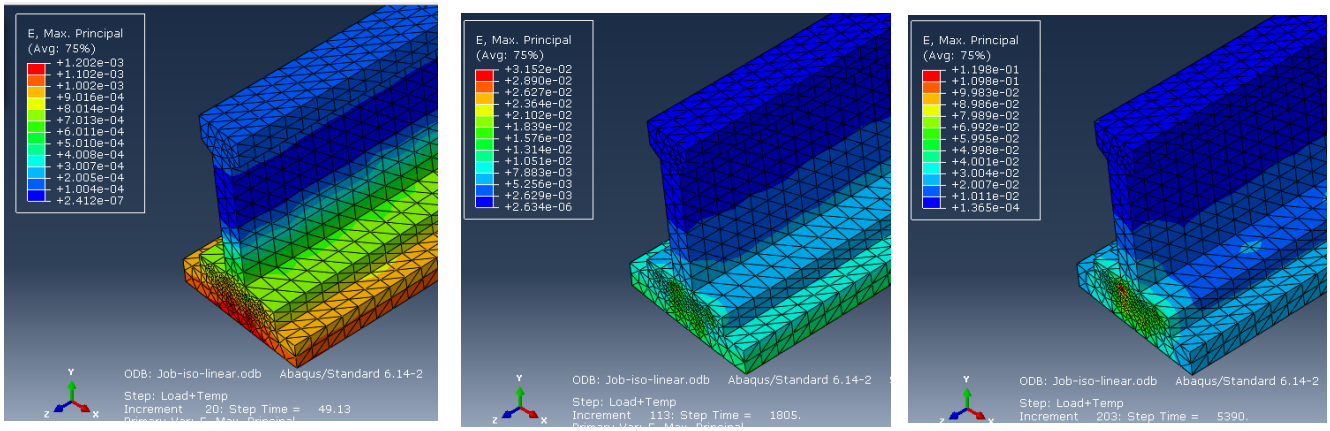

Figure 6-15: Total strain evolution over time (for three different steps)

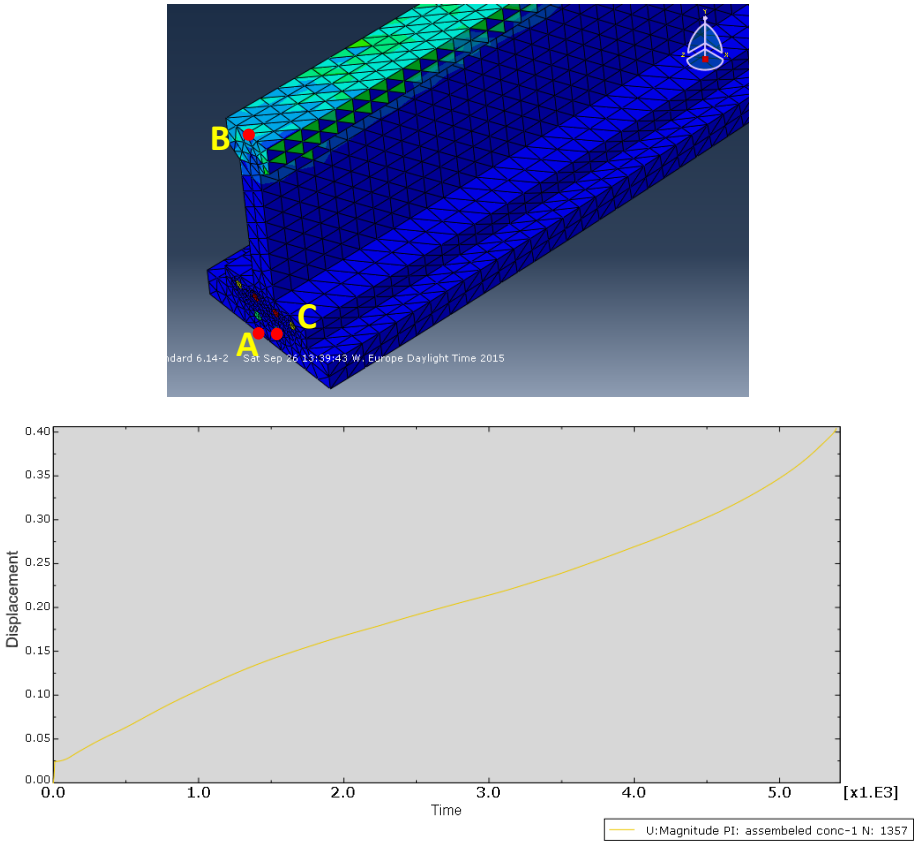

Figure 6-16: Displacement-time from FEM for center point

In the model a central point has been chosen to interpret the results. This point (A) is critical point since it is located at the bottom of the beam (tension zone) in mid-span and suffers the highest displacement. The results of Displacement-time of this point has been shown in Figure 6-16.

As it can be seen there is an initial increase in displacement and then there is an increasing trend until it reaches to failure. The initial increase in displacement is due to the mechanical loading act on the beam and it makes a maximum displacement in the center of the span which is around 0.0129 mm. Then the beam is going to expose fire ISO834 and experiences degradation in material strength which leads to increase displacement until it fails completely. As it can be seen in Figure 6-17, total strain of that point increases as well due to increase of temperature. For plastic strain, the results indicates that there is a primary plastic strain at the beginning while this value is small and constant over a specific period of time. Then, after 5000 seconds (83 min) it starts to increase and reaches to infinite value after 6 minutes which means that the beam collapsed after 89 minutes of fire exposure.

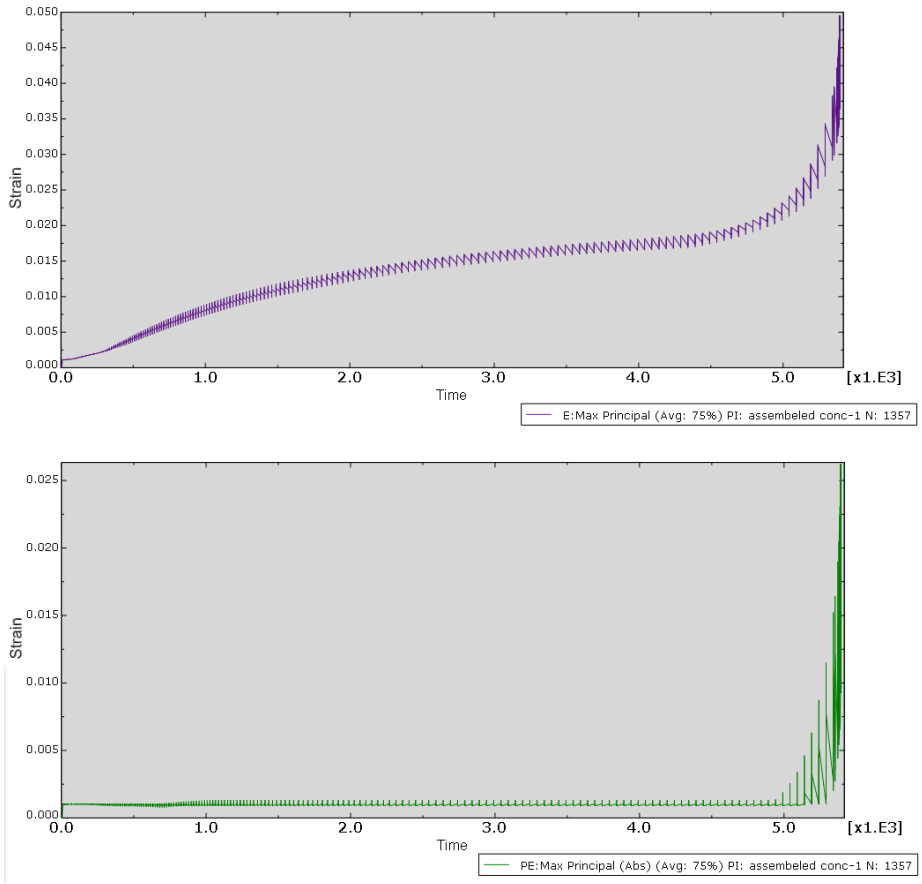

Figure 6-17: total and plastic Strain over time of a central point

Now, choose a node B located at top of the section (compression zone) in the center of the span. Observing the results which has been presented in Figure 6-18, shows that there is an elastic strain at the beginning of the analysis due to the mechanical loading and then as temperature increases the total strain increases due to the activation of plastic strains and its evolution over time.

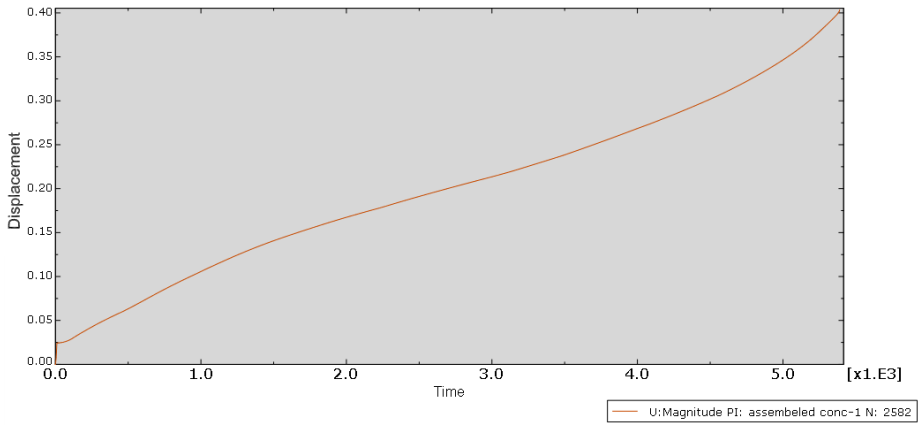

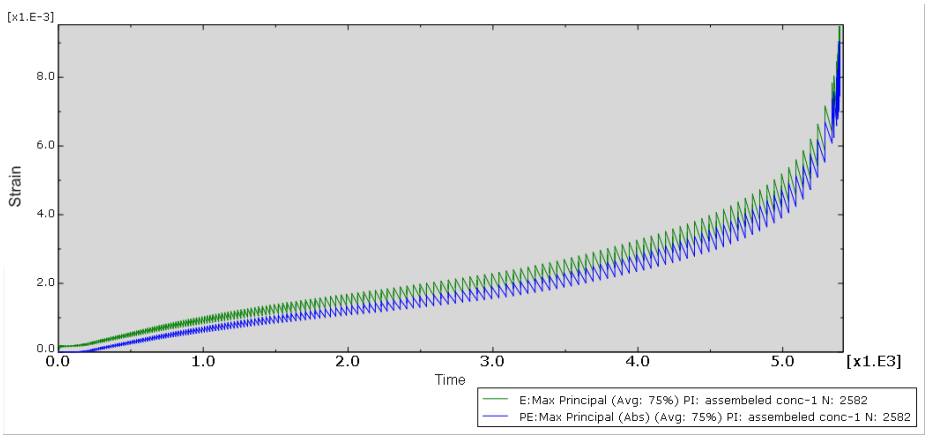

Figure 6-18: Total strain and plastic strain over time of a central point in compression zone

Point C was selected to study and is located in steel bars in the first layer and the result has been presented in Figure 6-19. It shows that there is an initial elastic strain due to the mechanical loading and by exposing to thermal loading this strain increases without any activation of plastic strains. Activation of plastic strain will occur after 7.5 minutes and it increases until it reaches to failure.

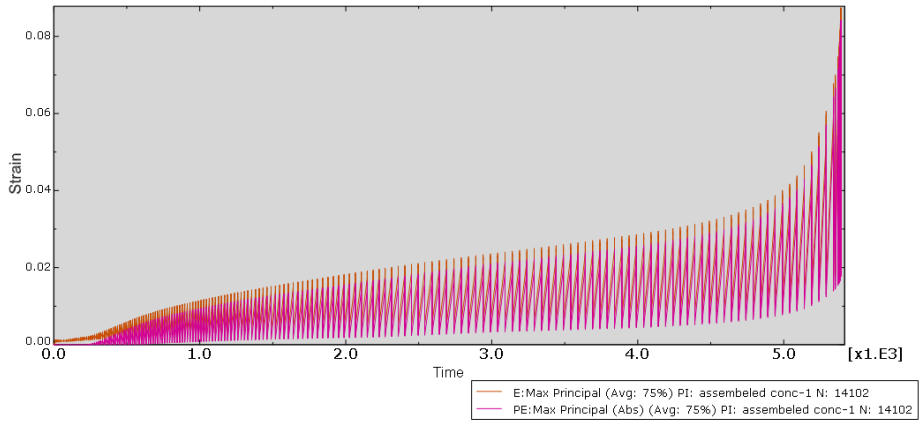

Figure 6-19: total strain and plastic strain of a central point in steel bars

6.1.9 Conclusion

One of the differences between plane section approach (2D) and FEM approach (3D) is the failure time. 3D model (finite element analysis) can resist more against fire. It can be because of contribution of the beam section at the center with transversal sections. On the other words, the bearing capacity of 3D model is proportional to the section and its surroundings' contributions which make confinement for the beam while in 2D analysis, only the cross section stands against the loads and the surrounding concretes is disregarded. This confinement can increase the bearing capacity in terms of bending moment and can make the beam more resistance against elevated temperature.

6.1.10 Different fire scenarios

Different fire scenarios are being considered in FEM model to find the effect of cooling phases. The model is the same used before only the fire table changed. Fire exposure can be considered with cooling phases that starts at different times such as 60 min, 70 min or after 80 min. Different fire scenarios are shown in Figure 6-20.

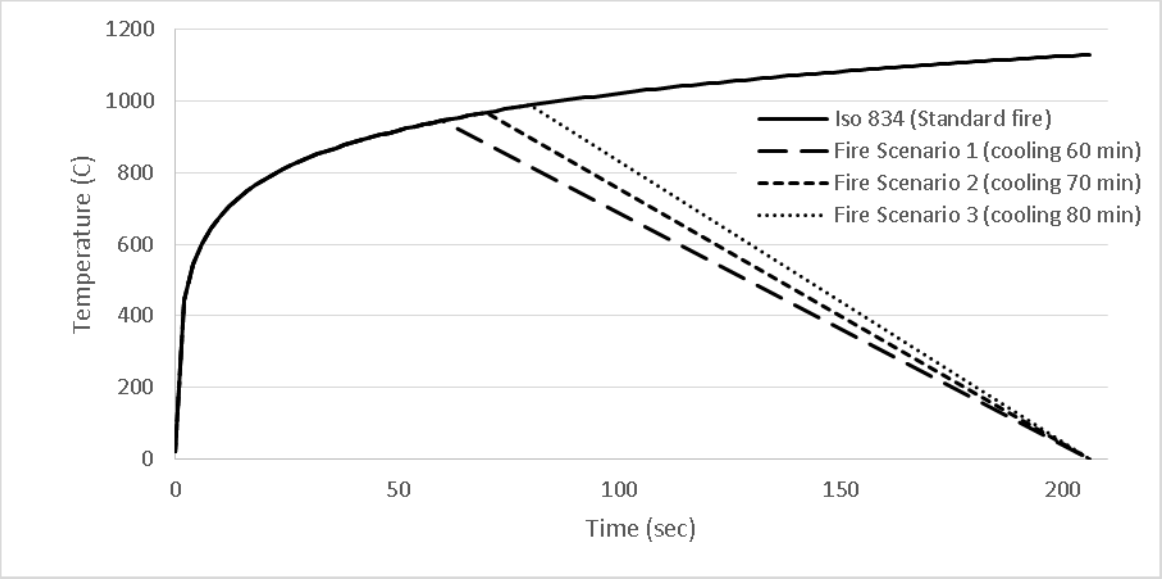

Figure 6-20: Fire exposure scenarios considered in 3D model

6.1.10.1 Results of different scenarios

The results reveals that the beam can stand against the loads completely if the cooling started before 70 minutes, while if the cooling started at any time after 80 minutes it cannot resist and will fail after some minutes. In the 3rd scenario, the cooling started after 80 minutes and the section fails at 92 minutes of total time period. However in other two scenarios that cooling started sooner (after 60 and 70 minutes), the beam will not fail and only experienced deflection.

In the 3rd scenario, the result of strain-time for a point located at the center and bottom of the beam reveals that the strain goes to infinite after 92 minutes (Figure 6-21).

This time is higher than the time of cooling started (80 min) and it is due to the penetration of temperature into the section and continue increasing of temperature in a certain depth over a specific time after cooling started.

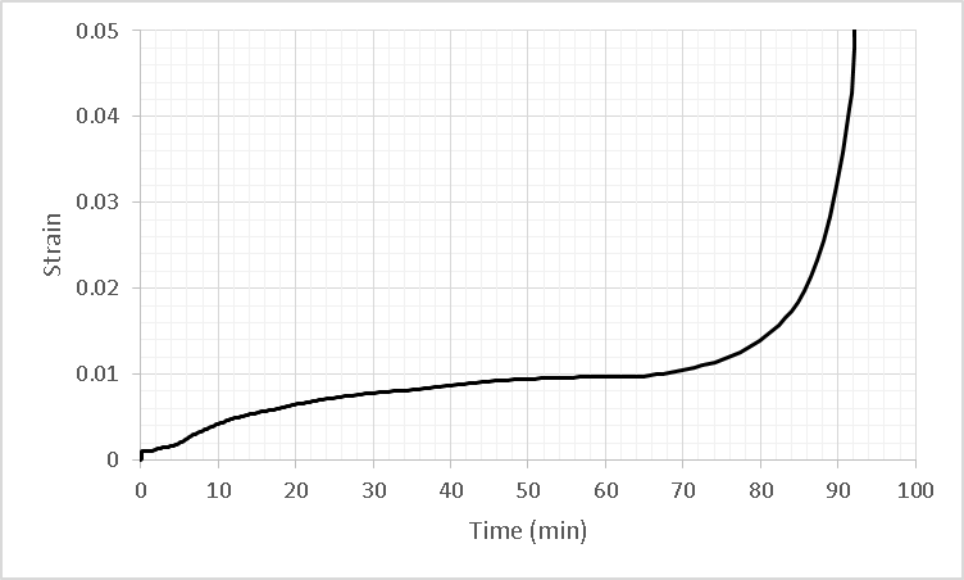

Figure 6-21: Strain-time of scenario 3 for a central point

The section will not fail if the cooling started after 80 minutes. If the cooling started at any time after 80 minutes, the analyses of FEM cannot complete means that the section will collapse. Result of the FEM with cooling started at 80 minutes is presented here. As we can see the beam can resist for 92 minutes and then collapse. According to

the results, the failure will occurs 12 minutes after cooling starts. Figure 6-22 shows the temperature distribution of beam at time of failure.

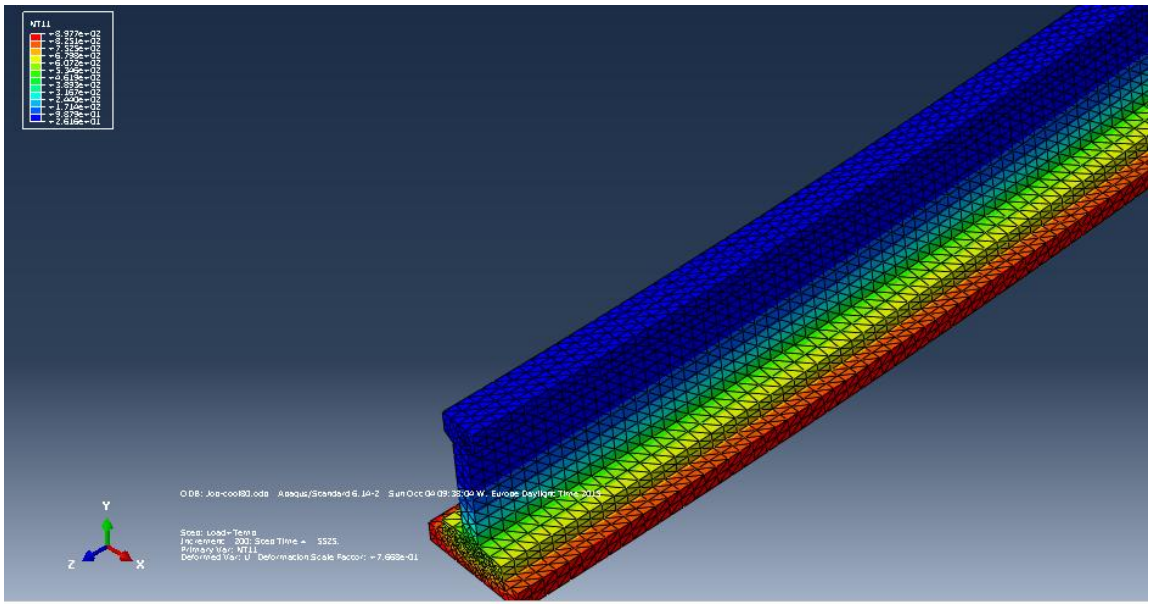

Figure 6-22: Thermal distribution of beam exposed to fire with cooling at 80 min

As we can in Figure 6-23, there is maximum tensile stresses in steel bars.

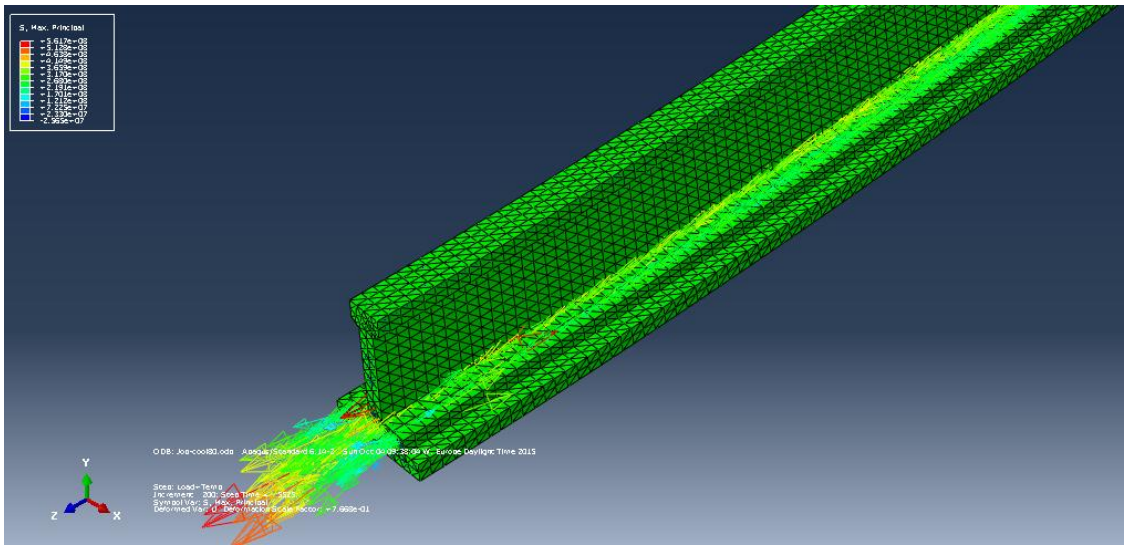

Figure 6-23: Maximum principal stresses on beam section at time of failure

6.1.11 Comparing results

Comparing the results of plane sectional approach (2D model) and 3D model for different time of cooling reveals that the 3D model stands more and failure will occur only in case of cooling after 80 minutes and there is no failure if the cooling started before 80 minutes. While in 2D model even if the cooling started at 30 min, the beam will fail after a while. It indicates that in 3D model there is contribution of transverse planes which made beam to be confined, therefore it leads to increase the bearing capacity.

7 Beam with slab (2D and 3D)

Model has been also considered with one-meter-length slab on the beam. The slab was added to the beam in both 2D and 3D approach and the bending moment capacity has been calculated in different scenarios.

1- Only bottom side of the beam exposed to fire ISO834 (No cooling),

2- both bottom sides of beam and slab exposed to fire with cooling phases

7.1.1 Geometry of beam with slab

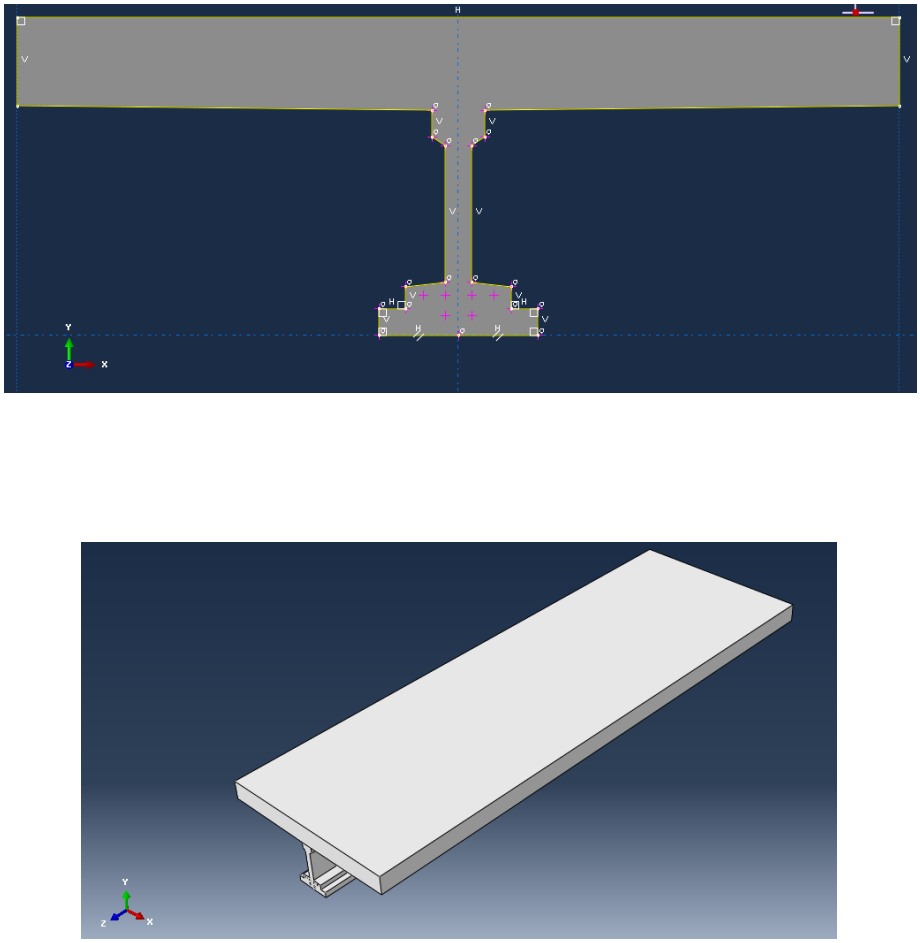

Figure 7-1:Model of beam with slab

7.1.2 Property of the Slab

In this part the property of the material used for slab is defined. The material used for beam is the same as before while for slab the material is normal fiber reinforced concrete (FRC), therefore the required fields for slab will be filled with the data of FRC given in chapter 2.

1- Density (General properties)

Used as uniform distribution and temperature dependent data

Density (kg/m3)	2300	2300	2250	2250
Temperature (C)	20	70	120	1220

Table 7-1: Density over temp input of numerical model

2- Conductivity (Thermal properties)

Used type as isotropic and temperature dependent data

Temperature (°C)	Conductivity (W/MK)	Temperature (°C)	Conductivity (W/MK)
20	1.960333	570	1.13075
70	1.864083	620	1.080333
100	1.808333	670	1.034083
120	1.772	720	0.992
150	1.71875	770	0.954083
170	1.684083	820	0.920333
200	1.633333	870	0.89075
220	1.600333	920	0.865333
270	1.52075	970	0.844083
320	1.445333	1020	0.827
370	1.374083	1070	0.814083
420	1.307	1120	0.805333
470	1.244083	1170	0.80075
520	1.185333	1220	0.800333

Table 7-2: Conductivity over temperature input of numerical model

3- Specific Heat (Thermal properties)

Used constant volume and temperature dependent data.

Temperature (C)	Specific Heat(J/kgK)	Temperature (C)	Specific Heat(J/kgK)
20	913.2222	570	1189.75
70	945.3056	620	1206.556
100	963.8889	670	1221.972
120	976	720	1236
150	993.75	770	1248.639
170	1005.306	820	1259.889
200	1022.222	870	1269.75
220	1033.222	920	1278.222
270	1059.75	970	1285.306
320	1084.889	1020	1291
370	1108.639	1070	1295.306
420	1131	1120	1298.222
470	1151.972	1170	1299.75
520	1171.556	1220	1299.889

Table 7-3: Temperature-specific heat of concrete of slab input of Abaqus

4- Elastic: Young modulus, Poisson's ratio (varies with temperatures)

Young's modulus and Poission's ratio of the concrete used is :

Young's Modulus ($\frac{N}{m^2}$)	Poisson's ratio	Temperature (°C)
28050000000	0.2	20

5- Expansion (Constant and equal to 2E-005)

6- Concrete damaged plasticity:

- Plasticity (constant),

Plasticity Properties	
Dilation Angle	38
Eccentricity	0.1
f_{b0}/f_{c0}	1/16
K	0.67
Viscosity parameter	0

Table 7-4: Plasticity properties of slab input of Abaqus

- Compressive behavior:

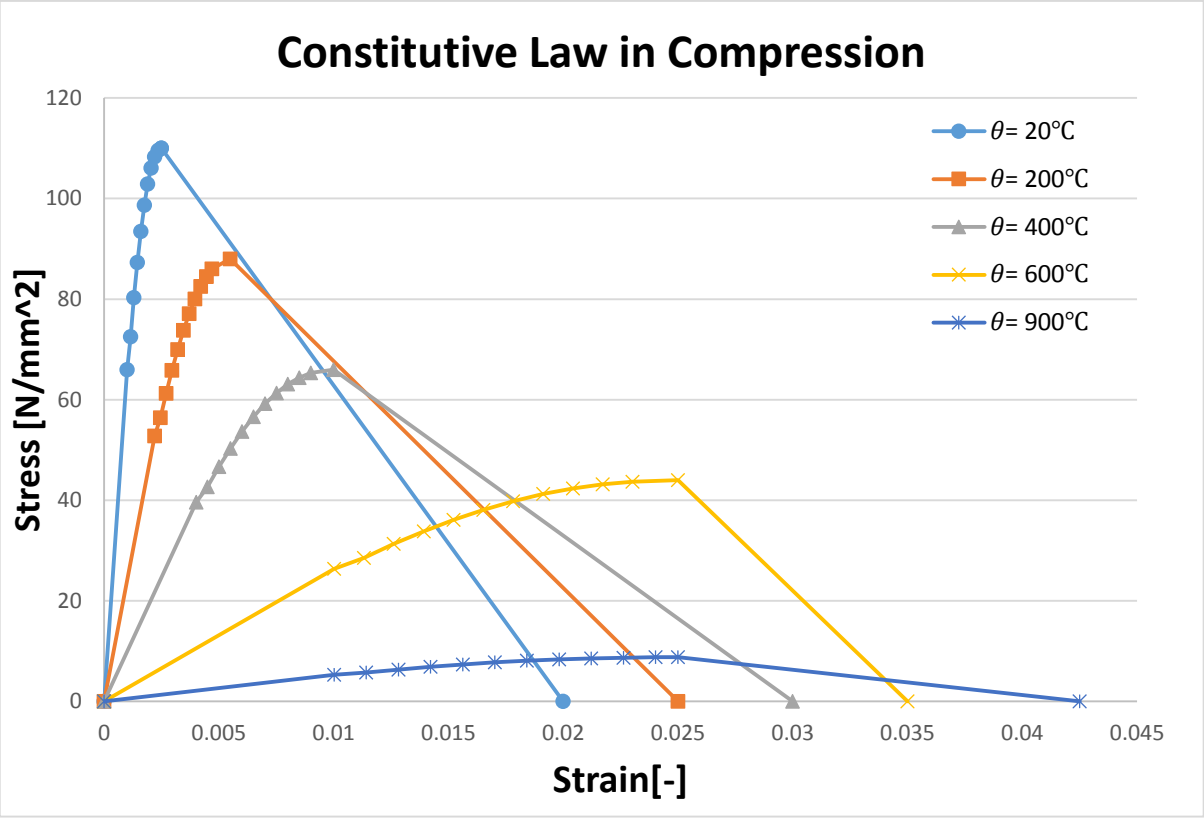

Figure 7-2: Constitutive law for slab in compression

Yield stress (N/m2)	Inelastic strain	Temperature	Yield stress (N/m2)	Inelastic strain	Temperature
27000000	0	20	10800000	0	600
29806297	0.00015	20	11689310	0.0013	600
33100177	0.0003	20	12811552	0.0026	600
36053038	0.00045	20	13844228	0.0039	600
38618211	0.0006	20	14775644	0.0052	600
40760971	0.00075	20	15596058	0.0065	600
42461207	0.0009	20	16298227	0.0078	600
43714604	0.00105	20	16877780	0.0091	600
44532250	0.0012	20	17333388	0.0104	600
44938855	0.00135	20	17666725	0.0117	600
44969955	0.0015	20	17882229	0.013	600
45000000	0.001437	20	18000000	0.014973	600
0	0.019037	20	0	0.024973	600
21600000	0	200	2160000	0	900
23084689	0.00025	200	2355705	0.0014	900

25073943	0.0005	200	2595313	0.0028	900
26931141	0.00075	200	2813710	0.0042	900
28639992	0.001	200	3008058	0.0056	900
30186209	0.00125	200	3176084	0.007	900
31558129	0.0015	200	3316220	0.0084	900
32747203	0.00175	200	3427694	0.0098	900
33748316	0.002	200	3510553	0.0112	900
34559925	0.00225	200	3565620	0.0126	900
35184001	0.0025	200	3594405	0.014	900
36000000	0.003294	200	3600000	0.014973	900
0	0.022794	200	0	0.032473	900
16200000	0	400			
17466797	0.0005	400			
19092369	0.001	400			
20595051	0.0015	400			
21959035	0.002	400			
23170926	0.0025	400			
24220441	0.003	400			
25100909	0.0035	400			
25809539	0.004	400			
26347430	0.0045	400			
26719350	0.005	400			
27000000	0.005989	400			
0	0.025989	400			

Table 7-5: Table of value of stress-strain over temperature for slab

- Tensile behavior (varies with temperatures)

In Abaqus, the model required displacement instead of strain, therefore, in order to convert strain to displacement the characteristic length has been used. The inputs of Abaqus are also started from the maximum stress when cracks starts to propagate.

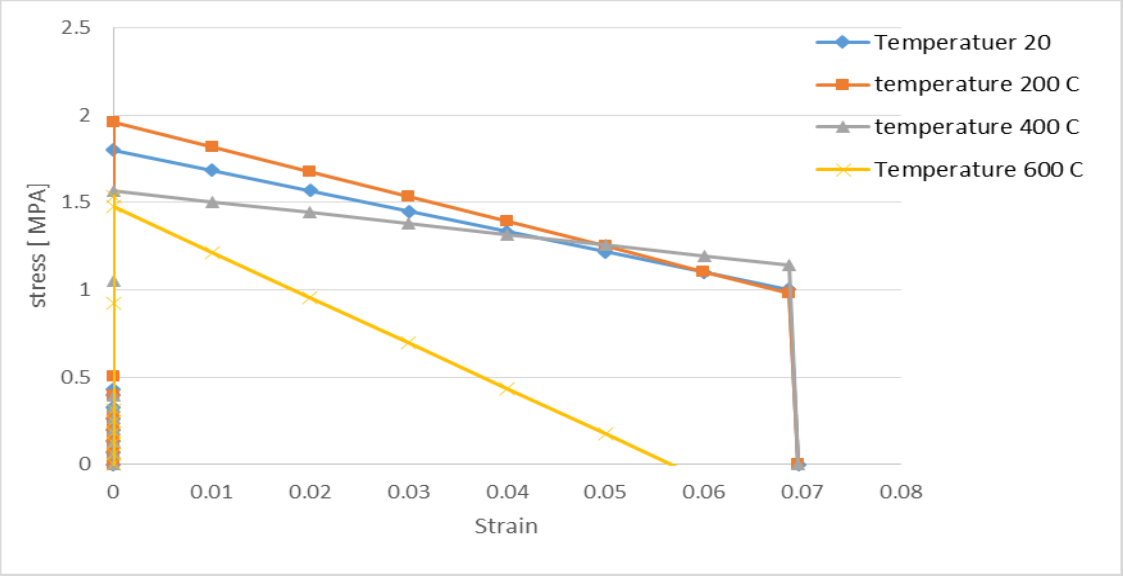

Figure 7-3: Constitutive law in tension for slab

Yield stress (N/m2)	Displacement (m)	Temperature	Yield stress (N/m2)	Displacement (m)	Temperature
1800000	0	20	1566000	0	400
1683458	0.000364	20	1503923	0.000364	400
1566915	0.000728	20	1441846	0.000728	400
1450373	0.001092	20	1379769	0.001092	400
1333830	0.001456	20	1317692	0.001456	400
1217288	0.00182	20	1255615	0.00182	400
1100746	0.002184	20	1193537	0.002184	400
1000000	0.002499	20	1140000	0.002498	400
0	0.002535	20	0	0.002535	400
1962000	0	200	1476000	0	600
1819220	0.000364	200	1215158	0.000364	600
1676439	0.000728	200	954315.4	0.000728	600
1533659	0.001092	200	693473.2	0.001092	600
1390878	0.001456	200	432630.9	0.001456	600
1248098	0.00182	200	171788.6	0.00182	600
1105317	0.002184	200	0	0.002148	600
982000	0.002499	200			
0	0.002535	200			

Table 7-6: Stress-displacement value of slab for different temperature

7.1.3 Load

In the part of "load", the loads will be applied to the model. It is worth noticing that since the model contains slab, the weight of slab should be cancelled from the load calculated in chapter 4. The program consider it automatically and do not need to consider this value in the calculations. Therefore value of 4000 N/m2 is the load applying on the model.

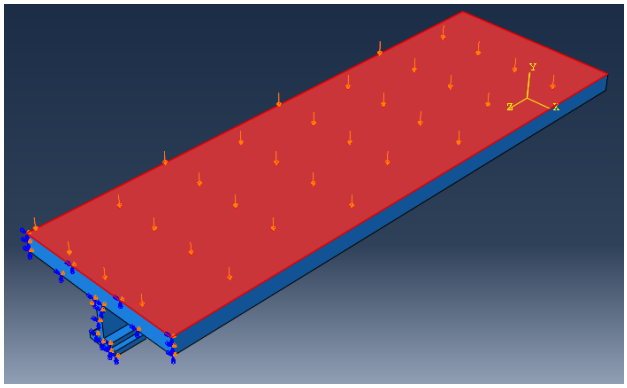

Figure 7-4: Loads acting on the beam with slab model

(The boundary condition and predefined field of temperature is the same as beam without slab.)

7.1.4 Mesh

Meshing is the same as beam without slab. Just the number of elements increases due to the existence of the slab.

Mesh of 3D model:

All regions in the assembly that require a mesh are meshed.

Total number of nodes: 72512

Total number of elements: 419072

419072 linear tetrahedral elements of type C3D4T

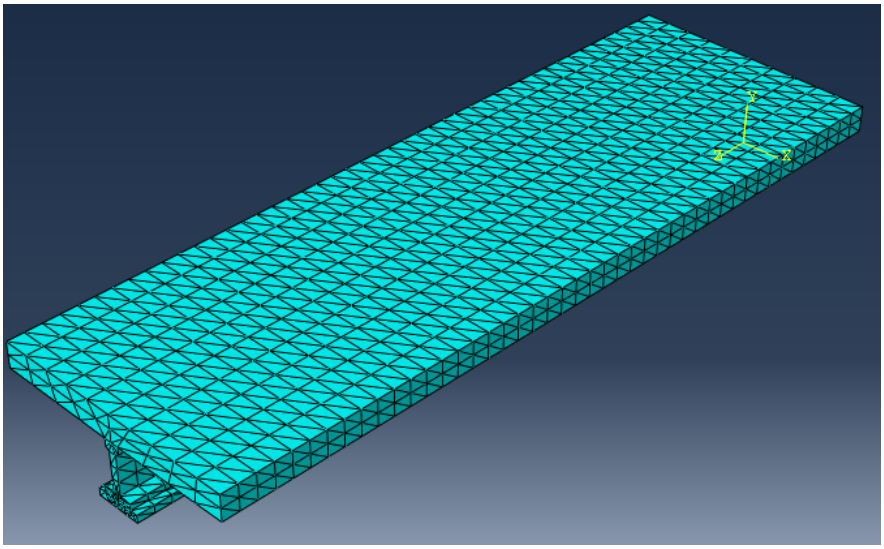

Figure 7-5: Mesh of beam with slab in 3D model

Mesh of 2D model:

All regions in the assembly that require a mesh are meshed.

Total number of nodes: 3430

Total number of elements: 6194

6194 linear triangular elements of type DC2D3

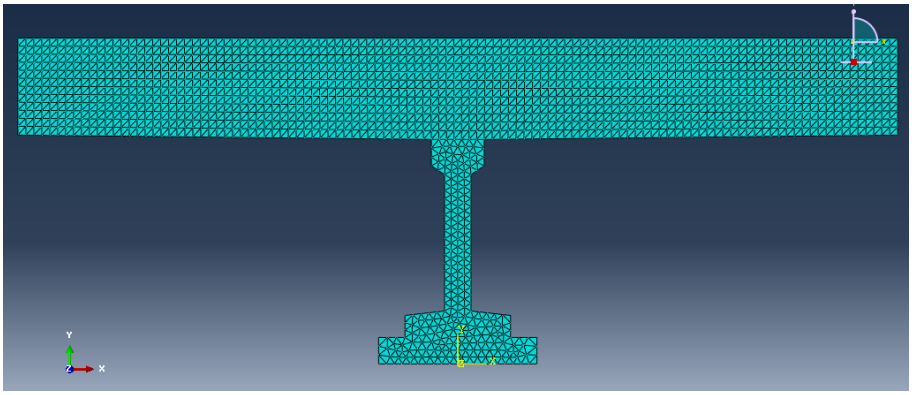

Figure 7-6: Meshing of beam with slab in 2D model

7.1.5 2D model

In 2D model, in addition to modelling beam in Abaqus, it is needed to use Matlab program to fine the bending moment capacity of the beam with slab. The results of FEM (temperature distribution over cross section in different times) has been used as an input for matlab. The slab geometry should be added to the previous geometry in the code. Number of discretization of section, number of curvatures, material properties, constitutive laws, degradation of material ... is the same as illustrated in chapter 5.

Temperature distribution over the cross section has been extracted from the numerical modelling for all sides exposed to fire with cooling 60. The result has been presented in Figure 7-7 and Figure 7-8.

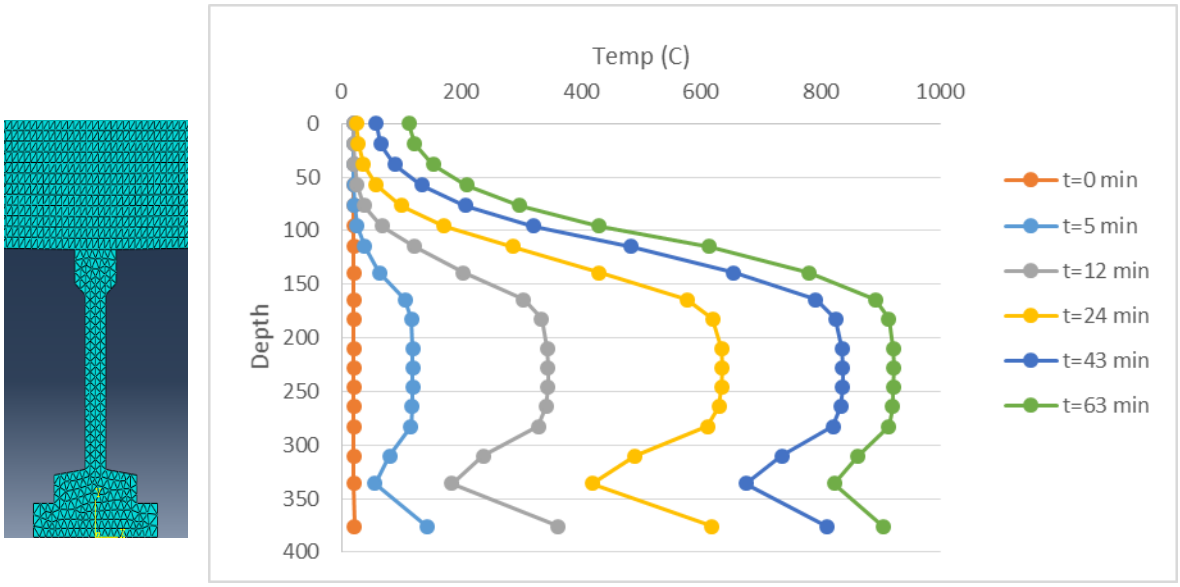

Figure 7-7:Results of FEM: both slab and beam are exposed to fire with cooling started at 60 min. Results at time 0, 5,12,24,43,63 minutes)

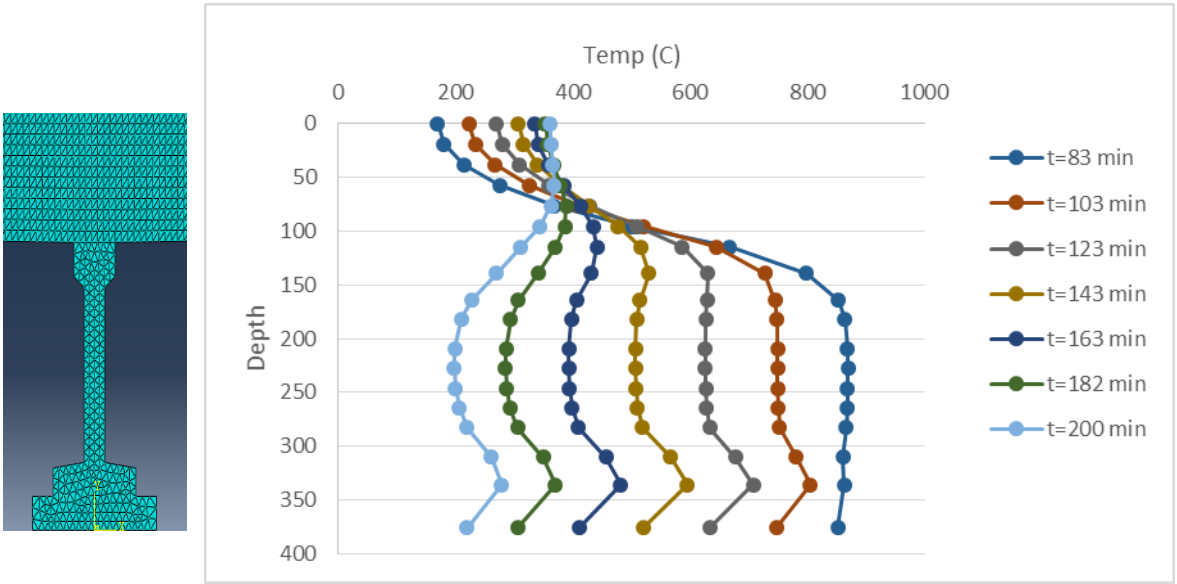

Figure 7-8: Results of FEM: both slab and beam are exposed to fire with cooling started at 60 min, Results at time 83,103,123,143,163,182 and 200 minutes)

For the other case, where the slab is not exposed to fire the temperature over the slab can be assumed to be constant and is the same with the temperature of top of the beam in result of without slab. Since the temperature at that layer are not high and the variation of temperature is negligible.

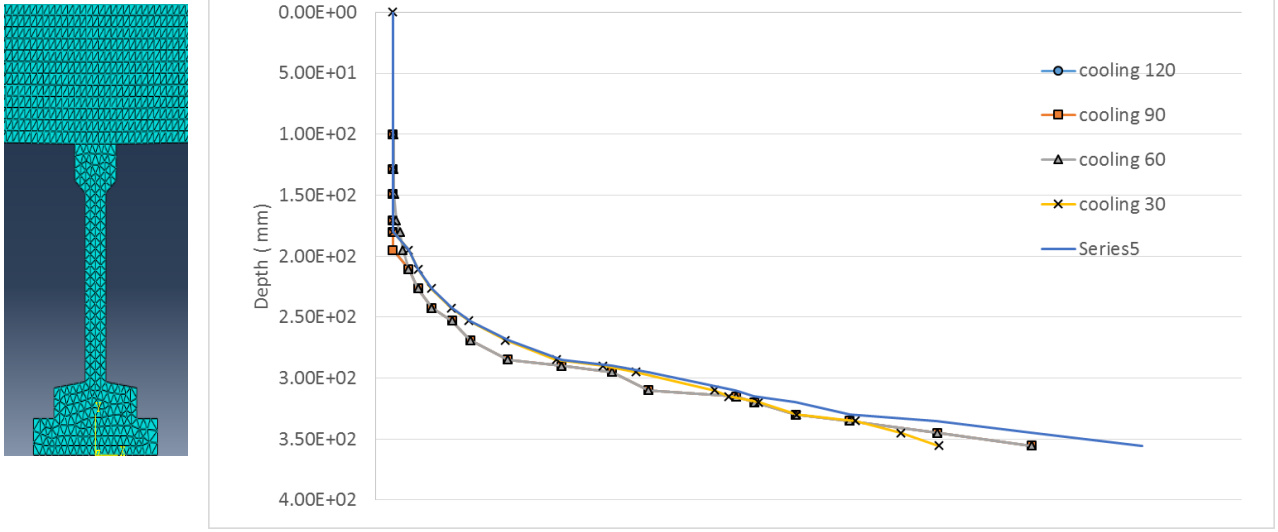

Figure 7-9: Temperature distribution over depth at time 60 min

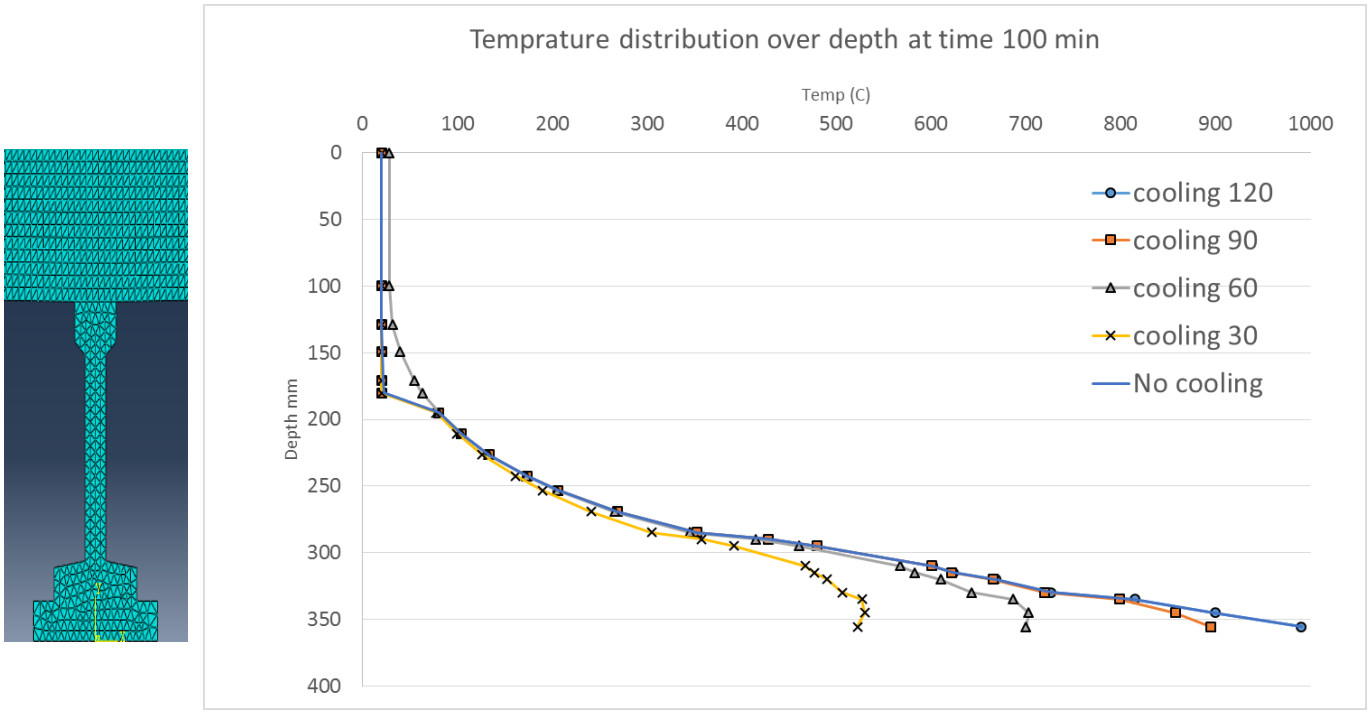

Figure 7-10: Temperature distribution over depth at time 100 min

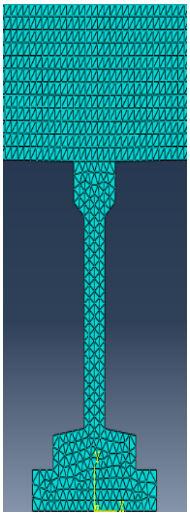

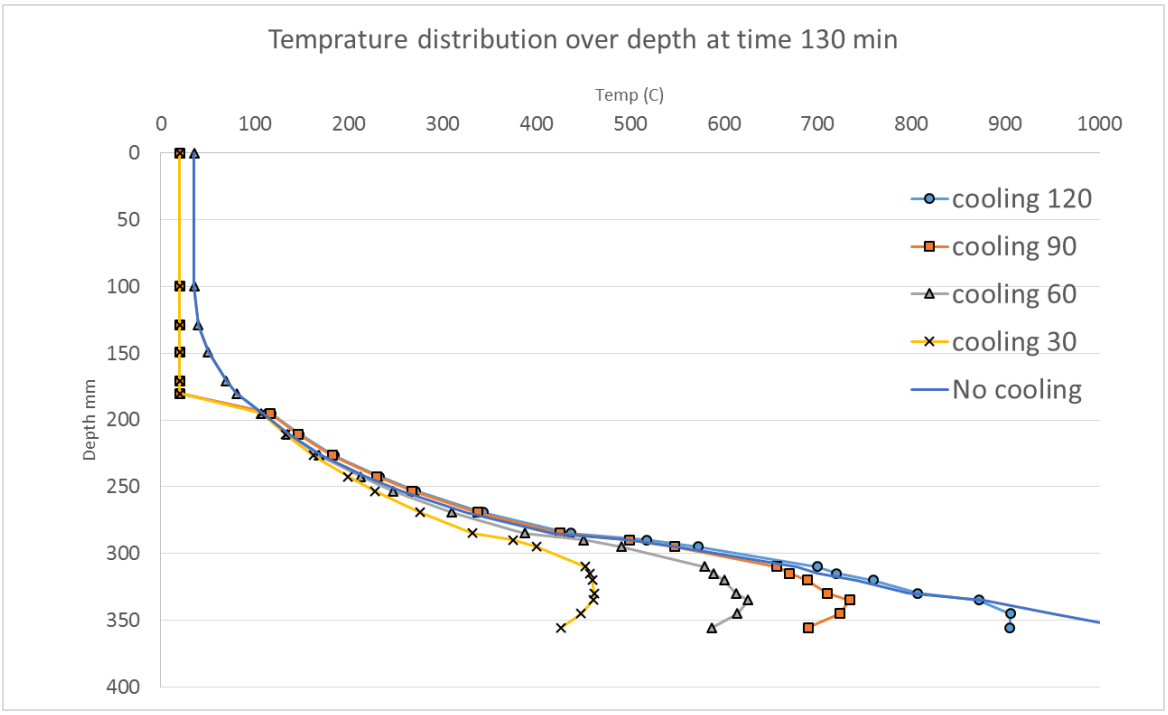

Figure 7-11: Temperature distribution over depth at time 130 min

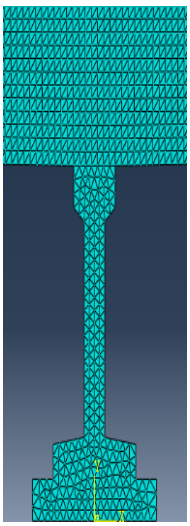

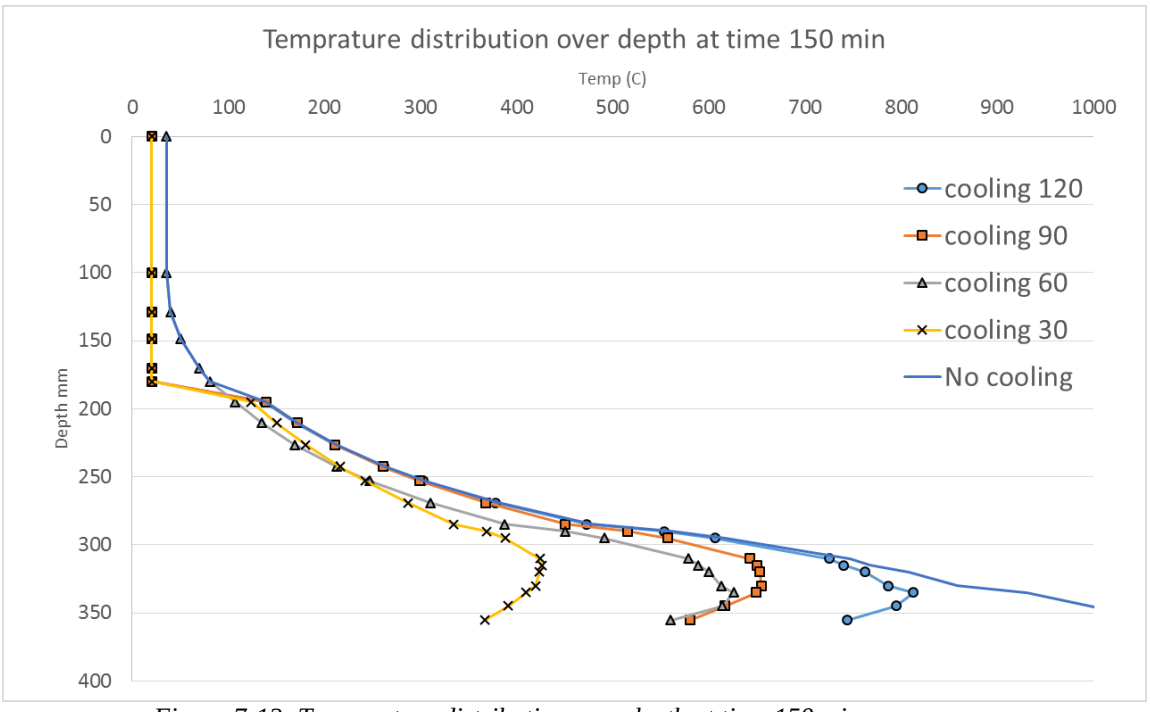

Figure 7-12: Temperature distribution over depth at time 150 min

For 2D model (plane section approach) the calculations have done in cooling scenarios such as; 30, 60, 90 and 120 (bottom of the beam exposed to fire).

After running the program, the final results in term of moment-curvature diagram have been extracted for each scenarios.

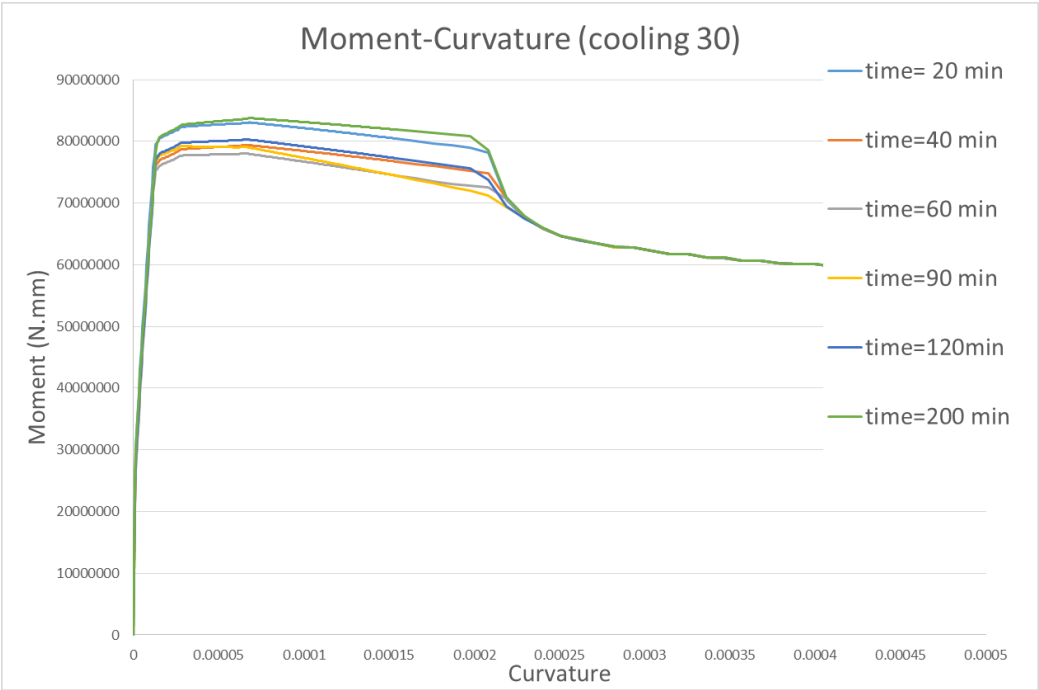

Figure 7-13:Moment-curvature of beam with slab for cooling started at 30 min

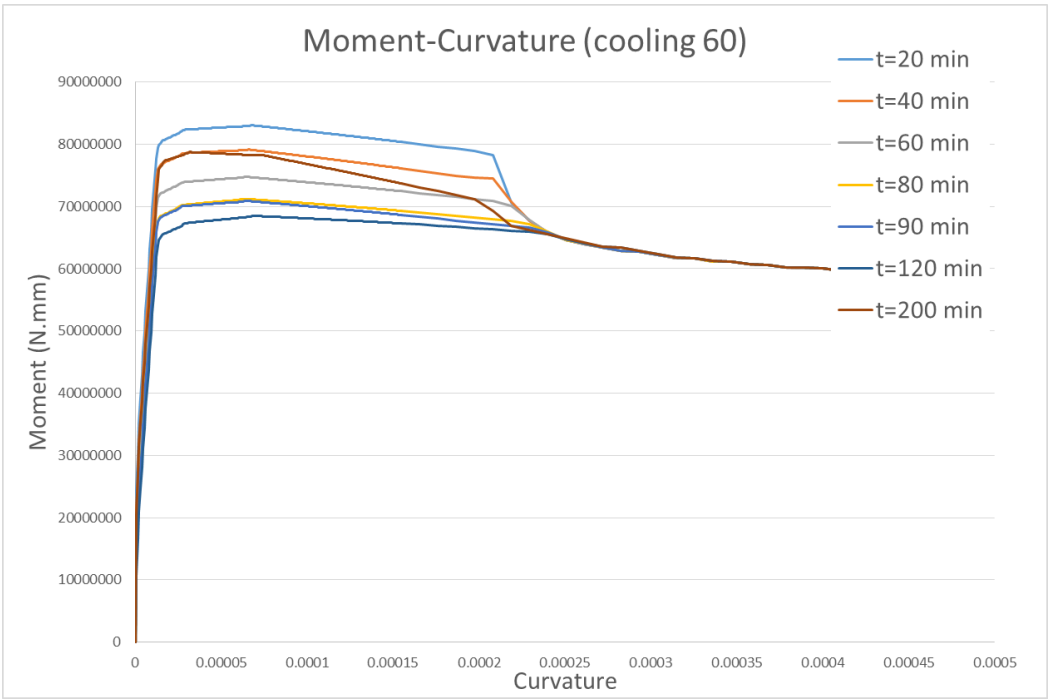

Figure 7-14:Moment-curvature of beam with slab for cooling started at 60 min

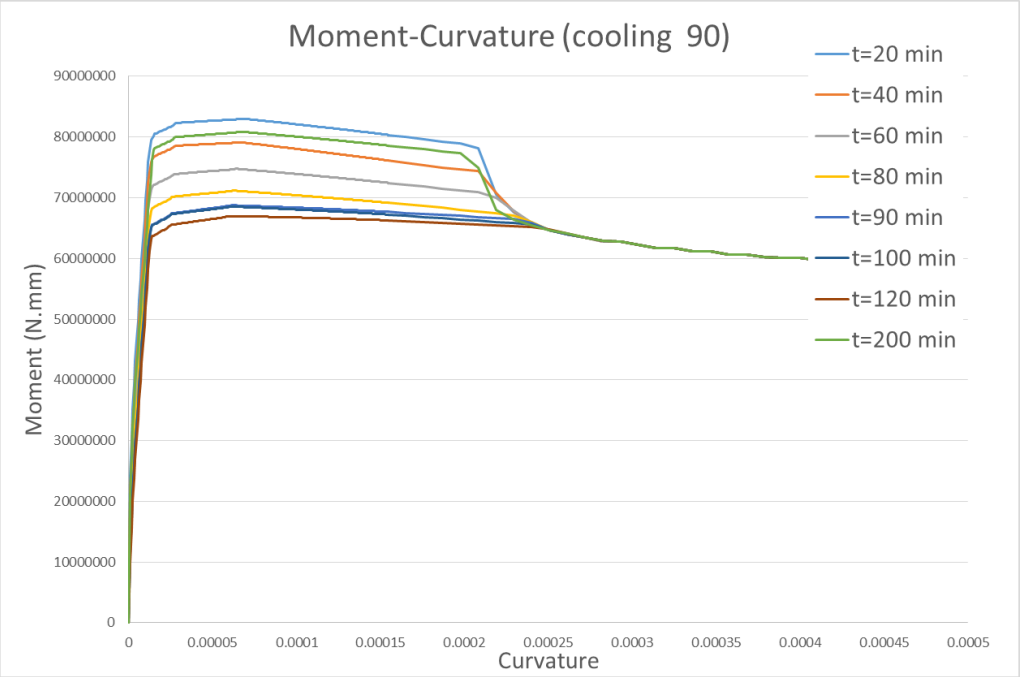

Figure 7-15:Moment-curvature of beam with slab for cooling started at 90 min

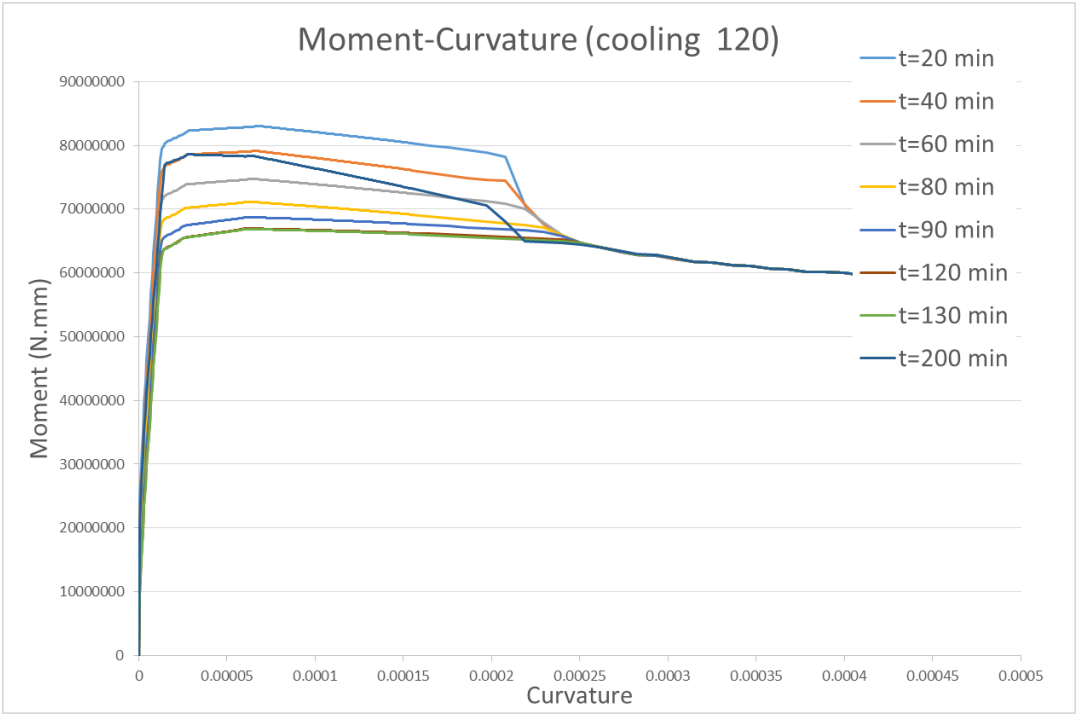

Figure 7-16:Moment-curvature of beam with slab for cooling started at 120 min

Bending moment capacity degradation over time can be found using the same procedure explained in chapter 5. Final results has been shown in Figure 7-17.

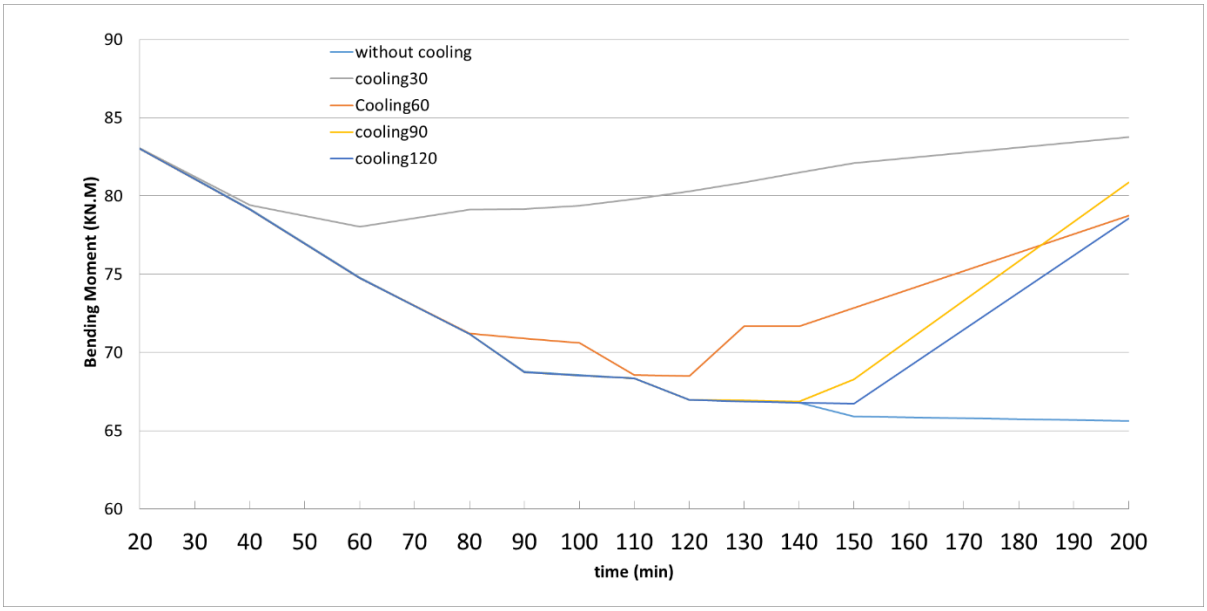

Figure 7-17: Moment-time diagram of beam with slab

Slab added to the beam section can increase the resisting bending moment of beam significantly. The results reveals that the failure will not occurs since the acting moment on the beam is around 28 (KN.M) and the bending moment capacity reaches at minimum of 65 (KN.M) in almost all the scenarios. It is worth noticing that in this analysis only fire exposed to the bottom of the beam and the slab is safe from degradation. In the next analysis the slab is also exposed to fire and the degradation of slab concrete will reduce the bearing capacity of the beam.

Figure 7-19 shows the situation when all the bottom surfaces of beam and slab are exposed to fire scenarios with cooling after 60 minutes. The results indicates that there is a significant degradation of bending moment capacity and the section will fail after 31 minutes of fire exposure. Knowing this results, it is suggested to design a barrier at least for slab in order to protect it against fire and keep the temperature of slab as low as possible.

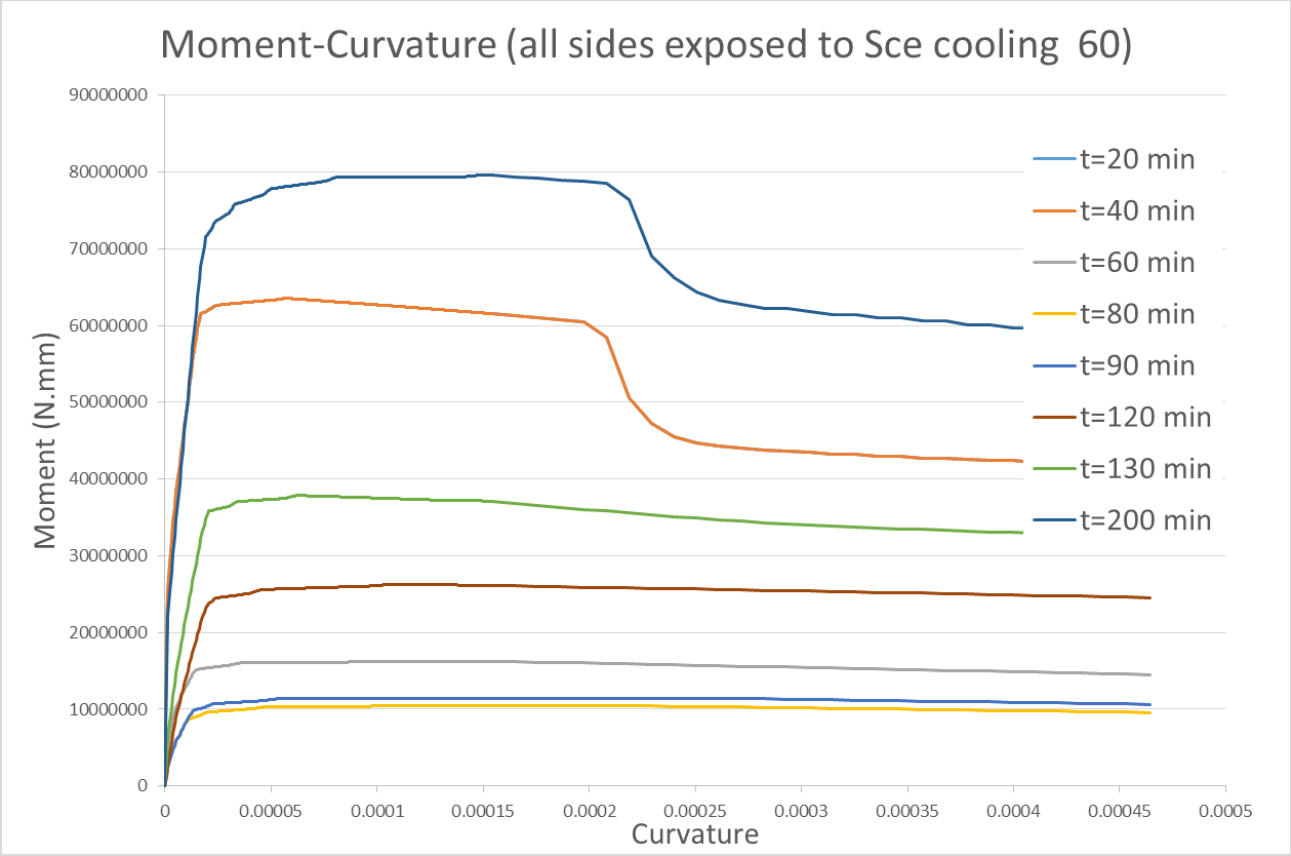

Figure 7-18:Moment-curvature of beam with slab for cooling started at 60 min (all sides are exposed to fire)

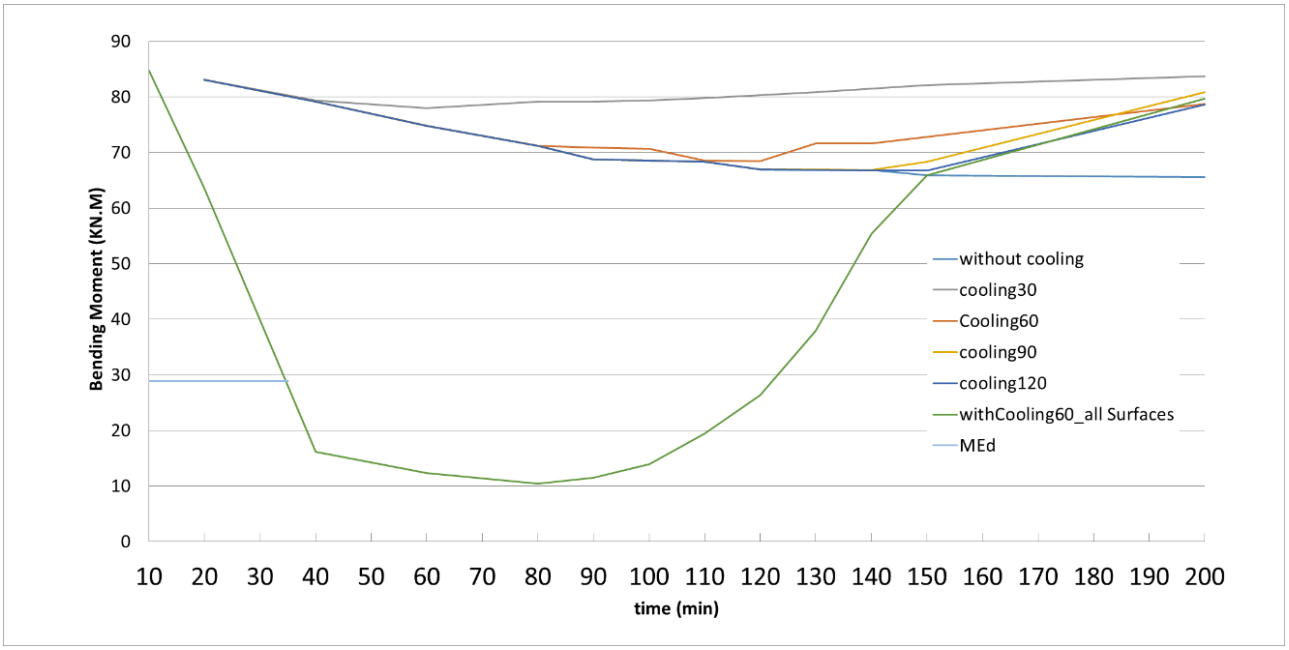

Figure 7-19: Slab exposed to fire scenario 60

7.1.6 3D model Results

In 3D model of beam with slab, only bottom of the beam exposed to fire iso834 without any cooling phases.

Results reveals that if the bottom of the beam exposed to fire there is no failure or collapse and the analysis of FEM will be completed successfully.

Starting form the result of temperature distribution, it is observed in Figure 7-20, nodal temperature increases as time grows. The zones that mostly experienced high temperature are the zones exist on bottom side of the beam where the surface exposed to fire. There is an initial displacement due to the external loading and then as temperature increase the displacement develops as well (Figure 7-22). The results of total strain shows that for a specific point which is located at the bottom of the beam in center there is evolution of strain from zero to 0.02 over time (Figure 7-23).

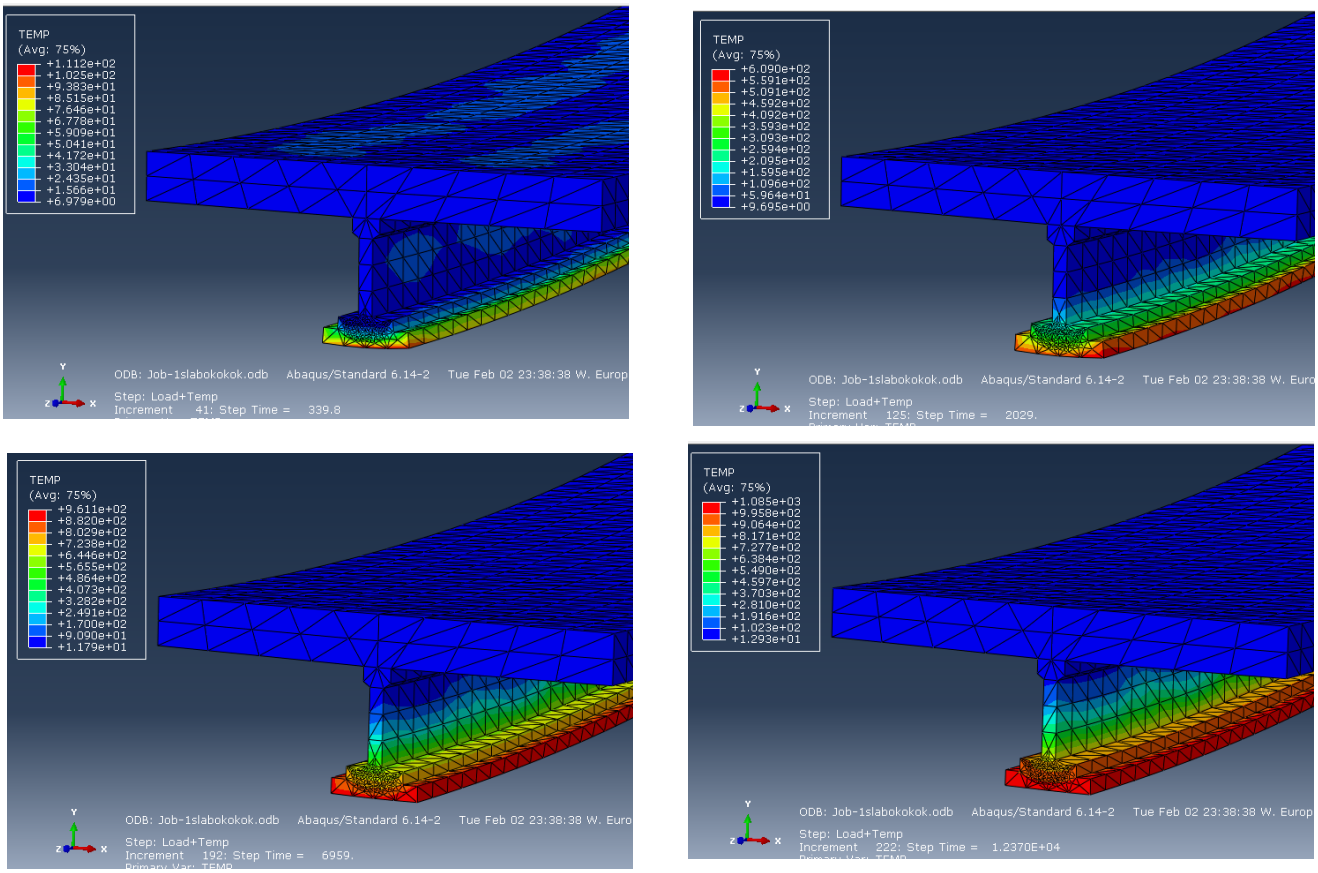

Figure 7-20: Nodal temperature for different steps (only bottom of the beam exposed to fire)

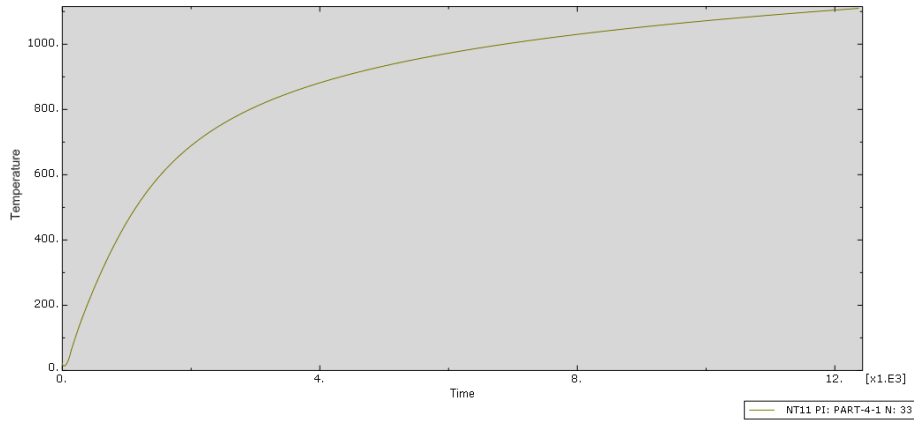

Figure 7-21: Temperature evolution over time for a specific point located at center and bottom of the beam

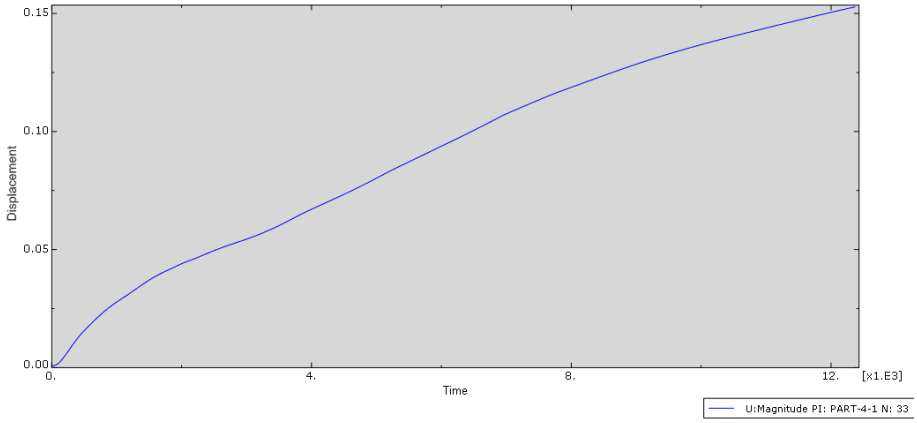

Figure 7-22: Displacement over time for a central point in the middle of the span

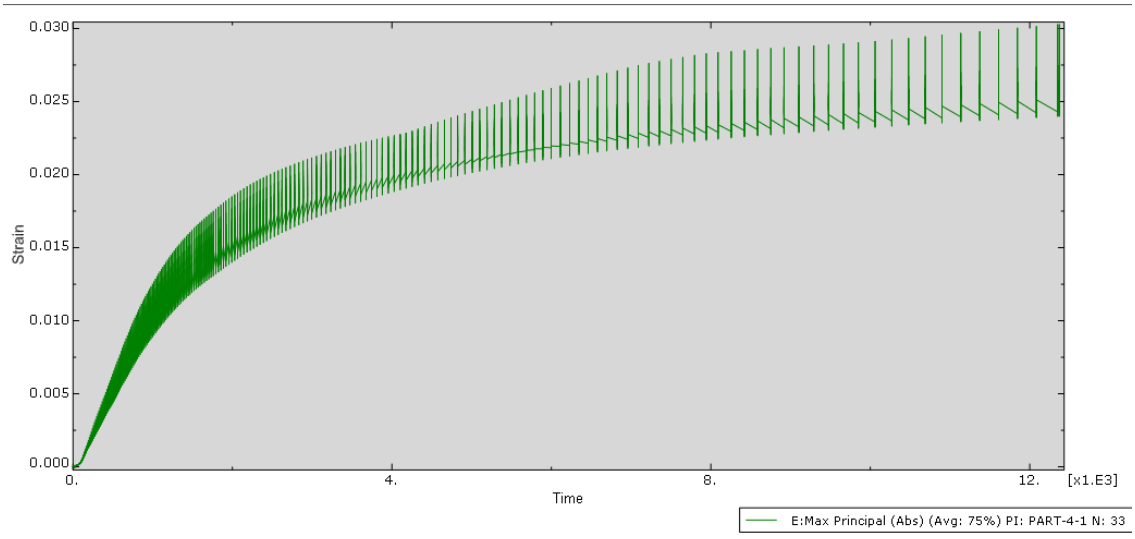

Figure 7-23: Strain evolution over time for a point in center and in bottom of the beam

Also results of stresses and strains have been shown graphically for 3 different steps (beginning, middle and end of the period) in Figure 7-24 and Figure 7-25.

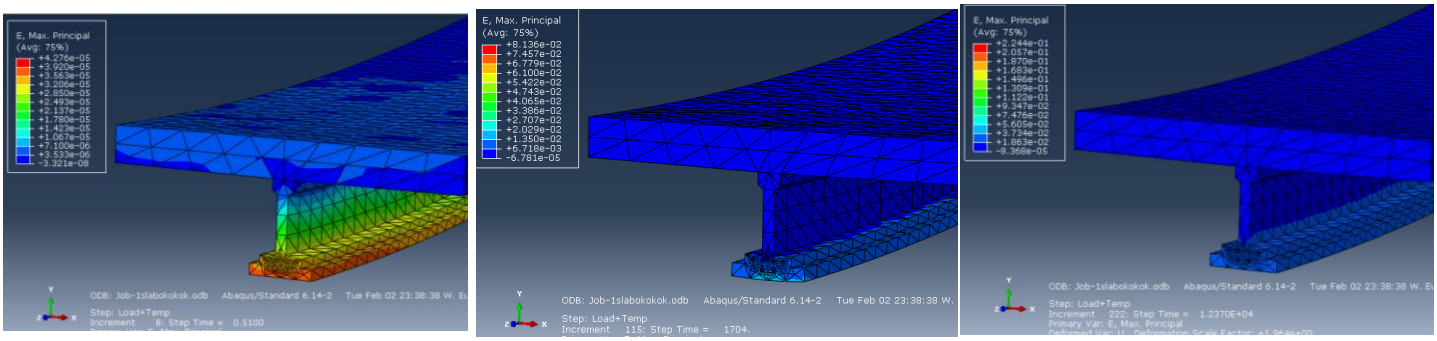

Figure 7-24: Strain evolution over time for beam in 3D view

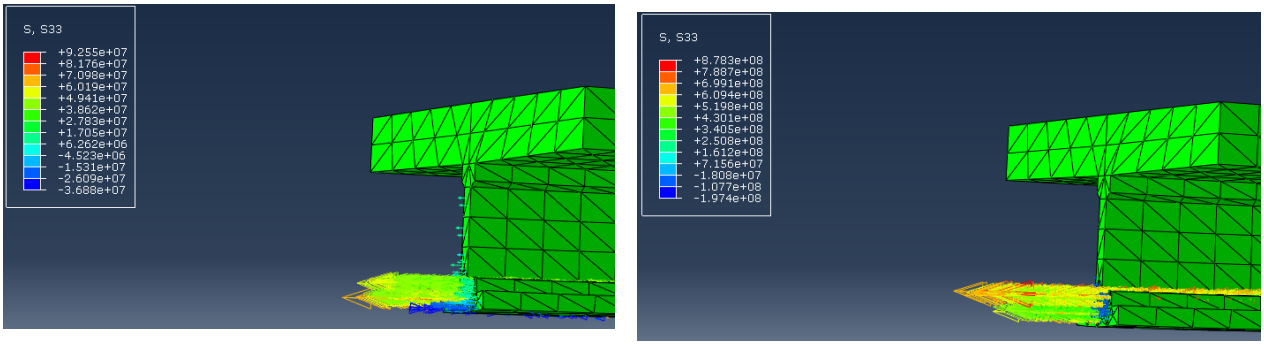

Figure 7-25: stress evolution over time for 3 steps in 3d view

The total strain which is elastic strain (plastic strain has not been activated) increasing over time from 4.27E-5 to 1.02E-2 for the points at the bottom of the beam in the center. Stresses shows that mostly the steel bars are carrying the load and the stresses exist in steel bars developed from an average value of 4.94E7 to 6.90E08 (N/mm2).

8 Conclusion

This thesis is studied for analyzing high performance steel fibre-reinforced concrete (HPFRC) subjected to bending moment when exposed to high temperature. The thesis is aimed to pave the way for deeper investigations especially to find the bearing capacity and time of failure of the HPFRC beam exposed to fire with or without cooling phases. For this purpose, from the numerical investigations carried out, some important conclusions may be highlighted.

1- Due to increase of temperature the properties of materials decrease. Therefore we have an increase in displacement because stiffness of material reduces. The numerical analysis carried out showed in both models (2D and 3D) there is failure after a certain time. Displacement as function of time was presented and shows that deformability increases over time and there is a time when materials are not able anymore to bear the loads. The difference between failure time in 2D (cross section) and 3D (whole structural element) shows that failure happens sooner in 2D rather than 3D.

2- In 2D model the failure time is smaller than failure time in 3D model. It indicates that designing structural elements such as beams using 2D model (plane section approach) leads to be in conservative side and/or not to be economical as well. Designing according to 3D FEM approach results to have smaller sections, because designer will take into account greater failure time. It is suggested that a value in between considered for the design against fire purposes.

3- The constitutive law has a great effect on the mode of failure and it can define a brittle or a ductile failure. In this study the constitutive laws were used according to FIB model code that leads to have ductile failure.

4- Fire exposure sides are very important and has significant effects on the results. If the fire exposes to both beam and slab, the results are very different compare with the condition when only beam is exposed to fire means that there is a fire barrier for the slab. It is recommended to use barrier to keep the temperature of the slab as low as possible.

5- Results of different cooling phases showed that the effect of cooling on structures are not always in favorable side. This is due to the penetration of temperature into the section and continue increasing of temperature in a certain depth over certain time after cooling started.

6- The height of the specimen plays a very important role on the achievement of the required bending moment capacity. The preliminary analytical model (beam) showed that if the slab has been considered in the model, the bearing capacity will increases significantly.

FUTURE PERSPECTIVES:

The numerical analysis performed in this thesis are referring only to the mechanical and thermal behavior of the material, but not measuring or taking into account the spalling phenomena as well as creep or shrinkage components of the strain. The further analysis could be done experimentally in order to investigate the complete response of material behavior.

Since the finite element analysis are giving reliable results, the comparison between the experimental tests, which includes total strain behavior, and the numerical tests, which consist of mechanical and thermal strains, would lead to understand the spalling phenomena. The proposed experimental models are the same of the numerical ones performed in the chapter 6. In this way, a better description of the tensile behavior of HPFRC under high temperatures could be developed.

Using other constitutive law (rigid or hardening behavior for cracks in tension) can lead to understand better the application of steel fibrers and comparing the results of different constitutive laws for tension. In this study only softening behavior of crack opening was assumed, that is not always the case and cannot completely described reality.

9 Bibliography

Hung, C. C., & Tawil, S. (December 2011). Seismic Behavior of a Coupled Wall System with HPFRC Materials in Critical Regions. *JOURNAL OF STRUCTURAL ENGINEERING © ASCE*, 1499-1507.

ACI, C. (1988). Design considerations for steel fiber reinforced concrte (ACI). *American concrete institute*.

ACI, c. (1997). State of the art report on fiber reinforced concrete. *ACI, american concrete institute*, 1-60.

Adebar, P., Mindess, S., Pierre, S., & Olund, B. (1997). Shear tests of fiber concrte beams without stirrups. *ACI structural journal* , 68-76.

Ayub, T., Shafiq, N., & Nuruddin, F. (2013). Mechanical Properties of High Performance Concrete Reinforcment with Basalat Fibers. *Elsevier* , 131-139.

Bažant, Z. P. (1997). Analysis of pore pressure, thermal stress and fracture in rapidly heated concrete,. *the International Workshop on Fire Performance of High Strength Concrete*, (pp. 155–164). Gaithersburg, Md, USA.

Bentur, A., & Mindess, S. (1990). *Fibre Reinforced Cementitious Composites.* India: E & FN spon.

Bhargava, P., Sharama, U., & Kaushik, S. (2006). Compressive Stress-Strain Behaviour of Small Sclae Steel Fibre Reinforced High Strenght Concrete Cylinders . *Journal of Advanced Concrete Technology* , 109-121.

Castillo, C. , Durrani, A.J. (Jan-Feb 1990). Effect of transient high temperature on high strenght concrete. *ACI materials Journal V.87*, 47-53.

Caverzan, A., Cadoni, E., & di Prisco, M. (2013). Dynamic tensile behaviour of high performance fibre reinforced cementitious composites after high temperature exposure. *Elsevier*, 87-109.

Caverzan, A., Colombo, M., Di Prisco, M., & Rivolta, B. (2015). High Performance steel fiber reinforced concrete: residual behaviour at high temperatue . *Materials and Structures*, 48:3317-3329.

Chanh, N. V. (n.d.). STEEL FIBER REINFORCED CONCRETE . *Vietnam joint seminar* , (pp. 108-116). Vietnam .

Dancygier, A. N., & Savir, Z. (2006). Flexural behavior of HSFRC with low reinforcement ratios. *Elsevier* , 1503-1512.

Diederichs, U., Jumppanen, U., & Schneider, U. (1995). high temperature properties and spalling behavior of high strength concrete. *Fourth Weimar Workshop on High performance concrete* (pp. 219-236). Weimar, Germany: Hochschule fur Architektur und Bauwesen.

Donoel, J. F. (2007). Fire safety and concrte structures. *FEBELCEM - Federation of Belgian cement industry* , 90.

Dwaikat, M.B., Kodur, V.K.R. (2009). Hydrothermal model for predicting fire-induced spalling in concrete structural systems,. *Fire Safety Journal*, 425-434.

Eren, O., & Celik, T. (1997). Effect of silica fume and steel fibers on some properties of high strengh concrte. *Constr Build Mater*, 373-82.

Fatih , A., Tefaruk, H., & Kamura, A. (2007). Effects of steel fiber addition on mechanical properties of concrete and RC beams. *Elsevier*, 654-661.

Felicetti, R., Gambarova, P., Natali Sora, M., & Khoury, G. (2000). Mechanical behaviour of hpc and uhpc in direct tension at high temperature and after cooling. *Fifth Symposium on Fiber Reinforced concrete (FRC)* (pp. 749-758). Lyon, France: BEFIB2000. RILEM.

GUERRINI, G. L. (2000). Applications of High-Performance fibre reinforced concrete. In *Applied Composite Materials 7* (pp. 195–207). Netherlands: 2000 Kluwer Academic Publishers.

Jansson, R. (2008). Material properties related to fire spalling of concrete. *Licentiate thesis, Lund institute of technology and Lund university*, 120.

Johnston, C. (1974). Steel fiber reinforced mortar and concrete. *A review of mechanical properties. In fiber reinforced concrete ACI* , 44.

Joost, C. W. (2009). High performance fiber reinforced concrete in knowledge and design codes . *Materials and Structures* , 1247-1260.

Kalifa, P., Menneteau, D., Quendard, D. (2000). Pore Pressure in HPC at High Temperatue . *Cement and Concrete Research* , 30. 1915-1927.

Kanmalai, W. C., Partheeban, P., & Felix, K. T. (2008). MECHANICAL PROPERTIES OF HIGH PERFORMANCE CONCRETE INCORPORATING GRANITE POWDER AS FINE AGGREGATE. *International Journal on Design and Manufacturing Technologies*, 67-73.

Kim, D., El-Tawil, S., & Naaman, A. (2009). Rate-dependent tensile behavior of high performance fiber reinforced cementitious composites. *Materials and Structures 42*, 399-414.

Kodur, V. (2003). Fiber reinforcement for minimizing spalling in HSC structural members exposed to fire . *Innovations in Fibre-Reinforced Concrete*, 216,-221-236.

Kodur, V. (2014). Properties of concrete at elevated temprature . *ISRN civil Engineering* , 15 pages.

Kodur, V. K. (May 2000). Spalling in high strength concrete exposed to fire—concerns, causes, critical parameters and cures,. *Advanced Technology in Structural Engineering* (pp. 1-9). ASCE Structures Congress.

Kodur, V., & Phan, L. (2007). Critical factors governing the fire performance of high strength concrete systems . *Elsevier*, 482-488.

Kristulovic, O. N., Dogan, E., Uang, C., & Haghayeghi, A. (1997). Flexural behaviour of composite R.C. -Slurry infiltrated Mat concrete (SIMCOM) members. *ACI Struct*, 502-512.

Krstulovic, O. N., Haghayeghi, A. R., & Uang, C. M. (1995). High performance construction material for seismic repari and rehabilitation. *IABSE reports = Rapports AIPC = IVBH Berichte*.

Kwak, Y. K., Eberhard, M. O., Kim, W. S., & Kim, J. (2002). Shear strenght of steel fiber reinforced concrete without stirrups. *ACI structural journal*, 530-538.

Kwak, Y. K., Elberhard, M. O., Kim, W. S., & Kim, J. (August 2002). Shear strength of steel fiber-reinforced concrete beams without stirrups. *ACI structural journal*, 530-538.

Lau, A., & Anson, M. (2006). Effect of high temperatures on high performance steel fibre reinforced concrete. *Elsevier*, 1698-1707.

Lau, A., & Anson, M. (2006). Effect of high tempratures on high performance fiber reinforced concrete . *Elsevier*, 1698-1707.

Levesque, A. (2006). Fire performance of Reinforced concrete slabs. *Master Thesis of worcester polytechnic institute* .

Markovic, I. (2006). *High performance hybrid fiber concrete: development and utilization.* TU Delft: PhD-thesis.

Meikandaan, P., Arunkumar, C., & PonPaul, R. S. (Dec 2012). Experimental studies on Bond between Fibre Reinforced Polymer and Concrete. *International Journal of Computer Trends and Technology (IJCTT)*, 12-18.

Mitsuo , O., & Hiroaki , M. (2014). Effects of various fibres on high-temperature spalling in high-performance concrete. *Elsevier*, 83-92.

Naaman, A. (23 Jun 1991). SIFCON: tailored properties for structural performance in high performance fiber reinforced cement composites. *Proceedings of the international workshop held by RILEM, ACI and others* , Mainz.

Naaman, A. E., & Reinhardt, H. W. (2006). Proposed classifiction of HPFRC composites based on their tensile response. *Materials and Structures* , 547-555.

Oral, B., & Denvid, L. (n.d.). *High Performance Concrete: Fundamentals and Application.* Massachusetts Institute of Technology.

Peng, G.-F., Duan, X.-J., Yang, X.-C., & Hao, T.-Y. (2014). Behavior of high performance steel-fiber concrete exposed to high temperature in terms of spalling and permeability. *10th International Symposium on High Performance Concrete - Innovation and Utilization, HPC* (pp. 252-258). Beijing; China: Trans Tech Publications Ltd.

Phan, L. (2005). Pore Pressure in High Strenght Concrete at High Temperature . *Peiformance, Innovations and Structural Implications .* Vancouver, Canada: the Third International Conference on Construction Materials.

Phan, l. (2007). spalling and mechanical properties of high strenght concrete at high temperature. *concrete under severe conditions: Environment and loading*.

Phan, L.T., Carion, N.J. (2003). Code Provisions for High Strength Concrete Strength-Temperature Relationship at Elevated Temperatures. In *RILEM Materials and Structures* (pp. v.36. 91-98).

Poon, C., Shui, Z., & Lam, L. (2004). Compressive behavior of fiber reinforced high performance concrete subjected to elevated temperatures. *Pergamon, Cement and concrete Research*, 2215-2222.

Poon, C., Shui, Z., & Lam, L. (2004). Compressive behavior of fiber reinforced high-performance concrete subjected to elevated temperature. *Pergamon*, 2215-2223.

Qian, C., & Stroeven, P. (2000). Development of hybrid polypropylene steel fiber reinforced concrete, . *Cem concr Res*, 63-69.

Shah, S. (1995). Recent Trends in the Science and Technology of Concrete. *Concrete Technology: New Trends industrial Applictions* , 1-18.

Soltanzadeh, F., Mazaheripour, H., Barros, J., & Sena, J. C. (2013). *Shear Capacity of HPFRC beams Flexurally Reinforced with steel and prestressed GFRP Bars.* UM, Guimarães.

Sun, W., Pan, G., Yan, H., Qi, C., & Chen, H. (1999). study on the anti exploding characteristics of fiber reinforced cement based composite. In *High Performance Fiber Reinforced Cement Composites* (pp. 565-574). Bagneux: RILEM Publications.

Svermova, L., & Bartos, P. (2002). Development of insito Sifcon for connections in precast concrete and seismic resistance structures. *our world in concrete and structures* , (pp. 29-30). Singapore.

Tamim, A., Faisal, F., & Talal, A. (1999). Mechanical Properties of Normal and High Strenght Concrete with Steel Fibers. *LKAUV*, 87-104.

Vatsal, P., & Niraj, S. (2013). A Survey of High Performance Concrete Developments in Civil Engineering Field. *Open Journal of Civil Engineering*, 69-79.

WAFA, F. F. (1990). Properties and Applications of Fiber Reinforced Concret. *JKAU: Eng. Sci*, 49-63.

Wasan, I. K., Ikbal, N. G., & Zeinab, R. M. (2012). BEHAVIOR OF HIGH PERFORMANCE FIBER REINFORCED CONCRETE COLUMNS. *ARPN Journal of Engineering and Applied Sciences*, Vol 7.

Wit, A. D. (2011). Behaviour and structural design of concrete structures exposed to fire. *Master of Science thesis, Stockholm, Sweden*.